

https://dspace.org/

Synthesis of biodiesel from rubber seed oil for internal compression ignition engine

Onoji, Samuel Erhigare

2017

https://hdl.handle.net/10539/25498

Onoji, Samuel Erhigare (2017) Synthesis of biodiesel from rubber seed oil for internal compression ignition engine, , University of the Witwatersrand, Johannesburg, <http://hdl.handle.net/10539/25498>

Downloaded from a DSpace repository. https://dspace.org/



SYNTHESIS OF BIODIESEL FROM RUBBER SEED OIL FOR INTERNAL COMPRESSION IGNITION ENGINE

Samuel Erhigare Onoji

A thesis submitted to the Faculty of Engineering and the Built Environment, University of the Witwatersrand, Johannesburg, in fulfillment of the requirements for the degree of Doctor of Philosophy.

Johannesburg, South Africa.

2nd December, 2017

DECLARATION

I declare that this thesis is my own, unaided work. It is being submitted for the Degree of Doctor of Philosophy in the University of the Witwatersrand, Johannesburg. It has not been submitted before for any degree or examination in any other University.



(Signature of candidate)

2nd.....Day of.....December, ...2017

ABSTRACT

Biodiesel has been identified as a good complement and plausible replacement of fossil diesel because of the overwhelming characteristic properties similar to fossil diesel in addition to its good lubricity, biodegradability, non-toxicity and eco-friendliness when used in diesel engines. The production of biodiesel from edible vegetable oils competes with food sources, thereby resulting in high cost of food and biodiesel. Studies have shown that rubber seed contains 35–45 % oil, which portrays a better competitor to other non-edible oil bearing plants in biodiesel production. In this study, non-edible vegetable oils from underutilized Nigerian NIG800 clonal rubber seeds were extracted from 0.5 mm kernel particle size using n-hexane as solvent to obtain a yield of 43 wt.% over an extraction time of 1 h. The oil was characterized for fatty acids by using gas chromatography-mass spectrometry (GC-MS), and for structural properties by Fourier transform-infrared (FT-IR) and nuclear magnetic resonance (NMR) analyses.

The optimization of the process conditions of the vegetable oil extraction was evaluated using response surface methodology (RSM) and artificial neural network (ANN) techniques both of which, were based on a statistically designed experimentation via the Box-Behnken design (BBD). A three-level, three-factor BBD was employed using rubber seed powder (X_1), volume of n-hexane (X_2) and extraction time (X_3) as process variables. The RSM model predicted optimal oil yield of 42.98 wt. % at conditions of X_1 (60 g), X_2 (250 mL) and X_3 (45 min) and experimentally validated as 42.64 wt. %. The ANN model predicted optimal oil yield of 43 wt. % at conditions of X_1 (40 g), X_2 (202 mL) and X_3 (49.99 min) and validated as 42.96 wt. %. Both models were effective in describing the parametric effect of the considered operating variables on the extraction of oil from the rubber seeds. On further examinations of the potentials of the vegetable oil, the kinetics of thermo-oxidative degradation of the oil was investigated. The kinetics produced a first-order reaction, with activation energy of 13.07 kJ/mol within the temperature range of 100–250 ^{o}C. In a bid to attain enhanced yield of

biodiesel produced via heterogeneous catalysis, coupled with the carbonaceous potentials of the pericarp and mesocarp of rubber seed shell casing as a suitable catalytic material, the rubber seed shells (RSS) were used to develop a heterogeneous catalyst. RSS was washed 3–4 times with hot distilled water, dried at 110 ^{o}C for 5 h, ground to powder, and calcined at 800 ^{o}C at a heating rate of 10 ^{o}C/min as a catalyst and analyzed for thermal, structural, and textural properties using thermogravimetric analyzer, x-ray diffractometer, and nitrogen adsorption/desorption analyzer, respectively. The catalyst was further analyzed for elemental compositions and surface morphology by x-ray fluorescence and scanning electron microscopy, respectively. The catalyst was then applied in biodiesel production from rubber seed oil. A central composite design (CCD) was employed together with RSM and ANN to obtain optimal conditions of the process variables consisting of reaction time, methanol/oil ratio, and catalyst loading on biodiesel yield. The optimum conditions obtained using RSM were as follows: reaction time (60 min), methanol/oil ratio (0.20 vol/vol), and catalyst loading (2.5 g) with biodiesel yield of 83.11% which was validated experimentally as 83.06$\pm$0.013%. Whereas, those obtained via ANN were reaction time (56.7 min), methanol/oil ratio (0.21 vol/vol), and catalyst loading (2.2 g) with a biodiesel yield of 85.07%, which was validated experimentally as 85.03$\pm$0.013%. The characterized biodiesel complied with ASTM D 6751 and EN 14214 biodiesel standards and was used in modern diesel test engine without technical modifications. Though the produced biodiesel has a lower energy content compared with conventional diesel fuel, in all the cases of blends considered, the optimal engine speed for higher performance and lower emissions was observed at 2500 rpm. In this study, the B20 blend has best engine performance with a lower emission profile, and was closely followed by B50 blend.

DEDICATION

To my lovely wife Mrs. Augustina Onoji, and my children Faith, Emmanuel, Deborah, and Mishael for their inestimable support, prayers and being my source of strength.

The work is also dedicated to my post-octogenarian Father, Mr. Iboyotete Onoji for his confidence in me and encouragement throughout my years of study. I will not fail to dedicate the work also to the memories of my mother, Mrs. Igogoma Onoji who has gone to be with the Lord.

ACKNOWLEDGMENTS

First and foremost, I appreciate God Almighty for the strength, knowledge and the grace He gave me to start and complete the research successfully.

My deep appreciation goes to Professor Sunny E. Iyuke for his thorough supervision, encouragement, guidance and valuable support he gave me while the project lasted. The three years under his supervision motivated me to develop a scientific rigour and effectiveness.

My profound gratitude goes to my co-supervisors, Professor Michael O. Daramola of the University of the Witwatersrand, Johannesburg, South Africa, and Professor Anselm I. Igbafe of Afe Babalola University, Ado-Ekiti, Nigeria, for their close supervision, expertise and valuable contributions to this study.

I acknowledged immensely the contributions of Dr. Julius I. Osayi of the Nanotechnology and Petroleum Research Group of the University of the Witwatersrand for the role he played throughout the duration of the research. Other members of the Nanotechnology and Petroleum Research Group are also appreciated for their immense contributions during our weekly research group meetings, and to Mr. Bruce Mothibeli for his laboratory assistance and materials provided for the practical work.

I would like to acknowledge the contribution of Dr. Diakanua B. Nkazi and Family for the hospitality showed to me during my stay in Johannesburg, and to Dr. Tunde F. Adepoju of Landmark University, Omu-Aran, Nigeria, for his encouragement and laboratory assistance.

I want to warmly appreciate Dr. Kevin I. Idehen and Dr. Reuben M. Umoh, both of the Petroleum Training Institute, Effurun, Nigeria for their valuable suggestions, insightful advice and support.

I sincerely appreciate His lordship, Bishop Dr. & Rev. (Mrs.) Curtis Fianu, Bishop of New Warri Bishopric Headquarters, Church of God Mission International Inc., Praise Centre, Effurun, Nigeria for their encouragement and prayers, and to all Pastors, Ordained Ministers, and Members of the Church for their support and goodwill.

Finally, I truly acknowledge the wonderful support of my beloved wife, Mrs. Augustina Onoji and my lovely children, Faith, Emmanuel, Deborah, and Mishael for their prayers, patience and sacrifice that strengthened me throughout the period of my study.

LIST OF REFERRED PUBLICATIONS

Onoji, S.E., Iyuke, S.E., Igbafe, A.I., & Nkazi, D. B. (2016). Rubber seed oil: A potential renewable source of biodiesel for sustainable development in sub-Saharan Africa. *Energy Conversion and Management*, *110*, 125–134.

Onoji, S.E., Iyuke, S.E., & Igbafe, A. I. (2016). *Hevea brasiliensis* (Rubber seed) oil: Extraction, characterization, and kinetics of thermo-oxidative degradation using classical chemical methods. *Energy & Fuels*, *30* (12), 10555–10567.

Onoji, S.E., Iyuke, S.E., Igbafe, A.I., & Daramola, M. O. (2017). *Hevea brasiliensis* (Rubber seed) oil: Modeling and optimization of extraction process parameters using response surface methodology and artificial neural network techniques. *Biofuels*, 1–15. doi:10.1080/17597269.2017.1338122.

Onoji, S.E., Iyuke, S.E., Igbafe, A.I., & Daramola, M. O. (2017). Transesterification of rubber seed oil to biodiesel over a calcined waste rubber seed shell catalyst: Modeling and optimization of process variables. *Energy & Fuels*, *31* (6), 6109–6119.

ORAL PRESENTATIONS AT CONFERENCES

Onoji, S.E., Iyuke, S.E., Igbafe, A.I., & Daramola, M. O. (2017, May). Synthesis of Rubber Seed (*Hevea brasiliensis*) Oil Methyl Esters over a Calcined Waste Rubber Seed Shell Catalyst: Modeling and Optimization of Process Variables. Paper presented at the 13th International African Scholar Academic Conference on *Delving into Issues and Resources for sub-Saharan Africa Growth in the Millennium Era: A Multi-Disciplinary Approach*. Universite de Sciences et Technologies de Côte d'Ivoire.

TABLE OF CONTENTS

Contents **Page**

DECLARATION.....i

ABSTRACT.....ii

DEDICATION.....iv

ACKNOWLEDGMENTS.....v

LIST OF REFERRED PUBLICATIONS.....vii

PRESENTATIONS AT CONFERENCES.....viii

CONTENTS.....ix

LIST OF FIGURES.....xvii

LIST OF TABLES.....xxii

NOMENCLATURE.....xxiv

CHAPTER 1: INTRODUCTION.....1

1.1 Research background and motivation.....1

1.2 Hypothesis.....3

1.3 Justification of study.....3

1.4 Research aims and objectives.....5

1.5 Thesis outline.....7

CHAPTER 2: LITERATURE REVIEW.....9

2.0 Introduction.....,9

2.1 The rubber tree.....9

2.2 Rubber seed capacity in sub-Saharan Africa.....13

2.3 Rubber seed collection and processing.....15

2.4 Biomass valorization processes.....15
2.5 Modeling and optimization approach to industrial research.....18
2.6 Qualitative and quantitative analytical procedures.....21
2.6.1 Thermogravimetric analysis.....22
2.6.2 Fourier transform infrared spectroscopy.....22
2.6.3 Scanning electron microscopy.....23
2.6.4 Brunauer- Emmett-Teller (BET) analysis.....23
2.6.5 Nuclear magnetic resonance.....24
2.6.6 Gas chromatography-mass spectroscopy.....24
2.6.7 X-ray diffraction and X-ray fluorescence.....25
2.7 Rubber seed analysis.....25
2.8 Rubber seed oil extraction methods.....29
2.8.1 Conventional extraction methods (mechanical and chemical) 30
2.8.2 Gas-assisted mechanical extraction method.....32
2.8.3 Microwave-assisted extraction (MAE) method.....32
2.8.4 Ultrasonic-assisted extraction method.....32
2.8.5 Aqueous enzymatic extraction method.....33
2.8.6 Supercritical fluid extraction (SFE) method.....33
2.9 Physico-chemical properties of rubber seed oil.....33
2.10 Thermo-oxidative analysis of rubber seed oil.....37
2.11 Industrial applications of rubber seed and oil.....39
2.12 Biofuels policies and sustainability in Africa.....40
2.12.1 Nigerian biofuel policy (A case study in Africa) 43
2.13 Catalysis.....45
2.13.1 Catalyst deactivation.....47

2.13.2 Physical adsorption and chemisorption in chemical reaction catalysis.....47

2.14 Gas-solid adsorption systems.....49

2.14.1 Langmuir model equation (linearized).....51

2.14.2 BET model equation.....51

2.14.3 Freundlich model equation.....52

2.14.4 The *t*-plot.....53

2.14.4.1 Harkins-Jura model.....54

2.14.4.2 Halsey equation.....55

2.14.5 Polanyi's potential theory.....55

2.14.6 Dubinin-Radushkevich equation.....56

2.14.7 Kelvin equation.....57

2.14.8 Thermodynamics of gas adsorption.....58

2.15 Biodiesel and its origin.....59

2.15.1 Biodiesel feedstock.....63

2.16 Catalysis in biodiesel production.....64

2.16.1 Acid-catalyzed esterification reaction.....64

2.16.2 Transesterification of oils using homogeneous catalyst.....65

2.16.2.1 Alkali-catalyzed transesterification reaction.....66

2.16.2.2 Two-step transesterification reaction.....67

2.16.2.3 Mechanisms for homogeneous catalysis.....67

2.16.3 Transesterification of oils using heterogeneous catalysts.....67

2.16.3.1 Heterogeneous acid transesterification reaction.....68

2.16.3.2 Heterogeneous base transesterification reaction.....69

2.16.4 Enzyme-catalyzed transesterification reaction.....71

2.16.5 Heterogeneous catalyst from natural sources.....71

2.17 Transesterification of rubber seed oil.....72
2.18 Transesterification methods for rubber seed oil.....73
2.18.1 The conventional method.....73
2.18.2 The in-situ method.....73
2.18.3 The enzymatic method.....74
2.18.4 The supercritical method.....74
2.18.5 The co-solvent assisted method.....74
2.18.6 The ultrasonic-assisted method.....74
2.18.7 The microwave-assisted method.....75
2.19 Factors affecting the transesterification of rubber seed oil.....75
2.19.1 FFA content of rubber seed oil.....75
2.19.2 Alcohol/oil molar ratio.....76
2.19.3 Catalyst concentration.....76
2.19.4 Reaction temperature and time.....77
2.19.5 Agitation speed.....77
2.20 Thermodynamics of internal combustion ignition engines.....78
2.20.1 Overview of reciprocating engines.....78
2.20.2 Air-standard assumptions.....80
2.20.3 Diesel cycle-The ideal cycle for compression ignition engines.....81
2.20.4 Mathematical models for internal compression ignition engines.....84
2.20.5 Models for gas mixture properties.....87
2.20.6 First and second laws of thermodynamics for internal combustion engines.....88
2.20.7 Second law of thermodynamics analysis (*availability*).....91
2.21 Performance evaluation of diesel engines.....95
2.21.1 Brake mean effective pressure.....96

2.21.2 Brake power.....96
2.21.3 Brake specific fuel consumption.....97
2.21.4 Brake thermal efficiency.....97
2.22 Performance and emissions evaluation of diesel engine using diesel-biodiesel blends of rubber seed oil.....97

CHAPTER 3: METHODOLOGY AND EXPERIMENTAL PROCEDURES.....100
3.0 Introduction…….....100
3.1 Materials and chemicals.....100
3.2 Experimental procedures for seed oil extraction……101
3.2.1 Rubber seed preparation……101
3.2.2 Extraction of the seed oil……102
3.3 Characterization of the seed oil……103
3.4 Spectroscopy analyses of the seed oil……..……104
3.4.1 Fatty acid profile of the seed oil…….....104
3.4.2 Fourier transform infrared spectroscopy.....105
3.4.3 Nuclear magnetic resonance spectroscopy...…….……105
3.5 Kinetics of thermal oxidative degradation of the seed oil.....106
3.6 Optimization study of the oil extraction process using RSM and ANN techniques.....107
3.6.1 Modeling of seed oil extraction process variables via RSM…….....108
3.6.2 Modeling of seed oil extraction process variables via ANN…….....111
3.7 Catalyst preparation and characterization.....113
3.8 Biodiesel production from the extracted seed oil and analysis…….....115
3.8.1 Acid-catalyzed esterification of rubber seed oil.....115
3.8.2 Biodiesel production from the esterified seed oil.....116

3.9 Characterization of the produced biodiesel…….....118

3.10 Reusability test for the catalyst used in biodiesel production….....119

3.11 Statistical analysis of the biodiesel production by RSM.....119

3.12 Analysis of variance (ANOVA) study for biodiesel production.....120

3.13 Modeling of biodiesel production process variables…….....120

3.14 Data validation for RSM and ANN models.....121

3.15 Combustion of biodiesel-diesel blends in internal compression ignition engine.....121

3.15.1 Biodiesel-diesel blending analysis via ultrasonication technique.....122

3.15.2 Methodology and experimental setup for combustion study of biodiesel blends.....123

CHAPTER 4: RESULTS AND DISCUSSION.....129

4.0 Introduction…….....129

4.1 Extraction of seed oil and determination of the best seed particle size.....129

4.2 Physical characterization of the seed and seed oil…….....130

4.3 Characterization of the seed oil…….....131

4.3.1Colour, pH, density and Specific gravity.....132

4.3.2 Iodine, peroxide, saponification and acid values.....132

4.3.3 Kinematic viscosity.....133

4.3.4 Cold flow properties.....134

4.3.4.1 Pour point.....134

4.3.4.2 Cloud point.....134

4.3.4.3 Cold filter plugging point.....135

4.3.5 Aniline point.....135

4.3.6 Boiling, freezing, flash and fire points.....135

4.3.7 Refractive index.....136

4.3.8 Other parameters.....136

4.3.8.1 Cetane number.....136

4.3.8.2 Diesel index.....137

4.3.8.3 Higher heating value.....137

4.3.8.4 Average molecular weight of rubber seed oil.....137

4.3.9 Fatty acid profile of the seed oil.....140

4.3.10 FT-IR and NMR spectroscopy of the seed oil.....142

4.3.10.1 FT-IR analysis of the seed oil.....142

4.3.10.2 ^{1}H NMR analysis of the seed oil…….....145

4.3.10.3 ^{13}C NMR analysis of the seed oil.....147

4.4 Kinetic study of thermo-oxidative degradation of rubber seed oil.....148

4.5 Parametric effects and optimization of oil extraction using RSM…….....154

4.5.1 Full quadratic regression model.....154

4.5.2 Optimization of oil extraction process variables based on RSM.....157

4.5.3 Analysis of variance (ANOVA) study for seed oil extraction.....158

4.5.4 Parametric effects of interactive factors on the seed oil yield.....161

4.6 Parametric effects and optimization of oil extraction using ANN model…….....164

4.7 Comparison of RSM and ANN models for the seed oil extraction.....169

4.8 Catalyst preparation and characterization…….....170

4.8.1 Thermo-gravimetric analysis of the rubber seed shell catalyst….....170

4.8.2 XRF elemental analysis and basic property of the rubber seed shell catalyst….....171

4.8.3 XRD analysis of the rubber seed shell catalyst.....172

4.8.4 SEM analysis of the rubber seed shell catalyst catalyst.....174

4.8.5 Surface properties of the rubber seed shell catalyst.....175

4.9 Biodiesel production from the extracted seed o…….....180

4.9.1 Characterization of the rubber seed oil biodiesel.....180

4.9.2 Reusability of the catalyst for biodiesel production.....182

4.10 Parametric effect and optimization of biodiesel production process variables.....183

4.10.1 Modeling and process variables optimization by RSM…….....183

4.10.2 Analysis of variance (ANOVA) for biodiesel production…….....188

4.10.3 Parametric effects of interactive factors on biodiesel yield using RSM….....191

4.10.4 Optimization and interactive effects of process variables on biodiesel yield by ANN model.....193

4.10.5 Comparison of RSM and ANN models for the biodiesel production.....197

4.11 Performance and emissions analysis of test engine using biodiesel-diesel blends.....198

4.11.1 Air/Fuel ratio.....198

4.11.2 Brake mean effective pressure.....199

4.11.3 Brake thermal efficiency.....200

4.11.4 Brake specific fuel consumption.....201

4.11.5 Engine brake power.....202

4.11.6 Engine torque.....203

4.11.7 Exhaust gas temperature.....204

4.11.8 CO emissions.....205

4.11.9 CO_2 emissions.....206

4.11.10 NO_x emissions.....207

4.11.11 Total hydrocarbons.....208

4.11.12 Smoke opacity.....209

CHAPTER 5: CONCLUSIONS AND RECOMMENDATIONS.....211

5.1 Conclusion.....211

5.2 Recommendations.....212

5.3 Contributions to knowledge.....213

REFERENCES.....214

APPENDIX.....240

Appendix A.....240

Appendix B.....244

Appendix C.....246

Appendix D.....248

Appendix E.....251

Appendix F.....259

Appendix G.....262

Appendix H.....269

Appendix I.....272

LIST OF FIGURES

Figure Page

1.1 Systematic approach employed in this research.....6

2.1 Rubber trees plantation.....11

2.2 Rubber seed.....12

2.3 Top ten leading producers of rubber seeds in 2014.....12

2.4 Overview of main biomass valorizations.....18

2.5 Multilayer structure of an ANN model.....20

2.6 General flowchart of Genetic Algorithm.....21

2.7 Flowchart of rubber seed oil processing.....30

2.8 Representation of the action of a catalyst.....47

2.9 Adsorption isotherm classified by *Brunauer*.....50

2.10 A typical structure of triglyceride molecule.....63

2.11 Scheme for stepwise transesterification of triglyceride to methyl esters.....66

2.12 Schematic diagram for a reciprocating engine cylinder.....79

2.13 P–v (a) and T–s (b) diagrams for the ideal Diesel cycle.....82

3.1 Flowchart of rubber seed powder preparation……..102

3.2 Schematic of 3-3-1 developed ANN topology.....111

3.3 Levenberg-Marquardt training flowchart for ANN model.....113

3.4 Experimental setup for biodiesel-diesel blending analysis.....123

3.5 Experimental TD202 test engine for performance and combustion analyses located at Petroleum Training Institute, Effurun, Nigeria.....124

3.6 A schematic layout of TD202 diesel test engine.....128

4.1 Effects of kernel particle size on the rubber seed oil yield.....130

4.2 Gas chromatogram of the rubber seed oil with identified peaks.....141

4.3 FT-IR spectrum of the rubber seed oil.....143

4.4 ^{1}H NMR spectrum of the rubber seed oil.....147

4.5 ^{13}C NMR spectrum of the rubber seed oil.....148

4.6 Overall process of oil degradation.....150

4.7 Acyclic polymer formations from oleic acid during thermal oxidation of oils.....151

4.8 ln (C_t/C_o) vs. time (min) for iodine values at 100, 150, 200 and 250 ^{o}C.....152

4.9 Arrhenius plot for kinetics of thermo-oxidative degradation of rubber seed oil.....153

4.10 Correlation of predicted and experimental oil yields of rubber seed oil extraction.....155

4.11 (a) Interactive effects between solvent volume and rubber seed powder weight on oil yield for RSM response surface (3D) plot.....162
4.11 (b) Interactive effects between extraction time and rubber seed powder weight on oil yield for RSM response surface (3D) plot.....163
4.11 (c) Interactive effects between extraction time and solvent volume on oil yield for RSM response surface (3D) plot.....164
4.12 Correlation of predicted yield and experimental yield of RSO by ANN model.....165
4.13 (a) Interactive effects of rubber seed powder weight and solvent volume on oil yield for ANN response surface (3D) and contour (2D) plots.....166
4.13 (b) Interactive effects of rubber seed powder weight and extraction time on oil yield for ANN response surface (3D) and contour (2D) plots.....167
4.13 (c) Interactive effects of extraction time and solvent volume on oil yield for ANN response surface (3D) and contour (2D) plots.....168
4.14 Percentage contribution of process variables to seed oil extraction via ANN model...169
4.15 TGA profile of the rubber seed shell (RSS) catalyst.....170
4.16 XRF analysis of the RSS: (a) raw and (b) calcined at 800 ^{o}C.....172
4.17 XRD diffractograms of the RSS: (a) raw, and (b) calcined at 800 ^{o}C.....174
4.18 SEM images for (a) raw, and (b) calcined RSS catalyst at magnification 2450x.....175
4.19 Nitrogen adsorption/desorption isotherms for the raw and calcined RSS.....176
4.20 Effects of reuse of different catalyst loadings (2, 2.2, 2.5, 3, and 3.5 g) on biodiesel yield (%) at optimum conditions.....182
4.21 Effects of Ca^{2+} ion leaching from reused catalyst on biodiesel yield (%) at optimum conditions.....183
4.22 Correlation of predicted vs. actual biodiesel yields (%) for the RSM model.....186

4.23 (a) RSM 3D plot for the interactive effect between reaction time and methanol/oil ratio on biodiesel (RSOME) yield.....191
4.23 (b) RSM 3D plot for the interactive effect between reaction time and catalyst amount on biodiesel (RSOME) yield.....192
4.23 (c) RSM 3D plot for the interactive effect between methanol/oil ratio and catalyst amount on biodiesel (RSOME) yield.....193
4.24 Correlation of predicted vs. actual biodiesel yields for ANN model.....194
4.25 ANN Surface plot for the interactive effect of methanol/oil ratio with reaction time on biodiesel (RSOME) yield.....195
4.26 ANN Surface plot for the interactive effect of catalyst amount with reaction time on biodiesel (RSOME) yield.....196
4.27 ANN Surface plot for the interactive effect of methanol/oil ratio with catalyst amount on biodiesel (RSOME) yield.....196
4.28 Percentage contribution of process variables to biodiesel production via ANN model.....197
4.29 Variation of air/fuel ratio with speed for diesel-biodiesel blends.....199
4.30 Variation of brake thermal efficiency with speed for diesel-biodiesel blends.....200
4.31 Variation of brake specific fuel consumption with speed for diesel-biodiesel blends.....201
4.32 Variation of engine power with speed for diesel-biodiesel blends.....203
4.33 Variation of engine torque with speed for diesel-biodiesel blends.....204
4.34 Variation of exhaust gas temperature with speed for diesel-biodiesel blends.....205
4.35 Variation of carbon monoxide emissions with speed for diesel-biodiesel blends.....206
4.36 Variation of carbon dioxide emissions with speed for diesel-biodiesel blends.....207
4.37 Variation of nitrogen oxides emissions with speed for diesel-biodiesel blends.....208

4.38 Variation of total hydrocarbons emissions with speed for diesel-biodiesel blends.....209

4.39 Variation of smoke opacity with speed for diesel-biodiesel blends.....210

C.1 Preparation of milled kernel for oil extraction 246

C.2 Oil soxhlet extractor used for the study.....246

C.3 Rotary evaporator used in the study.....247

C.4 Extracted rubber seed oil: (a) filtered, (b) crude.....247

E.1 Calcination of rubber seed shell (RSS) catalyst for biodiesel production.....259

F.1 Esterified oil separation into two layers.....260

F.2 Gravity settling of biodiesel, catalyst and glycerol phases….....260

F.3 Processed rubber seed oil methyl ester (biodiesel) for analysis.....261

F.4 Regression line (−), upper (−), and lower (−) prediction intervals and experimental data (■) of oxidation stability determination for biodiesel without additive.....261

G.1 ^{13}C NMR spectra of rubber seed oil (12–28 ppm) 265

G.2 ^{13}C NMR spectra of rubber seed oil (28.4–34.8 ppm) 266

G.3 ^{13}C NMR spectra of rubber seed oil (40–84 ppm) 266

G.4 ^{13}C NMR spectra of rubber seed oil (126.4–132.0 ppm) 267

G.5 ^{13}C NMR spectra of rubber seed oil (165–184 ppm) 267

G.6 Double bond peaks in the ^{13}C NMR spectrum for pure oleic acid, linoleic acid, and linolenic acid.....268

H.1 Nitrogen adsorption/desorption log plot for calcined RSS.....270

H.2 Nitrogen adsorption/desorption log plot for raw RSS.....270

H.3 BJH adsorption pore-size distribution log plot for calcined RSS.....271

LIST OF TABLES

Table Page

2.1 Estimated annual rubber seed oil and biodiesel production capacity for sub-Saharan Africa (SSA) countries in 2013.....14

2.2 Typical levels of cellulose, hemicellulose, and lignin in biomass.....17

2.3 Proximate analysis of rubber seed.....27

2.4 Amino acid profile of rubber seed.....28

2.5 Proximate analysis of RSS and RSK.....28

2.6 Ultimate analysis of RSS and RSK.....28

2.7 Extractives, holocellulose, hemicelluloses and cellulose contents of RSS and RSK.....29

2.8 Calorific value and oil yield of RSS and RSK.....29

2.9 Physico-chemical properties of rubber seed oil.....35

2.10 Fatty acids profile of rubber seed oil.....36

2.11 Fatty acid compositions of selected non-edible oils (%).....37

2.12 Africa countries which import and export energy.....42

2.13 SSA countries and their bioenergy policies.....43

2.14: Comparison between physisorption and chemisorption processes.....49

2.15 Methods of viscosity reduction in vegetable oils for biodiesel production.....62

3.1 Experimental range and levels of independent process variables for seed oil extraction via Box-Behnken design.....108

3.2 Experimental range and levels of independent process variables for biodiesel production via central composite design.....117

3.3 Technical specifications for TD 202 test diesel engine.....124

4.1 Physical characterization of rubber seed and the seed oil.....131

4.2 Physico-chemical properties and other characteristics of rubber seed oil.....139

4.3 Fatty acids profile of rubber seed oil.....140

4.4 Wavenumbers and their functional groups for FT-IR analysis of rubber seed oil.....144

4.5 ^{1}H NMR spectrum analysis of rubber seed oil.....146

4.6 ^{13}C NMR analysis of carbon type present in the rubber seed oil.....148

4.7 Effect of heating on peroxide, iodine, and refractive index values of rubber seed oil.....149

4.8 Kinetic parameters for degradation of rubber seed oil.....153

4.9 Box–Behnken design for the rubber seed oil extraction process optimization by RSM and ANN.....156

4.10 Analysis of variance (ANOVA) for response surface quadratic model.....159

4.11 RSM regression analysis for rubber seed oil extraction.....161

4.12 Summary report of N_2 adsorption/desorption analysis for raw RSS.....178

4.13 Summary report of N_2 adsorption/desorption analysis for calcined RSS (800 ^{o}C) ...179

4.14 Fuel properties of biodiesel from rubber seed oil.....181

4.15 Central composite design for optimization of biodiesel production process by RSM and ANN.....185

4.16 RSM regression coefficients analysis for the oil biodiesel production.....187

4.17 Analysis of variance (ANOVA) results for the fitted second-order polynomial model.....190

4.18 Properties of the test fuels.....198

D.1 Variation of oil yield with seed kernel particle size.....249

E.1 Variation of peroxide, iodine, and refractive index values of rubber seed oil with temperature and time.....258

F.1 Esterification parameters of rubber seed oil.....259

G.1 Infrared group absorption frequencies.....262

G.2 Assignment of signals of ^{1}H NMR spectra for vegetable oils (hazel nut and walnut)....265

H.1 XRF spectroscopic elemental analysis of rubber seed shells catalyst.....269

H.2 Biodiesel yields for fresh and reused catalyst loadings at optimum conditions.....271

I.1 Variation of engine speed with fuel and air parameters for B00 (diesel).....273

I.2 Variation of engine speed with fuel and air parameters for B10.....273

I.3 Variation of engine speed with fuel and air parameters for B20.....274

I.4 Variation of engine speed with fuel and air parameters for B30.....274

I.5 Variation of engine speed with fuel and air parameters for B50.....275

I.6 Variation of engine speed with fuel and air parameters for B100 (biodiesel).....275

I.7 Variation of brake thermal efficiency with engine speed.....276

I.8 Variation of brake specific fuel consumption with engine speed.....276

I.9 Variation of engine brake power with engine speed.....276

I.10 Variation of engine torque with engine speed.....276

I.11 Variation of exhaust gas temperature with engine speed.....277

I.12 Variation of carbon monoxide emissions with engine speed.....277

I.13 Variation of carbon dioxide emissions with engine speed.....277

I.14 Variation of oxides of nitrogen emissions with engine speed.....277

I.15 Variation of total hydrocarbons emissions with engine speed.....278

I.16 Variation of smoke opacity emissions with engine speed.....278

NOMENCLATURE

Description	Symbol
Adsorbate molecular area	A_m
Adsorbed volume	V_a
Adsorptive energy	E_n
Adsorption enthalpy change	ΔH_{ads}

Adsorption entropy change	ΔS_{ads}
Air-box differential pressure	ΔP
Avogadro's number	N
Brake thermal efficiency	η_{th}
Brunauer-Emmett-Teller constant	C
Carbon dioxide, Carbon monoxide	CO_2, CO
Clearance volume	V_c
Coefficient of discharge	C_d
Compression ratio	r
Concentration	C_t, C_o
Conference of the Parties	COP
Connecting rod	l
Crank angle	θ
Crank radius	α
Critical pressure, Critical temperature	P_c, T_c
Cutoff ratio	r_c
Engine speed	N
Exergy	a_i
Fuel	f
Hectares, Hour	ha, h
Internal energy, Velocity	U
Irreversibility	I
Langmuir constant	b
Langmuir specific surface area	S_L
Mass	m

Mass flowrate of air	$\dot{m}_a$
Minutes	min
Molecular mass	M
Monolayer volume	V_m
Number of moles, variables, and order of reaction	n
Orifice diameter	d
Oxides of nitrogen	NOx
Pressure	P
Process actual variable	*X*
Process coded variable	*x*
Quantity of heat	Q
Rate constant	k
Saturation pressure	P_o
Specific heat at constant pressure	C_p
Specific heat at constant volume	C_v
Specific heat ratio (C_p/C_v)	γ
Specific *volume*	*v*
Standard deviation of data	σ
Statistical thickness	*t*
Temperature, Torque	T
Time	t
Universal gas constant	R
Volume of biodiesel blends (%)	Bxx
Work	W

CHAPTER 1: INTRODUCTION

1.1 Research background and motivation

Industrial advancement in recent times has accelerated the need for sustained energy requirement across the globe. The depletion of non-renewable fossil materials (oil, gas, and coal) that arises from their continued usage, their price instability, energy insecurity, and the concern for the degraded environment stimulated global research for alternative sources of energy (Aldhaidhawi et al., 2017; Onoji et al., 2016a). Renewable energies from biomass, hydropower, solar, tidal waves, wind and geothermal have been proposed and considered as cheap sources of sustainable energies (Dwivedi et al., 2013; Thanh et al., 2012). The biomass source option, which appeared the cheapest or easiest to acquire will most certainly result to fast economic and sustainable growth of most developing countries in Africa (Onoji et al., 2016a; Thanh et al., 2012). Vegetable oils from biomass are seen as source materials for renewable energy production. The suitability of vegetable oils as source of biodiesel production has been reported in the literature by several researchers in recent times. Biodiesel is a mono-alkyl fatty acid methyl ester (FAME) produced by the transesterification of vegetable oils, animal fats and other sources of oils/fats with primary alcohols (methanol, in this study) in the presence of suitable catalysts (homogeneous, heterogeneous, and enzymes, etc) (Roschat et al., 2012; Guo et al., 2010).

The choice of biodiesel is based on its biodegradability, non-toxic, lower emissions, sulphur-free, low levels of polycyclic aromatic hydrocarbons (PAHs) and n-PAHs (Mofijur et al., 2014; Portet-Koltalo & Machour, 2013; Jaya & Ethirajulu, 2011; Kumar & Purushothaman, 2010).

In recent times, most of the biodiesel production routes are from edible oil plants such as palm oil, soybean, rapeseed, sunflower, and these compete with food/pharmaceutical and cosmetic uses, resulting to food-fuel crisis and high price of biodiesel generated thereof (Onoji et al.,

2016a; Ahmad et al., 2013; Asuquo et al., 2012; Ma & Hanna, 2012). To avert a food-fuel crisis, non-edible vegetable oils considered as low-grade oils that are not suitable for food uses, could be an attractive preference to edible oils for industrial applications (Dharma et al., 2016). One of the few versatile bioenergy crops with non-edible oil that has attracted the attention of researchers in recent times is the rubber tree (*Hevea brasiliensis*) (Ng et al., 2013).

Hevea brasiliensis is economically cultivated for the production of latex as a source of natural rubber for the production of various rubber products in use globally, while the seeds are underutilized (Takase et al., 2015; Atabani et al., 2013; Ng et al., 2013). However, the oil from the seed is the second most valuable product after the latex (Banković-Ilić et al., 2012). With the concept of sustainable development and the *Paris Agreement* on climate change (UNFCCC, 2015), the production of synthetic rubber would be reduced when the use of fossil materials is phased out in the dawn of next century. The cultivation of rubber tree to generate latex for natural rubber production, and the utilization of its seeds to produce non-edible oil for biodiesel production will boost the economy of most Africa countries that are poverty-ridden.

Homogeneous base catalysts such as NaOH, KOH and methoxides of sodium and potassium are most suitable for industrial transesterification of edible vegetable oils that are generally low in free fatty acids (FFAs). However, associated problems such as difficulty in catalyst-products separation, initial catalyst cost, soap formation, low-grade by-product glycerol, reactor corrosion and large volume of washing water requirements induced further research for environmental benign heterogeneous catalyst for biodiesel synthesis from non-edible oils though high in FFAs (Roschat et al., 2012; Zabeti et al., 2009). In addition, the use of homogeneous catalysts in transesterification of non-edible oils to biodiesel is hampered by the high FFAs of the oils that react with the catalyst resulting to low biodiesel yield. Uprety et al.

(2016) reported that heterogeneous catalysts are easily separated from reaction mixtures through simple filtration, and reused severally producing high-grade glycerol. Against this background, this study investigated the conversion of non-edible rubber seed oil to biodiesel over a catalyst derived from waste rubber seed shells (RSS). The results obtained from the study are promising and it is expected that this will further reduce the cost of biodiesel produced from rubber seed oil and make it more competitive to petro-diesel.

1.2 Hypothesis

- Industrial processes go faster to completion when homogeneous, heterogeneous, or enzymes catalysts are employed;
- Homogeneous catalysts are not suitable for the transesterification of non-edible rubber seed oil with high FFAs;
- Heterogeneous catalyst proposed in this research will attempt to solve the problems and will provide a better product output when employed for the transesterification reaction.
- When reactions take place in solid-liquid-vapour phase, mass transfer limitations are avoided, and the reaction may be enhanced if solid surface area becomes large;
- The structural and textural properties of the catalyst may offer insight to anticipated behaviour.

1.3 Justification of the study

During the Climate Change Summit (COP 21) held in Paris, from November 30 to December 12, 2015 to address the threat posed to humanity from climate change, world leaders, Policy makers, and scientists agreed that man is the major cause of climate change that results to increased global warming. A universal climate change agreement termed 'Paris Agreement' was reached and agreed that clean renewable energy sources would replace fossil materials for

energy generation in the dawn of next century (UNFCCC, 2015). The agreement will cause a reduction in the production of synthetic rubber from petrochemicals derived from fossil materials. The rubber tree (*Hevea brasiliensis*) from which natural rubber is sourced will play a significant role in the future energy mix. The underutilized rubber seeds will provide non-edible oil for biodiesel production to avert food-fuel crisis and enhance poverty-alleviation programme especially in the third world countries. The rubber seed shells (RSS) generated during oil extraction posed waste disposal problems to rubber seed oil millers. Synthesis of solid catalyst from waste RSS for use in biodiesel production in this study will further reduce the cost of biodiesel and make it more affordable.

Pursuant to government directives in 2005 for the diversification of Nigeria's economy through the mainstreaming of an Automotive Biomass Programme, the Nigerian National Petroleum Corporation (NNPC) was mandated to create a conducive environment for the take-off of a domestic bioenergy industry. The underlying objectives for government interest in a national biofuel programme are revenue diversification, reduced dependence on imported refined petroleum-derived products, improved agricultural productivity, job creation, meeting energy needs, and environmental benefits (Ishola et al., 2013; Abila, 2012). The Nigeria biofuel policy did not address the potential food-fuel conflicts that could arise from the use of food crops as biofuel feedstock (Ohimain, 2013). In Nigeria, about 18 million hectares (ha) of land are suitable for industrial cultivation of rubber trees in the southern region (Onoji et al., 2016a). The complete life cycle and environmental benefits of rubber trees in Nigeria is well investigated and defined compared to *Jatropha curca*s, a similar non-edible plant (Ishola et al., 2013), but detailed study on the benefits of rubber tree as a versatile bioenergy crop is limited as it was not mentioned as a plausible feedstock in the Nigeria's biofuels policy.

The outcomes of this research, as documented in this thesis, will encourage the continued cultivation of rubber trees for latex production, and harvesting the seed to produce oil for

biodiesel synthesis. It will also serve as a pool of information for the relevant Government Ministries, Departments, and Agencies that will serve as advocates for the implementation of the National Biofuels Policy across Nigeria's business strata with respect to biodiesel production from rubber seed oil and other African nations where rubber trees are cultivated.

1.4 Research aims and objectives

The main objectives of this research study were as follows:

- ✓ Extract, characterize, and determine the kinetics of thermo-oxidative degradation of rubber seed oil;
- ✓ Develop a mathematical model, and optimize the extraction of rubber seed oil using the developed model;
- ✓ Synthesize and characterize a solid catalyst from waste rubber seed shells for transesterification of rubber seed oil to biodiesel;
- ✓ Develop a mathematical model, and optimize the biodiesel production from rubber seed Oil using the developed model;
- ✓ Characterize the produced biodiesel and compare the properties with biodiesel Standards (ASTM D 6751 and EN 14214);
- ✓ Study the internal combustion of diesel-biodiesel blends using a test engine;
- ✓ Analyse the level of pollutants and emissions arising from the use of diesel, biodiesel, and diesel-biodiesel blends to ascertain their levels of environmental friendliness.

Figure 1.1 depicts the systematic approach employed in this research. The approach involves catalyst synthesis from waste rubber seed shells (RSS) calcined at 800 ^{o}C based on thermo-gravimetric analysis. The catalyst was characterized for structural and textural properties. Rubber seed oil (RSO) extracted from rubber seeds was esterified with methanol using 6% v/v sulphuric acid as catalyst. The esterified oil was then transesterified to biodiesel over a calcined

RSS as base catalyst. The biodiesel produced was blended with petro-diesel, and the blends were analysed in TD202 internal combustion diesel test engine for performance and emissions evaluation.

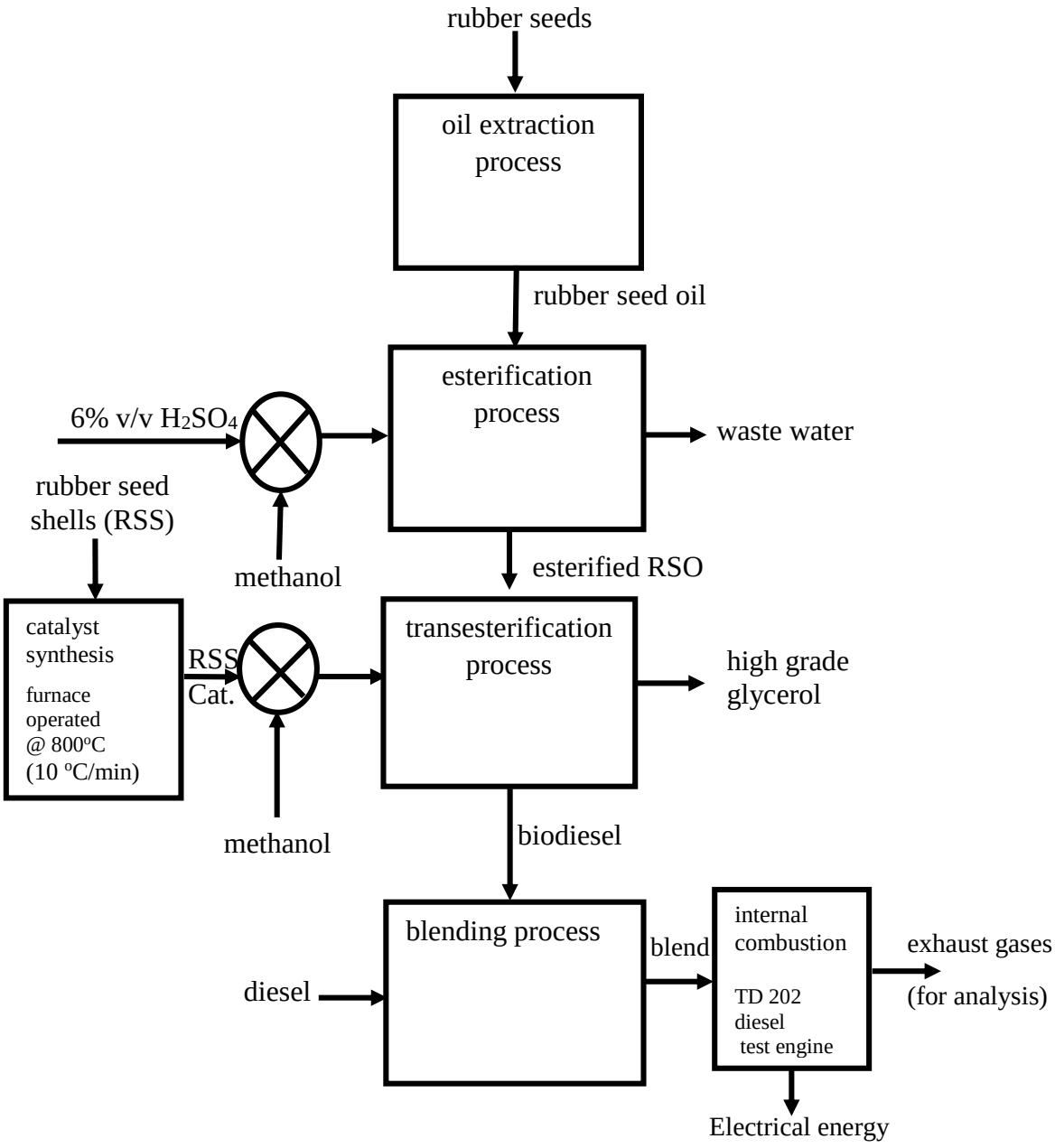


Figure 1.1: Systematic approach employed in this study

1.5 Thesis outline

The layout of the thesis is as follows:

This thesis investigated the conversion of non-edible and high free fatty acids rubber seed oil to biodiesel over a catalyst synthesized from waste rubber seed shells. The following chapters discuss the issues related to the synthesis and characterization of the catalyst, biodiesel production and evaluation of the performance and emission profiles of diesel-biodiesel blends using a diesel test engine.

Chapter 1 is the introductory chapter of the thesis and it provides information on the research background and motivation, hypothesis, and justification of the study. The chapter further discusses the aims and objectives, conceptual approach used to achieve the main goal of the research, and finally the thesis outline.

Chapter 2 presents the literature review and background information on rubber tree (*Hevea brasiliensis*). The chapter further highlights the benefits of biodiesel policies in sub-Saharan Africa (SSA); rubber seed capacity in SSA; industrial applications of rubber seeds; modeling and optimization in research. Others include oil extraction methods; kinetics of oil degradation; transesterification methods; catalysis; optimization of oil extraction and biodiesel production; and finally, the thermodynamics of the internal combustion of diesel-biodiesel blends for the evaluation of engine performance and emission analysis.

Chapter 3 contains details of the research methodology, experimental methods, and analytical procedures used in this research. The chapter presents materials and seed preparation; seed oil extraction; characterization of seed oil; oil degradation kinetics and optimization of oil extraction process. It also includes catalyst synthesis and characterization; biodiesel production and characterization; modeling and optimization of biodiesel production process; and engine performance and emission analysis of biodiesel-diesel blends.

Chapter 4 presents the experimental results and discussion on oil extraction, catalyst synthesis, biodiesel production, and their analyses. The chapter also discusses the performance of the blends in the internal compression ignition engine, and emission analysis. Results of previous researchers were compared with the findings of this research.

Chapter 5 concludes this research by providing a summary of the main findings, recommendations for future work, and contributions to knowledge.

CHAPTER 2: LITERATURE REVIEW

2.0 Introduction

The literature review presented in this chapter is a part of a review article, and experimental work on this research published in *Energy Conversion and Management, 2016 (issue 110*, pp. 125-134), and *Energy & Fuels, 2016 (issue 30*, number 12, pp. 10555-10567). The cover and abstract pages of the published papers are provided in Appendix A.

2.1 The rubber tree

The rubber tree (*Hevea brasiliensis*) shown in Figure 2.1, also known as the Para rubber belongs to the plant family *Euphorbiaceae* and it is the most economically important member of the genus *Hevea* that originated from Amazon region of Brazil in South America (Onoji et al., 2016a; Reshad et al., 2015; Kittigowittana et al., 2013**)**. *Hevea* exhibits morphological variability, with ten species (*H. brasiliensis, H. benthamiana, H. camorun, H. guianensis, H. microphylla, H. nitida, H. pauciflora, H. rigidifolia, H. camargoana,* and *H. spruceana)* identified that range from large forest trees to shrubs with latex in their parts (Venkatachalam et al., 2013). *Hevea brasiliensis* produces about 99% of the world's natural rubber (Aravind et al., 2015; Atabani et al., 2013). It was commercialized for latex production to boost the economy of Brazil in the 1800s. Several researchers investigated the properties of rubber latex (natural rubber) as it was an important product during the industrial revolution era. Notable among them was Charles Mariè de La Condamine who brought rubber seeds to Acadèmic Royale des Sciences of France in 1736 and published the first scientific properties of rubber (Charles, 2002).

Joseph Priestley, an English scientist discovered in 1770 the erasing nature of rubber on pencil mark on papers, earning it the name ‘rubber’. Vulcanization of rubber with sulphur to improve

its elastic and resistance properties was discovered by Charles Goodyear and Hancock in 1839 (Charles, 2002).

In 1876, Sir Henry Wickham, a British explorer took 70,000-Para rubber tree seeds out of Brazil to the Kew botanical gardens in London, England for research where different resistant varieties of the seeds were developed. The developed species were sent to the British colonies of Southeast Asia countries of Malaysia, Sri Lanka, and Singapore in 1876 for planting (Reshad et al., 2015). The most successful application of latex rubber was achieved in the 1880s when rubber was found to be the basic material for pneumatic tyres for automotive industry. Obviously, the well-organized plantations in the Southeast Asia countries resulted in a significant increase in productivity. The competition from Southeast Asia brought down the decades of rubber latex boom to an end for much of northern Brazil in the early 1900s. In the later part of the 19th century, Indonesia, Thailand, Malaysia, China, India, and Vietnam joined the league of natural rubber producers. Rubber seed (Figure 2.2) was introduced into Nigeria in 1895 from the Kews botanical gardens in London, and the first rubber plantation established at Sapele, Delta State in 1903 (Omo-Ikerodah et al., 2009). Rubber tree has 6-9 years of gestation period before tapping for latex, though the seeds are available between 4-6 years (Onoji et al., 2016a; Eka et al., 2010). A recent statistical analysis put the global harvested areas of rubber trees plantations at 11,096,400 ha (FAOSTAT, 2014), thus eliminating competition for land space with vegetable crops (Zhu et al., 2014). Rubber trees have been reported to grow to a height of 34 to 40 m in the wild (Takase et al., 2015; Ashraful et al., 2014; Kumar & Sharma, 2011). It requires warm humid climate with temperatures ranging from 20 to 35 ^{o}C, a fairly-distributed rainfall of about 1800 to 2000 mm throughout the year (Ashraful et al., 2014; Omo-Ikerodah et al., 2009) and growth is most rapid at altitudes below 200 m (Reshad et al., 2015). The analysis depicted in Figure 2.3 identified Southeast Asia countries of Indonesia, Thailand and Malaysia as major areas where rubber trees are cultivated; Nigeria and Côte

d'Ivoire are Africa dominant. Other Africa countries where rubber trees are cultivated include Democratic Republic of Congo, Cameroon, Republic of Congo, Central African Republic, Ghana, Liberia, Gabon and Guinea (Onoji et al., 2016a). Seeds from rubber tree considered as wastes over the years except for seed propagations (Kittigowittana et al., 2013), is the second most valuable product after the latex as source of non-edible oil (Banković-Ilić et al., 2012). Researchers in Asia (Zhu et al., 2014) investigated the factors influencing rubber seed yield through in-situ counting of rubber seeds in Xishuangbanna, China, and reported age, size and clonal types as dominant. Other factors include powdering mildew disease, abnormal leaf disease, phytophora disease, and weather (Iyayi et al., 2008). A typical rubber plantation has about 350-500 trees/ha with each tree yielding about 800 seeds and an average of 70 to 500 kg seed/ha on annual basis (Abdulkadir et al., 2014; Ebewele et al., 2010a; Eka et al., 2010).



Figure 2.1: Rubber trees plantation (Adapted from Onoji et al., 2016a)



Figure 2.2: Rubber seed (Adapted from Onoji et al., 2016a)

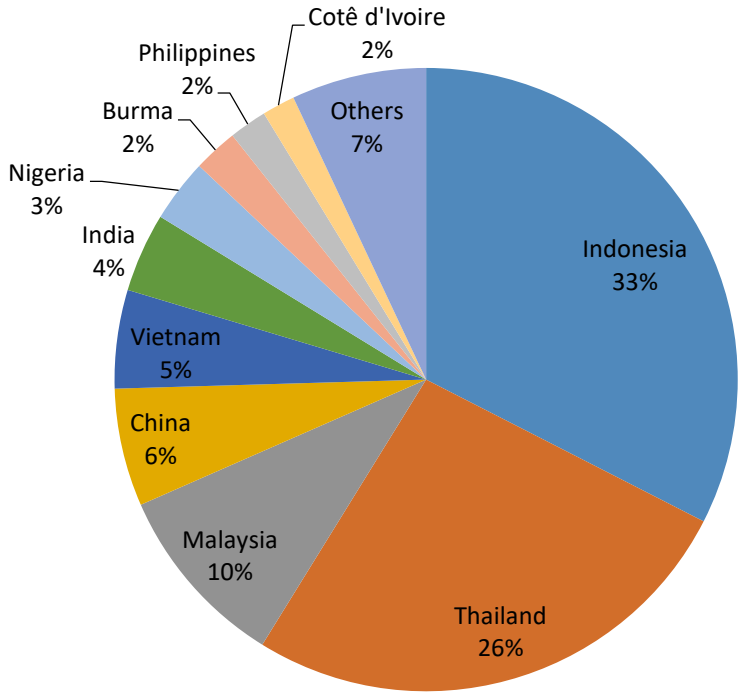


Figure 2.3: Top ten leading producers of rubber seeds in 2014 (Adapted from FAOSTAT, 2014)

2.2 Rubber seed capacity in sub-Saharan Africa

In consideration of the nature of non-edible oil plants such as rubber, jatropha, castor, linseed, moringa oleifera, cotton, neem, and tobacco for energy production to avert food-fuel crisis, rubber tree has fewer investigation on its potential in many sub-Saharan Africa (SSA) countries where it is cultivated for latex production. Onoji et al. (2016a) provided a holistic comparative data relevant to rubber seed as a significant source route of biodiesel production for the sustainable development of SSA countries. Using statistical data from Food and Agriculture Organization (FAO) of the United Nations for 2013, Onoji et al. (2016a) reported the hectares (ha) of rubber plantations cultivated in SSA as follows: Nigeria (345,000 ha), Côte d'Voire (135,000 ha), Liberia (76,000 ha), and Cameroon (55,000 ha). Others are Ghana (26,800 ha), Gabon (15,000 ha), Guinea (10,800 ha), Democratic Republic of Congo (50,500 ha), Republic of Congo (2,400 ha) and Central African Republic (CAR) (1,250 ha). With a plantation density of 350 trees/ha, 150 kg/ha and a projected 717,750 ha, the researchers reported that SSA could produce 17,947 ton (RSO) and 16,691 ton (biodiesel). Table 2.1 presents the details of their findings. The cultivation of rubber trees will sustain the production of rubber products from latex. It will also provide seed oils for biodiesel that will create additional financial benefits to the plantation farmers and reinvigorates the economies of the local communities in sub-Saharan Africa.

Table 2.1: Estimated annual rubber seed oil and biodiesel production capacity for SSA countries in 2013 (Onoji et al., 2016a)

Country	Harvested area (ha), A	Trees/ha	Trees (million)	Seed (ton/ha), B	Seed (ton) $A \times B = RS_{total}$	RSO (ton) $= RS_{total} \times 0.1667$	Biodiesel (ton) $= RSO \times 0.93$
Nigeria	345,000	350	120.75	0.15	51,750	8,626.725	8,022.854
Côte d'Voire	135,000	350	47.25	0.15	20,250	3,375.675	3,139.378
Liberia	76,000	350	26.6	0.15	11,400	1,900.380	1,767.353
Cameroon	55,000	350	19.25	0.15	8,250	1,375.275	1,279.006
D.R. Congo	50,500	350	17.675	0.15	7,575	1,262.753	1,174.360
Ghana	26,800	350	9.38	0.15	4,020	670.134	623.225
Gabon	15,000	350	5.25	0.15	2,250	375.075	348.820
Guinea	10,800	350	3.78	0.15	1,620	270.054	251.150
Rep. Congo	2,400	350	0.84	0.15	360	60.012	55.811
CAR	1,250	350	0.4375	0.15	187.5	31.256	29.068
Total	717,750		251.2125		107,662.5	17,947.339	16,691.025

2.3 Rubber seed collection and processing

The matured rubber seeds dehisce from the trees with a loud sound similar to that of a military rifle during the short period of dry season between the months of July and October in Nigeria (Onoji et al., 2016a), although it varies from one geographical region to another (Iyayi et al., 2008; Igeleke & Omorusi, 2007). Overgrown weeds make seed collection a difficult task as most seeds hide under the cover of weeds. During the period of rainfall, the seed pods will not dehisce to release the seeds as they pick up moisture that facilitates its deterioration (Iyayi et al., 2008). Sunshine is therefore a critical factor required to dehisce the seeds for a good yield. Igeleke & Omorusi (2007) listed excessive moisture, fungi, and pests such as insects and rodents as major causes of post-harvest deterioration of rubber seeds, and suggested that the seeds be dried to a moisture level of 7% or less, before storage. Aniamaka & Uriah (1990) suggested that the seeds should be collected as soon as they dehisce from the trees, and collection period repeated at least every fourth day to avoid deterioration. Seed that is not properly stored after harvesting could be affected by chemical reactions that may increase the free fatty acids content of the seed and reduce its potency for biofuels production. Drying of seeds at 70 ^{o}C or less will halt biochemical processes and reduce cyanide content; chemical treatment with 2% primiphos methyl and aluminum phosphide, and storage in polypropylene bags were suggested methods to extend the shelf life of post-harvested seeds in bulk storage (Igeleke & Omorusi, 2007). The seeds enclosed in a pod of 3-ellipsoidal capsules are mottled brown with glossy surfaces. They are oval-shaped, 2–5 cm long and average weight of 2–6 g (Onoji et al., 2016a).

2.4 Biomass valorization processes

Biomass covers organic matter that are traceable to plant or animal origin, either as raw (wood, energy crops, and agricultural residues, etc.) or processed (effluents, food processing residues,

and green wastes, etc.). Biomass materials are generally composed of cellulose, hemicellulose, lignin, lipids, proteins, simple sugars, and starches, depending on its origins (Claude et al., 2016). Among these compounds, cellulose, hemicellulose, and lignin are the three main constituents as shown in Table 2.2 (Zhang et al., 2010). The renewable aspect that is attributed to biomass can be explained by the carbon cycle: the carbon dioxide emitted during its use is compensated for by the carbon stock accumulated during its growing stage. Therefore, the biomass can only be considered as a clean and renewable energy source if obtained in a sustainable manner (Kumar et al., 2009). Bioenergy is a term that refers to all the processes whether industrial or not, that can produce energy from biomass. A general view of the worldwide energy consumption in 2013 depicts renewable energy accounting for about 19% (Claude et al., 2016). Biomass can be converted into energy or byproducts via versatile transformation technologies such as physico-chemical or thermo-chemical as shown in Figure 2.4. It is expected that at the dawn of the 22nd century when the use of fossil fuels would be limited, biodiesel that currently accounts for 0.15% of the share of renewable energy will become a major source of energy from biomass.

Table 2.2: Typical levels of cellulose, hemicellulose, and lignin in biomass (Zhang et al., 2010)

Component	Dry weight (%)	Description
Cellulose	40–60	A high-molecular weight (10^6 or more) linear chain of glucose linked by β-glycosidic linkage. This chain is stable and resistant to chemical attack.
Hemicellulose	20–40	Consists of short, highly branched chains of sugars (five-carbon sugars such as σ-xylose and ι-galactose, and six-carbon sugars such as σ-galactose, σ-glucose, and σ-mannose) and aromic acid. Lower molecular weight than cellulose. Relatively easy to be hydrolysed into basic sugars.
Lignin	10–25	A biopolymer rich in three-dimensional, highly branched polyphenolic constituents that provide structural integrity to plants. Amorphous with no exact structure. More difficult to be dehydrated than cellulose and hemicelluloses.

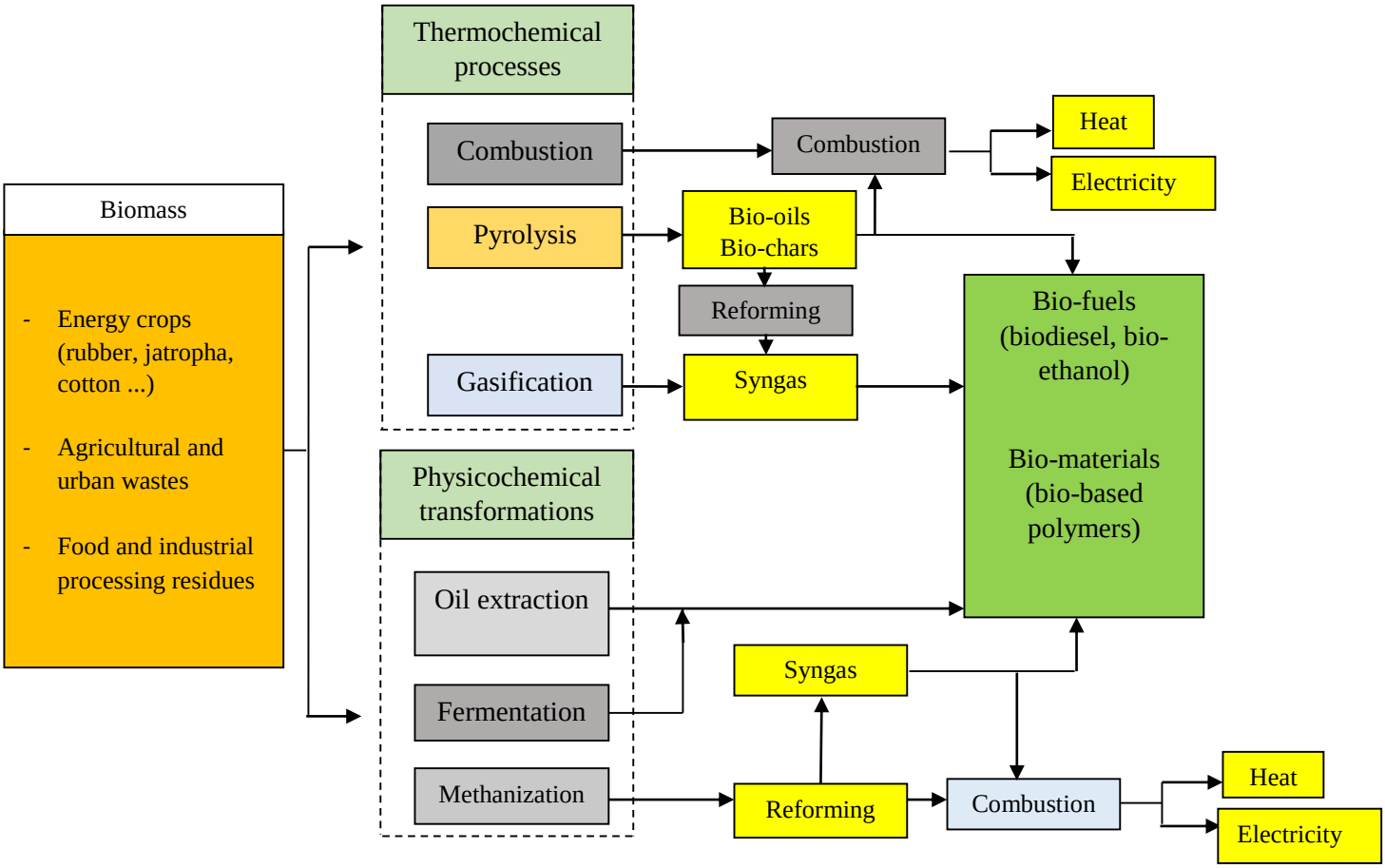


Figure 2.4: Overview of main biomass valorizations (Adapted and modified from Claude et al., 2016)

2.5 Modeling and optimization approach to industrial research

Modeling and optimization of process variables to increase the efficiency of a process is one of the most important stages in a biochemical process (Baş & Boyaci, 2007a). The traditional method of optimization is expensive, complex and time consuming due to large amount of experiments required. It considers one variable at a time, while other factors are kept constant and the interactive effects of the variables on the response of the system are neglected (Ma et al., 2016; Kostić et al., 2013; Baş & Boyaci, 2007a). The disadvantages of the traditional method prompted researchers to look for alternatives that will describe the entire system comprehensively. In the present day, industrial research uses response surface methodology

(RSM), and artificial intelligence tools such as artificial neural network (ANN) and genetic algorithm (GA), fuzzy logic (FL), ant algorithm (AA) and particle swarm optimization (PSO) to effectively optimize a process (Gueguim Kana et al., 2012).

Response surface methodology (RSM) is a collection of statistical and mathematical techniques useful for developing, improving, and optimizing processes in which responses of interest are influenced by several process variables and the objective is to optimize these responses (Kostić et al., 2013; Baş & Boyaci, 2007b). RSM defines the effect of these variables, alone and/or their interactive effects on the response of the process. RSM offers a large amount of information from a small number of experiments to explain the behavior of the system (Baş & Boyaci, 2007b). RSM generates a second-order polynomial predictive model that relates the response of a process to the independent variables considered. On the other hand, ANN is a modeling tool inspired by biological neural networks which consists of interconnected group of artificial neurons (input, hidden and output), and processes information using a connectionist approach to computation (Kostić et al., 2013). In an ANN, a neuron sums the weighted inputs from several connections and then applies a transfer function (e.g. sigmoid) to the sum. The resulting value is propagated through outgoing connections to other neurons. Figure 2.5 depicts a typical multilayer structure of an ANN model (Gueguim Kana et al., 2012). The ANN model describes processes that exhibit nonlinearities better than RSM, since it does not require theoretical knowledge or experience during the training process (Zahedi & Azarpour, 2011). It has the inherent ability to learn and generalize data by producing reasonable outputs, for inputs that were not encountered during the training process, and update easily when new set of data are submitted to it. The limitation in process optimization by ANN model is overcome by coupling a cost-effective and less time-consuming GA as described in Figure 2.6 (Chuahy & Kokjohn, 2017). Design of experiments (DOEs) such as central composite design (CCD), Box–

Behnken design (BBD), and Taguchi experimental design (TED) employing RSM and ANN–GA optimization techniques are commercially available for research. Dhawane et al. (2015) employed CCD approach using RSM to study the influence of process variables (methanol/oil ratio, catalyst loading, temperature) at a reaction time of 1 h on the yield of biodiesel produced from *Hevea brasiliensis* oil. They reported an optimal yield of 89.3% at the following conditions: methanol/oil ratio (15:1), catalyst loading (3.5 wt.%), and reaction temperature (60 ^{o}C). A BBD-RSM was used by Dwivedi & Sharma (2015) to study the optimization of biodiesel synthesized from pongamia oil and reported a yield of 98.4% at optimal process conditions of MeOH/oil ratio (11.06:1), KOH catalyst loading (1.43% w/w), reaction time (81.43 min), and reaction temperature (56.6 ^{o}C). Taguchi optimization method was used to investigate the influence of process variables (MeOH/oil ratio, reaction temperature, and catalyst amount) at constant reaction time (3 h) on biodiesel yield from Kapok (*Ceiba pentandra*) oil (Norazahar et al., 2012). They reported 98% maximum yield at conditions of 55 ^{o}C, 2 wt % KOH catalyst, and 8:1 methanol/oil ratio.

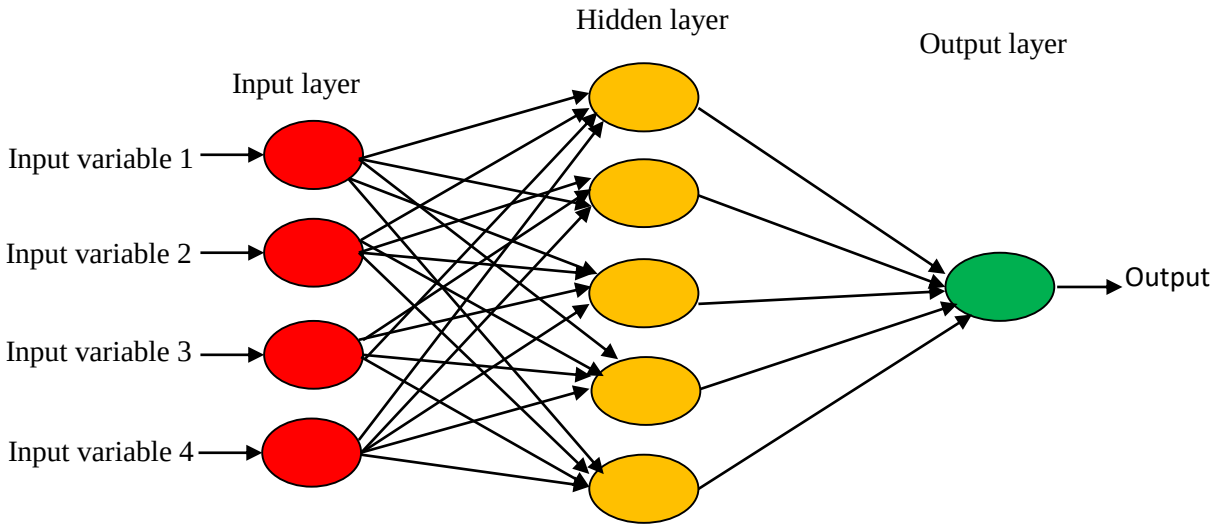


Figure 2.5: Multilayer structure of an ANN model (Adapted and modified from Gueguim Kana et al., 2012)

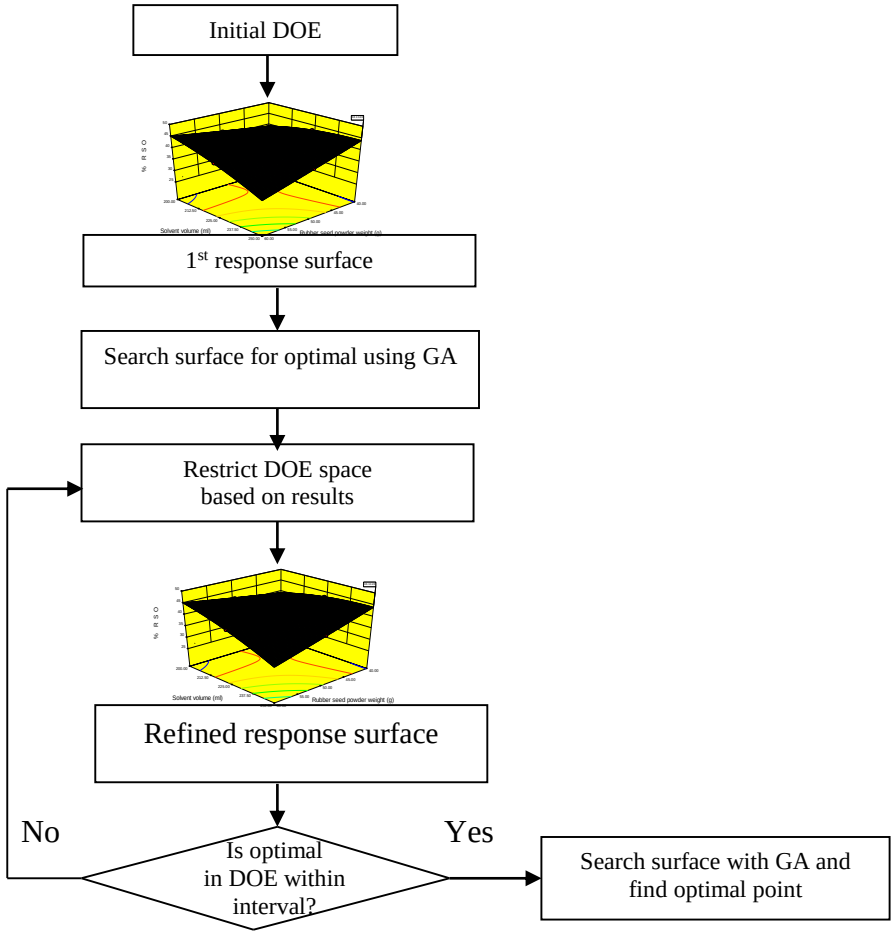


Figure 2.6: General flowchart of Genetic Algorithm (Adapted and modified from Chuahy & Kokjohn, 2017)

2.6 Qualitative and quantitative analytical procedures

Various spectroscopy methods of analysis have been developed to quantify and/ or quantify the relative proportions of different materials present in compounds such as lipids and solids (Guillèn & Ruiz, 2003). These methods are relatively fast, and provide great deal of information on the material under consideration. Some of the spectroscopy methods include Fourier transform infrared and scanning electron microscopy. Others include Brunauer-Emmett-Teller analysis, nuclear magnetic resonance, gas chromatography-mass spectroscopy,

x-ray diffraction, and x-ray fluorescence. These methods of analyses and information obtainable from them are discussed below.

2.6.1 Thermogravimetric analysis (TGA)

The application of thermal techniques of analysis has gained much attractiveness in recent years. Thermal techniques of investigation are methods used to characterize a system, an element of a compound (Coats & Redfern, 1963). Thermogravimetry analysis has received immense patronage in the understanding of solid fuel substrate degradation to release energy (Islam et al., 2016). The TGA traces the thermal degradation patterns of fresh biomass, char and hydro-char under air and inert environment for subsequent kinetic studies (Molintas & Gupta, 2011). The patterns revealed the response of heating rates, the inherent biomass properties and severity that define the char combustion profiles in the form of thermographs (Ceylan & Goldfarb, 2015). The degradation of biomass by pyrolysis occurs over wide temperature ranges. For instance, holocellulose was reported to decompose between 200 and 380 ^{o}C, and lignin component degrades over wide temperatures (180–600 ^{o}C) to char (Slopiecka et al., 2012). A typical TGA studies reveal three stages of differential weight loss of biomass combustion that include dehydration, devolatilization and char oxidation (Islam et al., 2016). The two leading methods include; differential thermal analysis and thermogravimetric analysis, where changes in the system weight are measured as a function of temperature (Coats & Redfern, 1963).

2.6.2 Fourier transform infrared spectroscopy (FT-IR)

One of the most common spectroscopic techniques applied by organic and inorganic chemists is the Fourier infrared spectroscopy. FT-IR is used to study surface chemistry of materials or substance and equipped with the ability of conveying information about the

molecules in a specimen with their respective concentrations (Smith, 2011), and where all infrared frequencies in a specimen are detected simultaneously (Bohre, 2013). FT-IR as an analytical technique has been widely used to monitor the quality of biodiesel/diesel blends, including checking for fuel adulteration (Valente et al., 2016). It has been reported for use in the analysis of free fatty acids (Ismail et al., 1993), anisidine determination (Man & Setiowaty, 1999), and monitoring of the transesterification of oils with methanol to biodiesel (Knothe, 1999). Infrared spectroscopic analysis is also used to identify the chemical functional groups present in a specimen undergoing analysis (Bohre, 2013).

2.6.3 Scanning electron microscopy (SEM)

Scanning electron microscopy is a technique used to investigate morphology of a designated sample by scanning with a beam of electron (Khan, 2014). Interactions between electrons and atoms in a sample creates signals that are detected, and convey information about the sample's composition, morphology and surface topology. The sample to be analysed should be conductive (Hosmani, 2014). A non-conductive material to be analysed is usually coated with a conductive material such as gold, gold/palladium alloy, or platinum prior to analysis.

2.6.4 *Brunauer- Emmett-Teller* (BET) Analysis

The *Brunauer-Emmett-Teller* explains the theory behind the physical adsorption of gas molecules on a solid surface. It serves as a basis for an analytical technique to measure the specific area of a solid and other textural properties such as pore size and pore volume that play important role in its catalytic behaviour (Lowell et al., 2004). Since the surface area of a solid cannot be calculated directly from particle size information,

a method to do this is to determine its surface area at an atomic level. The amount of gas adsorbed is a function of the total amount of exposed surface. It is also a function of temperature, gas pressure and the strength of interaction between gas and solid (Lowell et al., 2004). Nitrogen gas is commonly used for *BET* analysis because of high purity, availability, and relatively strong interaction with most solid surfaces.

2.6.5 Nuclear magnetic resonance (NMR)

Proton (^{1}H) and carbon-13 (^{13}C) NMR spectroscopy is a technique that is useful to determine the proportion of different acyl groups present in oils and fats, and other liquids in a very short time (Onoji et al., 2016b). The area of the signals of the ^{1}H NMR spectra is proportional to the number of hydrogen atoms that produce the signals. This method has many advantages in relation to the classical methods because it does not involve chemical modification of the sample.

2.6.6 Gas chromatography-mass spectroscopy (GC-MS)

Gas chromatography is a process of separating component (s) from the given sample by using a gaseous mobile phase. It involves a sample being vapourized and injected onto the head of the chromatographic column (Karger et al., 1973). The sample is transported through the column by the flow of inert gas (Helium or nitrogen) or hydrogen gas. The components are recorded as a sequence of peaks as they leave the column. The peaks can be read and analysed to determine the exact components of the mixture. The components are recorded as a sequence of peaks as they leave the column. The peaks can be read and analysed to determine the exact components of the mixture (Skooge at al., 2007). The number of peaks determines the number of components in a sample. The amount of a given component in a sample is determined by the area under the peaks. The identity of components can be determined by the given retention

times. Detecting the mass of the individual compound allows for conclusive of the sample (Willard et al., 1981). This is confirmed by the mass spectrometer coupled to it to obtain the compound's molecular weight.

2.6.7 X-ray diffraction and X-ray fluorescence of solid materials

The powder X-ray diffraction is a non-destructive technique used to identify crystalline phases and orientation of materials. It determines the structural properties and atomic orientation/arrangement of the material. The diffractometer will create the IRD pattern of the sample, measure d- spacing and obtain integrated intensities. The data are compared with known standards in the Joint Committee on Powder Diffraction Standards (JCPDS) site, which are for random orientations (Cullity, 1978).

XRF is a non-destructive technique used for the determination of elemental compositions of a material. An X-ray source is used to irradiate the sample and to cause the elements in the sample to emit (or fluoresce) their characteristics X-rays. A detector system (Wavelength dispersive) is used to measure the position and intensity of peaks of the emitted X-rays for qualitative and quantitative measurements of the elements and their amounts.

2.7 Rubber seed analysis

Eka et al. (2010) analysed rubber seed to determine its potential use as proteins, fats, carbohydrate and amino acids as food supplements for livestock. They reported that well processed rubber seed could be used as food claiming that good storage and heat treatment can reduce the levels of poisonous hydrogen cyanide present in the seed. The results of the proximate analysis and amino acids profile of rubber seed are presented in Table 2.3 and Table 2.4, respectively. The use of rubber seed shell (RSS) and rubber seed kernel (RSK) as source materials for biofuel has been reported in literature. Hassan et al. (2014) investigated RSS and

RSK before oil extraction as raw materials for bio-oil production. They determined their proximate (Table 2.5) and ultimate (Table 2.6) compositions, extractives, cellulose, holocellulose and hemicelluloses content (Table 2.7) and, calorific value and oil yield (Table 2.8). The ultimate analysis from their report shows that carbon and oxygen are the major components of RSS and RSK while other elements are in minority. The proximate analysis indicates that volatile matters in both samples are a major component. High amount of volatile matter indicates that the material could liquefy easily. The knowledge of the number of extractives (Waxes, fats, resins, gum, sugars, starches, sterols, flavonoids, etc.) helps to estimate exact amount of fermentable sugar present in biomass, and should be extracted before processing the lignocelluloses material as a biofuel feedstock (Sasmal et al., 2012). The report also shows that cellulose contents of RSS and RSK are significantly different. Kim et al. (2012) reported that cellulose content of approximately 40% would be useful for biofuel production. From the analysis presented by Hassan et al. (2014), RSK is a more suitable material for biofuel production than RSS. The results presented in Table 2.8 shows that the calorific value of both samples is in the range 23–28 MJ/kg, and the highest oil yield of 33.1% was obtained from RSK. The TGA results presented show that major degradation of RSS and RSK was observed at 300 and 350 ^{o}C, respectively. The differential thermo-gravimetric analysis (DTG) showed two major weight losses for both samples. The first major loss occurred within 250–350 ^{o}C and the second around 400 ^{o}C. Weight losses resulting from hemicelluloses and cellulose occurred at the region between 250–350 ^{o}C, while the lignin degradation starts at 500 ^{o}C. Sun & Jiang (2010) investigated the use of RSS as a raw material for the production of activated carbon by the physical activation with steam. Their results of the proximate analysis (Table 2.5) obtained for RSS were very close to those reported by Hassan et al. (2014). Other results presented by Sun & Jiang (2010) show that RSS is a good precursor for activated carbon. The optimal activation conditions, reported are pyrolyzed temperature (880 ^{o}C), steam flowrate (6 kg/h),

and residence time (60 min). The characteristics of the activated carbon from RSS with a yield (30.5%) reported are specific surface area (S_{BET}) 948 m^2/g, total volume (0.988 m^2/kg), iodine number of adsorbent (q_{iodine}) 1.326 g/g, amount of methylene blue adsorption of adsorbent (9 mb) 265 mg/g, and hardness 94.7%. The results of TGA show two stages of decomposition as follows: stage one (273–385 ^oC) and stage two (385–800 ^oC). Little weight loss was observed at temperature below 270 ^oC because the rubber seed had been dried under 105 ^oC for 3 h. The TGA results from both researchers are very similar as presented above. The DSC analysis presented by Sun & Jiang (2010) shows a little drop at a temperature of 100 ^oC, because the sample needs heat to evaporate the remaining water. The reported decomposition temperatures for hemicelluloses and cellulose are 180 and 240 ^oC, respectively. When temperature was about 320 ^oC, DSC arrived at valley, where hemicellulose and cellulose decomposed and produced abundant organic compounds (wood tar, ketone and methanol) which would vapourized by adsorbing large heat. At 500 ^oC, DSC curves climbed up steeply and reached at a peak, because at this step lignin pyrolyzed and emitted abundant heat. At 800 ^oC, DSC curve reached a base line, pyrolysis reaction was over and the residue reported as graphite carbon and ash (Sun & Jiang, 2010).

Table 2.3: Proximate analysis of rubber seed (Eka et al., 2010)

Parameter	Value
Moisture, %	3.99 ± 0.01
Protein, g/100g	17.41 ± 0.01
Fat, g/100g	68.53 ± 0.04
Ash, g/100g	3.08 ± 0.01
Total Carbohydrate, % (by difference)	6.99

Table 2.4: Amino acid profile of rubber seed (Eka et al., 2010)

Non-essential amino acids (g/100g protein)		Essential amino acids (g/100g protein)	
Aspartic acid	11.18 ± 1.57	Threonine	3.72 ± 0.42
Serine	5.89 ± 0.38	Valine	7.08 ± 0.27
Glutamic acid	16.13 ± 0.34	Methionine	1.37 ± 0.31
Glycine	5.14 ± 0.00	Lysine	4.26 ± 0.41
Histidine	2.95 ± 0.25	Isoleucine	3.28 ± 0.04
Arginine	12.45 ± 0.19	Leucine	6.81 ± 0.08
Alanine	4.71 ± 0.15	Phenylalanine	4.88 ± 0.46
Proline	6.77 ± 0.02		
Cysteine	0.78 ± 0.79		
Tyrosine	2.99 ± 0.25		

Table 2.5: Proximate analysis of RSS and RSK (Hassan et al., 2014; [a] Sung & Jiang, 2010)

Biomass	Moisture	Ash	Volatile mater	Fixed carbon
RSS	14.3, 14.37[a]	0.1, 0.17[a]	71.7, 71.76[a]	13.9, 13.97[a]
RSK	4.3	0.2	89.4	6.1

Table 2.6: Ultimate analysis of RSS and RSK (Hassan et al., 2014)

Biomass	C	H	N	S	O*
RSS	48.8	5.9	1.5	0.1	43.7
RSK	64.5	8.2	3.6	0.3	23.4

Table 2.7: Extractives, holocellulose, hemicelluloses and cellulose contents of RSS and RSK (Hassan et al., 2014)

Biomass	Extractives	Holocellulose	Hemicelluloses	*Cellulose
RSS	7.8	92.2	66.4	25.8
RSK	3.6	96.4	26.9	69.5

*calculated by difference

Table 2.8: Calorific value and oil yield of RSS and RSK (Hassan et al., 2014)

Biomass	Calorific value (MJ/kg)	Oil yield (%)
RSS	23.9	8.7
RSK	27.5	33.1

2.8 Rubber seed oil extraction methods

Industrially, several methods are employed for oil extraction such as mechanical (hydraulic and screw press), solvent extraction, enzymatic, aqueous, supercritical fluid extraction, and their combinations (Onoji et al., 2016b). Mechanical type of extraction is widely used and well adapted to rural communities with moderate initial and operating costs, but oil yield is low (Subrotoet al., 2015; Willems et al., 2008; Olajide et al., 2007). Modeling and optimizing the extraction process variables is paramount to obtaining a higher oil yield. Such optimized parameters could provide vital information to researchers and industrialists. Figure 2.7 depicts a typical flowchart for rubber seed oil processing with a combination of mechanical and chemical methods. The seeds are dried, crushed, and milled to reduce particle size. Milled seed (meal) was conditioned with scorching gas in a heated rotary dryer for 10–20 min at 60–70 ^{o}C (Iyayi et al., 2008). It was then introduced into a mechanical screw press to recover rubber seed

oil, cake and foots (wastes). Rubber seed oil was recovered from the foots using a filtration unit and stored for further use. More rubber seed oil was further extracted from the oily cake in a solvent extraction unit using n-hexane. The cake was stored in a storage unit, and oil-hexane mixture vacuum evaporated to recover the oil, while n-hexane solvent recycled.

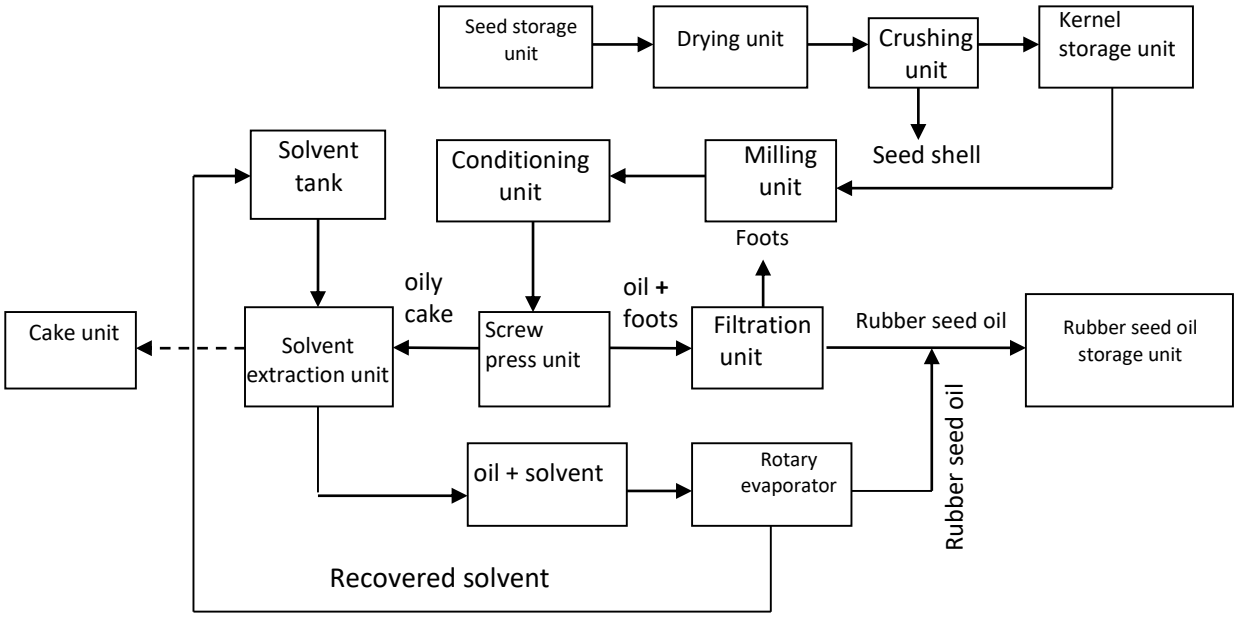


Figure 2.7: Flowchart of rubber seed oil processing (Adapted from Onoji et al., 2016a)

2.8.1 Conventional extraction method (Mechanical and chemical)

Conventional method uses mechanical and chemical means to extract the oil. The mechanical type (mainly hydraulic and screw press) is relatively inexpensive after the initial capital costs (Onoji et al., 2016a; Li et al., 2013). Quality of the oil is high, but it has low yield compared to other extraction methods (Ebewele et al., 2010a). Mechanical screw press is relatively inefficient because it leaves 8–14% of the available oil in the de-oiled cake (Ali & Watson, 2014). Singh & Bargale (2000) recommended the use of double-stage compression expellers to enhance oil recovery. With increased pressure and heated screw press head, oil could easily be extracted from pre-treated seeds (Ebewele et al., 2010a; Zheng et al., 2003). The chemical method is widely used in the laboratory using n-hexane or other suitable organic solvents as

extractive media. Co-extraction of undesirable components in the oil results to low quality. Boiling point of solvent, solvent/seed ratio, seed size, moisture content, drying and extraction time are some of the parameters that affect the yield (Onoji et al., 2016b). Ebewele et al. (2010a) employed hydraulic press to study the influence of extraction variables-pressure (5–8 MPa), temperature (40–90 ^{o}C), moisture content (7–16%), and particle size (1.16–3.36 mm) on the oil yield of different rubber species. They reported that optimal yields for the different species were obtained at 8 MPa, 70 ^{o}C, 10%, and 1.16 mm. Sabarish et al. (2016) studied the effects of drying time, drying temperature, pressing time, and pressure on the yield of rubber seed oil extracted with hydraulic press using design of experiment and a 2^4-full factorial design for the response surface analysis. The analysis of variance (ANOVA) report indicates that the maximum oil yield was obtained at the following conditions: drying temperature 55 ^{o}C, drying time 1 h, pressure 35 kg/cm^2, and pressing time 25 min. Sayyar et al. (2009) in their study on the extraction of oil from jatropha seed using n-hexane solvent reported variation in oil yields (46–47.3%) at 8 h extraction time, 0.16 solute/solvent ratio and particle size (0.5–0.75 mm). Kostić et al. (2013) considered the effect of solvent/seed ratio (3:1, 6.5:1 and 10:1 ml/g), extraction temperature (20, 45 and 70 ^{o}C) and extraction time (5, 10 and 15 min) on hempseed oil yield using RSM and ANN optimization techniques. They reported optimal yield of 29.56% based on ANN conditions: solvent/seed ratio (10:1), temperature (70 ^{o}C) and extraction time (10 min). Bokhari et al. (2012) reported similar observations on extraction of rubber seed oil using RSM. They obtained an optimal yield of 33.56% with n-hexane as solvent at 0.027 g/ml solute/solvent ratio and 4.5 h extraction time. Reshad et al. (2015) also applied RSM using central composite design for the extraction of oil from rubber seeds with n-hexane as solvent. They reported a maximum yield of 49.36% at optimal conditions of 0.08 g/ml solute/solvent ratio, 1 mm particle size, and 8 h extraction time.

2.8.2 Gas-assisted mechanical extraction method

This process involves the dissolution of supercritical CO_2 fluid into the milled seed followed by the screw pressing process (Ebewele et al., 2010a). It allowed for the use of lower pressure, while maintaining higher yield without compromising quality (Onoji et al., 2016a).

2.8.3 Microwave-assisted extraction (MAE) method

Microwaves are electromagnetic waves; a combination of a vertical magnetic field and an electrical wave, with wavelengths ranging from 1 mm to 1 m (Ma et al., 2016). Microwave irradiation follows two mechanisms; viz. dipolar rotation and ionic conduction that generate electromagnetic field that accelerates the extraction process (Ma et al., 2016; Li et al., 2013). The process allows shorter time, low solvent consumption, higher yield and much lower energy requirements compared to the conventional methods (Ali & Watson, 2014). Gimbun et al. (2012) in their study on rubber seed oil extraction compared the efficacy of MAE with Soxhlet method. They obtained a higher oil yield of 40% with MAE and 36% with Soxhlet technique. They further reported a shorter extraction time of 15 min for MAE and 6 h for Soxhlet method. The efficiency of MAE is due to good interactive effect of microwave with solvent molecules.

2.8.4 Ultrasonic-assisted extraction method

The process involves the formation and collapse of microscopic bubbles that release huge amount of energy, pressure and mechanical shear. The ultrasound penetrates the seeds' cell tissues and extracts the oil into the solvent by disrupting the cell walls (Ali & Watson, 2014; Li et al., 2004). Shorter time and low solvent consumption are some of its advantages (Onoji et al., 2016a; Ali & Watson, 2014).

2.8.5 Aqueous enzymatic extraction method

The high efficiency and specificity of enzymes allow them to be useful extractive media. They hydrolyze and rupture the cell walls of the seed kernels and release their oil constituent. Since no solvent is involved, this method is eco-friendly with low initial cost accompanied with the ease of processing of the de-oiled cake into livestock feeds (Li et al., 2004).

2.8.6 Supercritical fluid extraction (SFE) method

SFE is a separation process where the substances are dissolved in a fluid that is able to modify its dissolving power under specific condition above their supercritical regions-critical temperature (T_c) and pressure (P_c) (Rodríguez-Solana et al., 2014). Supercritical fluids have the ability to penetrate into the micropores of a solid and good transport properties (Raventós et al., 2002). Among the available supercritical fluid, carbon dioxide is considered the best because of its inherent advantages of non-toxic, non-flammable, cost-effective, and it has a low T_c (304.15 K). Efficiency of CO_2 can be enhanced by adding a co-solvent such as methanol that is capable of hydrogen bonding and dipole-dipole interactions with the contents of the seed (Murga et al., 2000).

2.9 Physico-chemical properties of rubber seed oil (RSO)

The physicochemical properties of rubber seed oil reported by various researchers are available in literature. The determination of these properties enables the evaluation of the oil as a source of potential industrial feedstock for biodiesel production and other uses (Onoji et al., 2016a). The common fatty acids reported for rubber seed oil are palmitic (C16:0), stearic (C18:0), oleic (C18:1), linoleic (C18:2) and linolenic (C18:3) (Kittigowittana et al., 2013; Widayat & Kiono, 2012; Ramadhas et al., 2005). Other types of acid may be present in smaller proportions (Ashraful et al., 2014). The reports indicate that rubber seed oil consists mainly of unsaturated

fatty acids with polyunsaturated acids in higher proportion. The values reported by researchers may be different depending on the extraction processes, clonal types, analytical methods used, and geographical locations of the rubber tree (Onoji et al., 2016a). Tables 2.9 and 2.10 present the physico-chemical properties and the fatty acid compositions, respectively, of rubber seed oil found in literature. These properties are comparable to other non-edible vegetable oils found in literature (Table 2.11).

Table 2.9: Physico-chemical properties of rubber seed oil

Parameters	Researchers [a, b, c]	This study [d]
Colour	golden yellow, light/dark brown	dark brown
Density, g/cm^3 @ 25 ^{o}C	0.857–0.943	0.886 ± 0.002
Specific gravity @ 15 ^{o}C	0.91	0.909 ± 0.002
^{o}API gravity @ 15 ^{o}C	NA	24.1 ± 0.282
Ph	6	6 ± 0.141
Oil content (wt.%)	35–60	43 ± 0.141
Iodine value, g I_2/100 g oil	113–146	137.02 ± 0.028
Peroxide value, meq. O_2/kg oil	1.6–16	10.46 ± 0.098
Saponification value, mg KOH/g oil	183.91–235.28	195.30 ± 0.282
Acid value, mg KOH/g oil	1.68–42.41	18.20 ± 0.141
Free fatty acid (%FFA as oleic acid)	0.84–42.412	9.10 ± 0.07
Kinematic viscosity, mm^2/s @ 40 ^{o}C	6–66	40.18 ± 0.028
Refractive index @ 20 ^{o}C	1.46–1.47	1.4707 ± 0.00028
Pour point, ^{o}C	–9 to –1.5	–6
Cloud point, ^{o}C	3–4	5.5
Cold filter plugging point, ^{o}C	NA	–0.025
Flash point, ^{o}C	72–295	240.3
Fire point, ^{o}C	298	256
Aniline point, ^{o}C (^{o}F)	NA	21 (69.8)
Boiling point, ^{o}C	NA	119
Freezing point, ^{o}C	NA	–18
Cetane number	45–49.73	43.42
Higher heating value (HHV), MJ/kg	36.1–44	39.37
Mean mol. weight of fatty acids (g/mol)	NA	286.74
Average mol. weight of RSO (g/mol)	NA	898
Diesel index	NA	15.71

[NA] means not available; values are mean ± standard deviation of duplicate data.

[a] Onoji et al. (2016a); [b] Aravind et al. (2015); [c] Reshad et al. (2015); [d] Onoji et al. (2016b)

Table 2.10: Fatty acids profile of rubber seed oil

Fatty acid/Systemic name	Chemical formulae	Composition (%)	
		Researchers [a]	This study [d]
Myristic ($C_{14:0}$) / Tetradecanoic	$C_{14}H_{28}O_2$	2.2	-
Palmitic ($C_{16:0}$)/ Hexadecanoic	$C_{16}H_{32}O_2$	0.23–10.6	13.85
Palmitoleic ($C_{16:1}$)/ Hexadec-9-enoic	$C_{16}H_{30}O_2$	0.23–0.25	-
Stearic ($C_{18:0}$)/ Octadecanoic	$C_{18}H_{36}O_2$	5.69–12	16.82
Oleic ($C_{18:1}$)/ *cis*-9-Octadecenoic	$C_{18}H_{34}O_2$	12.7–42.08	64.11
Linoleic($C_{18:2}$)/ *cis*-9-*cis*-12-Octadecadienoic	$C_{18}H_{32}O_2$	39.6–52.84	-
α-Linolenic ($C_{18:3}$)/ *cis*-9-*cis*-12-*cis*-15-Octadecatrienoic	$C_{18}H_{30}O_2$	2.38–26	-
Arachidonic ($C_{20:0}$)/ Eicosanoic	$C_{20}H_{40}O_2$	0.66–0.97	-
Erucic acid ($C_{22:1}$)/*cis*-13-Docosenoic	$C_{22}H_{42}O_2$	-	5.22
Total saturated		8.78–23.57	30.67
Total monounsaturated		12.93–42.33	69.33
Total polyunsaturated (linoleic, linolenic, etc)		41.98–78.84	Trace

[a] Onoji et al. (2016a); [d] Onoji et al. (2016b)

Table 2.11: Fatty acid compositions of selected non-edible oils (%) (Onoji et al., 2016a)

Fatty acid	Rubber	Jatropha	Neem	Linseed	Tobacco
Myristic acid (C14:0)	2.2	0.3–1.4	0.2–0.26	0.045	0.09–0.17
Palmitic acid (C16:0)	0.23–10.6	12.6–16.0	16–33	5.85–6.21	8.46–10.96
Palmitoleic acid (C16:1)	0.23–0.25	0.57–3.5	0.24	0.3	0.2
Stearic acid (C18:0)	5.69–12	5.97–7.4	9–24	5.47–5.63	2.64–3.34
Oleic acid (C18:1)	12.7–42.08	34.3–44.7	25–54	20.17–24.05	11.24–14.54
Linoleic acid (C18:2)	39.6–52.84	31.4–43.2	6–16	13.29–14.93	69.49–75.58
α-Linolenic acid (C18:3)	2.38–26	0.8–3.4	0.56	46.10–51.12	0.69–4.20
Arachidonic acid (C20:0)	0.66–0.97	0.17–0.3	1.04	0.2	0.25
Behenic acid (C22:0)	–	0.5–0.7	0.3	0.3	0.12
Oil content (%)	35–60	20–60	20–30	35–45	35–49

Cxx: y means number of carbon atoms: number of double bonds

2.10 Thermo-oxidative analysis of rubber seed oil

Generally, seed oils deteriorate when handled defectively with the major decomposition reaction being oxidation in the presence of atmospheric air (oxygen). The oxidative stability of oils is an important indicator of performance and shelf life, and it depends on the fatty acid compositions and conditions to which it is subjected (Onoji et al., 2016b; Guillèn and Cabo, 2002). Poor oxidative stability, unpleasant odor, filter clogging tendency, low temperature fluidity and other conditions that make them unsuitable for long-term storage before use are some of the characteristics of vegetable oils (Oderinde et al., 2009). Thermal oxidation of seed oil on prolonged heating occurs through a free radical mechanism. This is characterized by the initial emergence of a sweetish and unpleasant odor that becomes progressively worse until it

attains a characteristic smell of rancid fat, yielding peroxides and unstable hydroperoxides as primary products (Gouveia de Souza et al., 2004; Guillèn & Cabo, 2002). The primary products degrade easily to produce secondary products such as aldehydes, ketones, acids and alcohols (Gouveia de Souza et al., 2004; Santos et al., 2002). Oxidative stability of vegetable oils can be improved by use of various antioxidant additives available in markets or more importantly by increasing the saturated fatty acids and oleic acid contents in oil by genetic modification of oil bearing plants (Borugadda & Goud, 2013). Such thermal oxidative reactions can be investigated using thermo-analytical methods such as differential scanning calorimetry (DSC), thermogravimetry analysis (TGA), derivative thermogravimetry (DTG) and Fourier transform-infrared (FT-IR) spectroscopy (Onoji et al., 2016b; Borugadda & Goud, 2013; Gouveia de Souza et al., 2004). A good thermal decomposition profile of oil can be obtained at a heating rate of 10 ^{o}C/min under inert atmosphere (Borugadda & Goud, 2013). Reshad et al., (2015) estimated the thermal properties of rubber seed oil (RSO), rubber seed kernel (RSK), and cake by TGA and DSC analyses. They reported single-stage decomposition for RSO, while cake and kernel occurred in two and three stages, respectively. A negligible weight loss (<0.2%) of RSO was observed at 90 ^{o}C due to the presence of moisture (free water). Sudden decrease in weight of the oil sample started from 250–470 ^{o}C which was reported to be due to decomposition of heavier hydrocarbon molecules to lower molecular hydrocarbons, and non-hydrocarbon gases such as CO_2 and CO. TGA confirms RSO is thermally stable up to temperature of 290 ^{o}C (onset point) higher than kernel (210 ^{o}C) and cake (120 ^{o}C). These reports collaborated with the findings of Aravind et al. (2015) who investigated the thermal degradation of RSO, coconut oil, sunflower oil and SAE20W40 under oxygen environment in the temperature range 0–500 ^{o}C and reported that RSO is thermally stable up to 250 ^{o}C and that gradual degradation occurs after 300 ^{o}C. The TGA curve of RSO is similar to that of SAE20W40 as the degradation is gradual unlike coconut and sunflower oil. However, simple

and low-cost classic chemical analysis such as determination of the concentration of peroxide value, iodine value, acid value and refractive index has been effectively employed to evaluate the kinetics of oils degradation under thermal conditions that influence the mechanisms of degradation process (Onoji et al., 2016b; Oderinde et al., 2009).

2.11 Industrial applications of rubber seed and oil

Recent scientific studies show that rubber seed and seed oil have several potential industrial applications such as biodiesel (Onoji et al., 2016a; Vipin et al., 2016; Reshad et al., 2015), semi-drying oil (Eka et al., 2010; Ebewele et al., 2010a), paints and coating (Aigbodion & Pillai, 2000), printing ink (Iyayi et al., 2008; Igeleke & Omorusi, 2007). Others are livestock feeds and fertilizer (Iyayi et al., 2008; Igeleke & Omorusi, 2007), lubricants (Aravind et al., 2015), powdered activated carbon (Sung & Jiang, 2010; Okieimen et al., 2005a), cosmetic (Kittigowittana et al., 2013), liquid soap and hair shampoo (Igeleke & Omorusi, 2007) and as a carrier for copper fungicide (Ebewele et al., 2010a). Matured fresh rubber seed contains 40-50% kernels (Banković-Ilić et al., 2012), 37% shell (Atabani et al., 2013) and 20–25wt. % moisture (Gimbun et al., 2012). The seed contains protein, essential and non-essential amino acids (Eka et al., 2010), while the dried kernel contains 40-50% oil (Onoji et al., 2016a; Widyarani et al., 2014). Rubber seed contains toxic substances such as cyanogenic glycoside (186 mg) and about 638-749 mg HCN per kg of fresh kernel (Eka et al., 2010; Iyayi et al., 2008). HCN constituent can be reduced on storage for a period not less than 2 months at room temperature (Iyayi et al., 2008). With the emergence of biodiesel industry in SSA countries, rubber plantation farmers will earn extra profit by harvesting rubber seeds for biodiesel production. This will also encourage the cultivation of new plantations that will reinvigorate the economy of these local communities, which had abandoned their plantations due to low demand for rubber latex in the past (Onoji et al., 2016a).

2.12 Biofuels policies and sustainability in Africa

The African continent is plagued with poverty and unrests because of lack of good governance and accountability. Africa has about 9.5% of the world proven reserves of crude oil that are concentrated in four countries (Nigeria, Algeria, Egypt, and Libya) and contributes about 12% to global oil production (Onoji et al., 2016a; Yang et al., 2014; Amigun et al., 2011). The rest African countries are net importers of energy (Table 2.12) and that places a heavy economic burden and reduces energy security and sovereignty. Thus, there is an urgent need to invest in domestic energy infrastructure driven by the private sector for quick economic recovery and growth within the continent (Yang et al., 2014).

Biofuels production in Africa could be commercialized to diversify energy and agricultural activity in best practices, reduce dependence on crude oil and contribute to economic growth in a sustainable manner.

The advantages of biofuels such as biodiesel, bioethanol, biohydrogen, biogas, biomethanol, etc. are renewability, biodegradability, lower Sulphur and aromatic content, higher combustion efficiency, lower emissions and amongst others. However, biodiesel and bioethanol are the two alternative fuels promoted with potential to reduce dependence on fossil oil derived products imports (Demirbaş, 2009). The development of biodiesel industry in most African countries is still in the infancy stage with *Jatropha curcas* as the main non-edible oil source (Yang et al., 2014). Advanced countries of US, Germany, France, Spain, Italy, and emerging economies like Brazil and India, have well-articulated and sustainable biofuels policies that enhance their development. Availability of adequate arable land for bioenergy crops cultivation is a major challenge to these nations (Amigun et al., 2008).

Onoji et al. (2016a) suggested that African countries should articulate institutional policies and regulatory frameworks to guard against deforestation and biodiversity challenges. This is due to the presence of foreign investors that will invest in bioenergy crops cultivation for biodiesel production. Most of the bioenergy policies in draft forms in African countries targeted food crops as biofuels feedstock. These policies are counterproductive as most Africans depend heavily on these crops for food. Available reports in literature support rubber tree seeds as plausible source of non-edible oil to complement jatropha seed oil for biodiesel production in sub-Saharan Africa (Onoji et al., 2016a). However, none of the sub-Saharan African countries where rubber trees exist in large quantity considers it as a feedstock for biodiesel production in their bioenergy policies shown in Table 2.13. This is a policy oversight considering the multiple applications of rubber plant in automotive and biofuel industry. A case study of Nigeria is presented to show the lapses in biofuel policies in Africa and energy insecurity.

Table 2.12: Africa countries which import and export energy (Yang et al., 2014)

Major energy exporters [a]	Net energy exporters	Importers [b]
Algeria	Angola	Benin
Rep. Congo	Cameroon	Eritrea
Egypt	Congo	Ethiopia
Gabon	Côte d'Voire	Ghana
Libya	D.R. Congo	Kenya
Nigeria	Gabon	Morocco
South Africa	Sudan	Mozambique
		Namibia
		Senegal
		Tanzania
		Togo
		Zambia
		Zimbabwe

[a] Major energy exporter are in excess of 0.5 quads.

[b] Most of the African countries' imports are very small (less than 0.3 quads).

Table 2.13: Sub-Saharan African countries and their bioenergy policies (Onoji et al., 2016a)

Country	Biodiesel feedstock	Presence of policies
D.R. Congo	rubber*, oil palm, melon, sesame	draft energy policy
Cameroon	rubber*, oil palm, melon,	None
Rep. Congo	rubber*, oil palm, melon	policy under development
CAR	rubber*, melon, sesame	None
Nigeria	rubber*, jatropha, oil palm, sesame	energy policy, biofuels strategy
Ghana	rubber*, jatropha, oil palm	energy policy, renewable energy
Côte d'Ivoire	rubber*, sesame, tobacco	policy under development
Liberia	rubber*, pongamia pinnata, oil palm	draft biofuel policy
Gabon	rubber*, oil palm, pongamia pinnata	None
Guinea	rubber*, oil palm, sesame	None

* means available but wasted, and are not listed as feedstock in biofuels policies.

2.12.1 Nigerian biofuel policy (A case study in Africa)

With estimated reserves of 37.2 billion barrels, a daily production output of 2.2 million barrels of crude oil and gas reserves of about 187 trillion cubic feet, Nigeria is still facing energy challenges with about 49% of the population lacking access to electricity. Energy output rated at about 4000 MW is grossly inadequate, and demand is expected to increase over the next 20 years (Ishola et al., 2013). The declining capacity for energy generation in Nigeria has deeply entrenched the dependence on renewable biomass fuels for cooking (Abila, 2012). The adoption of biofuel policy in Nigeria in 2007 holds a diversity of opportunities and potentials to project Nigeria into a bioeconomy and increase her energy generation (Abila, 2012). Demirbaş et al. (2009) classified the importance of the biofuel industry as economic, environmental, and energy security. The biofuel industry could attract investment in new

technology, boost rural development through industrialization, and create employment leading to poverty reduction. It could also reduce dependence on revenue from oil, recycle carbon dioxide, reduce rural-urban drift of unemployed youths (Wohlgemutgh, 1999), and increase the income of smallholder farmers integrated into the biofuel supply chain (Malik, 2009). Ohimain (2013) however reviewed the Nigerian biofuel policy and incentives released in 2007 and observed that:

- the policy narrowly classified biofuel to include only bioethanol and biodiesel neglecting other biofuels and energy carriers obtainable from biomass such as biohydrogen, biogas, biomethanol, biocrude, biobutanol, dimethyl ether, and other products of Fisher-Tropsch (FT) synthesis- FT diesel, FT gasoline, and chemicals;
- The policy classified the biofuel enterprise as an agro-allied industry, yet the policy is driven by the petroleum sector;
- The policy inadvertently refers to food crops as biofuel feedstock and did not address the potential food-fuel crisis that could arise from the use of food crops as biofuel feedstock;
- The policy did not adequately address issues pertaining to technology transfer, biomass collection, waste management (environmental impact) and transportation of biofuel feedstock;
- The policy did not encourage expansion of feedstock sources by investing in research and development on second and third generation biofuel feedstock that do not compete with food;
- That modern biomass conversion technology issues were not addressed by the policy.

The researcher suggested upgrade of the policy to accommodate the observed lapses. Ishola et al. (2013) reported similar observations in US$3.86 billion investment in nineteen ethanol bio-refineries in Nigeria with unsatisfactory results. This could be attributed to limited availability of food crops as biofuel feedstock. Many of the food crops are staple food in Nigeria and their

use as biofuel feedstock is counterproductive. The report however, did not highlight any expenditure on biodiesel programme. The adoption of rubber seed as a source of non-edible oil feedstock will drive the Nigerian biofuel policy to fruition. Nigeria has the capacity to produce over 8,000 ton of biodiesel/annum from rubber seed oil and this figure could increase with proper management (Onoji et al., 2016a). Despite the potentials and availability of rubber seeds in Nigeria, there is no trial production of biodiesel from rubber seed oil except on research scale, which is even limited.

2.13 Catalysis

A catalyst is a substance that affects the rate of a reaction (positive or negative) without been substantially affected by the process. Catalysts are neither reactants nor product, and have been used by man for over 2000 years in several industrial applications (Levenspiel, 2005). Catalysis is the occurrence, study, and use of catalysts and catalytic processes that involve the constant search for new ways of increasing product yield and selectivity (Fogler, 2008). There are two broad classes of catalysts: (1) Enzymes - operate at close to ambient temperature with biochemical systems, (2) Man-made catalysts - operate at high temperature (homogeneous and heterogeneous). Homogeneous catalysis concerns processes in which a catalyst is in solution with at least one of the reactants. A heterogeneous catalytic process involves more than one phase; usually the catalyst is a solid and the reactants and products are in liquid or gaseous form. A heterogeneous catalytic reaction occurs at or very near the fluid-solid. Because a catalytic reaction occurs at the fluid -solid interface, a large interfacial area is essential in attaining significant reaction rate. In many catalysts, this area is providing by an inner porous structure needed for the high rate of reaction (Fogler, 2008). A typical silica-alumina cracking catalyst has a pore volume of 0.6 cm^3/g, average pore radius of 4mm, and a corresponding surface area of 300 m^2/g (Fogler, 2008). In some cases, a catalyst may contain some minute

particles of an active material dispersed over a less active substance called a support. The active material is frequently a pure metal or a metal alloy. Catalysts can also have small amounts of active ingredient added called promoters, which increase the activity of the solid catalysts. Although a catalyst can easily speed up the rate of a reaction in several folds, when varieties of reactions are encountered, the catalyst selectivity enables it to affect a single reaction, leaving the rest unaffected. Thus, in the presence of an appropriate catalyst, products containing predominantly the material(s) desired could be obtained from a given feed. The following are some general observations made by Levenspiel (2005) on catalyst:

- The selection of a catalyst to promote a reaction is not well understood. In practice, extensive trial and error may be needed to produce a satisfactory catalyst;
- Duplication of the chemical constitution of a good catalyst is no guarantee that the solid produced will have any catalytic activity;
- Various theories have been proposed to explain the action of catalyst, and it is thought that reactant molecules are changed, energized, or affected to form intermediates in the regions close to the catalyst surface;
- In terms of the transition-state theory, the catalyst reduces the potential energy barrier over which the reactants must pass to form products (Figure 2.8);
- Though a catalyst may speed up a reaction, it never determines the equilibrium or endpoint of a reaction. Thus, with or without a catalyst, the equilibrium constant for a reaction is always the same.

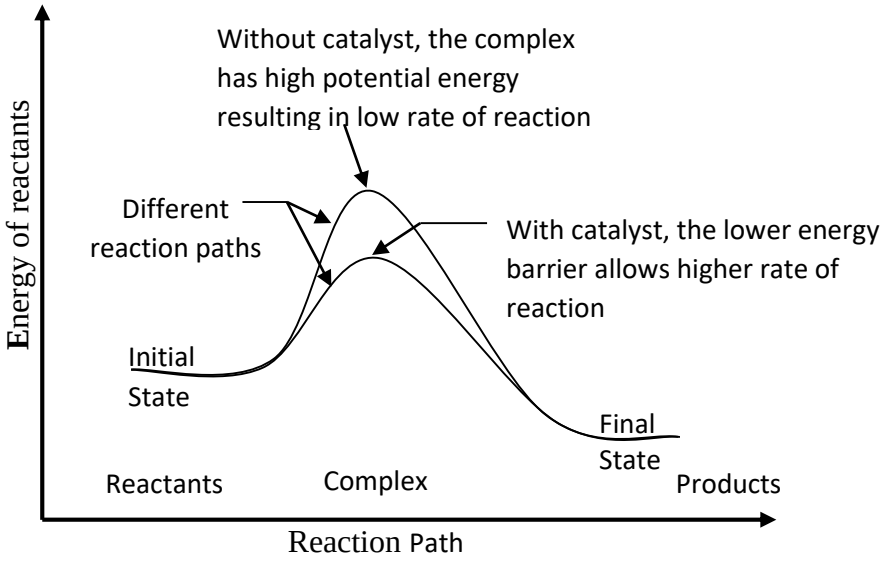


Figure 2.8: Representation of the action of a catalyst (Adapted from Levenspiel, 2005)

2.13.1 Catalyst deactivation

Most catalysts do not maintain their activities at the same levels for indefinite periods. They are subjected to deactivation, which causes a decline in catalyst's activity as time progresses. Catalyst deactivation may be caused by: (1) Aging -This is a gradual change in surface crystal structure; (2) Poisoning-This is the irreversible deposition of substances on the active site; or (3) fouling or coking- This is the deposition of reversible carbonaceous or other material on the entire surface.

2.13.2 Physical adsorption and chemisorption in chemical reaction catalysis

For a catalytic reaction to occur, at least one, or frequently all of the reactants must be attached to the surface of the catalyst (Wu, 2004). This attachment known as adsorption, takes place by two different processes: physical adsorption (physisorption) and chemisorption (chemisorption) (Mechrafi, 2002). Physical adsorption mainly caused by van der Waals forces is the result of low energy exchange between the adsorbate and the adsorbent on the solid

surface (Desjardins, 1997). The adsorbate is relatively free to move on the surface, as the attraction is not fixed to a specific site. Physisorption is relatively reversible and capable of multilayer adsorption (Madani, 2004). The process is similar to condensation, with small exothermic heat of adsorption (4.2–63 kJ/mol) (Fogler, 2008). In chemisorption, the adsorbed atoms or molecules are held to the surface by valence forces of the same type as those that occur between bonded atoms in molecules (Fogler, 2008). In this case, the adsorbed molecules are not free to move on the solid surface; thus, the adsorption process depends on the functional groups present on the adsorbent and not on the surface area. As a result, the electronic structure of the chemisorbed molecule is perturbed significantly, causing it to be extremely reactive. Due to the stronger molecular electronic structure that results from the formation of chemical bonds between adsorbate and adsorbent, chemisorption is an irreversible process. It occurs at a higher temperature that requires more energy. Like physical adsorption, chemisorption is exothermic process, but the heats of adsorption are generally of the same magnitude as the heat of a chemical reaction (i.e., 40–400 kJ/mol). Table 2.14 presents the comparisons between physisorption and chemisorption.

Table 2.14: Comparison between physisorption and chemisorption processes

Physisorption	Chemisorption
Adsorbates are molecules	Adsorbates are atoms or radicals
Multilayer adsorption process	Monolayer adsorption process
Attraction is a result of van der Waals forces	Attraction is a result of chemical bonds
Reversible process	Irreversible process
Molecules are adsorbed on available sites	Molecules are adsorbed on active sites only
Adsorption temperature must be below the boiling point of the Adsorbate	It occurs at any temperature
Heat of Adsorption is less than 50 kJ/mol	Heat of Adsorption can be more than 100 kJ/mol (Christmann, 2012)

2.14 Gas-solid adsorption systems

The ability of the surface of a solid to adsorb gases and vapour is considered as its most characteristic property. Surface area and porosity are important properties in the field of catalyst design and heterogeneous catalysis (Storck et al., 1998). The physisorption method as routine tool is the most widely used technique for the characterization of micropores (diameter < 2 nm), mesopores (diameter 2–50 nm) and macropores (diameter> 50 nm) of new materials for catalysts design. Gas-solid adsorption has been carried out extensively in the past few years due to the comparative ease of experimental work (Shanavas et al., 2011). The results of physisorption experiments are usually presented in graphical forms as isotherms. The *Langmuir* equation is the simplest equation for the gas-solid adsorption systems upon which other isotherms were derived. The earliest reports on gas-solid adsorption were classified by *Brunauer-Emmett-Teller* (BET) based on their derived models type I, II, III, IV and V

isotherms (Figure 2.9), although *Freundlich* isotherm was reported as the oldest (Iyer & Kunji, 1992).

The *Langmuir* model and the BET isotherms are used to obtain the monolayer values from which the specific surface areas are calculated. The monolayer values and the molecular areas estimated by *Langmuir* and *BET* isotherms are inaccurate, resulting to errors in surface areas estimations. BET admitted that their equation be strictly applied in the range of relative pressures between 0.05 and 0.35 for adsorption process, since the equation did not fit the experimental data for all relative pressures (De Boer et al., 1966). The Langmuir equation has only limited applicability, for it is valid for type I isotherm of *Brunauer's* classification.

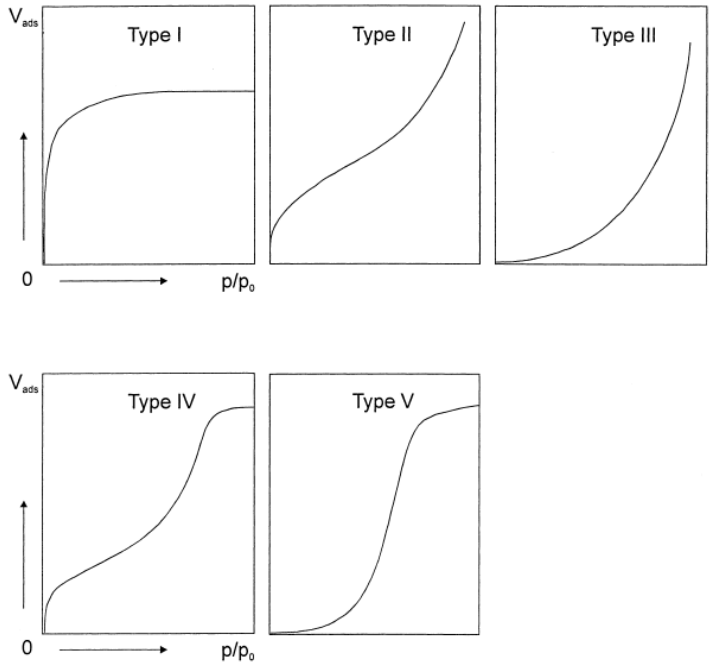


Figure 2.9: Adsorption isotherm classified by *Brunauer* (Adapted from Storck et al., 1998)

2.14.1 Langmuir model equation (linearized)

The linear form of the *Langmuir* equation is described as:

$$\frac{P}{V} = \frac{P}{V_m} + \frac{1}{bV_m} \tag{2.1}$$

Where: *'b'* is the *Langmuir* constant related to the affinity of binding sites, P, P_o, and V_m are as defined earlier. A plot of $\frac{P}{V}$ versus P yields a straight line from Langmuir V_m and b can be evaluated. The quantity V_m obtained from the Langmuir equation is the monolayer value, which is used to determine the Langmuir specific surface area (S_L) of the adsorbent by using Equation (2.2) (Shanavas et al., 2011).

$$S_L = V_m \times N \times A_m \tag{2.2}$$

Where: N is the Avogadro's number; and A_m is the adsorbate molecular area (0.162 nm^2 for nitrogen).

The *Langmuir* equation derived from the adsorption on the nonporous surface adsorption, gives the type I isotherm. In physical adsorption, however, the type I isotherm is obtained from microporous adsorbents such as active carbons or zeolites. In such microporous adsorbents, the type I isotherm can be explained by filling of the adsorbate molecules into micropores observed as initial sharp rise of the isotherm. The flat region of the isotherm appears when the micropores are completely filled by adsorbate. It is reasonable to conclude that the monolayer volume (V_m) of microporous adsorbent obtained from the *Langmuir* plot corresponds to the microspore volume. The surface area of microporous adsorbent estimated from V_{im} occasionally gives the abnormally high value.

2.14.2 BET model equation

The assumptions of the *BET* equation are:

- Estimates monolayer capacity;

- Adsorption occurs layer by layer;
- Molecules in the first layer interact with the solid, and molecules in the following layers behave as in bulk liquid;
- Heat of adsorption for the first layer is higher than successive layers;
- Heat of adsorption for second and successive layers equals the heat of liquefaction;
- Lateral interactions between adsorbed molecules are ignored.

$$\frac{x}{V(1-x)} = \left(\frac{C-1}{V_m C}\right)x + \frac{1}{V_m C} \tag{2.3}$$

where: 'x' is the relative pressure (P/P_o); P is the partial pressure; Po is the saturation pressure; V_m is the maximum amount of gas adsorbed/unit mass of solid at high pressure conditions required to form a complete monolayer over the entire surface of the solid, and C is the *BET* constant related to the heat of adsorption. A plot of $\frac{x}{V(1-x)}$ versus x yields a straight line from which V_m and C are calculated. The volume of the monolayer (V_m) is converted to a specific surface area (S_{BET}) by assuming that each molecule in the monolayer occupies a given surface (0.162 nm^2 for nitrogen).

2.14.3 Freundlich model equation

The Freundlich isotherm represents the isothermal variation of adsorption of a quantity of gas adsorbed by unit mass of solid adsorbent with pressure. The isotherm is obeyed when the adsorbate forms a monomolecular layer on the surface of the adsorbent. It was determined experimentally that the extent of adsorption varies directly with pressure until saturation pressure P_o is reached. Beyond that point, the rate of adsorption saturates even after applying higher pressure. The Freundlich isotherm indicates that:

- At low pressure, the extent of adsorption varies linearly with pressure, $\frac{x}{m} \propto P^1$;

- At high pressure, it becomes independent of pressure, $\frac{x}{m} \propto P^0$

Thus, Freundlich adsorption isotherm fails at higher pressure.

Mathematically, the model equation is expressed as:

$$\frac{x}{m} = K_F P^{\frac{1}{n}} \tag{2.4}$$

Equation (2.4) in linearized form becomes:

$$\log\left(\frac{x}{m}\right) = \log K_F + \frac{1}{n}\log P \tag{2.5}$$

where, x = mass of adsorbate

m = mass of adsorbent

P = equilibrium pressure of adsorbate

$K_{F\ and}$ n are constants for a given adsorbate and adsorbent at a particular temperature. The value of n is always greater than 1; indicating that the amount of gas adsorbed does not increase as rapidly as the pressure.

2.14.4 The *t*-plot

Various thickness equations have been developed and reported in literature to relate thickness of adsorbed film to pressure in gas-solid adsorption. The characteristics of these equations are:

- ✓ Compares an isotherm of a mesoporous materials with a standard type II isotherm of a nonporous adsorbent with BET C constants similar to that of the microporous sample;
- ✓ Existence of a direct relation between thickness and specific volume of gas adsorbed;
- ✓ Thickness equation predicts V at various pressures for nonporous materials;
- ✓ Plotting experimental data against thickness equation data yields a straight line for nonporous solids, and a deviated line for porous solids.

The *t*-values are in practice calculated with a thickness equation that describes the particular standard reference curve

Practically, an adsorbate has never been reported to cover an adsorbent with a film of uniform thickness. In many instances, it is assumed that the film thickness on pore walls is uniform which then allows for the calculation of statistical thickness (*t*) from gas adsorption isotherms. Several model equations have been reported in the literature developed to calculate statistical thickness. The *t*-plot method permits the determination of micropore volume, surface area, and help to obtain in principle information about the average pore size of the adsorbent.

De Boer et al. (1966) in their study of gas-solid adsorption proposed a master *t*-curve multimolecular N_2-adsorption to overcome limitations of *Langmuir* and the *BET* isotherms. Their reports indicated an identical multilayer adsorption curves for variety of adsorbents considered; provided no capillary condensation occur and no narrow pores are excluded during the adsorption process. A master *t-curve* in terms of an average thickness of the adsorbed layer for the adsorption of nitrogen at 78 K over the range 0.1–0.75 P/P_o was developed. This developed curve gave the same surface area with a fitted BET isotherm. If the statistical thickness (*t*) of one layer is 3.5 Å, then a value of 3.54 (Å) indicates an adsorption of $n = \left(\frac{V}{V_m} \right)$ layers where V is the adsorbed volume, and V_m the monolayer capacity both in cm^3/g STP adsorbent.

2.14.4.1 Harkins-Jura model

Harkin-Jura model that was derived from an empirical equation of state for condensed films, attempts to modify earlier models of *Langmuir* and *BET*. The model proposes that the adsorptive film is of the condensed type (liquid) and hence its surface pressure, the difference of the surface tension of the bare surface and film-covered surface is a linear function of the area per molecule (Shanavas et al., 2011). The isotherm does not rely on parameters such as molecular area and monolayer values, and thus gives reliable results compared to *Langmuir* isotherm. The *Harkins-Jura* model is given as:

$$\log x = B - \frac{A}{(V_a)^2} \tag{2.6}$$

where $x = \frac{P}{P_o}$, A and B are constants, V_a is the adsorbed volume.

A similar thickness equation was obtained by De Boer et al. (1966), which represents nitrogen adsorption on solid adsorbents at 77 K:

$$\log x = 0.034 - \frac{13.99}{t^2} \tag{2.7}$$

And,

$$t(\text{Å}) = \left[\frac{13.99}{0.034 - \log(P/P_o)}\right]^{0.5} \tag{2.8}$$

For carbon-like derived materials, a developed thickness equation is given as:

$$t(\text{Å}) = 0.88(\text{P/P}_\text{o}) + 6.45(P/P_o) + 2.98 \tag{2.9}$$

2.14.4.2 Halsey equation

The *Halsey* equation provides another alternative to calculate the statistical thickness. The equation for nitrogen adsorption at 77 K was described as:

$$t(\text{Å}) = 3.54\left[\frac{-5}{\ln(P/P_o)}\right]^{1/3} \tag{2.10}$$

2.14.5 Polanyi's potential theory

The Polanyi's potential theory occupies a unique position in the study of physisorption. For different number of adsorbents, the theory has been successfully used to correlate data at different temperatures and for different adsorbates, although it is reported not consistent with monolayer adsorption on heterogeneous surfaces (Harris, 1969). The theory explained that the adsorption process is facilitated by the existence of potential fields around the surface of the

adsorbent, and the adsorptive potential energy (E_n) needed to energize the adsorbate from its equilibrium pressure to the saturation pressure is described by (Polany et al., 1970; Harris, 1969):

$$E_n = \int_{Pequil}^{Psat} VdP = \int_{Pequil}^{P_{sat}} \frac{RT}{P} dP = RT \ln\left(\frac{P_{sat}}{P_{equil}}\right) \tag{2.11}$$

2.14.6 Dubinin-Radushkevich equation

Dubinin-Radushkevich method, which is based on the Polanyi's potential theory, is widely used to describe adsorption in microporous solids such as activated carbon and zeolites. The equation has a semi-empirical origin and is based on the assumptions of a change in the potential energy between the gas and adsorbed phases and a characteristic energy of a given solid. This equation yields a macroscopic behaviour of adsorption loading for a given pressure (Nguyen & Do, 2001). The proposed equation allows the calculation of micropore volume from the adsorption isotherm.

In its basic form, the *Dubinin-Radushkevich* can be described as (Nguyen & Do, 2001; Misra, 1969):

$$\frac{V}{V_o} = \exp\left[-\left(RT \ln\left(\frac{P}{P_o}\right)/E\right)^2\right] \tag{2.12}$$

$$\log_e V = \log_e V_o - \left(\frac{RT}{E}\right)^2 \log_e^2\left(\frac{P}{P_o}\right) \tag{2.13}$$

where, V = volume adsorbed (cm^3/g); Vo = micropore volume (cm^3/g). A plot of $\log_e V$ vs. $\log_e^2 p/p_o$ known as a characteristic curve plotted to test the suitability of the equation and/ or to determine its range of applicability. If the model equations were applicable, the plot would be a straight line with an intercept $\log_e V_o$ and a slope $-(RT/E)^2$, from which micropore volume and characteristic energy (E) can be obtained (Nguyen & Do, 2001).

2.14.7 Kelvin equation

The *Kelvin* equation provides a correlation between pore diameter and pore condensation pressure. The relative pressure where the pore condensation occurs depends on the pore radius. Basic assumptions are:

- Pores of cylindrical shapes;
- No fluid-wall interactions;
- Zero (0) contact angle (θ).

The basic form of the *Kelvin* equation is described by (Siboni & Volpe, 2008; Mitropoulos, 2008; Aylmore, 1974):

$$\ln\frac{P}{P_o} = -\frac{2\gamma V_l Cos\theta}{RT}\left(\frac{1}{r_m}\right) \tag{2.14}$$

If contact angle $\theta = 0$, then Equation (2.14) becomes:

$$\ln\frac{P}{P_o} = -\frac{2\gamma V_l}{RT}\left(\frac{1}{r_m}\right) \tag{2.15}$$

where θ *is* the contact angle between solid and the condensed phase, and:

$$r_P = r_K + t \tag{2.16}$$

When fluid-wall interactions are considered, the modified *Kelvin* equation for nitrogen at a temperature of 77 K becomes:

$$r_K(\text{Å}) = \frac{4.15}{\log(\mathrm{P_o}/P)} \tag{2.17}$$

where γ *is* the surface tension of liquid adsorbate (N/m), V_l is the molar volume of the bulk liquid adsorbate (vol/mol) and the value is 34.68 cm^3/mol for nitrogen at 77 K, r_m is the mean radius of curvature of the liquid/gas interface; r_K is the Kelvin radius; r_p is the pore radius; *R*

is the universal gas constant; *T* is the absolute temperature; and *t* is the statistical thickness of the adsorbed film (deposited or retained).

For many practical purposes, this model is commonly a cylinder with infinite length and for many mesoporous materials; the adsorption isotherm is of type IV. Hysteresis in capillaries open at both ends, results from the fact that in desorption, evaporation takes place from a hemispherical meniscus while in adsorption, condensation occurs from a cylindrical film. In both cases, condensation or evaporation occurs at some distance *t* from the pore walls (Mitropoulos, 2008). On assumption of zero contact angle, r_m for a hemispherical meniscus will be equal to $r_m = r_K$.

where r_K is Kelvin radius, $r_K = r_P - t$ while for a cylindrical interface, $r_m = 2r_K$.

2.14.8 Thermodynamics of gas adsorption

Adsorption process is exothermic in nature, and the heats released might be the result of energetic interactions between the adsorbate and adsorbent species. The thermodynamic relation of gas adsorption is given by Equation (2.18).

$$\Delta G_{ads} = \Delta H_{ads} - T\Delta S_{ads} \tag{2.18}$$

where ΔG_{ads}, $\Delta H_{ads,}$ and ΔS_{ads} are the Gibbs free energy change of adsorption, the enthalpy changes of adsorption, and the entropy change of adsorption, respectively. ΔG_{ads} is negative because gas adsorption proceeds spontaneously. Furthermore, ΔS_{ads} is negative because the molecules moving at random in gas phase are fixed on the solid surface by adsorption. The adsorbate amount and the heat released during the adsorption process could be used to determine the thermodynamic quantities. The isosteric method is used to measure the molar enthalpy at different temperatures and from which the heat of adsorption is calculated (van

Dongen & Broekhoff, 1969). The isosteric adsorption enthalpy and entropy can be determined from the gradient and y-intercept of $\ln\frac{P}{P_o}$ versus $\frac{1}{T}$ from the following equation:

$$\ln\frac{P}{P_o} = \frac{\Delta H_{ads}}{R}\frac{1}{T} - \frac{\Delta S_{ads}}{R} \tag{2.19}$$

The equation above is similar to the *Clausius-Clapeyron* relation given by:

$$\Delta H_{ads} = -RT^2\frac{\partial}{\partial T}\left(\ln\frac{P}{P_o}\right) \tag{2.20}$$

2.15 Biodiesel and its origin

Biodiesel is a long chain fatty acid mono-alkyl esters (FAME) produced from acyl glycerol (triglyceride) in vegetable oils and animal fats via transesterification with short chain alcohols (in this study, methanol) (Issariyakul & Dalai, 2014). Biodiesel has good properties like renewability, biodegradability, lower emission profile and excellent lubricity amongst others (Sajjadi et al.,2016; Guo et al., 2010). Triglyceride (Figure 2.10) is the major component of vegetable oils composed of three esters of fatty acid chain (acyl group) attached to the glycerol backbone (glycerol group). Typical fatty acid chains attached to triglycerides found in vegetable oils are usually from 10 to 24 carbon atoms. The major difference between various vegetable oils is the type of fatty acids attached to triglyceride molecule. Rudolf Diesel (1858-1913) invented the diesel engine in 1892 (Marchetti & Errazu, 2008) out of his desire to improve on the steam engines of the late 1800s that were considered dangerous. In 1900, he demonstrated the newly designed engine running on peanut oil at Paris World Exhibition (Marchetti & Errazu, 2008). The diesel engine later became the engine of choice for power, reliability and high fuel economy. Shortly after death of Rudolf Diesel in 1913, cheap diesel fuel from petroleum became available. With the availability of cheap petroleum, the diesel engine design was modified to match the properties of petro-diesel (Ma & Hanna, 1999) and

this discourages the use of vegetable oils in that era. Several researchers (Aransiola et al., 2014) have reviewed the use of vegetable oil as a source of fuel. Their publications show satisfactory performance of vegetable oils as plausible source material as fuels for use in diesel engines. In spite of the benefits of vegetable oils as fuel in diesel engines, their high viscosity is a major drawback when used as fuels in direct-injection diesel engines resulting in poor atomization and engine deposits (Issariyakul & Dalai, 2014).

The World War II and the oil crises of the 1970s saw a brief interest in the use of vegetable oils to fuel diesel engines. Unfortunately, the newer diesel engine designs could not run on traditional vegetable oils, due to high viscosity compared to petro-diesel. In the early 1980s, concerns over the degradation of the environment, energy security, and agricultural over production once again brought the use of vegetable oils to the forefront. A renewed effort was focused on the use of vegetable oils as sources of fuels and was debated at the first International Conference on plants and vegetable oils as fuel in Fargo, North Dakota in August 1982 (Ma & Hanna, 1999). Four major technologies adapted to reduce the viscosity of vegetable oils, such as direct blending with petrol-diesel, micro-emulsification, pyrolysis, and transesterification have been suggested by Subramaniam et al. (2013), Boro et al. (2012), and Schwab et al. (1987) for use in biodiesel production. The advantages and disadvantages of these methods as listed in Table 2.15 show that transesterification is the best choice. Currently, transesterification is the most commonly employed method for biodiesel production. The biodiesel produced through this process is burned directly in unmodified diesel engines, with very low deposit formation. The idea of transesterification dated back to 1938 when it was found that the glycerin component of the triglyceride has no calorific value and was likely to cause excessive carbon deposit on the engine. The residue fatty acid of the oil after the removal of the glycerin part through a catalyzed chemical reaction (transesterification) with a simple short chain alcohol, is referred to as biodiesel, a term that made its first appearance in a paper published in

1988 (Issariyakul & Dalai, 2014). Over 90% biodiesel produced, is currently sourced from edible vegetable oils that compete with food use (Sajjadi et al., 2016; Ashraful et al., 2014). Food is a necessity of man after shelter; and the use of edible vegetable oils as biodiesel source materials is counterproductive. Feedstock accounts for about 60–95% of the total cost of biodiesel (Banković-Ilić et al., 2012) and the production of biodiesel from low-cost materials will reduce its price and makes it more competitive with fossil-diesel. Non-edible rubber seed oil can be exploited as low-cost industrial oil for biodiesel production and this will reduce biodiesel cost and avoid food-fuel crisis in future (Morshed et al., 2011). Homogeneous base catalysts such as NaOH, KOH and methoxides of sodium and potassium are most suitable for industrial transesterification of edible vegetable oils that are generally low in free fatty acids (FFAs). However, associated problems such as difficulty in catalyst-products separation, initial catalyst cost, soap formation, low-grade by-product glycerol, reactor corrosion and large volume washing water requirements induced further research for environmentally benign heterogeneous catalyst for biodiesel synthesis from non-edible oils (Roschat et al., 2012; Zabeti et al., 2009). Heterogeneous (solid) catalysts are separated from reaction mixtures by simple filtration process. They are reused and recycled severally producing high-grade glycerol (Uprety et al., 2016). In the recent past, successful ventures were reported on the utilization of calcined wastes such as eggshell (Piker et al., 2016) and animal bones (Nisar et al., 2017) to generate CaO as low-cost solid base catalysts for transesterification of oil to biodiesels with yields above 96%. Betiku and Ajala (2014) also used a solid catalyst obtained from waste plantain peels calcined at 500 ^{o}C for 3.5 h as direct basic heterogeneous catalyst to transesterify pretreated yellow oleander (*Thevetia peruviana*) oil to biodiesel with a yield > 95% (w/w) at RSM optimized conditions of methanol/oil ratio (0.3 v/v), reaction time (1.5 h), and calcined plantain peels catalyst (3.0 w/v).

Table 2.15: Methods of viscosity reduction in vegetable oils for biodiesel production (Adapted from Boro et al., 2012)

Methods	Definition	Advantages	Disadvantages
Pyrolysis or thermal cracking	Method of conversion of one substance into another by application of heat with the aid of the catalyst in the absence of air or oxygen	1.Lower processing cost, compatibility with infrastructure, engines and fuel standards, and feed stock flexibility 2.The final products are similar to diesel fuel in composition	Energy intensive
Micro-emulsions	A micro-emulsion is a colloidal equilibrium dispersion of optically isotropic fluid microstructures with dimensions generally in the range of 1–150 and spontaneously formed from two normally immiscible liquids and one or more ionic or non-ionic amphiphiles.	1. Fuel viscosity is lowered 2. They can improve spray characteristics by explosive vaporization of the low boiling constituents in the micelles	Lower cetane number and energy content
Direct use and blending	Either use vegetable oil directly or is blended with diesel	Liquid nature and portability. Heat content ~80% of diesel fuel) readily available; renewability	1. Higher viscosity 2. Lower volatility 3. The reactivity of unsaturated hydrocarbon chains
Transesterification	Transesterification (also called alcoholysis) is the reaction of a fat or oil with an alcohol to form esters and glycerol	Renewability; higher cetane number; lower emissions; higher combustion efficiency	Glycerol disposal and waste water problem

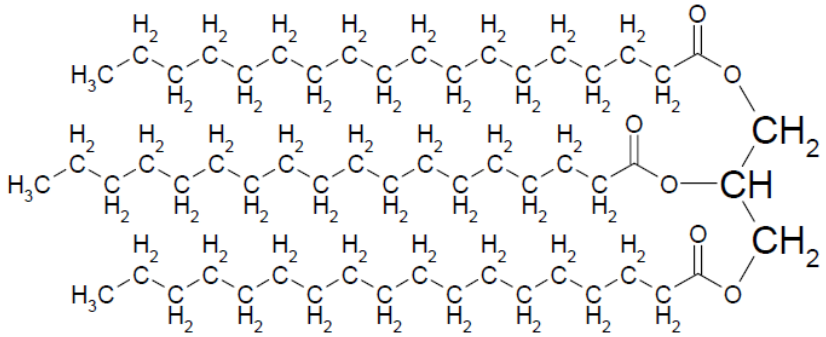


Figure 2.10: A typical structure of a triglyceride molecule

2.15.1 Biodiesel feedstock

Lipids and simple alcohols are the main feedstock required for the production of biodiesel. There are over 350 oilseed crops identified worldwide as sources of lipids suitable for biofuels (Ashraful et al., 2014). Lipids can also include animal fats, and more recently, micro-algae and cyanobacteria (Kings et al., 2017). Over 95% of biodiesel are sourced from edible vegetable oils that are regionally based: rapeseed and sunflower in European countries and Canada; soybean oil in United States; palm oil in tropical countries such as Indonesia and Malaysia; coconut oil in the Philippines (Bankovic-Ilic et al., 2012; Ashraful et al., 2014). Several researchers have reported that the cost of biodiesel depends on the feedstock that accounts for about 60-95% (Ashraful et al; 2014; Morshed et al., 2011). The debate over the food versus fuel crisis on the use of edible oils for biofuel production simulated research into the use of non-edible and used oils as a veritable source of raw material for biodiesel production (Onoji et al., 2016a).

Oil seed bearing plants such as rubber tree, jatropha *curcas*, and karanja just to mention a few have been described as promising sources of non-edible oil for biodiesel production to avert food shortage. The rubber tree with a high seed oil yield (35–60%) and with the potential to generate natural rubber for production of various rubber products placed it at an advantageous position over other non-edible oilseeds (Onoji et al., 2016a; Atabani et al., 2013). The rubber

is the bioenergy crop of the next century considering its versatile use in biofuels and automobile industry.

The most frequently used alcohols for biodiesel production are short-chain alcohols, such as methanol (CH_3OH), ethanol (C_2H_5OH) and butanol (C_4H_9OH). The choice of alcohol depends on cost, sustainability, and performance characteristics (Encinar et al., 2007). In Brazil, for example, ethanol is preferred because it is readily available, cheap and sustainable. In transesterification with ethanol, unreacted ethanol forms an azeotrope that is expensive to purify during recovery. Methanol is much cheaper than ethanol and the literature on biodiesel is replete with methyl esters rather than ethyl esters (Yuan et al., 2008). Methanol is more easily recycled because it does not form an azeotrope. Ethanolysis forms stable emulsions depicting difficulty in product separation and this is contrary to unstable emulsions resulting from methanolysis. The reaction rate is relatively slow with ethanol because the formation of ethoxide anion is more difficult than that of the methoxide (OM Tapanes et al., 2008).

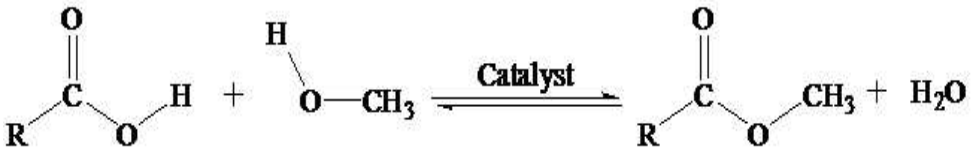
2.16 Catalysis in biodiesel production

Esterification and transesterification reactions are commonly employed in biodiesel synthesis. Vegetable oils that have high content of FFAs will undergo pretreatment process (esterification reactions) to reduce the levels of FFAs to an acceptable limit ($<1\%$) prior to transesterification process with base catalysts.

2.16.1 Acid-catalyzed esterification reaction

This method is suitable for processing biodiesel feedstock with high FFAs and other low-grade oils that are not suitable for direct base transesterification. The catalysts used include sulphuric, hydrochloric, sulfonic and phosphoric acids (Aransiola et al., 2014). However, the downstream processing of huge waste water, high oil/methanol ratio, corrosiveness, catalyst recovery

problem, longer reaction time, and modulate temperatures and pressures are some of its disadvantages. The esterification reaction is a simple reversible reaction as shown in Equation (2.21) (Guo & Fang, 2011). FFA supplies hydroxide and the methanol supplies proton without intermediate process and FFA is converted to ester (biodiesel) and water as a byproduct.



(2.21)

2.16.2 Transesterification of oils using homogeneous catalyst

Transesterification has been widely accepted as the most viable method to produce biodiesel. Transesterification is the chemical reaction of vegetable oils, waste oils, animal fats, or microalgae oils with excess primary alcohol in the presence of a suitable catalyst. The choice of catalyst and biodiesel production route depends on the physicochemical properties of the selected oil. The catalysts used are classified as: homogeneous (acid and base), heterogeneous (acid and base), and enzymes. The triglyceride is converted stepwise to diglyceride and monoglyceride intermediates, and finally to glycerol with biodiesel (FAME) formed at each step (Issariyakul & Dalai, 2014; Thanh et al., 2012; Guo & Fang, 2011) as depicted in Figure 2.11. The breakdown of the triglyceride structure requires three steps:

1. The first step produces an intermediate tetrahedral;

2. The second step involves the breakdown of the unstable intermediate tetrahedral into diglyceride ion and fatty acid ester (biodiesel), and;

3. The final step that involves the recovery of the catalyst by proton transfer.

The three mechanisms are repeated for cleavage of each fatty acid ester and then finally, three fatty acid esters (biodiesels) and a glycerol is formed as shown in the overall Equation (2.22) (Thanh et al., 2012).

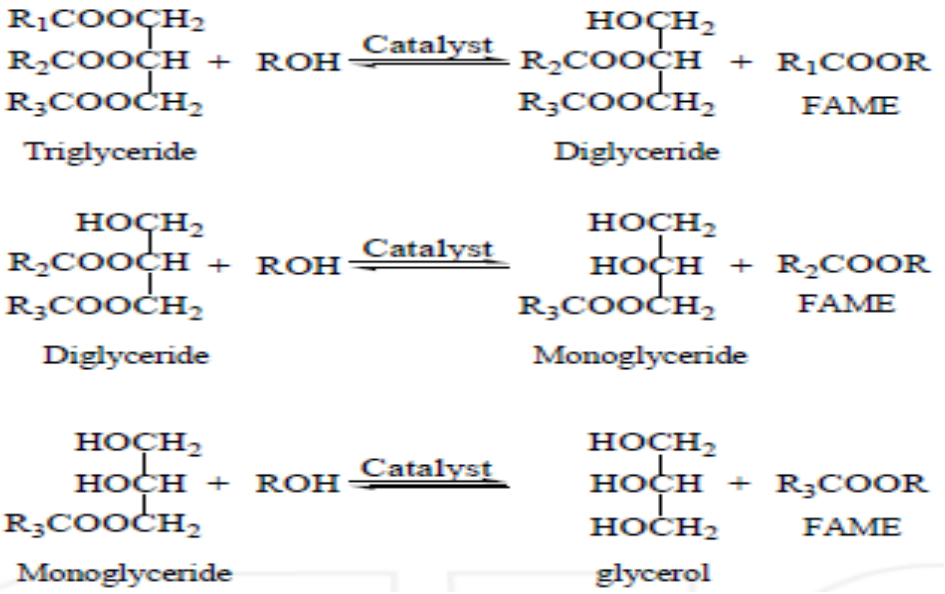
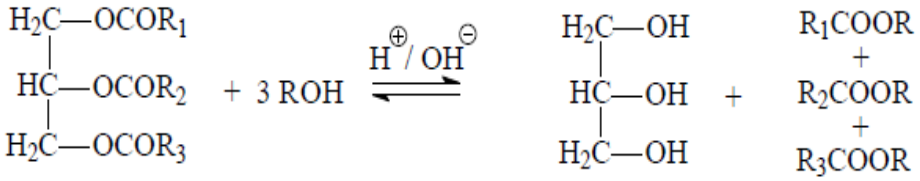


Figure 2.11: Scheme for stepwise transesterification of triglyceride to methyl esters (Adapted from Guo & Fang, 2011)



where R, R_1, R_2 and R_3 are alkyl groups. (2.22)

2.16.2.1 Alkali-catalyzed transesterification reaction

Hydroxides and alkoxides of alkaline metals as well as the carbonates of sodium and potassium metals catalyze these reactions. The process is widely used in the laboratory, pilot and industrial scale levels. The catalysts show a very high performance when the feedstock have low content of FFAs such as edible vegetable oils of rapeseed, soybean, sunflower etc. However, the shortcomings of this method such as energy intensive, glycerol recovery problems, corrosiveness, and food-fuel crisis, have generated debates about their use in different form in the past few years.

2.16.2.2 Two-step transesterification reaction

The method involves acid-catalyzed esterification followed by alkali-catalyzed transesterification, and useful for processing high FFAs feedstock to biodiesel. It is a combination of the process as described in Section (2.16.1), followed by a second step, alkali-catalyzed transesterification, as described in Section (2.16.2.1) (Betiku & Ajala, 2014).

2.16.2.3 Mechanisms for homogeneous catalysis

Homogeneous catalysts used for oil transesterification are either acid or base, and usually in liquid form. The protonation of the carbonyl group in the triglyceride molecule and the alcohol attacking the protonated carbon to create a tetrahedral intermediate form the basis of acid catalysis (Aransiola et al., 2014). However, in a homogeneous-base catalyzed reaction, the creation of nucleophilic alkoxides from the alcohol to attack the electrophilic part of the carbonyl group of the triglycerides forms the basis of the reaction. The mechanisms for acid-catalyzed and base-catalyzed are well documented in the literature (Thanh et al., 2012). These reactions demonstrate the conversion of triglyceride into diglyceride. The reaction mechanisms of diglyceride and monoglyceride, which convert into monoglyceride and glycerol, respectively, take place in the same way as for triglyceride. The overall reactions were earlier shown in Equation (2.22).

2.16.3 Transesterification of oils using heterogeneous catalysts

Solid catalysts of acid and base origins are known as heterogeneous catalysts. They were developed to overcome the limitations of homogeneous catalysts, although they have similar mechanisms to the homogeneous type. Aransiola et al. (2014) report various types of heterogeneous catalysts and their preparatory methods in their review paper.

2.16.3.1 Heterogeneous acid transesterification reaction

Heterogeneous acid catalysts have ability to catalyze both esterification and transesterification reactions simultaneously, and are less corrosive, less toxic, and generate fewer environmental problems (Zhang et al., 2011), and thus produce a low-cost biodiesel that is competitive with commercial diesel. The acids contain variety of acid sites with different strengths of Brönsted or Lewis acidity as compared to homogeneous acid catalysts despite their lower activity (Aransiola et al., 2014; Thanh et al., 2012). At low temperature, the activity of acid catalysts in transesterification is normally quite low, and to obtain a sufficient reaction rate, it is necessary to increase the reaction temperature (> 170 ^{o}C) and this could increase the capital costs thus the cost of biodiesel (Di Serio et al., 2008). Several solid acid-catalysts such as Nafion-NR50, acid ion-exchange resins, sulfated zirconia (SZ), tungstated zirconia (WZ), supported acid catalysts (with metal oxides as supports), zeolite-based catalyst (e.g., zeolite β, HYzeolite) and heteropoly acids have been reported in the literature for the transesterification of oil to biodiesel with good yields.

The mechanism of solid acid-catalyzed esterification reaction consists of the following steps: Firstly, solid catalysts provide protons, and carbonyl carbon is protonated. This is followed by nucleophilic attack of CH_3OH on the carbonium ion to form a tetrahedral intermediate. The last stage involves the migration and reformation of proton with the breakdown of intermediate to produce biodiesel (Guo & Fang, 2011). As discussed in Section (2.16.2), three consecutive reactions are required to complete the transesterification of a triglyceride molecule. The mechanisms of solid acid-catalyzed transesterification of triglycerides show that triglycerides are protonated at the carbonyl group on the surface of the catalyst. A nucleophilic attack by the alcohol forms an unstable tetrahedral intermediate that leads to proton migration, followed by breakdown of the tetrahedral intermediate with the assistance of solvent. After twice repetitions, three new esters products are produced and the catalyst regenerated. During the

catalytic process, protonation of carbonyl group boosts the catalytic effect of solid-acid catalysts by increasing the electrophilicity of the adjacent carbonyl carbon atom (Guo & Fang, 2011). Issariyakul & Dalai (2014) presented the mechanisms of solid acid-catalyzed reactions for both esterification and transesterification in a more compacted form. In the esterification process, free fatty acid initially adsorbs on the active acid site of the catalyst that leads to carbonation during their interaction. This is followed by an attack of methanol to produce an unstable tetrahedral intermediate that finally leads to the removal of water molecule to produce methyl ester (biodiesel). The reaction mechanism for the transesterification part occurs in a similar manner to that of esterification. The formation of methyl ester stems from an elimination of diglyceride, monoglyceride, and glycerol from the tetrahedral intermediate when triglyceride, diglyceride, and monoglyceride are adsorbed in the acidic site, respectively.

2.16.3.2 Heterogeneous base transesterification reaction

The use of heterogeneous base catalyst has received a wider research attention over the last decade. Such catalysts are known to transesterify low-quality oils with moderately high FFAs and water contents. Though low in catalytic activity, their performance could be improved by simple calcinations process. Heterogeneous base catalysts are available in different forms such as hydrotalcites, metal oxides, mixed-metal oxides, metallic salts, supported-based catalyst and base zeolites to mention a few (Guo & Fang, 2011). They can be generated from low-cost waste materials such as eggshell (Piker et al., 2016), plantain peels (Betiku & Ajala, 2014) and animal bones (Nisar et al., 2017) with their catalytic activity enhanced by calcinations. Hydrotalcites (HTs) are a class of anionic and basic clays known as layered double hydroxides (LDHs) with the formula $Mg_6Al_2(OH)_{16}CO_3.4H_2O$. HTs consist of positively charged brucite-like layers and interstitial layers formed by CO_3^{-2} anions and water molecules compensate the positive charge resulting from the substitution. LDHs have strong alkali sites and high stability with good

adjustability of composition and structure (Guo & Fang, 2011). Metal oxides are composed of cations possessing Lewis acid and anions with Brönsted base. They are classified as single metal oxides (e.g., CaO, MgO and SrO) and mixed metal oxides (e.g., A-B-O type metal oxides, where A is alkaline-earth metal (Ca, Ba, Mg), alkaline metal (Li) or rare earth metal (La) and B is a transition metal (Ti, Mn, Fe, Zr, Ce) (Kawashima et al., 2008; Liu et al., 2008). Reports on the use of inorganic solid bases (metallic salts) are rare in literature, although such materials are easy-to-use and could be sourced from low-cost materials. Available reports indicate that sodium silicate, vanadyl phosphate, calcium zincate and calcium methoxide have been investigated as heterogeneous catalysts for biodiesel synthesis with yield of almost 100% under certain conditions (Guo & Fang, 2011).

Alkali metals (Li, Na, K) and alkaline-earth metals (Mg, Ca, Ba) are the most common sources of super basicity, and selected as the active species of supported solid base catalysts for biodiesel synthesis. They are frequently used in the metallic form or as various ionic forms of hydroxide, halide, carbonate and nitrate. Alumina, silica, zinc oxide, zirconium oxide and zeolite have been used as supports for these catalysts (Issariyakul & Dalai, 2014; Guo & Fang, 2011) in their preparation by impregnation followed by calcinations. The reaction mechanism pathway for solid base-catalyzed transesterification seems to follow a similar mechanism to that of a homogeneous base catalyst. First, ion exchange proceeded after methanol adsorbed on the surface of solid base, producing active specie (CH_3O^-) which is strongly basic and highly active. Secondly, nucleophilic attack of CH_3O^- on the carbonyl carbon of triglyceride formed a tetrahedral intermediate. Thirdly, rearrangement of the intermediate results in the formation of ester (biodiesel). Finally, protons are converted to diglyceride ion to generate diglyceride. This sequence is then repeated twice to yield glycerol and biodiesel.

2.16.4 Enzyme-catalyzed transesterification reaction

Lipases as enzyme-catalysts for biodiesel synthesis have been classified as environmentally friendly approach to solving energy problems. This new area of research seems to overcome the challenges of using conventional catalysts-feedstock pretreatment, high energy requirements, catalyst removal problems and waste water treatment (Aransiola et al., 2014). Lipases as biocatalysts can be classified as: extracellular lipases and intracellular lipases, and are produced by microorganisms, animals and plants (Gog et al., 2012; Antczak et al., 2009). The main drawbacks of lipase-catalyzed transesterification reaction are the high cost of enzyme production, higher reaction times as compared to base-catalyzed reaction, potential hazard of explosion, regeneration and reuse of biocatalyst limited with a long operating time. However, in order to reduce cost of operation and improve catalyst stability and reusability, lipases can be immobilized on several materials (Modi et al., 2007; Noureddini et al., 2005), and have been characterized by high selectivity and efficiency, absence of side reactions, and high yield of biodiesel (Koh et al., 2011; Dizge & Keskinler, 2008).

2.16.5 Heterogeneous catalyst from natural sources

Sourcing for sustainable heterogeneous catalysts derived from waste biomass materials and other natural sources as alternative to conventional heterogeneous catalysts of chemical origin is a promising area of research (Aransiola et al., 2014). The conventional heterogeneous catalysts (acid or base) require high synthesis cost, and sometimes-expert skills are required for processing them. Therefore, sourcing for solid base catalysts from biomass could reduce the cost of biodiesel and serve as a platform for converting waste to wealth. Betiku and Ajala (2014) obtained 95% yield of yellow oleander oil biodiesel with calcined biomass (waste plantain peels) as solid base catalyst. In addition, the catalytic activity of CaO obtained from natural and biological waste materials such as eggshell, limestone calcite, dolomite and animal

bones through calcinations has been investigated as solid base catalysts for oil transesterification (Nisar et al., 2017; Piker et al., 2016).

2.17 Transesterification of rubber seed oil

Transesterification reaction is a process generally employed to produce fatty acid mono-alkyl ester (FAME) popularly called biodiesel when vegetable oil or animal fats reacts with excess short-chain alcohol (in this case, methanol) in the presence of a suitable catalyst (acid, base or enzymes) with glycerol as by-product (Onoji et al., 2016a). The free fatty acids (FFAs) and moisture contents of the oil/fats determine the choice of the catalyst. The transesterification processes available in literature for rubber seed oil biodiesel production are conventional method, in-situ, enzymatic, supercritical, co-solvent, ultrasonic-assisted, and microwave-assisted. Several factors such reaction time, temperature, FFAs and moisture contents, pressure, capital cost, catalyst type and reagents determine the applicable method of production. Edible vegetable oils with low FFA (<1 wt. %), commonly employ homogeneous base catalysts such as NaOH and KOH. Homogeneous base catalyst will form soap during transesterification of rubber seed oil with simple alcohols because of its high FFA. In a 2-step process, esterification reaction of rubber seed oil with excess alcohol in the presence of homogeneous acid catalyst (H_2SO_4) will reduce the FFA content. The esterified oil is transesterified with homogeneous base catalyst to produce a higher yield of rubber seed oil's biodiesel and glycerol as waste. However, the downstream processing of the biodiesel to recover the catalyst and other waste products possess challenges to industrialists with the attendant high capital costs. Heterogeneous catalyst that catalyzes both esterification and transesterification reactions is seen as a better option for high FFA oils. They are stable, active at low temperature, have high selectivity, relatively cheap and could be locally sourced (Di Serio et al., 2008).

2.18 Transesterification methods for rubber seed oil

The transesterification methods available for biodiesel production from RSO are conventional, in-situ, enzymatic, supercritical, co-solvent, ultrasonic-assisted and microwave-assisted.

2.18.1 The conventional method

The common conventional homogenous base catalysts for RSO transesterification reaction are NaOH, KOH, carbonates and the alkoxides of Na and K (Ahmad et al., 2014a; Ibrahim & Pillai, 2011) with biodiesel yields ranging from 86.7-97.8 wt.%. Homogeneous acid catalysts such as H_2SO_4, HCl, and H_3PO_4 are used for RSO esterification (pre-treatment) process prior to transesterification reaction (Ahmad et al., 2014b, Ahmad et al., 2014c; Bokhari et al., 2014). Heterogeneous catalysts such as cation exchange resin, solid metal oxides and their silicates are tolerant to high FFAs RSO and can be used several times without much loss to activity (Omorogbe et al., 2013). Gimbun et al. (2012) used lime-based catalyst derived from cement clinker to obtain 96.9 wt. % yield of biodiesel from high FFA RSO. Krishnakumar et al. (2013) synthesized biodiesel from rubber seed oil with solid CaO catalyst calcined at 850 ^{o}C for 1.5 h and reported a yield of 98 wt. %.

2.18.2 The in-situ method

This involves contacting the raw-milled seed directly with the alcohol in the presence of a catalyst (acid/alkali) instead of the pre-extracted oil. The advantages of the process include reduced reaction time, higher yield, smaller wastewater formation and lower consumption of reagents (Ma & Hanna, 1999). Abdulkadir et al. (2014) and Widayat et al. (2013) employed in-situ method and obtained optimum biodiesel yields of 75 wt. % and 91.05 wt. percentage respectively during RSO transesterification.

2.18.3 The enzymatic method

This method uses enzymes such as lipases as biocatalysts. Though characterized by low reaction rates, when the enzymes are immobilized, they can be re-used several times (Ma & Hanna, 1999). The process is FFA friendly and the milder conditions allowed biodiesel yield of at least 90% (Awolu & Layokun, 2013) and can be used to transesterify rubber seed oil to biodiesel.

2.18.4 The supercritical method

This process is tolerant to high FFA and moisture content and recommended by researchers for variety of feeds such as rubber seed oil and waste vegetable oils (Sanjel et al., 2014). Under the supercritical conditions, the alcohol becomes "super acid" thereby eliminating the use of catalyst creating a single phase with low reaction time (2-4 min) and low mass transfer limitations are reduced. The high temperature (300–400 ^{o}C), high pressure (80–100 atm) and high molar alcohol/oil ratio (42:1) are some of its inherent disadvantages (Thanh et al., 2012).

2.18.5 The co-solvent assisted method

This is a new greener biotechnological method because of minimum waste generation and low energy demand. The co-solvent creates a single phase that gives rise to increased reaction rates within a short time. Among the researched co-solvents such as tetrahydrofuran (THF), 1-4-dioxane, acetone and di-ethyl ether, THF was the first reported co-solvent used for biodiesel production (Thanh et al., 2012).

2.18.6 The ultrasonic-assisted method

The immiscibility of alcohol and vegetable oils hinders mass transfer rates between the phases. This limits the reaction rates and the yield of biodiesel (Guo & Fang, 2011). Widayat and Kiono

(2012) employed ultrasonic-assisted technology in the extraction and transesterification of rubber seed oil simultaneously to biodiesel at 40 ^{o}C and 40 Hz. A developed model equation for the transesterification step based on response surface methodology shows that ultrasound could reduce process time and increase biodiesel yield significantly.

2.18.7 The microwave-assisted method

This is an alternative heating method to the conventional method of heating because the microwave energy selectively energizes the catalyst's interaction with the reactants (Hincapie et al., 2014; Di Serio et al., 2008). Microwave is non-ionizing radiations with low energy. The changing electrical field component of microwave radiation interacts with the dipoles of the reactants molecules increasing their rotations. This reflects an increase in reaction rates and higher biodiesel yield in shorter time, as compared to conventional systems heating (Hincapie et al., 2014; Guo & Fang, 2011).

2.19 Factors affecting the transesterification of rubber seed oil

Transesterification of rubber seed oil to synthesize biodiesel is affected by number of factors. The parameters considered in this thesis are as follows:

2.19.1 FFA content of rubber seed oil

The FFA content of rubber seed oil is reportedly high with the range 23.471–45 wt. % (Ahmad et al., 2014a; Omorogbe et al., 2013; Ebewele et al., 2010b). The reduction of FFA values of crude rubber seed oil is significant to avoid soap formation and downstream processing problems when a homogeneous base catalyst is used in transesterification reaction (Ibrahim & Pillai, 2011). Homogeneous acid catalyst such as H_2SO_4 is employed in esterification of the oil with alcohol to reduce the FFA to less than 1 wt.% prior to transesterification. Catalyst

concentration followed by alcohol/oil ratio is the most influential parameters compared to reaction temperature and time (Ahmad et al., 2014b).

2.19.2 Alcohol/oil molar ratio

Alcohol/oil molar ratio is one important variable that affects the yield of biodiesel. The stoichiometric ratio for transesterification requires three moles of alcohol and one mole triglyceride to yield three moles of fatty acid esters and one mole of glycerol (Ma & Hanna, 1999). The molar ratio depends on the catalyst type and may be as high as 30:1 for acid catalyzed reaction and 6:1 for base reaction for butanol-soybean oil (Freedman et al., 1986). Various researchers (Bokhari et al., 2014; Ahmad et al., 2014b; Abdulkadir et al., 2014) reported a 6:1 molar alcohol/oil ratio for maximum biodiesel yield of 75–96.8 wt. % when homogeneous catalyst such as KOH is employed for rubber seed oil transesterification. Ahmad et al. (2014b) observed that alcohol/oil molar ratio is the most influencing factor in rubber seed oil biodiesel production up to certain limit, beyond which the amount of methanol has no effect on the biodiesel yield while a higher methanol concentration may result to downstream processing problems.

2.19.3 Catalyst concentration

Different catalyst loadings for the successful transesterification of rubber seed oil to biodiesel have been reported in the literature. Gimbun et al. (2012) reported an optimum 6 wt. % with a yield of 92.3% using a limestone-based catalyst for rubber seed oil transesterification. Optimal conditions such as catalyst loading, calcination temperature and time are usually determined through optimization process (Ahmad et al., 2014a; Ahmad et al., 2014c). Catalyst loading was reported the second most influencing factor that determines higher of biodiesel (Ahmad et al., 2014b; Widayat & Kiono, 2012). The physical appearances of rubber seed oil biodiesel are

determined by the concentration of the catalyst with higher concentration giving rise to a darker colour (Widayat et al., 2013). Dhawane et al. (2015) studied the influence of using flamboyant pods derived steam activated carbon as catalyst (0.5–5 wt.%) on the transesterification of rubber seed oil at 60 ^{o}C, 15:1 methanol/oil ratio, 750 rpm, and 60 min reaction time. they reported a maximum FAME yield of 89.3% at catalyst loading of 3.5 wt.%. Further increase in catalyst concentration decreases the yield due to soap formation during the reaction, viscous and emulsified reaction mixture at higher catalyst loadings.

2.19.4 Reaction temperature and time

Generally, increase in temperature increases the rate of a chemical reaction and the yield of rubber seed oil biodiesel (Abdulkadir et al., 2014; Gimbun et al., 2012). Dhawane et al. (2015) reported 60 ^{o}C as most desirable temperature for transesterification reaction when methanol is used. Gimbun et al. (2012) observed that increasing the temperature above the boiling point of methanol (65 ^{o}C) to about 70 ^{o}C reduces the yield from 96.9 to 95.8 wt. % when rubber seed oil was transesterified with derived CaO as a base catalyst. The decrease yield is explained by the evaporation of methanol when reaction temperature is above 65 ^{o}C. Most work cited in literature suggests that 1 h reaction time is sufficient for the completion of a transesterification reaction with base catalyst. Solid catalyst leaching may increase may increase when a higher reaction time is considered (Dhawane et al., 2015).

2.19.5 Agitation speed

Agitation speed plays significant role in the esterification and transesterification of vegetable oils to esters because of mass transfer limitations imposed by the immiscibility of the reaction mixtures. Dhawane et al. (2016) in their study reported the influence of agitation speed on the optimization of Iron (II) doped carbonaceous catalyst for biodiesel production from rubber seed

oil at 12:1 methanol/oil ratio, 55 ^{o}C, and 1 h reaction time. They observed that at 500 rpm, the yield was 94.5%, and subsequently decreases to 85.01% at 750 rpm that was attributed to the leaching of the adsorbed Iron (II) from the surface into the reaction mixture. Further reduction in yield to 75.34% was reported when agitation speed increases to 100 rpm.

2.20 Thermodynamics of internal combustion ignition engines

The reaction paths for complex fuel mixtures such as diesel, biodiesel or gasoline are not well defined compared to the actual path of combustion process for simple fuels such as hydrogen and methane. However, the first and second laws of thermodynamics can be applied to analyze the combustion performance of internal combustion ignition engines. First law of thermodynamics can be used to relate the end states of mixtures undergoing a combustion process, and its application does not require the details of the process as it fails to give the best insight into the engine's operation (Abassi et al., 2010). Energy balance on the cylinder is made with the aim of obtaining power and efficiency using first law. Otto and Diesel cycles are the common methods applied to analyze the performance of engines using the first law.

2.20.1 Overview of reciprocating engines

A reciprocating engine also called internal combustion ignition engine is a piston cylinder device (Figure 2.12) that has a wide range of applications in automobiles, truck, light aircraft, ships, and electric power generators. The piston reciprocates in the cylinder between two fixed positions, known as the top dead center (*TDC*) and the bottom dead center (*BDC*). The TDC is the position of the piston when it forms the smallest volume in the cylinder, while the *BDC* is the position of the piston when it forms the largest volume in the cylinder (Çengel & Boles, 1994). The distance between the *TDC* and BDC is the largest distance that the piston can move in one direction, and it is called the stroke of the engine. The diameter of the piston is called

the bore. The air or air-fuel mixture is drawn into the cylinder through the intake valve, and the combustion products expelled from the cylinder through the exhaust valve. The minimum volume formed in the cylinder when the piston is at *TDC* is the clearance volume, while the volume displaced by the piston as it moves between *TDC* and *BDC* is the displacement volume. The ratio of the maximum volume formed in the cylinder to the minimum (clearance) volume is the compression ratio (r) of the engine (Çengel & Boles, 1994):

$$r = \frac{V_{\max}}{V_{\min}} = \frac{V_{BDC}}{V_{TDC}} \tag{2.23}$$

Reciprocating engines are classified as either compression-ignition (CI) engines (e.g., diesel engine) or spark-ignition (SI) engines (e.g., petrol engine) depending on how the combustion process is initiated. They operate as either four-stroke or two-stroke internal combustion engines depending on designs.

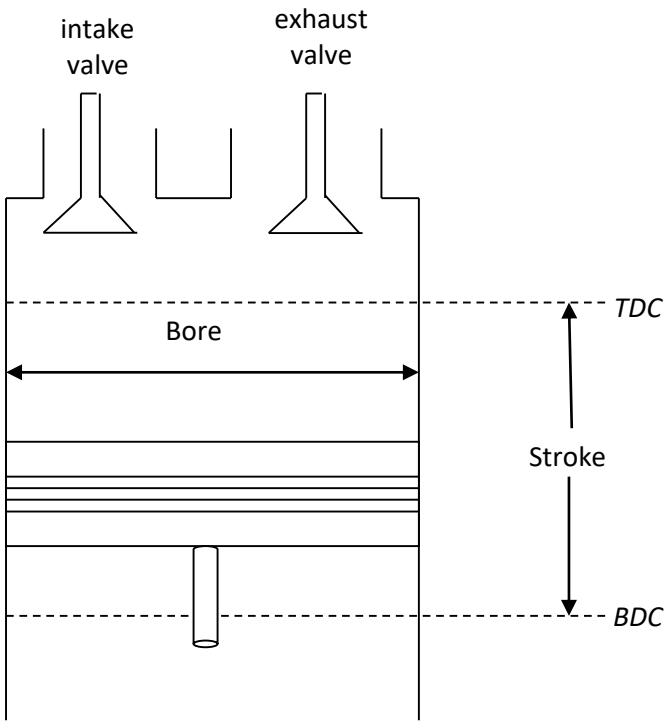


Figure 2.12: Schematic diagram for a reciprocating engine cylinder (Adapted from Çengel & Boles, 1994)

2.20.2 Air-standard assumptions

The working fluid remains a gas throughout the entire cycle in the gas power cycle. Compression-ignition (diesel), spark-ignition (petrol), and the conventional gas turbine engines are devices that operate on gas cycle. During the combustion process, the composition of the working fluid changes from air and fuel to combustion products during the course of the cycle. The working fluid closely resembles air at all times because air is predominantly nitrogen that hardly undergoes chemical reactions in the combustion chamber. The working fluid is expelled as exhaust gases instead of returning to its initial state at a point in the cycle. This tells us that the working fluid does not undergo a complete thermodynamic cycle, though internal combustion engines operate on a mechanical cycle (i.e., the piston returns to its starting position at the end of each revolution). To simplify the analysis of actual gas power cycles, the following air-standard assumptions are usually applied:

- ✓ The working fluid is air. It circulates continuously in a closed loop, and behaves as an ideal gas,
- ✓ All the processes which make up the cycle are internally reversible,
- ✓ The combustion process is replaced by a heat addition process from an external source,
- ✓ A heat rejection process that restores the working fluid to its initial state replaces the exhaust process.

The air-standard assumption is called the cold-air standard assumption if the air has constant specific heats whose values are determined at room temperature (25 ^{o}C). This simplified model enables us to study qualitatively the influence of major parameters on the performance of the actual engines (Çengel & Boles, 1994).

2.20.3 Diesel cycle-The ideal cycle for compression ignition engines

The Diesel cycle (Figure 2.13) is the ideal cycle for CI reciprocating engines. The CI engine, first proposed by Rudolf Diesel in the 1890s is very similar to the SI engine. In SI engines, the air-fuel mixture is compressed to a temperature below the auto-ignition temperature of the fuel, and the combustion process is initiated when a spark plug is fired (Çengel & Boles, 1994). In CI engines, only air is compressed to a temperature above the auto-ignition temperature of the fuel, and combustion starts on contact as the fuel is injected into the hot air. Therefore, a fuel injector in diesel engines replaces the spark plug and carburetor. In gasoline engines, a mixture of air and fuel is compressed during the compression stroke, and the compression ratio is limited by the onset of auto-ignition or engine knock. In diesel engines, only air is compressed during the compression stroke, thereby eliminating the possibility of auto-ignition. Therefore, diesel engines can be designed to operate at much higher compression ratios, typically between 12 and 24 (Çengel & Boles, 1994).

The fuel injection process in diesel engines starts when the piston approaches *TDC* and continues during the first part of the power stroke. Therefore, the combustion process in these engines takes place over longer intervals and thus, diesel cycle is approximated as a constant-pressure (process 2 → 3) heat addition process. This is the only process where Diesel cycle differs from Otto cycle. The remaining three processes are the same for both ideal cycles (processes 1 → 2, 3 → 4, and 4 → 1). Diesel cycle, like the Otto cycle, is executed in a closed system (piston-cylinder).

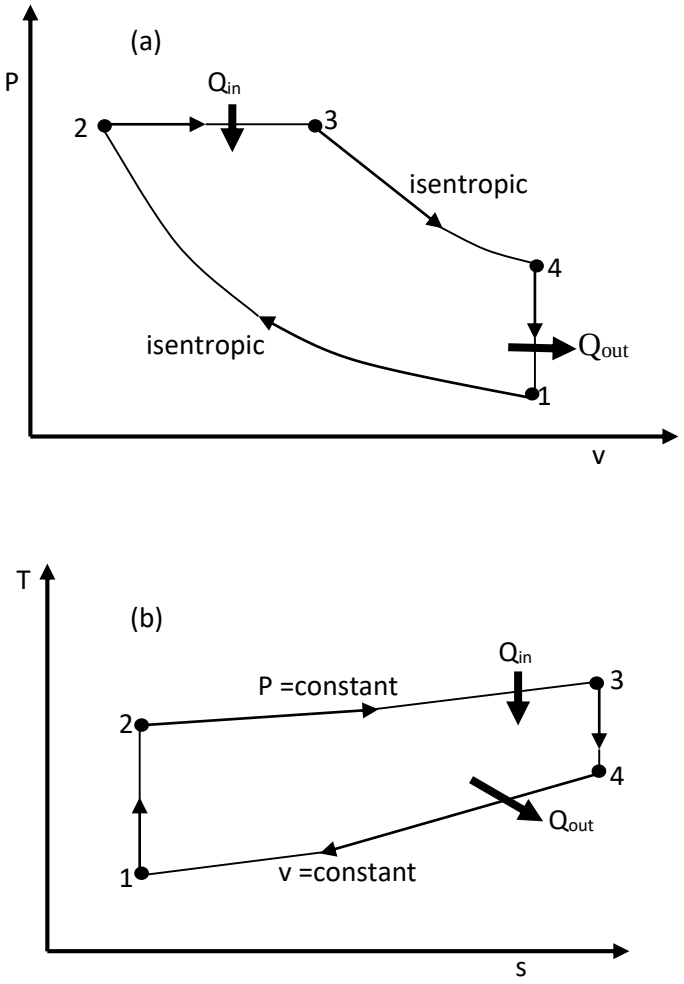


Figure 2.13: P–v (a) and T–s (b) diagrams for the ideal Diesel cycle (Adapted from Çengel & Boles, 1994)

Under the cold-air standard assumptions, the amount of heat added to the working fluid at constant pressure and rejected at constant volume can be expressed as:

$$Q_{in} = Q_{2\to3} = W_{2\to3} + (\Delta U)_{2\to3} = P_2(v_3 - v_2) + (U_3 - U_2) \tag{2.24}$$

$$Q_{in} = h_3 - h_2 = C_p(T_3 - T_2) \tag{2.25}$$

$$Q_{out} = -Q_{4\to1} = -W_{4\to1} - (\Delta U)_{4\to1} = U_4 - U_1 = C_v(T_4 - T_1) \tag{2.26}$$

$$W_{4\to1} = 0 \tag{2.27}$$

The thermal efficiency of the ideal diesel cycle under the cold-air standard assumptions becomes:

$$n_{th,Diesel} = \frac{W_{net}}{Q_{in}} = 1 - \frac{Q_{out}}{Q_{in}} = \frac{T_4 - T_1}{\gamma(T_3 - T_2)} = 1 - \frac{T_1\left(\frac{T_4}{T_1} - 1\right)}{\gamma T_2\left(\frac{T_3}{T_2} - 1\right)} \tag{2.28}$$

where $\gamma = \frac{C_p}{C_v}$, the specific heat ratio and equal to 1.4 for ideal gas (Azoumah et al., 2009).

If (r) is defined as the engine's compression ratio and (r_c) represents the cutoff ratio, expressed as the ratio of the cylinder after and before the combustion process, then Equation (2.28) can be expressed as (Azoumah et al., 2009):

$$n_{th,Diesel} = 1 - \frac{1}{r^{\gamma-1}}\left[\frac{r_c^{\gamma} - 1}{\gamma(r_c - 1)}\right] \tag{2.29}$$

where $r = \frac{V_1}{V_2}$, and $r_c = \frac{V_3}{V_2}$; V_1 is the maximum volume, and V_2 represents the clearance volume as earlier discussed.

The combustion chamber temperature (T_3) under ideal conditions can be evaluated from the measured exhaust gas temperature (T_4) by the relation (Azoumah et al., 2009):

$$T_3 = T_4\left(\frac{r}{r_c}\right)^{\gamma-1} \tag{2.30}$$

The compression stroke (process 1 → 2) is assumed an isentropic process, and the following equations used to determine the pressure and temperature at stage 2.

$$T_2 = T_1\left(\frac{V_1}{V_2}\right)^{\gamma-1} \tag{2.31}$$

$$P_2 = P_1\left(\frac{V_1}{V_2}\right)^{\gamma} \tag{2.32}$$

Process 2 →3 ($P =$ constant heat addition to the air-fuel mixture, i.e. $P_2 = P_3$):

$$\frac{P_2 V_2}{T_2} = \frac{P_3 V_3}{T_3} \tag{2.33}$$

$$T_3 = T_2 \left(\frac{V_3}{V_2} \right) \tag{2.34}$$

Process 3 → 4 (isentropic expansion of the combustion gases):

$$T_4 = T_3 \left(\frac{V_3}{V_4} \right)^{\gamma - 1} \tag{2.35}$$

$$P_2 = P_3 \left(\frac{V_3}{V_4} \right)^{\gamma} \tag{2.36}$$

Process 4 →1 (constant-volume heat rejection process with no work interactions is shown in Equations (2.26) and (2.27), respectively.

The mean effective pressure (MEP) is determined as:

$$MEP = \frac{W_{net}}{V_{\max} - V_{\min}} = \frac{W_{net}}{V_1 - V_2} \tag{2.37}$$

2.20.4 Mathematical models for internal compression ignition engines

The analysis of the performance of internal compression ignition (diesel) engines based on the second law of thermodynamics is made possible by first-law mathematical modeling of the various processes inside the cylinder and its subsystems. Examples of such mathematical models include zero-dimensional models also referred to as single-zone models, two-zone, four-zone or multi-zone models (Rakopoulos & Giakoumis, 2006). The single-zone model assumes the working fluid in the engine to be a thermodynamic system (mixture of gases) that undergoes energy and mass exchange with the surroundings, and the energy released is computed using first law of thermodynamics. In the two-zone models, the working fluid in the engine is split into two zones (burned and unburned gases) that are analyzed separately (Hago

& Morin, 2010; Rakopoulos & Giakoumis, 1997). Computer simulations of internal combustion engine cycles have been of tremendous use in design studies, as diagnostic tools in analyzing data obtained from experiments, and in understanding the complex processes occurring in the combustion chamber. Quasi-dimensional model, a double-zone model has been the most frequently used model because it predicts the performance of the engine better than the single zone models (Rakopoulos & Giakoumis, 1997).

As discussed above, the Diesel cycle is useful for analyzing diesel engine's performance. The compression stroke of Diesel engine can be simulated from the following equations based on ideal gas behaviour.

$$PV = nRT \tag{2.38}$$

$$\frac{dp}{d\theta} = \frac{1}{V}\left[-\left(1+\frac{R}{C_v}\right)P\frac{dv}{d\theta} - \frac{R}{C_v}\right] \tag{2.39}$$

The volume of the cylinder at any crank angle (θ) can be defined as (El-Seesy et al., 2017; Heywood, 1988):

$$V = V_c\left[1+\frac{1}{2}(r_c-1)\left[\beta+1-Cos\theta-\left(\beta^2-Sin^2\theta\right)^{0.5}\right]\right] \tag{2.40}$$

$$\beta = \frac{l}{\alpha} \tag{2.41}$$

where V_c = clearance volume as earlier defined, r_c = cutoff ratio, l = connecting rod length (m), and α = crank radius (m).

Differentiating Equation (2.40) with respect to the crank angle (θ) gives:

$$\frac{dV}{d\theta} = V_c\left[\frac{1}{2}(r_c-1)\left[Sin\theta-0.5(-2Sin2\theta)\right]\right] \tag{2.42}$$

The net heat release rate (HRR) in the cylinder during the combustion process using a single-zone combustion model can be determined from the expression described by (Bayindir et al., 2017; Ibrahim, 2016):

$$\frac{dQ}{d\theta} = \frac{\gamma}{\gamma - 1} P \frac{dV}{d\theta} + \frac{1}{\gamma - 1} V \frac{dP}{d\theta} \tag{2.43}$$

The cumulative heat release (CHR) is the integral of HRR over a restricted crank angle (θ) interval that depends on the HRR curve and given as (Guardiola et al., 2017):

$$\int dQ = \int \left(\frac{\gamma}{\gamma - 1} \right) PdV + \int \frac{1}{(\gamma - 1)} VdP \tag{2.44}$$

Where $Q =$ apparent heat release rate (J), $P =$ cylinder pressure (bar), and V instantaneous volume of cylinder (m^3).

Computer software like MATLAB can be used to simulate Equation (2.38) to Equation (2.44) and the results obtained can be compared with those from experiments.

To model the performance of a compression ignition (CI) engine according to the first law of thermodynamics, Rakopoulous & Giakoumis (2006) suggested the following simplifying assumptions:

(a) Spatial homogeneity of pressure for two-zone models;

(b) Spatial homogeneity of temperature for the whole cylinder or for each zone considered;

(c) Working fluid is considered an ideal gas;

(d) Gas properties (enthalpy, internal energy, etc.) are modeled using polynomial relations with temperature (and pressure);

(e) Heat released from combustion is distributed evenly throughout the cylinder;

(f) Blow-by losses are neglected;

(g) Enthalpy associated with pressure of injected fuel is negligible;

(h) Spatially averaged, instantaneous (time resolved) heat transfer rates are used to estimate heat transfer to the cylinder walls;

(i) Dissociation is usually, but not always neglected;

(j) No heat transfer occurs between burned and unburned zones;

(k) Work required to transfer fluid from the unburned zone to the burned zone is negligible.

2.20.5 Models for gas mixture properties

One of the processes that control engine power, efficiency, and emission inside the diesel engine cylinder, is the combustion of fuel-air mixture (Heywood, 1988). The components that make up the working fluid in the engine cylinder such as oxygen, carbon dioxide, carbon monoxide, water vapour, fuel vapour, nitrogen, etc. are treated as ideal gases for simplification in engine performance evaluations.

Thus,

$$PV = \frac{m}{M} RT = nRT \tag{2.45}$$

where $P =$ pressure, $V =$ volume, $m =$ mass of gas, $T =$ temperature, $R =$ universal gas constant, $M =$ molecular weight, and $n =$ number of moles.

The mixture of diesel and biodiesel properties can be determined from individual properties using the following relations:

$$\in_{mix} = \sum_{i=1} \in_i \; x_i \tag{2.46}$$

where $\in_{mix}$ is the property of the mixture, $\in_i$ is the property of pure diesel or biodiesel, and x_i is the fraction of diesel or biodiesel.

Air-fuel ratio is defined by:

$$\left(\frac{A}{F}\right)_{mix} = \sum_{i=1} \frac{\in_i \; x_i}{\in_i \; x_i \left(A/F\right)_i} \tag{2.47}$$

The lower heating value (LHV) of the fuel mixture as given by Bayraktar (2005) is:

$$LHV_{mix} = \frac{\sum_{i=1} \in_i \; x_i \left(LHV\right)_i}{\sum_{i=1} \in_i \; x_i} \tag{2.48}$$

The general chemical reactions occurring in the engine cylinder for diesel/biodiesel blend-air mixture with humid air is approximated by the following reactions (Meisami et al., 2017).

$$aC_{14}H_{25} + bC_{18}H_{34}O_2 + c(O_2 + 3.76N_2 + xH_2O) \rightarrow dCO_2 + eCO + fO_2 + gNO + hNO_2 + iN_2 + jH_2O \quad (2.49)$$

where $O_2 + 3.76N_2 + xH_2O$ is the inlet air entering the combustion chamber.

$$x = 7.655\omega \quad (2.50)$$

$$\omega = 0.622\frac{P_v}{P_a} \quad (2.50\text{-a})$$

where ω represents specific humidity of air, P_v and P_a are the partial pressure of vapour and dry air, respectively, and combustion reaction based on one mole of the fuel $(a + b = 1)$.

Özkan (2015) in a comparative study on energy and exergy analyses of a diesel engine reported a combustion equation for diesel fuel (No. 2) based on Equation (2.49).

$$C_{14}H_{25} + 35.264(O_2 + 3.76N_2) \rightarrow 14.929O_2 + 0.017CO + 14.04CO_2 + 0.00236C_{14}H_{25} + 0.4911NO + 0.0161NO_2 + 132.343N_2 + 12.363H_2O \quad (2.51)$$

2.20.6 First and second laws of thermodynamics for internal combustion engines

Energy analysis of a process is based on the first law of thermodynamics, which embodies the principle of energy conservation. It is a traditional method used to assess the performance and efficiency of energy systems and processes. The first law deals with the quantity of energy and does not fully analyze the performance of internal combustion ignition engine.

According to the first law, the energy balance for steady-state control volume (combustion chamber volume) of the engine is given as:

$$\Delta Q - \Delta W = \Delta H \quad (2.52)$$

where ΔQ represents the heat transfer through the combustion chamber to cooling water and lubrication systems per mole of fuel, ΔW represents the mechanical useful work done by the engine in one cycle per unit mole of fuel, and ΔH represents the enthalpy change between the products $\left(\bar{H}_p\right)$ and reactants $\left(\bar{H}_r\right)$.

Thus,

$$\Delta H = \bar{H}_p - \bar{H}_r \tag{2.53}$$

When we substitute Equation (2.53) into Equation (2.52), we obtain an expression:

$$\Delta Q + \bar{H}_r = \Delta W + \bar{H}_p \tag{2.54}$$

The enthalpy terms can be evaluated from the following equations:

$$\bar{H}_r = \sum_r n_i \left(\bar{h}_f^0 + \Delta \bar{h} \right)_i \tag{2.55}$$

$$\bar{H}_p = \sum_p n_e \left(\bar{h}_f^0 + \Delta \bar{h} \right)_e \tag{2.56}$$

where, n_i and n_e are the moles number of reactants and products, respectively, per mole of fuel obtained directly from the balanced combustion equation, $\bar{h}_f^0$ is the standard enthalpy of formation and $\Delta \bar{h}$ represents the difference in enthalpy between any given state and the enthalpy of ideal gas at 25 ^{o}C and 1 atm.

Introducing Equation (2.55) and Equation (2.56) into Equation (2.54) yields:

$$\Delta Q + \sum_r n_i \left(\bar{h}_f^0 + \Delta \bar{h} \right)_i = \Delta W + \sum_p n_e \left(\bar{h}_f^0 + \Delta \bar{h} \right)_e \tag{2.57}$$

where ΔQ, ΔW, $\bar{H}_r$, and $\bar{H}_p$ are in kJ/kmol of fuel.

The lower heating value (LHV) at constant pressure equals the enthalpy at complete combustion when water is present as a vapour and based on first law, it is described by the relation (Caton, 2000):

$$LHV = -(\Delta H)_{P_0, T_0} = \sum_r n_i \bar{h}_{f,i}^0 - \sum_p n_e \bar{h}_{f,e}^0 \tag{2.58}$$

where $(\Delta H)_{P_0,T_0}$ represents the enthalpy of the combustion at reference dead state pressure (P_0) and temperature (T_0).

The second law of thermodynamics can be used to obtain a model expression for the maximum useful work an engine can deliver, based on the assumption that an internal combustion engine is an open system that exchanges heat and work with its surrounding. Exergy (also called *Availability*) is defined as the maximum amount of useful work that can be obtained by bringing a system to a state of thermodynamic equilibrium (thermal, mechanical, and chemical) with the common components of the environment by means of a reversible process (Peduzzi et al., 2016). Exergy analysis based on the second law of thermodynamics is a thermodynamic analysis technique for systems and processes that deal with the quality of energy. It has been increasingly applied on energy systems over the last few decades because of its advantages over energy analysis based on first law (Abassi et al., 2010; Rakopoulos & Giakoumis, 1997). In evaluating exergy, the characteristics of the reference environment (temperature, pressure, and chemical composition) must be specified. Thus, exergy depends on the properties of the system or process, and the environment. Exergy is not conserved like energy, but destroyed by processes such as combustion, friction, mixing and throttling that decrease the ability of the system to produce useful work (Abassi et al., 2010; Rakpoulos & Giakoumis, 1997). The destruction of exergy, called *irreversibility* is the source of non-maximum conversion of fuel energy into useful mechanical work in a diesel (and Otto) engine. The reduction of irreversibility can lead to better engine performance through a more efficient exploitation of fuel (Rakopoulos & Giakoumis, 2006).

From the second law of thermodynamics, the heat transfer (ΔQ) can be expressed as follows:

$$\frac{\Delta Q}{T_A} \leq \Delta S \tag{2.59}$$

where T_A is the temperature of the surrounding and ΔS is the entropy.

Combining Equation (2.52) and Equation (2.59) results in:

$$\Delta W \leq -\left(\Delta H - T_A \Delta S\right) \tag{2.60}$$

Maximum work is achieved when the pressure and temperature of the products equals that of the atmosphere.

Under these conditions:

$$\Delta W_{\max} = -\left(\Delta G\right)_{P_A, T_A} \tag{2.61}$$

where $\left(\Delta G\right)_{P_A, T_A}$ represents the change in the Gibbs free energy for the conversion of reactants $\left(r\right)$ to products $\left(p\right)$ at atmospheric temperature and pressure, and will be at its maximum at the complete combustion of the fuel (Caton, 2000).

The *availability* (exergy) conversion efficiency $\left(\varepsilon\right)$, which measures the effectiveness of any internal combustion engine is determined from the ratio of the actual work delivered compared with this maximum work, and expressed as follows:

$$\varepsilon = \frac{\Delta W}{\Delta W_{\max}} = \frac{\Delta W}{-\left(\Delta G\right)_{P_A, T_A}} \tag{2.62}$$

2.20.7 Second law of thermodynamics analysis (*availability*)

The second law of thermodynamics analysis applies exergy (*availability*) equations in the engine cylinder of internal combustion ignition engine. The different forms of availability that exist for the analysis of the engine cylinder are chemical availability, flow availability, thermal availability, mechanical availability and fuel availability (Caton, 2000).

The chemical exergy (*fuel availability*) associated with the burning of fuel in the cylinder, and for hydrocarbon liquid fuel of the general type, $C_x H_y$ on kg basis is given as (Rakopoulos & Giakoumis, 2006):

$$a_{fch} = LHV\left(1.04224 + 0.011925\frac{y}{x} - \frac{0.042}{x}\right) \tag{2.63}$$

For fuel of the form $C_z H_y O_p S_q$ (Meisami et al., 2017; Özkan, 2015; Rakopoulos & Giakoumis, 2006; Stepanov, 1995):

$$a_{fch} = LHV\left[1.041 + 0.1728\frac{y}{z} + 0.0432\frac{p}{z} + 0.2196\frac{q}{z}\left(1 - 2.0628\frac{y}{z}\right)\right] \tag{2.64}$$

Thermo-mechanical availability is another form cited by Rakopoulos & Giakoumis (1997):

$$a_{ftm} = U + P_0 V - T_0 S - G_0 \tag{2.65}$$

where G_0 is the working medium's Gibbs free enthalpy at ambient pressure P_0, and temperature T_0, calculated based on dead state compositions, and neglecting kinetic and potential energy terms.

When the system moves from one state to another, the change in exergy as defined by Lior & Rudy (1988) for ideal Otto cycle is also applicable for Diesel cycle.

$$\Delta a_{ftm} = C_P\left(T_{n+1} - T_n\right) - T_n\left[C_P \log_e\left(\frac{T_{n+1}}{T_n}\right) + R\log_e\left(\frac{P_0}{P_i}\right)\right] \tag{2.66}$$

$$P_i = x_i P \tag{2.67}$$

where n (0, 1, 2, 3, 4) represents the state of the components, P_i represents the partial pressure of component i.

If T_1 represents the intake temperature, and T_0 equals the temperature of the environment, then $T_1 = T_0$ for n = 0 (i.e., the environment), and the exergy for the intake process becomes:

$$\Delta a_{ftm,0\to1} = -RT_0 \log_e\left(\frac{P_0}{P_i}\right) \tag{2.68}$$

The exergy of the exhaust gases includes thermo-mechanical exergy and chemical exergy components described by (Meisam et al., 2017; Özkan, 2015):

$$a_{ftm} = \sum_i y_i \left[\left(\bar{h}_{i,T} - \bar{h}_{i,T_0} \right) - T_0 \left(\bar{s}_{i,T} - \bar{s}_{i,T_0} \right) + RT_0 \log_e \frac{P}{P_0} \right] \tag{2.69}$$

$$a_{fch} = RT_0 \sum_i y_i \log_e \left(\frac{y_i}{y_{i,0}} \right) \tag{2.70}$$

$$a_{fexh} = a_{ftm} + a_{fch} \tag{2.71}$$

where a_{ftm} represents the thermo-mechanical exergy, a_{fch} represents the chemical exergy and a_{fexh} represents the total exhaust exergy in molar basis.

The availability balance can be made on the inlet manifold and the exhaust manifold for each fuel composition and the results can be used to estimate the exergy efficiency of the engine for different fuel composition as follows (Rakopoulos & Giakoumis, 2006):

$$\varepsilon = \frac{Availability\ out\ in\ product}{Availability\ in} = 1 - \frac{Loss + destruction}{Input} \tag{2.72}$$

If we consider the cylinder as a closed system and for a four-stroke engine based on second-law, Meisami et al. (2017), Rakopoulos & Giakoumis (2006), and Heywood (1988) describe the exergy efficiency per cycle as:

$$\varepsilon_1 = \frac{W_b}{\dot{m}_{f1} a_{fch}} \tag{2.73}$$

where W_b represents the brake work production, and $\dot{m}_{f1}$, represents the total mass flowrate of fuel entering the cylinder per cycle.

The efficiency (ε_1) can then be compared to the brake thermal efficiency η_{th} as defined by first law of thermodynamics (Meisami et al., 2017; Rakopoulos & Giakoumis, 2006).

$$\eta_{th} = \frac{W_b}{\dot{m}_{f1} LHV} \tag{2.74}$$

Thus,

$$\varepsilon_1 = \eta_{th} \frac{LHV}{a_{fch}} \tag{2.75}$$

Another approach to second-law exergy efficiency for the cylinder is as defined by Alkidas (1988):

$$\varepsilon_2 = \frac{W_b}{W_{\max}} = \frac{W_b}{W_b + I} \tag{2.76}$$

where I represents irreversibilities due to combustion and heat transfer.

For a closed system considered for the cylinder, mass transfer is limited in or out of the cylinder during a single cycle, and the exergy of the fuel is described by the relation (Lior & Rudy, 1988):

$$a_{fch,closed} = a_{fch} - (P - P_i)v \tag{2.77}$$

where, v = specific volume (vol/mol), P_i is the partial pressure of the components (diesel and biodiesel once vapourized) which is determined by using Raoult's law as follows:

$$P_i = x_i P \tag{2.78}$$

The specific volume (v) is calculated from equations of state assuming ideal gas behaviour for the air-fuel mixture.

$$v = \frac{RT}{P} \tag{2.79}$$

where R is the ideal gas constant, T is the temperature, and P is the pressure in the cylinder.

If the assumption of zero work done by the exhaust gases as they return to the environment as discussed earlier (Equation (2.27)) is applied, then the following changes in exergy for the process could be written as (Lior & Rudy, 1988):

Exergy added during compression (process $1 \rightarrow 2$) $= a_2 - a_1$ (2.80)

Exergy lost during combustion (process $2 \rightarrow 3$) $= a_2 - a_3$ (2.81)

Exergy extracted during expansion (process $3 \rightarrow 4$) $= a_3 - a_4$ (2.82)

Exergy lost from exhaust (process $4 \rightarrow 1$) $= a_4 - a_1$ (2.83)

Therefore, the effectiveness of the closed system (piston-cylinder) on the premise of only one control mass is given below:

$$\in_{sys,eff} = \frac{(a_3 - a_4) - (a_2 - a_1)}{a_{in}} \tag{2.84}$$

where:

$(a_3 - a_4) - (a_2 - a_1)$ represents the net exergy extracted for intended use, and

a_{in} represents decrease in input fuel exergy.

2.21 Performance evaluation of diesel engines

The ruggedness, fuel economy, and high-power delivery of diesel engines has attracted its use as engines of choice in industrial applications. The performance and efficiency of an engine is determined by evaluating engine parameters such as brake mean effective pressure (BMEP), brake power (BP), brake specific fuel consumption (BSFC), brake thermal efficiency (BTE %), engine torque, and observing the exhaust gas temperature. The gaseous emissions from diesel engines increased in the past few decades due to increase in the number of operating power plants, vehicles, ships, light aircrafts, and agricultural tractors using diesel as fuel. Due to increasing stringent environmental regulations to protect the environment, the use of diesel-biodiesel blends has been encouraged to reduce the levels of exhaust gas emissions such as carbon monoxide (CO), carbon dioxide (CO_2), smoke opacity, particulate matters (PM), and oxides of nitrogen (NO_x), etc into the environment (Aldhaidhawi, et al., 2017). The high content of oxygen (10–12 %) in biodiesel enables near 100% combustion of diesel-biodiesel blends in diesel engines. The analyses of these parameters will determine the level of effectiveness of the engine and compliance to environmental laws.

2.21.1 Brake mean effective pressure (BMEP)

$BMEP$ is the average mean pressure in the cylinder that would produce the measured brake power output. This pressure is calculated as the uniform pressure in cylinder as the piston rises from top to bottom of each power stroke. The $BMEP$ is that part of the indicated mean effective pressure $IMEP$ the gives the brake power.

$$BMEP = IMEP - Losses = \frac{BP}{C_e \times N} \tag{2.85}$$

where C_e represents the engine capacity, N represents the number of working cycles per second, and for a 4-stroke engine, $N = \frac{rev/s}{2}$; for a 2-stroke engine, $N = rev/s$.

2.21.2 Brake power (BP)

The brake power (also called engine shaft power) of an engine is the difference between the indicated power (IP) and the power lost to mechanical friction (FP). The indicated power is the actual rate of work done by the working fluid (e.g. diesel oil) on the piston measured in kilowatts. The mechanical efficiency is the measure of the ability of the engine to overcome the frictional power loss that includes frictions in the bearings, pistons, and other mechanical parts of the engine (Dwivedi et al., 2013).

$$BP = IP - FP = 2\pi N_s \frac{60}{T_e} \tag{2.86}$$

$$IP = IMEP \times A \times l \times N \tag{2.87}$$

$$\eta_{mech} = \frac{BP}{IP} \tag{2.88}$$

where, η_{mech} represents the mechanical efficiency, IP is in Watts, N_s represents the shaft speed in rev/s, T_e represents the effective Torque (Nm), $IMEP$ is in Pa, A is the area of piston (m^2), l is the length of stroke (m), and N as defined in Section (2.21.1).

2.21.3 Brake specific fuel consumption (Bsfc)

$Bsfc$ is defined as the rate of fuel by the engine per brake horsepower developed, and it is a measure of the efficiency of the engine in converting the fuel supplied to produce useful work. It is desirable to obtain a lower value of $Bsfc$ because it indicates that the engine is more efficient.

$$Bsfc = \frac{\dot{m}_f}{BP} \tag{2.89}$$

where $\dot{m}_f$ is the mass flowrate of fuel.

2.21.4 Brake thermal efficiency (BTE %)

This is the ratio of the brake power to the energy generated from the engine by burning the fuel. The energy in the fuel is usually assumed as the lower heating value (LHV).

$$\eta_{th} = \frac{BP}{\dot{m}_f\,(LHV)} \tag{2.90}$$

2.22 Performance and emissions evaluation of diesel engine using diesel-biodiesel blends of rubber seed oil

Few studies have examined the utilization of rubber seed oil biodiesel as an alternative engine fuel. Onoji et al. (2016a) in their review, confirm the appropriateness of such promising fuel for use in diesel engines to boost the economy of most sub-Saharan African countries that depend on imported fuel. Ramadhas et al. (2005a) examined the performance of unmodified diesel engine that run on rubber seed oil, diesel, and rubber seed oil biodiesel-diesel blends at different loads. In all cases considered, the thermal efficiency increases with load to a certain limit, and begins to decrease. The lower blends of biodiesel increase the thermal efficiency and reduce the fuel consumption. The low thermal efficiency for pure biodiesel (B100) is due to

the reduction in calorific value of biodiesel that results to increased fuel consumption compared to B10 (10% biodiesel-90% diesel). Pure rubber seed oil has the lowest thermal efficiency in all cases considered, and for all loads.

The *brake specific fuel consumption* (*Bsfc*) variation with engine loads for all cases considered, decreases with increase in the load. Lower values of *Bsfc* were observed for lower blends of biodiesel/diesel, but the trend reverses for higher blends of B50-B100. This is because biodiesel is about 14% lower in calorific value than diesel fuel. The *Bsfc* of rubber seed oil was higher than those of the blends and diesel because of high viscosity and low atomization.

The carbon monoxide emission increases with load capacity in all the cases considered. This is typical with all internal combustion engines since the air-fuel ratio decreases with increase in load, and becomes greater than the stoichiometric value. Biodiesel blends have lower CO emissions compared to those from diesel, biodiesel and rubber seed oil.

The profile of carbon dioxide emissions in the all cases considered by the researchers increases with load. The CO_2 emissions for the blends are lower than those reported for diesel and biodiesel. Biodiesel combustion emits more CO_2 than diesel fuel because of oxygen content (10–12 %) of biodiesel that aids higher combustion rate.

In consideration of the variation of smoke opacity of the different fuels considered with loads, lower values were observed for biodiesel blends compared to diesel and rubber seed oil. The blend of B20 appears to give the lowest opacity while rubber seed oil and diesel gave similar results.

The exhaust gas temperature increases with loads for all the cases considered by the researchers and for all fuels tested. The exhaust gas energy loss is lower for blends up to B20 because of lower exhaust gas temperature observed. This fact is confirmed by the higher brake thermal efficiency and lower brake specific fuel consumption obtained for B20 and below. Pure rubber

seed oil gave the highest exhaust gas temperature in all loads, indicative of higher energy loss and higher concentration of NO_x in the exhaust gas stream.

The foregoing results of engine performance and emissions analyses for blends of rubber seed oil biodiesel tested by Ramadhas et al. (2005a) are similar to those reported for biodiesel from pongamia oil (Prabhahar et al., 2011), jatropha *curcas* (Elango & Senthilkumar, 2011), other non-edible oil biodiesels (Ashraful et al., 2014), and rubber seed oil-diesel blends (Ramadhas et al., 2005b). The NO_x emissions for diesel and biodiesel blends follow an increasing trend with loads for all types of biodiesels. NO_x is generally formed at higher combustion temperatures, and lower values are for diesel fuel compared with the blends. In all cases, pure biodiesel (B100) generates higher concentration of NO_x compared with diesel and the blends (Elango & Senthilkumar, 2011). Geo et al. (2010) injected diethyl ether (DEE) through the intake port during suction stroke at different flowrates of 100, 150, and 200 g/h into rubber seed oil that was injected directly inside the cylinder at the end of compression stroke in order to study the engine performance. Their results indicate that the brake thermal efficiency improves from 26.5% with neat rubber seed oil to a maximum of 28.5% with DEE injection rate of 200 g/h. Smoke opacity also reduce from 6.1 to 4 BSU along with marginal reduction in hydrocarbons and CO emissions with DEE injection. Other researchers (Senthilkumar & Purushothaman, 2012) examined the use of high FFA rubber seed oil biodiesel-diesel blend in a diesel engine with respect to performance and emission analysis. Their report for B00, B5, and B100 indicated similar trends for Bsfc, BTE, and CO emissions up to 100% load with those reported by Ramadhas et al. (2005a).

CHAPTER 3: METHODOLOGY AND EXPERIMENTAL PROCEDURES

3.0 Introduction

This chapter documents all methods and techniques used to achieve results in this thesis. This includes, but not limited to the collection of rubber seeds, seed oil extraction, characterisation, and the determination of the physicochemical properties of the extracted oil. It also discusses the experimental procedures and methods used in the transesterification process, and the modelling approach used in this thesis. The oil extraction process was modeled to determine the optimum extraction process variables. The kinetics of the oil degradation under thermal conditions was studied. The synthesis and characterisation of catalyst from waste rubber seed shell for transesterification of the rubber seed oil to biodiesel is reported in this chapter.

Finally, the produced biodiesel was characterised, and tested in an unmodified diesel engine to determine its performance and emission evaluation in compliance with environmental laws.

3.1 Materials and Chemicals

Matured and fresh rubber seeds (*Hevea brasiliensis*) used in this work was handpicked from different clones of NIG800 series at the plantations of Rubber Research Institute of Nigeria (RRIN), Iyanomo, Benin City.The seeds are usually available in the early months of dry season, usually July to August each year but could be harvested until October.

Various sizes of Duran beakers, flasks, measuring cylinders and separating funnels were used in this work. Other glass wares used include density bottles, pipettes, burettes, etc. Muslin cloth with Whitman filter paper was used to enclose a known weight of milled rubber seed powder into the extraction thimble during the extraction process.

All chemical reagents used in this study were of analytical grades manufactured by BDH Chemicals Ltd., Poole England and GFS Chemicals, Inc., 867 McKinley Ave., Columbus, OH 43223, and they include n-hexane, NaOH, KOH, $CaCl_2$, methanol, ethanol, phenolphthalein,

starch, KI, CCl_4, $Na_2S_2O_3$, ethanoic potassium hydroxide, HCl, p-anisidine, iso-octane, diethyl ether, and ethyl alcohol.

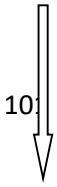
3.2 Experimental procedures for seed oil extraction

This work was carried out in the Biochemical Engineering Laboratory at the Department of Chemical Engineering, Landmark University, Omu-Aran, Kwara State, Nigeria, using the experimental procedures described in this section.

3.2.1 Rubber seed preparation

Figure 3.1 shows the flowchart for the preparation of rubber seed powder from which oil was extracted. The rubber seeds were examined for freshness, washed 3–4 times with hot distilled water to get rid of dust and solid impurities, and dried at room temperature for 48 h (Onoji et al., 2017a). Separation of the chaffs from the seeds was carried out by winnowing. Approximately 500 g of seeds were de-shelled manually using laboratory mortar and pestle to free the kernels from the shells. The seed shells and kernels were weighed separately and their weights recorded (see Section B.1 of Appendix B for calculations). About 100 g of seed kernel was dried for 5 h at 105 ^{o}C using U CLEAR heating drying oven (*Model DHG-9053A*) to constant weight to determine the initial moisture content of the seeds. Moisture content after conditioning was determined by calculating the weight difference of the sample before and after oven drying (see Section B.1 of Appendix B for calculations). The remaining seed kernels were processed to 15% absolute moisture content required for higher oil yields before extraction (Bhuiya et al., 2015). A portion of the processed kernel was milled and sieved into five-particle sizes (0.5, 1, 1.5, 2 and 2.5 mm) and were used to determine which particle size would give the maximum oil yield from the available sizes (Onoji et al., 2017a).

Raw rubber seeds



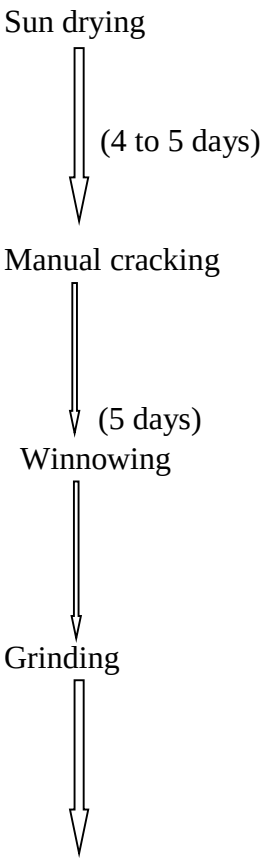


Figure 3.1: Flowchart of rubber seed powder preparation

3.2.2 Extraction of the seed oil

The main industrial process parameters influencing oil extraction are as follows: type of solvent, kernel particle size, seed/solvent ratio, extraction time and temperature (Elkhaleefa & Shigidi, 2015). The solvent chosen is usually based on cost, behaviour towards the matrix, and toxicity. In this study, five-particle sizes of rubber seed kernel (0.5, 1, 1.5, 2 and 2.5 mm) were considered to determine the particle size that will give the maximum oil yield (Onoji et al., 2016b). For each particle size considered, the extractor was charged with 50 g of milled rubber seed kernel packed in a muslin cloth (Figure C.1 of Appendix C), and placed in a thimble of

the Soxhlet extractor. A 500-mL round-bottom glass flask was filled with 225 mL n-hexane solvent and tightly fixed to the end of the extractor (Figure C.2 of Appendix C). Heating was provided for the setup by a heating mantle regulated at 60 ^{o}C for 45 min. Extraction time was considered to end when the first drop of the extracting solvent recycled back into the thimble. Each experiment was conducted in three replicates, and the mixture was concentrated at 65 ^{o}C using rotary evaporator (Figure C.3 of Appendix C) under vacuum to recover the extracted oil (Figure C.4 of Appendix C) (Onoji et al., 2017a, 2016b). The oil yield was gravimetrically determined using Equation (3.1), and average values recorded in Table D.1 of Appendix D and presented in Figure 4.1. The particle size that gave the maximum oil yield was employed for further oil extraction.

$$RSO\ yield\ (wt.\%) = \frac{mass\ of\ extracted\ oil\ (g)}{mass\ of\ rubber\ seed\ kernel\ used\ (g)} \times 100 \quad (3.1)$$

3.3 Characterization of the seed oil

The physico-chemical properties of the extracted rubber seed oil were determined to ascertain its industrial applications. Standard procedures as described by *American Society for Testing and Methods* (ASTM) and *Association of Official Analytical Chemists* (AOAC, 1990) were used to characterize the oil. The extracted rubber seed oil was analyzed for density, specific gravity, ^{o}API, saponification value, acid value, % free fatty acids (FFA), iodine value, peroxide value, kinematic viscosity, refractive index and pH using standard procedures as described by ASTM and AOAC (1990).

The acid value was determined by titration method, while the iodine value was obtained by Wijs' method. The specific gravity measurement was carried out at room temperature using standard specific gravity bottles. The state and colour of the oil were noted using visual inspection at room temperature (Onoji et al., 2016b). Other parameters evaluated are aniline point, diesel index, cetane number (Mofijur et al., 2014), higher heating value (HHV)

(Demirbaş, 1998), mean molecular mass of fatty acids (Ajiwe et al., 1995), and average molecular mass of oil (Fillières et al., 1995). The procedures and calculations of these parameters are presented in Sections E.1.1 through E.1.12 of Appendix E. ASTM standard procedures were followed to determine cloud, flash, freezing, boiling, and pour points, respectively. The cold filter plugging point (CFPP) was estimated using the correlation cited by Verma et al. (2016).

3.4 Spectroscopy analyses of the seed oil

The extracted oil was characterized by gas chromatography-mass spectroscopy (GC-MS), Fourier transform infrared spectroscopy (FT-IR) and nuclear magnetic resonance (NMR) techniques.

3.4.1 Fatty acid profile of the seed oil

The fatty acid profile was determined qualitatively using GC-MS (*QP2010 Plus Shimadzu, Japan*) system equipped with flame ionization detector (FID) with capillary column DB-1 (length 30 m x diameter 0.25 mm x film thickness 0.25 μm). Helium was used as carrier gas with a linear velocity of 49.2 cm/s and a purge flow of 3 mL/min. The column oven temperature was programmed at 70 ^{o}C and was quickly ramped at 10 ^{o}C/min until it reached 280 ^{o}C and held for 5 min. A sample of the oil was mixed with 1 mL HPLC grade n-hexane. A portion of this mixture (0.5 μL) was injected into the GC at 250 ^{o}C at split ratio of 20:1. A column pressure of 116.9 kPa and column flowrate of 1.80 mL/min was maintained. The mass spectrometer (MS) was operated in electron ionization mode with the following parameters: ion source temperature 200 ^{o}C, interface temperature 250 ^{o}C and solvent cut time 2.5 min. It was scanned from m/z 30 to 350, and identification of the peaks was performed by comparing retention times with those of National Institute of Standards and Technology (NIST) library analyzed

under the same conditions (Onoji et al., 2016b). The area percentage method was used to estimate the amount of fatty acid compositions of the oil (Sanjel et al., 2014).

3.4.2 Fourier transform infrared spectroscopy

FT-IR spectroscopy can be employed to identify the various functional groups present in oils and gives an insight into formation of primary and secondary oxidation products when the oil is under thermal stress (Ogbu & Ajiwe, 2016). In this study, FT-IR was used to characterize the oil at room temperature (28 ^{o}C) in order to assess the oxidation state of the oil prior to thermal treatment using FT-IR spectrometer (Model: TENSOR 27, Bruker Optics Inc, USA) equipped with a detector having a spectral range 4000–500 cm^{-1}. The FT-IR was analyzed using OPUS spectroscopy software supplied with the instrument.

3.4.3 Nuclear magnetic resonance spectroscopy

The NMR spectroscopy is a useful nondestructive tool that complements GC-MS in the characterization of lipids and identification of compounds present. In this study, the ^{1}H NMR spectrum was recorded on *Bruke*r ultra-shield TM 500-MHz NMR spectrophotometer using deuterated chloroform ($CDCl_3$) as solvent (δ = 7.26 ppm) containing a small amount of tetramethylsilane (TMS) as an internal standard (δ = 0 ppm) and put in a 5-mm diameter tube. The ^{13}C NMR experiments were performed using the same equipment, and the carbon atom in $CDCl_3$ was taken as 77.42 ppm. All other peaks were assigned with respect to it. About 25–30 mg of RSO was dissolved in 1 mL of $CDCl_3$, and the experiments were performed at 25 ^{o}C (Onoji et al., 2016b).

3.5 Kinetics of thermal oxidative degradation of the seed oil

Vegetable oils (mainly triglycerides) undergo chemical reactions such as oxidation, isomerization, polymerization and hydrolysis when subjected to prolonged heating process (Onoji et al., 2016b). These reactions affect the physico-chemical properties of these oils and their quality. The thermal study of oils before their industrial applications permits data to be obtained on the influence of time and temperature on their thermal oxidation (Gouveia de Souza et al., 2004).

In this study, classical chemical analysis methods were used to determine the change in peroxide value, iodine value and refractive index of RSO when subjected to heat treatment (Oderinde et al., 2009). Rubber seed oil has been reported to be thermally stable up to 250 ^{o}C under heat treatment (Aravind et al., 2015). For this reason, the peroxide value, iodine value and refractive index were determined at 100, 150, 200 and 250 ^{o}C at various time intervals using methods prescribed by ASTM and AOAC (1990). The procedures outlined in Sections E.1.7, E.1.8, and E.1.9 of Appendix E was followed at the conditions of temperature and time considered for each case. The iodine value is a measure of the degree of unsaturation to quantify the amount of double bonds present in the oil. It reflects its susceptibility to oxidation (Hrušovský et al., 2013), and was used in the present study to generate data for kinetic plots.

The broad reaction rate expression proposed by several researchers for the kinetics of thermo-oxidative degradation of RSO is expressed in Equation (3.2) (Santos et al., 2002; Van Boekel, 1996; Ramaswamy et al., 1989).

$$-dC/dt = kC^n \tag{3.2}$$

where 'C' is iodine value at any time, 'n' is order of reaction, and 'k' is the reaction rate constant whose temperature dependence is commonly described by Arrhenius Equation (3.3).

$$k = A_o \exp(-E_a/RT) \tag{3.3}$$

T is the absolute temperature, R is the universal gas constant, E_a is the activation energy, and A_o is the pre-exponential factor. The thermo-oxidative degradation of vegetable oils generally follows a first-order reaction as given in Equation (3.4) (Ramaswamy et al., 1989).

$$ln\, C_t/C_o = kt \tag{3.4}$$

where $C_t$iodine value at time t is, C_o is initial iodine value.

3.6 Optimization study of the oil extraction process using RSM and ANN–GA techniques

RSM based on Box–Behnken experimental design, and ANN–GA was used to model and optimize the extraction process conditions for rubber seed oil production. A three-level, three-factor design was employed in this study (Table 3.1). The extraction process parameters investigated were rubber seed powder weight (X_1), solvent volume (X_2) and extraction time (X_3). The BBD generated 17 experimental runs that were randomized to minimize the unpredictable variations in the observed responses due to uncontrolled extraneous factors. The experimental runs included 12 factorial points, and 5 centre points that provide information on the interior of the experimental regions to evaluate the curvature effect. The experiments were carried out in series as described in the preliminary assay for the determination of optimum particle size. An average particle kernel size of 0.5 mm that gave the maximum oil yield was used to obtain experimental oil yields that were employed in RSM and ANN modeling (Onoji et al., 2017a)

Table 3.1: Experimental range and levels of independent process variables for seed oil extraction via Box-Behnken design (Onoji et al., 2017a)

Independent process variables	Symbols (uncoded)	Coded factor levels		
		−1	0	+1
Rubber seed powder weight (RSPW) (g)	X_1	40	50	60
Solvent volume (mL)	X_2	200	225	250
Extraction time (min)	X_3	40	45	50

3.6.1 Modeling of seed oil extraction process variables via RSM

The experimental oil yields obtained from BBD, and the process parameters were statistically analyzed using RSM and least-squares method to fit a second-order polynomial model generated by the Design-Expert software trial version 8.0.3.1 (*Stat-Ease Inc., Minneapolis, MN, USA*) for the complete BBD (Onoji et al., 2017a). The relationship between the response and the input variables is given in Equation (3.5) (Baş & Boyaci, 2007b):

$$Y = f(X_1, X_2, ...X_n) + \varepsilon \tag{3.5}$$

where Y is the response, f is the unknown function of the response, X_1, X_2, …. Xn denote the actual independent process variables, n is the number of the independent variables and ε the statistical error that represents other sources of variability not accounted for by f. It is generally assumed that ε has a normal distribution with mean zero and variance (Baş & Boyaci, 2007b). The relationship between independent coded and actual values is defined by Equation (3.6):

$$x_i = \frac{X_i - \overline{X}_i}{\Delta X_i} \tag{3.6}$$

where x_i is the coded value of the ith factor, X_i is actual (experimental) value of the ith factor in the uncoded units, $\overline{X}_i$ is the average of the low and high values for the ith factor, and ΔX_i represents the step change for the ith factor.

The general second-order polynomial regression model shown in Equation (3.7) was used to develop the empirical model that establishes the correlation between the coded process parameters (x_1, x_2 and x_3) and the response variable Y (% yield).

$$Y = \beta_o + \sum_{i=1}^{k} \beta_i x_i + \sum_{i=i}^{k} \beta_{ii} x_i^2 + \sum_{i<j}^{k} \beta_{ij} x_i x_j + \varepsilon \quad (3.7)$$

where β_o, β_i, β_{ii}, and β_{ij} represent the regression coefficients of intercept, linear, quadratic and interactive terms, respectively, while x_i and x_j represent the coded process parameters.

The regression coefficients of Equation (3.7) were estimated using the least square estimation method based on multiple regression technique. In this method, it is assumed that random errors are identically distributed with a zero mean and a common unknown variance. The residual is an estimate of the corresponding ε_i which is the difference between the actual value (Y_i) and the predicted value as shown in Equation (3.8).

$$\varepsilon_i = Y_{i,exp} - Y_{i,pred} \quad (3.8)$$

The objective of the optimization step is to minimize the sum of the squares of the residuals, often called the sum of squares of the errors (SSE). Thus,

$$SSE = \sum_{i=1}^{n} \varepsilon_i^2 = \sum_{i=1}^{n} \left(Y_{i,\exp} - Y_{i,pred}\right)^2 \quad (3.9)$$

The residuals may be expressed in different as in Equation (3.10), and *SSE* may be written as shown in Equation (3.11) (Baş & Boyaci, 2007b).

$$\varepsilon = Y - x\beta \quad (3.10)$$

$$SSE = \varepsilon^T \varepsilon = \left(Y - x\beta\right)^T \left(Y - x\beta\right) \quad (3.11)$$

Differentiating the SSE with respect to β, yields a vector of partial derivatives (Equation (3.12)), as follows:

$$\frac{\partial}{\partial \beta}\left(SSE\right) = -2x^T \left(Y - x\beta\right) \quad (3.12)$$

When Equation (3.12) is equated to zero, we have $x\beta = Y$ that is solvable directly to obtain the coefficients β from Equation (3.13).

$$x^T x\beta = x^T Y \tag{3.13}$$

The rearrangement of Equation (3.13) in matrix form is given in Equation (3.14) (Baş & Boyaci, 2007b):

$$\beta = Cx^T Y \tag{3.14}$$

where $C = \left(x^T x\right)^{-1}$ is a squared matrix. After the regression coefficients are obtained from Equation (3.14) using the experimental response Y, the model-predicted response could be easily calculated using the developed model from Equation (3.7) with all the regression coefficients incorporated.

The developed second-order regression model that adequately describes the behavior of the process with respect to the operating variables was used to create contour (2D) and surface responses (3D) plots. This was used to explore the designed space, and to predict the optimal conditions for RSO extraction yield. The variability of the response variable was determined by the adjusted multiple coefficient of determination ($R^2_{adj.}$) which is a measure of the amount of variation around the mean explained by the model and adjusted for the number of terms in the model. In addition, the adequate precision (signal-to-noise ratio) was calculated using Equation (3.15) to verify that the quadratic regression model is adequate (Onoji et al., 2017a; Cerino Córdova et al., 2011).

$$Adequateprecision = \frac{\text{Max } (Y) - Min\,(Y)}{\sqrt{\frac{\omega\sigma^2}{n}}} \tag{3.15}$$

where Max (Y) is the maximum predicted oil yield; Min (Y) is the minimum predicted oil yield; ω is the number of model parameters (including β_o); σ^2 is residual mean square; and n is the number of experimental runs.

3.6.2 Modeling of seed oil extraction process variables via ANN

A commercial ANN program, Neural Power trial version 2.5 (CPC-X software) was employed in this study. RSO yield was predicted by using back-propagation multi-layer feed-forward neural network algorithm. A topology of 3–3–1 network (Figure 3.2) corresponding to the number of neurons within the input, hidden and output layers, respectively was used for the training. A sigmoid transfer function was adopted for the study. The input vector consisted of the rubber seed powder weight (X_1), solvent volume (X_2), and extraction time (X_3) while the output vector (Y) was the rubber seed oil (RSO) yield (Onoji et al., 2017a). The functional relationship to be estimated by the ANN model could be expressed as follows:

$$Y = f\left(X_1, X_2, X_3\right) \tag{3.16}$$

where X_1, X_2, X_3, and Y are as defined earlier. The output of a neuron is computed from Equation (3.17) (Shokri et al., 2011):

$$O_i = f\left(\sum_{j=1}^{n} w_{ij} I_j + b_i\right) \tag{3.17}$$

where O_i is output of the i^{th} neuron, f is transfer function, b_i is bias of the i^{th} neuron, w_{ij} is synaptic weight corresponding to j^{th} synapse of i^{th} neuron, I_j is j^{th} input signal to the i^{th} neuron and n is number of input signals to the i^{th} neuron.

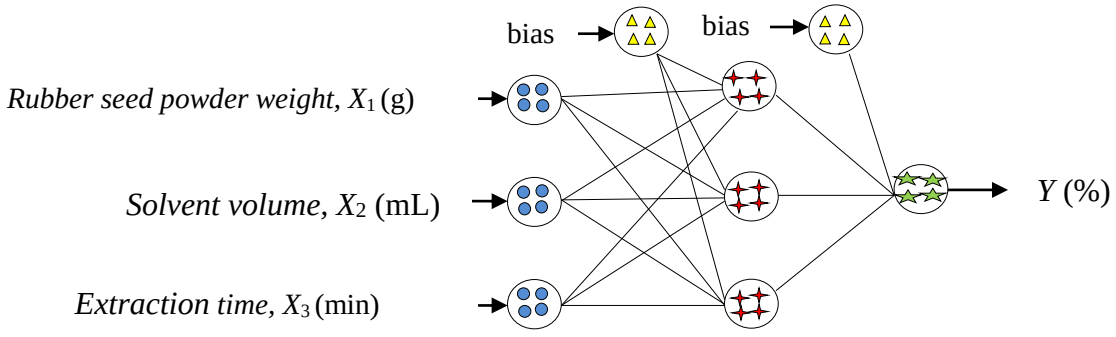


Figure 3.2: Schematic of 3-3-1 developed ANN topology (Onoji et al., 2017a)

The experimental oil yields obtained from the 17 experimental runs of BBD was divided into two sets. Experimental oil yields of 14 set of data was used for ANN training and cross validation, and the other set of 3 data was used for testing of the trained network. The network was trained using the back-propagation method implemented by Levenberg-Marquardt algorithm depicted in Figure 3.3 (Onoji et al., 2017a). The training was carried out by adjusting the connection weights and biases between neurons with the aim of reducing the mean square error (MSE) between the predicted and experimental outputs below an acceptable threshold (Gueguim Kana et al., 2012). A network will memorize results instead of generalizing when it is over trained. In such a case, the resulted model can perfectly predict the data similar to training data, but will perform poorly if new set of data are submitted to it. The training was completed when the network is able to predict the given output. The trained model was validated by using it to predict RSO yield of the 3 data that were not used during the training phase. The validated model was subsequently used as evaluation function (Equation 3.18) for Genetic Algorithm (GA) optimization process to predict the optimal values of RSO extraction variables (X_1, X_2, X_3 *and Y)* applied in developing the model (Onoji et al., 2017a; Kostić et al., 2013; Gueguim Kana et al., 2012).

$$f(X) = \frac{1}{1+e^{-X}} \tag{3.18}$$

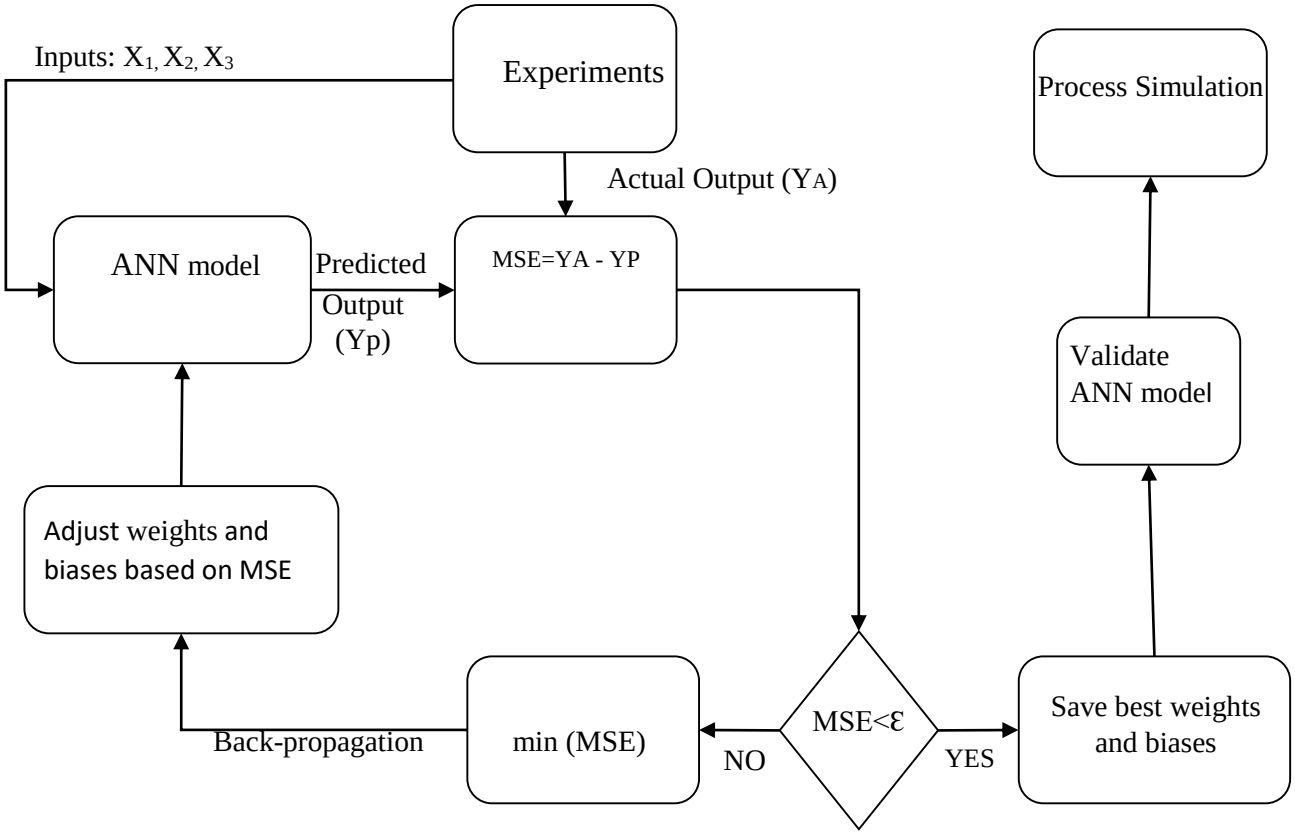


Figure 3.3: Levenberg-Marquardt training flowchart for ANN model (Adapted from Onoji et al., 2017a).

3.7 Catalyst preparation and characterization

The rubber seed shells (RSS) freed from the kernels in Section 3.2.1 were stored in polyethylene bags for analyses. The RSS was washed 3–4 times with hot distilled water to get rid of dust and solid impurities. It was then dried in a laboratory oven at 110 ^{o}C for about 5 h, and stored in a desiccator. The cooled dried RSS was ground to powder with a grinder, and sieved through a 60-mesh size. The powdered raw RSS was analyzed by thermo-gravimetric analyzer (TGA) in the range of 30–950 ^{o}C at 10 ^{o}C/min, under nitrogen environment to determine a suitable calcination temperature of the catalyst (Onoji et al., 2017b). The RSS powder was calcined from 40–800 ^{o}C at heating rate of 10 ^{o}C/min in an electric muffle furnace (Carbolite, Parson Lane, Hope Valley S33 6RB, England, *Model:* RWF 12/5) for about 3 h to

remove organic materials in it and stored in screwed bottles for analyses. Raw and calcined RSS (Figure E.1 of Appendix E) were dissolved in deionized water to determine the basic property (pH). Energy dispersive X-ray spectroscopy (EDX 3600B-XRF Skyray Instrument) analysis was employed to determine the elemental compositions of the raw and the calcined RSS. Samples were pulverized using *Knife Mill GRINDOMIX* (*model: GM20*), and pelletized with *Mini-pellet press kit Asia* (*model: GS01152*). The equipment was calibrated using pure silver standard sample. The diffraction patterns of raw and calcined RSS samples were analyzed with a diffractometer (*XRD EMPYREAN mini-material analyzer*, manufactured by PANalytical B.V., Holland) to observe their amorphous and crystalline structures. Sample was pulverized to homogeneous size and loaded into XRD sample holder. The diffractometer equipped with PIXcel-3D detector employed Cu-Kα1 radiation source (λ =1.54059 Å) at 45 kV and 40 mA. Scanning was recorded in a continuous mode over 2^{o}-Theta range from 4.0131^{o} to 79.9849^{o} with a step size 0.026^{o} at 13.77 second per step. The size and morphology of catalyst was examined with scanning electron microscope (*SEM-Phenom ProxMVE 016477830*, manufactured by Phenom World, Eindhoven, Netherlands). The RSS sample was dispersed on a stub using a sticky carbon tape before coating with palladium gold. Vacuum was created before carrying out the analysis by inserting the stub into the equipment (Onoji et al., 2017b).

Surface area and porosity, pore volume, and pore-size distribution are important parameters in heterogeneous catalysis and catalyst design (Storck et al., 1998). Prior to analysis, about 335.3 mg of raw sample was weighed and outgassed at 250 ^{o}C for 11 h under a stream of nitrogen gas to remove moisture and impurities. Similar analysis was carried out using 382.7 mg calcined RSS catalyst at same conditions. These analyses were to evaluate the textural properties of the raw and calcined RSS in order to determine the influence of calcination temperature (Onoji et al., 2017b).

The accessibility of active sites is determined by the total surface area, and thus related to catalytic activity. *Gold App surface area and porosity analyzer* (*Model: V-sorb 2800p*) was used to estimate the surface textural properties of the raw and calcined RSS from isotherms generated by *Brunauer-Emmett-Teller* (BET) model (Equation 3.19) (Vasudevan et al., 2011) using nitrogen adsorption/desorption at 77.3 K.

$$\frac{(P/P_o)}{V[(1-P/P_o)]} = \frac{(C-1)}{V_m C} \times \frac{P}{P_o} + \frac{1}{V_m C} \tag{3.19}$$

where P is the partial pressure, P_o is the saturation pressure, V_m is the maximum amount of nitrogen adsorbed/unit mass of catalyst at high pressure conditions required to form a complete monolayer over the entire surface of the catalyst, and C is the BET constant related to isosteric heat of adsorption. *Barrett-Joyner-Halenda* (BJH) model calculated the pore-size distributions of the raw and calcined RSS. The total pore volume is defined as the volume of liquid N_2 corresponding to the amount adsorbed at a relative pressure of $P/P_o = 0.997$, after which N_2 desorption commences.

3.8 Biodiesel production from the extracted seed oil and analysis

The rubber seed oil used for the biodiesel production was earlier extracted as in Section 3.2.2. The high FFA of the oil allows for two-step production routes: Esterification and transesterification.

3.8.1 Acid-catalyzed esterification of the seed oil

The rubber seed oil used in the study had an initial acid value of 18.02±0.141 mg KOH/g oil, and FFA level of 9.01±0.07% (Onoji et al., 2016b). Reduction of FFA to <1% prior to transesterification reaction is necessary to avoid catalyst consumption in soap formation and a low yield of biodiesel because of the basic nature of the synthesized catalyst (Betiku & Ajala, 2014). 100 mL rubber seed oil was measured into a 250-mL one-neck glass reactor and

preheated to 105 ^{o}C on a magnetic stirrer hot plate to remove moisture and volatile impurities. Then, 1.5 % vol/vol H_2SO_4 catalyst based on methanol volume was mixed with 45 mL of analytical grade methanol (>99%) and stirred for 5 min. The mixture was added to the oil maintained at 60 ^{o}C, and the reaction continued for 1 h at a stirring rate of 600 rpm. The esterified oil was transferred into a separating funnel and allowed to stand for 2 h (Figure F.1 of Appendix F). The pretreated oil was separated from the water formed (Equation (3.20)), and excess methanol was evaporated in a rotary evaporator prior to acid value determination by standard titration procedure described by ASTM. Similar experiments were carried out using 3, 4.5, and 6 % vol/vol H_2SO_4 and their acid values determined were recorded in Table F.1 of Appendix F. The 6% vol/vol H_2SO_4 obtained for <1% FFA (90.5% conversion) was employed to esterify the oil used for transesterification reaction (Onoji et al., 2017b).

$$\underset{\text{FFA}}{RCOOH} + \underset{\text{methanol}}{CH_3OH} \xrightarrow{H_2SO_4\ (\text{catalyst})} \underset{\text{methyl ester}}{RCOOCH_3} + \underset{\text{water}}{H_2O} \qquad (3.20)$$

3.8.2 Biodiesel production from the esterified seed oil

A three-factor, three-level (Table 3.2) central composite design using Design-Expert® dx8 software version 8.0.7.1 (*Design Ease Inc., USA*) coupled with response surface methodology was used to statistically analyze the experimental data that consisted of 8 factorial points, 6 axial points, and 6 center points. A transesterification reaction of the esterified seed oil was performed according to the experimental design set by RSM and designed by employing CCD. Twenty experimental runs were carried out for the optimization process under different combination of process variables. In each run, and for the reaction time (X_1), 180 mL of oil specified by methanol/oil ratio (X_2), and RSS catalyst (X_3) as depicted in Table 3.2 were reacted in a 500 mL three-necked round bottom reactor equipped with a reflux condenser, and magnetic

stirrer maintained at 400 rpm throughout the experiment (Onoji et al., 2017b). Heat was supplied by magnetic hot plate at 60 ^{o}C for a reaction time set by the CCD. At the end of the reaction time, the reaction was quenched in an ice-bath and the content of the reactor was transferred into a separating funnel for 2 h to separate glycerol and other impurities from the biodiesel (rubber seed oil methyl ester) phase (Figure F.2 of Appendix F). The biodiesel was poured into a rotary evaporator to remove excess methanol, and washed thrice with deionized water at 50 ^{o}C to remove entrained glycerol and residual catalyst. Washed biodiesel was dried over anhydrous sodium sulphate at 50 ^{o}C (Dhawane et al., 2016). Dried biodiesel (Figure F.3 of Appendix F) was decanted and filtered to remove sodium sulphate, and the yield was estimated using Equation (3.21).

$$Biodiesel\ yield\ (\%) = \frac{Weight\ of\ product\ obtained \times FAME\%}{Weight\ of\ refined\ rubber\ seed\ oil} \times 100 \qquad (3.21)$$

where FAME% is the concentration of fatty acid methyl esters (FAME) analyzed by gas chromatography-mass spectrometry (GC-MS).

Table 3.2: Experimental range and levels of independent process variables for biodiesel production via central composite design

Independent process variables	Symbols (uncoded)	Coded factor levels		
		–1	0	+1
Reaction time (min)	X_1	60	65	70
Methanol/oil ratio (v/v)	X_2	0.20	0.25	0.30
RSS catalyst (g)	X_3	2.5	3.0	3.5

3.9 Characterization of the produced biodiesel

The physico-chemical properties such as density, color, moisture content, ^{o}API gravity, kinematic viscosity, acid value, saponification value, iodine value, and calorific value were determined. These properties including oxidation stability at 110 ^{o}C, cetane number, diesel index, pour point, cloud point, flash point, fire point and cold filter plugging point of the methyl ester (biodiesel) produced at optimum conditions were determined following the procedures prescribed by ASTM standards and other methods (Onoji et al., 2017a). The oxidation stability was determined by using PetroOXY automatic oxidation stability tester (Protest® Instruments GmbH & Co. KG, Dahlewitz, Germany). Figure F.4 of Appendix F and Equation (3.22) developed by Botella et al. (2014) with adjusted R^2 of 0.915 at 95% confidence interval was used to estimate the Rancimat value of the oxidation stability of the produced biodiesel without additive.

$$Rancimat\ (min) = [(31.89 - 20.63f)(PetroOXY(min)) + \ (-214.65 + 319.68f)] \tag{3.22}$$

where f = 0 if no additive is used, and 1 if an additive has been mixed with biodiesel while PetroOXY (min) is the value obtained from the Tester.

The fatty acid methyl ester (FAME) content of the biodiesel was determined by GC Agilent© 7890B and MS Pegasus 4D GCXGC (LECO) located in Wits University Johannesburg, and the value obtained was compared with the correlation of Equation (3.23) developed by Felizardo et al. (2006).

$$FAME\ (\%) = -45.055 ln\mu + 162.85 \tag{3.23}$$

whereμ is the kinematic viscosity (mm^2/s) at 40 ^{o}C.

3.10 Reusability test for the catalyst used in biodiesel production

Different loadings (2, 2.2, 2.5, 3, and 3.5 g) of the prepared catalyst at optimum reaction conditions of RSM, and at 60 ^{o}C were used to produce biodiesel in order to determine the level of loss in activity in the reusability test. After the completion of each reaction, the biodiesel yield was determined. The catalyst was separated from the reaction mixture by filtration, centrifuged, washed with acetone to remove impurities blocking the active sites, and oven dried at 110 ^{o}C for 3 h before each successive reuse. Leaching of active sites into the reaction mixture was determined by atomic absorption spectroscopy (AAS) (Onoji et al., 2017b).

3.11 Statistical analysis of the biodiesel production by RSM

The general second-order polynomial regression model described by Equation (3.24) was used to develop the empirical model that describes the correlation between the transesterification uncoded process parameters (X_1, X_2, and X_3), and the predicted response variable, RSOME yield (%) (Onoji et al., 2017b).

$$RSOME\ (\%) = \beta_o + \sum_{i=1}^{\alpha} \beta_i x_i + \sum_{i=i}^{\alpha} \beta_{ii} x_i^2 + \sum_{i<j}^{\alpha} \beta_{ij} x_i x_j + e \quad (3.24)$$

where β_o, β_i, β_{ii}, and β_{ij} represent the regression coefficients of intercept, linear, quadratic, and interactive terms, respectively, while x_i and x_j, represent the coded independent process parameters as defined in Equation (3.25), and 'e' the experimental error of analysis.

$$x_i = \frac{X_i - \overline{X}_i}{\Delta X_i} \quad (3.25)$$

X_i is actual (experimental) value of the ith factor in the uncoded units, $\overline{X}_i$ is the average of the low and high values for the ith factor, and ΔX_i represents the step change for the ith factor.

The adequate precision ratio (signal-to-noise ratio) which verifies the adequacy of the developed model was estimated by Equation (3.26) (Cerino Córdova et al., 2011).

$$Adequate\ precision = \frac{\text{Max } (Y) - Min\ (Y)}{\sqrt{\frac{\omega\sigma^2}{n}}} \quad (3.26)$$

where Max (*Y*) is the maximum predicted RSOME yield (%), Min (*Y*) is the minimum predicted RSOME yield (%), ω is the number of model parameters (including β_o), σ^2 is residual mean square, and *n* is the number of experimental runs. The derived model was used to create surface (3-D) plots to explore the designed space, and predict the optimal conditions for RSOME.

3.12 Analysis of variance (ANOVA) study for biodiesel production

One-way analysis of variance (ANOVA) was used for evaluating statistical significance of the experimental polynomial model, coefficients, process factors, and the quality of the model fit. Optimal process conditions for maximizing the yield of RSOME were determined by solving the model equation using the Design-Expert® dx8 software version 8.0.7.1. The coefficient of variance (% C.V.), a ratio of standard deviation to mean value was determined to check the capability of the model to accurately predict yields, and a low value is desirable.

3.13 Modeling of biodiesel production process variables by ANN

ANN Neural Power trial version 2.5 (cpc-x software) was employed in the study. RSOME yield (%) was predicted using the supervised back-propagation multilayer feed-forward algorithm. The network consists of an input layer (three neurons), hidden layer (three neurons), and output layer (one neuron). The same process parameters and experimental data used for the RSM modeling were deployed in the ANN architectural design. Training of the network, cross validation and testing were carried out, and the ANN-Genetic Algorithm model was successfully used as an evaluation function for the optimization of its input space to predict the

optimal values (Onoji et al., 2017a) of RSOME yield (%) and process parameters (X_1, X_2, *and* X_3) applied in developing the model.

3.14 Data validation for RSM and ANN models

The predicted optimized responses obtained from RSM and ANN models were compared with the average experimental values from triplicate runs obtained using the optimum conditions in order to evaluate the efficiencies of these optimization techniques. The percent relative error (PRE) (Zahedi & Azarpour, 2011) and absolute average deviation (AAD) (Betiku & Ajala, 2014) were determined and these were used to identify the best model by comparing evaluated values. The PRE and AAD values were calculated using Equations (3.27) and (3.28), respectively.

$$PRE\ (\%) = \frac{optimal\ actual\ yield - optimal\ predicted\ yield}{optimal\ actual\ yield} \times\ 100 \tag{3.27}$$

$$AAD\ (\%) = \left\{\left[\sum_{i=}^{n}\left(\frac{RSOME_{i,actual} - RSOME_{i,pred}}{RSOME_{i,actual}}\right)\right]\frac{1}{n}\right\} \times 100 \tag{3.28}$$

Where n is the number of experimental runs, while $RSOME_{i,\ actual}$ is the actual yield (%), and $RSOME_{i,\ pred}$ is the predicted yield (%).

3.15 Combustion of biodiesel-diesel blends in internal compression ignition engine

Five litres of commercial diesel was purchased from Nigerian National Petroleum Corporation (NNPC) fuel station located at Refinery road, Effurun, Delta State, Nigeria. The diesel and the rubber seed oil biodiesel were characterized to ascertain its uniformity with ASTM (American Society for Testing and Materials) standards for biodiesel and diesel fuels. The biodiesel-diesel

blends were prepared and tested for performance, and combustion characteristics using internal compression ignition engine.

3.15.1 Biodiesel-diesel blending analysis via ultrasonication technique

Figure 3.4 depicts the experimental setup for the blending of biodiesel mixtures using the ultrasonication blending technique. Four different blends of B10, B20, B30, and B50 were prepared on volumetric basis for test in internal compression ignition engine. Pure diesel (B00) and biodiesel (B100) fuels were also tested to determine their levels of environmental friendliness with those of their blends. For each blend (Bxx), where B stands for biodiesel blend, and xx for the % volume of biodiesel in the blend (e.g. B10 means 10% vol biodiesel, and 90% vol diesel), the measured volume of biodiesel was poured into a batch blender. The ultrasonicator horn was lowered to a depth of 2 cm within the biodiesel and then switched on. Then, an appropriate measured volume of diesel was added to the biodiesel at a constant rate and allowed to blend for 5 min under standard atmospheric conditions. The ultrasonicator is then switched off and the mixture emptied into a measuring cylinder for combustion analysis in an internal compression ignition engine.

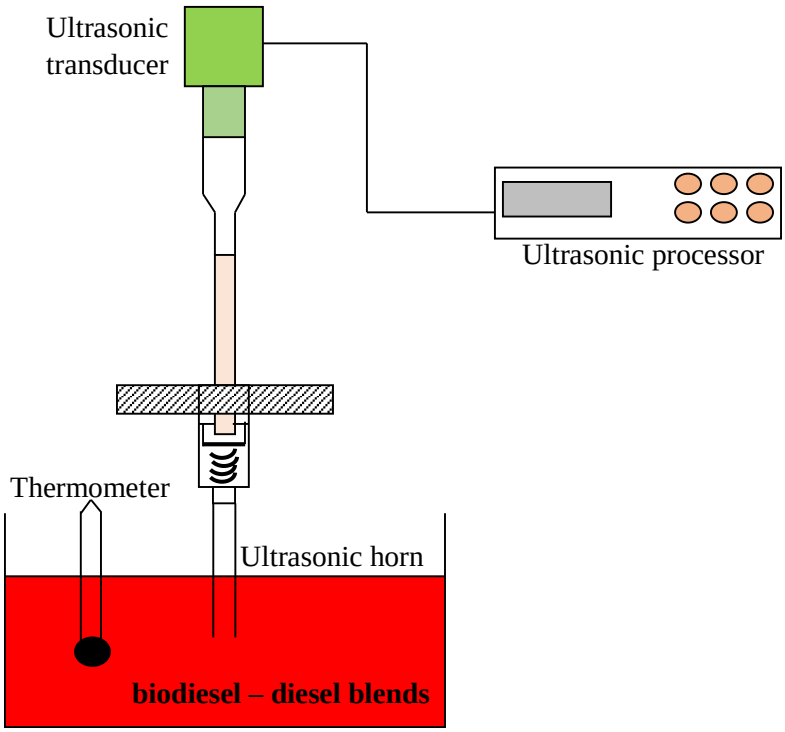


Figure 3.4: Experimental setup for biodiesel-diesel blending analysis

3.15.2 Methodology and experimental setup for combustion study of biodiesel blends

The experimental research was performed on a naturally aspirated single-cylinder, four-stroke, direct-injection, air-cooled, TecQuipment TD202 (*Model*: *1B20*) Hatz diesel test engine that was coupled to TecQuipment TD200 small engine test bed shown in Figure 3.5, and connected to a separate Versatile Data Acquisition System (VDAS) to accurately monitor and record all measured data on a computer system. The test engine is located in the Biofuels Laboratory at Petroleum Training Institute, Effurun, Nigeria. The detailed technical specifications of the test engine are listed in Table 3.3.



Figure 3.5: Experimental TD202 diesel test engine for performance and combustion analyses located at Petroleum Training Institute, Effurun, Nigeria

Table 3.3: Technical specifications for TD 202 diesel test engine

Engine make/model	Hatz/1B20
Engine type	Single cylinder, direct injection and air-cooled
Displacement (Capacity)	232 cm^3
Number of strokes	4
Aspiration/starting system	Natural/Recoil starter
Cylinder bore/connecting rod length	69 mm/104 mm
Stroke/crank radius	62 mm/31 mm
Compression ratio	22:1
Absolute maximum power	3.5 kW at 3600 rpm
Continuous rated power	3.1 kW at 3000 rpm
Orifice diameter/Coefficient of discharge	0.0185 m/0.6

The test engine set included a robust cost effective and efficient hydraulic dynamometer to control the engine load as shown schematically in Figure 3.6. There are no load resistors needed because the engine power is dissipated into the water that passes through the dynamometer. The engine was allowed to warm up before the experiments were conducted to ensure parameters were being analyzed at steady state (Özener et al., 2014). The performance and operating parameters, such as the engine torque (Nm), engine power (Watts), exhaust gas temperature (^oC), ambient air temperature, T_A (^oC), air-box differential pressure, ΔP (P_a), and ambient pressure, P_A (mbar) were measured at the engine speeds of 1500, 2000, 2500, 3000, and 3500 rpm at fixed 100% engine loading and were digitally displayed on instrument modules. They were recorded after the conditions of the engine stabilized. The parameters considered for the engine performance and emission analysis that indicate the applicability of the produced biodiesel in the engine are air/fuel ratio, brake mean effective pressure (BMEP), brake thermal efficiency (BTE %), break power (BP), engine torque, brake specific fuel consumption (BSFC), and exhaust gas temperature for performance evaluation consideration. The CO, CO_2, NO_x, total hydrocarbons (THCs), and smoke opacity were considered for the emission analysis with respect to the test engine. The engine power (Watts) was displayed digitally on the instrument module (Figure 3.5) and could be calculated using the module displayed speed (rpm) and the torque (Nm) based on Equation (3.29) used by Ude et al. (2017).

$$BP = \frac{T \times N}{9549.3} \tag{3.29}$$

where:

BP represents the engine brake power (kW); T represents the developed torque (Nm), and N is the engine speed (rpm).

The air velocity (m/s), air flowrate (kg/s), air/fuel ratio, and the brake mean effective pressure (bar) are described by Equations (3.30), (3.31), (3.32), and (3.33), respectively (TecQuipment Ltd, 2011).

$$U = \sqrt{\frac{2\Delta P}{\rho_{air}}} \tag{3.30}$$

$$\dot{m}_a = \frac{C_o \pi d^2}{4} \sqrt{\frac{2 P_A \Delta P}{R_a T_A}} \tag{3.31}$$

$$\frac{Air}{Fuel}\ ratio = \frac{\dot{m}_a}{\dot{m}_f} \tag{3.32}$$

$$BMEP = \frac{60 \times BP \times (Stroke/2)}{0.1 \times Speed \times Engine\ Capacity} \tag{3.33}$$

where:

U = velocity of air (m/s);

ΔP = air-box differential pressure (P_a);

ρ_{air} = density of air (1.2754 kg/m^3);

d = diameter of the orifice plate (= 0.0185 m for the test engine used);

C_o = coefficient of discharge (= 0.6 for the test engine used);

$\dot{m}_a$ = mass flowrate of air (kg/s);

$\dot{m}_f$ = mass flowrate of fuel (kg/s)

P_A = ambient pressure (P_a); T_A = ambient air temperature (K);

R_a = Gas constant for air (287 J/kg K)

BMEP = brake mean effective pressure (bar);

BP = brake power (Watts);

Engine capacity = 232 cm^3 for the test engine used, and speed expressed in rpm.

Stroke = 4, for the test engine.

The engine speed was measured using an optical sensor, while the torque was measured using a load cell. The volumetric flowrate of fuel at each engine speed, for each blend was calculated using the time (measured by a stopwatch) the engine takes to consume 8 mL of fuel using the 8-mL pipette fitted gauge (AVF1 option). The inlet air flowrate was measured using an orifice plate of diameter 18.5 mm. A k-type thermocouple and a differential pressure transducer were fitted near the orifice plate in order to measure the air temperature and pressure, respectively, needed for the inlet air flowrate calculation. An engine cycle analyzer (ECA 100) received the signals of both the pressure transducer and shaft encoder.

A *Quintox* flue gas analyzer (*Model*: KM 9106) manufactured by KANE International Ltd., Swallow fields, Welwyn Garden City, Herts, AL 1JG, UK, and supplied with combustion analysis display unit was employed to measure the exhaust gas emissions (CO, CO_2, NO_x, and THC) at the above stipulated engine speeds, while the smoke opacity was measured with AVL DiSmoke 4000 opacity smoke meter.

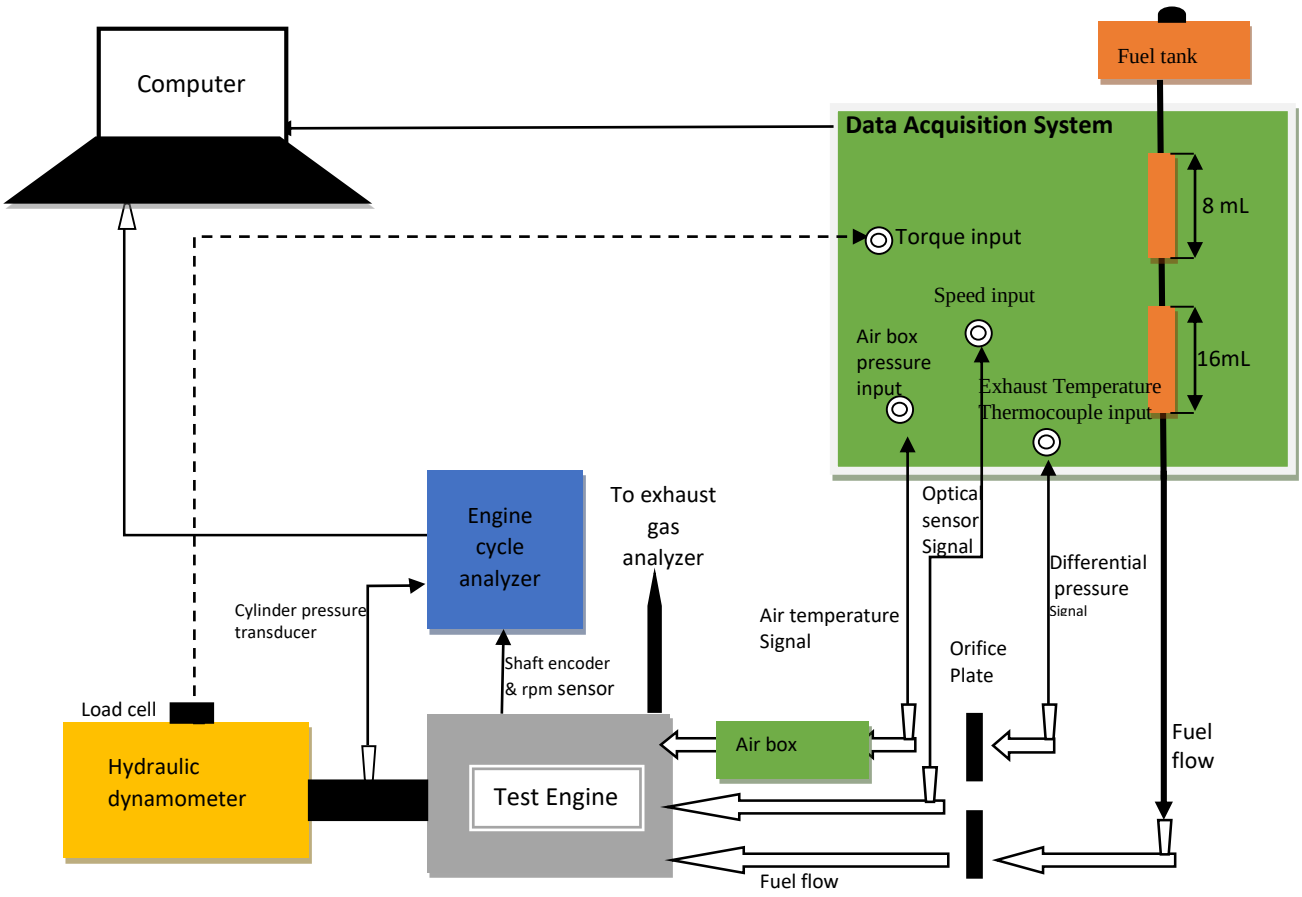


Figure 3.6: A schematic layout of experimental TD202 diesel test engine

CHAPTER 4: RESULTS AND DISCUSSION

4.0 Introduction

This chapter documents and discusses all the results obtained in this study. The results were compared with the literature, and discrepancies if any were explained.

4.1 Extraction of seed oil and determination of the best seed particle size

The results depicted in Figure 4.1 showed that a seed particle size of 0.5 mm gave the maximum oil yield of 40.3 wt. % among the available sizes during the oil extraction (Onoji et al., 2017a). The data for the plots are shown in Table D.1 of Appendix D. The findings of this study concur with those of Menkiti et al. (2015) who extracted *Terminalia catappa L* seed oil using n-hexane solvent, and obtained a yield of 60.45 wt. % from the smallest kernel particle size 0.5 mm compared to the other sizes (1, 1.5, 2, and 2.5 mm) considered. A similar trend in the reported work of Reshad et al. (2015) where the smaller particle size of 1 mm gave a rubber seed oil yield of 49.36 wt. % for 8 h extraction time was also observed. The smaller particle size creates a larger surface area that enhances oil yield by facilitating solvent diffusivity in the seed powder. In the present study, particle size of 0.5 mm was considered for oil extraction for the modeling and optimization processes, and chemical analyses. However, for industrial application, 1 mm particle size with a yield of 40.1 wt. % is preferred to 0.5 mm size as less energy is required to process the 1 mm kernel size (Onoji et al., 2017a).

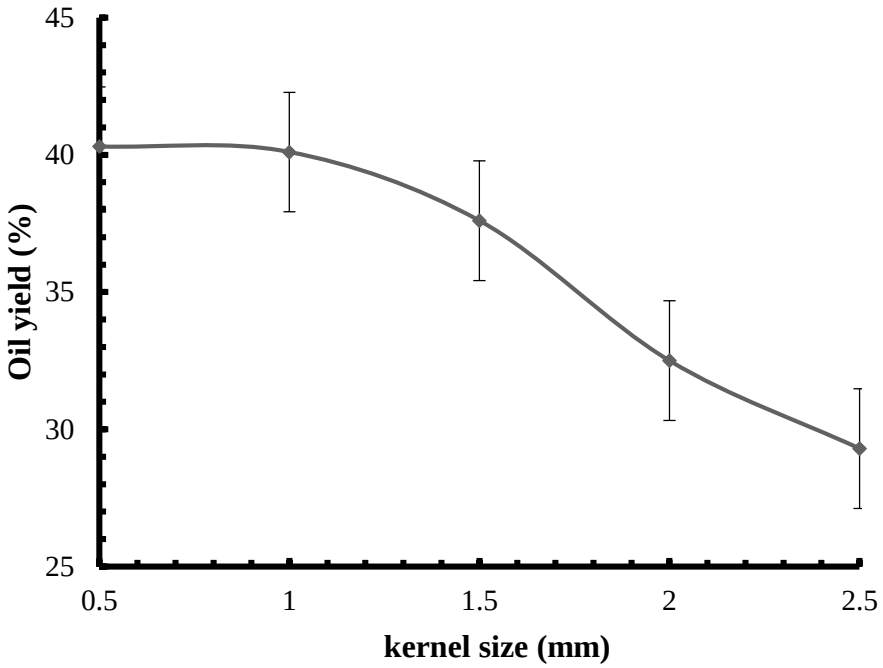


Figure 4.1: Effects of kernel particle size on the rubber seed oil yield

4.2 Physical characterization of the seed and seed oil

Table 4.1 presents the analysis of rubber seed and the extracted seed oil (Onoji et al., 2016b). The computations are presented in Section B.1 of Appendix B. The kernels moisture content (9.7 wt.%) of rubber seed evaluated was higher than the reported value of 6.5 wt.% for yellow horn seed kernels (Li et al., 2013). The determined rubber seed oil moisture content is low (1.73 wt.%) compared to castor oil (8 wt.%) and shea nut oil (10 wt.%) (Asuquo et al., 2012), *Afzelia africana* oil (2.10 wt.%) and *Hura crepitans* oil (1.90 wt.%) (Ogbu & Ajiwe, 2016). High moisture content initiates oxidation process that reduces the oil's shelf life. The low value for this oil is an indication that it could be stored for a long period without appreciable deterioration in value. The ash content of the rubber seed oil (0.001 wt.%) is lower than the prescribed ASTM ash limit (0.01 wt.% max) and those of *Afzelia africana* oil (0.006 wt.%) and *Hura crepitans* oil (0.004 wt.%) (Ogbu & Ajiwe, 2016). The low ash value is an indication that the oil lacks trace metals that catalyze oxidation reactions that cause rancidity, high acidity and

other unpleasant characteristics during storage. The carbon residue (0.4 wt.%) is close to the ASTM standard limit of 0.35 wt.% max for diesel fuels (Demirbaş, 1998), but higher than other vegetable oils such as sunflower (0.03 wt.%), rapeseed (0.05 wt.%) and olive (0.09 wt.%) (Anastopoulos et al., 2009). The high volatile content of the oil suggests that it could be a plausible source material for biodiesel synthesis for use in internal compression ignition engines.

Table 4.1: Physical characterization of rubber seed and the seed oil

Parameter	Composition (wt.%)
Rubber seed	
Kernel	40.47 ± 0.07
Kernel moisture	9.7 ± 0.07
Shell	49.83± 0.14
	100
Rubber seed oil	
Conradson carbon residue	0.4 ± 0.028
Moisture content	1.73 ± 0.028
Ash content	0.001 ± 0.0001
Volatile matter	97.869± 0.056
	100

values are mean ± standard deviation of duplicate data.

4.3 Characterization of the seed oil

The extracted rubber seed oil was subjected to physico-chemical analysis following the procedures prescribed in AOAC (1990) and ASTM methods. A comparison of the properties of the oil with values in the literature (Onoji et al., 2016a; Aravind et al., 2015; Reshad et al.,

2015) for rubber seed oil is presented in Table 4.2. The results of the analyses indicate the potentials of rubber seed oil as an alternative feedstock to edible oils for commercial production of biodiesel, and other industrial applications of oils where non-edible oil is preferable (Onoji et al., 2017a).

4.3.1 Colour, pH, density and Specific gravity

The colour of the rubber seed oil was dark brown after clarification, and it remained liquid at room temperature (Onoji et al., 2016b). The pH value of 6.0 obtained for the oil compares favorably with those reported for castor oil (6.8) and luffa cylindrica seed oil (3.93) (Asuquo et al., 2012). This value is an indication of the presence of reasonable amount of free fatty acid and the advantageous utilization of the oil in soap making (Hosamani & Katagi, 2008). The density at 25 ^{o}C was determined using a pycnometer and was found to be 0.886 g/cm^3, which implies that the oil is less than water with the absence of heavy elements. The specific gravity at 15 ^{o}C was determined as 0.909 using standard specific gravity bottles and the ^{o}API gravity of 24.1 was calculated for the oil (Onoji et al., 2016b). Specific gravity is an indication of the energy content of a fuel. A fuel with a high specific gravity (low ^{o}API) has a higher heating value than a fuel with a low specific gravity (high ^{o}API). The physical characteristics seem to be similar to other common vegetable oils, and the oil was validated as environmentally friendly.

4.3.2 Iodine, peroxide, saponification and acid values

Iodine value (IV) measures the degree of unsaturation in a fat or vegetable oil and determines its oxidative stability. The iodine value of rubber seed oil (137.02 g I_2/100 g oil) was estimated by Wijs' method and falls within the range specified for semi-drying oils (100–150 g I_2/100 g) (Asuquo et al., 2012). The higher iodine value may be due to high-unsaturated fatty acid

content, as observed in GC-MS analysis of oil. The peroxide value (PV) determines the extent to which the oil has undergone rancidity when stored, heated, or in contact with air and could be used to assess the quality and stability of oils. Oils become rancid when the PV range from 20–40 mequiv O_2/kg oil (Bora et al., 2014). Standard Organization of Nigeria (SON, 2000) and the Nigerian Industrial Standards (NIS, 1992) specify a peroxide value of 10 mequiv O_2/kg oil for edible oils. The PV obtained for rubber seed oil in this study was 10.46 mequiv O_2/kg oil, and it is within the range reported in literature for RSO (1.6–16 mequiv O_2/kg oil) (Onoji et al., 2016a), and close to Nigerian standards for edible oils. This indicates that the rubber seed oil can be stored for a long period without deterioration. The saponification value (SV) indicates the amount of alkali required to convert the oil into soap and is an index of average molecular mass of fatty acid in the oil sample (Toscano et al., 2012; Anastopoulos et al., 2009). As oil is mainly triglycerides, it allows for comparison of the average fatty acid chain length. The SV of 195.3 mg KOH/g RSO obtained in this study (Onoji et al., 2016b) lies between those of sunflower (186) and coconut oils (265) (Aravind et al., 2015), and within the range of 195–205 mg KOH/g oil for edible palm oils as specified by SON (2000) and NIS (1992). This shows that rubber seed oil has lesser tendency to saponify at elevated temperatures than coconut oil. The acid value (AV) of rubber seed oil was 18.20 mg KOH/g oil, which indicates high levels of free fatty acids (9.10 wt.%), a limiting factor in its use as a source of food. The acceptable limit for edible oils is ≤ 10 mg KOH/g oil. Therefore, chemical re-esterification or physical refining would be required to de-acidify the oil (Ebewele et al., 2010b). However; this value is low enough and is within the limits for industrially useful oils (Oyedeji & Oderinde, 2006).

4.3.3 Kinematic viscosity

Kinematic viscosity (KV) is a measure of the resistance of oil to shear. The dynamic (absolute) viscosity for the rubber seed oil was digitally determined at 40 ^{o}C using Brookfield DV - I +

Viscometer (*Model LVDV* - |+) manufactured by Brookfield Engineering Laboratories Inc., Middleboro, MA 02346 USA. It was operated at 100 rpm with spindle No. 61 and a Torque of 59.2%. The average KV of the RSO was calculated as 35.6 cP and converted to 40.18 mm^2/s based on Equation (4.1). This is a low value compared to jatropha *curcas* L. oil (77.4 mm^2/s) but higher than that of conventional diesel (<5 mm^2/s) (Reshad et al., 2015).

$$Kinematic\ viscosity\ (mm^2/s) = \frac{Absolute\ viscosity\ (cP)}{Density\ (g/cm^3)} \quad (4.1)$$

4.3.4 Cold flow properties

The flow properties of RSO were observed under low temperatures, and the parameters considered are pour point (PP), cloud point (CP) and cold filter plugging point (CFPP), respectively.

4.3.4.1 Pour point (PP)

The PP is the lowest temperature at which the oil suffers from gel formation and attains semi-solid state and become deprived of its flow ability (Verma et al., 2016). The value of –6 ^oC observed for this rubber seed oil is lower than that of Jatropha oil (4 ^oC) (Reshad et al., 2015; Mazumdar et al., 2012) and castor oil (–2 ^oC), comparable to waste cooking oil (–7 ^oC), but higher compared to canola (–18 ^oC) (Reshad et al., 2015). The value obtained is close to reported value of –9 ^oC for RSO (Aravind et al., 2015). This suggests that it can be employed under cold climatic conditions as a source material for lubricating oil formulation.

4.3.4.2 Cloud point (CP)

CP is the temperature at which a cloud or haze first appears in a liquid when cooled under carefully controlled conditions. The observed CP for rubber seed oil was 5.5 ^oC. This value is lower than 10–11 ^oC reported for Jatropha oil (Mazumdar et al., 2012). This suggests that RSO

is mainly unsaturated and a good source material for biodiesel synthesis for use in cold regions compared to Jatropha oil (Onoji et al., 2016b).

4.3.4.3 Cold filter plugging point (CFPP)

The CFPP measures the lowest temperature at which a fuel gives trouble-free flow in a fuel system. The CFPP value of –0.025 ^{o}C was estimated from Equation (4.2) cited by Verma et al. (2016).

$$CFPP = 0.8537 \times CP - 4.72 \quad (4.2)$$

The low CFPP confirms that the rubber seed oil is mainly unsaturated fatty acids and its use is favourable in cold climatic regions.

4.3.5 Aniline point

The aniline point (AP) of oil is defined as the minimum temperature at which equal volumes of aniline and oil are miscible. It is a measure of the aromatic content of oil and an evaluating factor for diesel index determination and cetane number. At room temperature (28 ^{o}C), complete miscibility of rubber seed oil with an equal volume of aniline was observed. The oil was cooled to 10 ^{o}C in an ice-bath and mixed with equal volume of aniline to form a 2-phase mixture. The mixture was heated gradually until complete miscibility was observed at 21 ^{o}C (69.8 ^{o}F) as the aniline point (Onoji et al., 2016b).

4.3.6 Boiling, freezing, flash and fire points

The boiling point was determined as 119 ^{o}C using Stanhope-Setastill apparatus (*Model: 11860-3U*). This suggests that moisture present could be removed at 105 ^{o}C without affecting its properties prior to industrial applications such as biodiesel and lubricant synthesis. The freezing point was observed at –18 ^{o}C using Stanhope-Seta Cloud and Pour Point Refrigerator Surrey,

England (Test Bath No. 4) calibrated to –51 ^{o}C. The fire and flash points were determined by using Stanhope-Seta Pensky-Martens (A and B closed Cup-Model 34100-2/34000-0U) multi-flash equipment. The flash and fire points were observed as 240.3 and 256 ^{o}C, respectively. This shows that the oil can be stored safely at room temperature.

4.3.7 Refractive index (RI)

The refractive index (RI) is the ratio of the velocity of light in vacuum to the velocity of light in a medium (in this case, RSO) and an indication of the level of saturation of the oil. RI was determined at 20 ^{o}C using Abbe Refractometer (*Model: 60/ED*) and calibrated chart. The value of 1.4707 calculated for RSO falls within the range reported in the literature for vegetable oils (Rashad et al., 2015).

4.3.8 Other parameters

Other parameters determined for RSO are cetane number, diesel index, higher heating value, and average molecular weight.

4.3.8.1 Cetane number (CN)

Cetane number is a measure of the tendency a fuel to knock in a diesel engine. It is an indication of the ignition quality of a fuel. CN for RSO was calculated as 43.42 using the correlation developed by Mofijur et al. (2014) as expressed in Equation (4.3).

$$CN = 46.3 + (5458/SV) - (0.225 \times IV) \quad (4.3)$$

This value compares favourably with those reported in the literature (45–49.73) for RSO (Omorogbe et al., 2013; Kumar et al., 2010). However, with the recent price instability of crude oil in the world markets, there is renewed interest in the use of vegetable oils such as RSO to produce biodiesel for use in diesel engines.

4.3.8.2 Diesel index (DI)

The diesel index of RSO is computed using Equation (4.4) as follows:

$$Diesel\ index(DI) = \frac{Aniline\ point\ (°F) \times API\ gravity\ (60\ °F)}{100} \quad (4.4)$$

The value 15.71 obtained is below minimum standard of 50 specified for diesel fuel. Therefore, this oil cannot be used directly on diesel engines without chemical conversion because of its high viscosity that will result to poor atomization in engine during operation.

4.3.8.3 Higher heating value (HHV)

The HHV of vegetable oils can be calculated by using SV and IV obtained from simple chemical analyses using common laboratory equipment. In this study, a simple correlation (R^2 = 0.9999) developed by Demirbaş (1998) as expressed in Equation (4.5) was used to estimate HHV for RSO.

$$HHV\ (MJ/kg) = 49.43 - [0.041(SV) + 0.015(IV)] \quad (4.5)$$

The value obtained (39.37 MJ/kg) is within the range reported in literature for RSO (36.1–44 MJ/kg) (Onoji et al., 2016a; Reshad et al., 2015) and comparable to those reported by Rahman et al. (2014) for jatropha *curcas* L. oil (38.66).

4.3.8.4 Average molecular weight of rubber seed oil

Vegetable oils are mainly triglycerides of three fatty acid chains with a glycerol backbone. The average molecular weight of vegetable oils can be estimated using simple analytical processes in laboratories. Higher molecular mass indicates higher heating values for the oil. The determination of the molecular weight of vegetable oil is important for biodiesel production reactions because the quantity of reagents used is based on molecular weight of the vegetable

oil. The average molecular weight of the RSO was calculated using Equation (4.6) reported by Fillières et al. (1995).

$$Avg.molecular\ weight\ of\ oil\ (g/mol.) = 3M_{w_{FA}} + M_{w_{gly}} - 3M_{w_{water}} \quad (4.6)$$

where $M_{w_{FA}}$ is the mean molecular weight of fatty acids present, $M_{w_{gly}}$ is the molecular weight of glycerol (92.09), and $M_{w_{water}}$ is the molecular weight of water (18.01).

The mean molecular weight of fatty acids of RSO was estimated from Equation (4.7) reported by Ajiwe et al. (1995) and calculated as 286.74.

$$Mean\ molecular\ weight\ of\ fatty\ acids = (56/SV) \times 1000 \quad (4.7)$$

The average molecular weight of the RSO estimated from Equation (10) is 898 g/mol. The value obtained compares favourably with those reported by Anastopoulos et al. (2009) for sunflower oil (876), rapeseed oil (992), olive oil (857), and used frying oil (882).

Table 4.2: Physico-chemical properties and other characteristics of rubber seed oil.

Parameters	Refs.[a, b, c]	This study
Colour	Golden yellow, light/dark brown	Dark brown
Density, g/cm^3 @ 25 ^{o}C	0.857–0.943	0.886± 0.002
Specific gravity @ 15 ^{o}C	0.91	0.909± 0.002
^{o}API gravity @ 15 ^{o}C	NA	24.1± 0.282
Ph	6	6± 0.141
Oil content (wt.%)	40–50	43± 0.141
Iodine value, g I_2/100 g oil	113–146	137.02± 0.028
Peroxide value, meq. O_2/kg oil	1.6–16	10.46± 0.098
Saponification value, mg KOH/g oil	183.91–235.28	195.30± 0.282
Acid value, mg KOH/g oil	1.68–42.41	18.20± 0.141
Free fatty acid (%FFA as oleic acid)	0.84–42.412	9.10± 0.07
Kinematic viscosity, mm^2/s @ 40 ^{o}C	6–66	40.18± 0.028
Refractive index @ 20 ^{o}C	1.46–1.47	1.4707± 0.0003
Pour point, ^{o}C	–9 to –1.5	–6
Cloud point, ^{o}C	3–4	5.5
Cold filter plugging point, ^{o}C	NA	–0.025
Flash point, ^{o}C	72–295	240.3
Fire point, ^{o}C	298	256
Aniline point, ^{o}C (^{o}F)	NA	21 (69.8)
Boiling point, ^{o}C	NA	119
Freezing point, ^{o}C	NA	–18
Cetane number	45–49.73	43.42
Higher heating value (HHV), MJ/kg	36.1–44	39.37
Mean mol. weight of fatty acids, (g/mol)	NA	286.74
Average molecular weight of RSO, (g/mol)	NA	898
Diesel index	NA	15.71

[a] Onoji et al., 2016a; [b]Aravind et al., 2015; [c] Reshad et al., 2015.

NA: means not available; values are mean ± standard deviation of duplicate data.

4.3.9 Fatty acid profile of the seed oil

Gas chromatography-mass spectrometry (GC-MS) analysis was employed to characterize the oil to determine its fatty acid profile. The identification of compounds and their structures was based on data from NIST library. The results presented in Table 4.3 and Figure 4.2 indicates that the oil is mainly unsaturated. The fatty acids present are palmitic (13.85%), stearic (16.82%), oleic (64.11%), and *cis*-erucic (5.22%). The total unsaturated fatty acid composition of the rubber seed oil was 69.33% with a saturated content of 30.67% (Onoji et al., 2016b).

Table 4.3: Fatty acids profile of rubber seed oil

Fatty acid/systemic name	Chemical formulae	Compositions (wt. %) Ref.[q]	This study
Myristic ($C_{14:0}$) / Tetradecanoic	$C_{14}H_{28}O_2$	2.2	–
Palmitic ($C_{16:0}$)/ Hexadecanoic	$C_{16}H_{32}O_2$	0.23–10.6	13.85
Palmitoleic ($C_{16:1}$)/ Hexadec-9-enoic	$C_{16}H_{30}O_2$	0.23–0.25	–
Stearic ($C_{18:0}$)/ Octadecanoic	$C_{18}H_{36}O_2$	5.69–12	16.82
Oleic ($C_{18:1}$)/ *cis*-9-Octadecenoic	$C_{18}H_{34}O_2$	12.7–42.08	64.11
Linoleic($C_{18:2}$)/ *cis*-9-*cis*-12-Octadecadienoic	$C_{18}H_{32}O_2$	39.6–52.84	–
α-Linolenic ($C_{18:3}$)/ *cis*-9-*cis*-12-*cis*-15-Octadecatrienoic	$C_{18}H_{30}O_2$	2.38–26	–
Arachidonic ($C_{20:0}$)/ Eicosanoic	$C_{20}H_{40}O_2$	0.66–0.97	–
Erucic acid ($C_{22:1}$)/*cis*-13-Docosenoic	$C_{22}H_{42}O_2$	–	5.22
Total saturated		8.78–23.57	30.67
Total monounsaturated		12.93–42.33	69.33
Total polyunsaturated (linoleic, linolenic, etc)		41.98–78.84	Trace

[q] Onoji et al., 2016a

Although the composition of this oil did not follow the trend of some of the reported fatty acid profile for rubber seed oil in the literature (Onoji et al., 2016a), genetic variations could be

responsible for the disparity observed in the fatty acid profile of seed oil from NIG 800 clonal series of Nigerian rubber seeds. The high content of oleic acid and the presence of *cis*-erucic acid indicate the potential use of seed oils from the NIG800 series as a source of oleo chemicals. This could replace the oleo chemicals from petroleum currently used for the oleo chemical and steel industries. The mean molecular weight of fatty acids present in the rubber seed oil was computed as 280.81 using Equation (4.8). This value compares favourably with 286.74 obtained using chemical analysis method earlier shown in Equation (4.7) with 2.06 % deviation.

$$Mean\ molecular\ weight\ of\ fatty\ acids = \frac{\sum f_i}{\sum \frac{f_i}{M_{wi}}} \tag{4.8}$$

where f_I = % composition of fatty acids from GC-MS analysis and M_{wi} = molecular weight of a fatty acid.

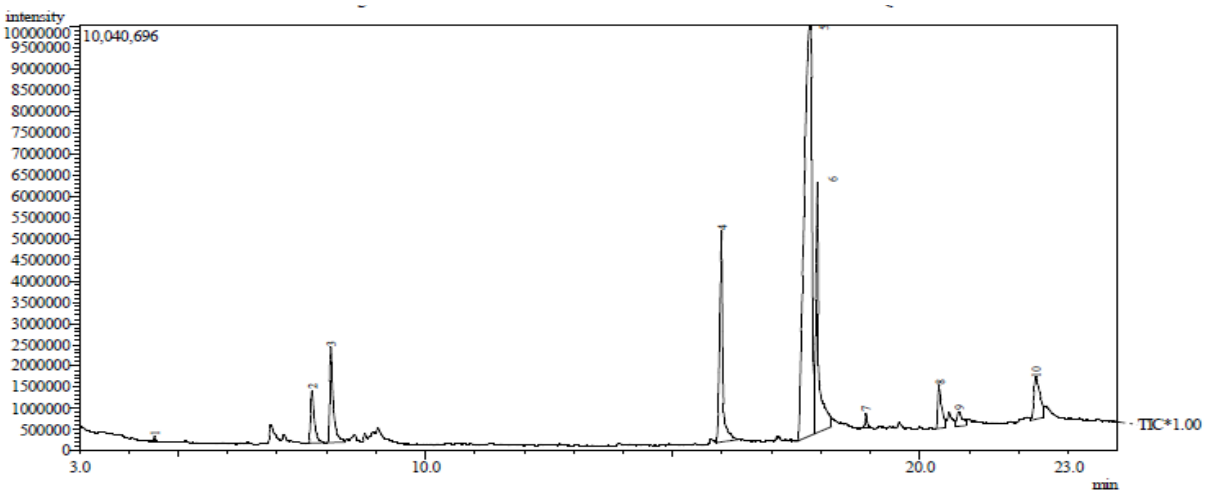


Figure 4.2: Gas chromatogram of the rubber seed oil with identified peaks: peak 4 (palmitic acid), peak 5 (oleic acid), peak 6 (stearic acid), peak 10 (*cis*-erucic acid) (Onoji et al., 2016b)

4.3.10 FT-IR and NMR spectroscopy of the seed oil

The structural characterizations of rubber seed oil were further performed by FT-IR, ^{1}H NMR, and ^{13}C NMR analyses to confirm results from GC-MS analysis. These analyses are essential for industrial applications of the oil.

4.3.10.1 FT-IR analysis of the seed oil

Further insight into the chemical compositions of the rubber seed oil was provided by the FT-IR spectrum at room temperature (28 ^{o}C) based on Table G.1 of Appendix G. It has been reported that very low proportions of compounds present in a mixture exhibit very weak band which are not detectable in the IR spectrum (Guillèn & Cabo, 2002). The absorption bands of vegetable oils at intervals of 3200 and 3600 cm^{-1} are usually due to O–H stretching vibration of alcohols, carboxylic acids, and hydroperoxides (Ogbu & Ajiwe, 2016). These bands range is conspicuously absent at room temperature for the oil under study. This indicates the absence of a free hydroxyl functional group (O–H) for alcohols, phenols, primary and secondary oxidation products for the extracted oil, as shown in the FT-IR spectrum (Figure 4.3). Data showed that triglyceride (TG) was the main component in this rubber seed oil. The strong absorption band of the ester carbonyl functional group of TG, i.e. C=O was observed around 1742 cm^{-1}. The stretch vibration of C–O at 1160 cm^{-1} is attributed to the presence of ester groups. The FT-IR spectrum presents a fingerprint region (1461–585 cm^{-1}) that can be used as an analytical tool to detect rubber seed oil adulteration. Table 4.4 shows the functional groups and modes of vibration present in this rubber seed oil at room temperature (Onoji et al., 2016b). The results compared favourably and within the ranges reported for rubber seed oils by other researchers (Reshad et al., 2015; Bakare et al., 2006).

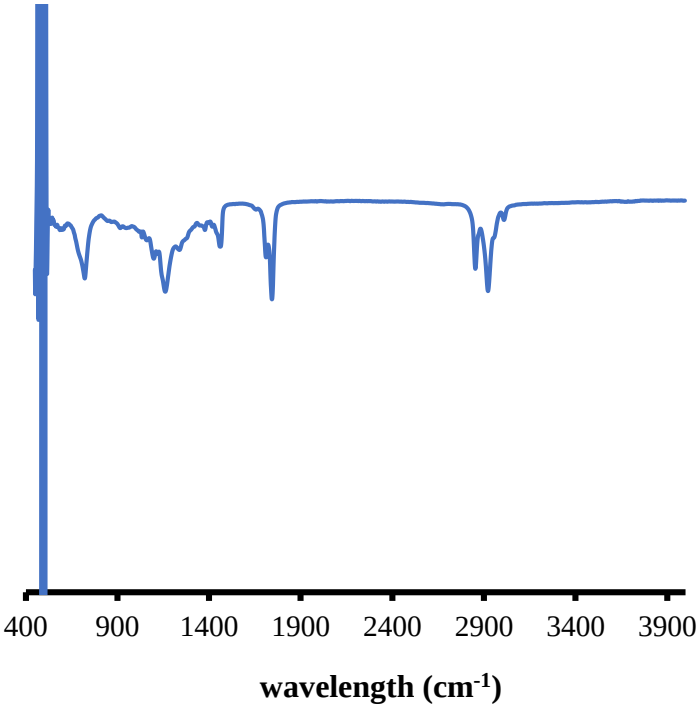


Figure 4.3: FT-IR spectrum of the rubber seed oil

Table 4.4: Wavenumbers and their functional groups for FT-IR analysis of the rubber seed oil

Wavenumber (cm^{-1})	Functional group	Description of vibration
3009	Alkenes	This is due to =C–H stretching of non-conjugated unsaturation (methylene group)
2921–2853	Alkanes	These strong peaks are attributed to the stretching of C–H (methyl group)
1742	Carbonyl	This strong and sharp peak is attributed to –C=O stretching of esters
1710	Carboxylic acids	This assigned peak is due to stretching vibration of C=O
Fingerprint region (1461–585 cm^{-1})		
1461	Alkenes	The medium signal can be attributed to bending frequency of C–H
1377	Alkenes	The assigned peak is due to C–H bending vibrations of alkenes (CH_2 group)
1238	Carboxylic acids, Esters	The assigned peak is attributed to stretching vibration of C–O
1160	Esters	C–O stretching vibration attributed to ester groups
1118–1033	Esters	=C–O–C stretching vibration of ester groups
721	Aromatics	Assigned to out-of-plane bending vibration of saturated carbon atom (C–H)
585	Alkanes	The weak signal is due to C–H vibration

4.3.10.2 ^{1}H NMR analysis of the seed oil

The assignments of the signals of the rubber seed oil spectrum to the different kinds of hydrogen atoms of the acyl chains based on the literature provided by Guillén & Ruiz (2003) as in Table G.2 of Appendix G are presented in Table 4.5. The ^{1}H NMR spectrum of the rubber seed oil shown in Figure 4.4, with ten different signals of variably significant intensity depending on the proportions of the different acyl groups, is comparable with those of most vegetable oils reported in the literature (Guillén & Ruiz, 2003) and that of rubber seed oil presented by other researchers (Reshad et al., 2015; Bakare et al., 2006; Okieimen et al., 2005b).

The signals are due to the protons of the triacylglycerols and are proportional to the number of hydrogen atoms of each kind that are present in the oil sample. Signal 1 (Figure 4.4 and Table 4.5) is produced by overlapping of doublet signals of methyl group protons of the saturated and omega-9 (i.e. oleic acid) acyl groups, and it appears at 0.80 and 0.81 ppm, respectively. Signal 2 is a singlet due to methyl protons of erucyl group (i.e. *cis*-erucic acid) and appears at 0.89 ppm. Signal 3 is due to the protons of the saturated methylene group of all acyl chains and appears at 1.19 and 1.23 ppm. Signals 4 and 6 are due to methylene protons in the β and α position and appear at 1.53 and 2.22 ppm, respectively. Signal 5, between 1.94 and 1.98, are due to α-methylene protons in relation to a single double bond (allylic protons). Signal 7, an overlapping signal between 2.68 and 2.72 ppm, is due to signals from α-methylene protons in relation to double bonds (bi-allylic protons). Signal 8, which appears between 4.05 and 4.23 ppm, is due to the protons on carbon atoms 1 and 3 of the glyceryl group. Signal 9, which appears at 5.25, is due to the proton on carbon atom 2 of the glyceryl group that overlaps with signal 10 (olefinic protons of different acyl groups) at 5.26 ppm.

Table 4.5: ^{1}H NMR spectrum analysis of the rubber seed oil

Signal	Chemical shift (ppm)	Functional group	Assignments
1	0.80 and 0.81	$–CH_3$ (terminal methyl protons (saturated and oleic acids)	all acyl chains except linolenyl
2	0.89	$–CH_3$ (terminal methyl protons (*cis*-erucic acid)	acyl chains
3	1.19 and 1.23	$–(CH_2)_n$ - (saturated methylene proton)	all acyl chains
4	1.53	$–OCO–CH_2–CH_2–$ (β-methylene protons (carbonyl)	acyl chains
5	1.94-1.98	$–CH_2–CH=CH$ (allylic methylene protons)	all acyl chains
6	2.22	$–OCO–CH_2–$ (α-methylene protons)	acyl chains
7	2.68 and 2.72	$=HC–CH_2–CH=$ (bis-allylic methylene protons)	acyl chains
8	4.05-4.23	$–CH_2OCOR$ (methylene protons on carbons 1, 3)	glyceryl group
9	5.25	>CHOCOR (proton on carbon atom 2). It overlaps with signal 10	glyceryl group
10	5.26	–CH=CH– (olefinic protons)	acyl chains

^{1}H NMR chemical shift (2.8 ppm) (Sadowska et al., 2008) usually attributed to the presence of linolenic and linoleic chains ($CH=CHCH_2CH=CH$), is not present in rubber seed oil used in this study. This is in satisfactory agreement with the GC-MS and ^{13}C NMR analyses of the oil.

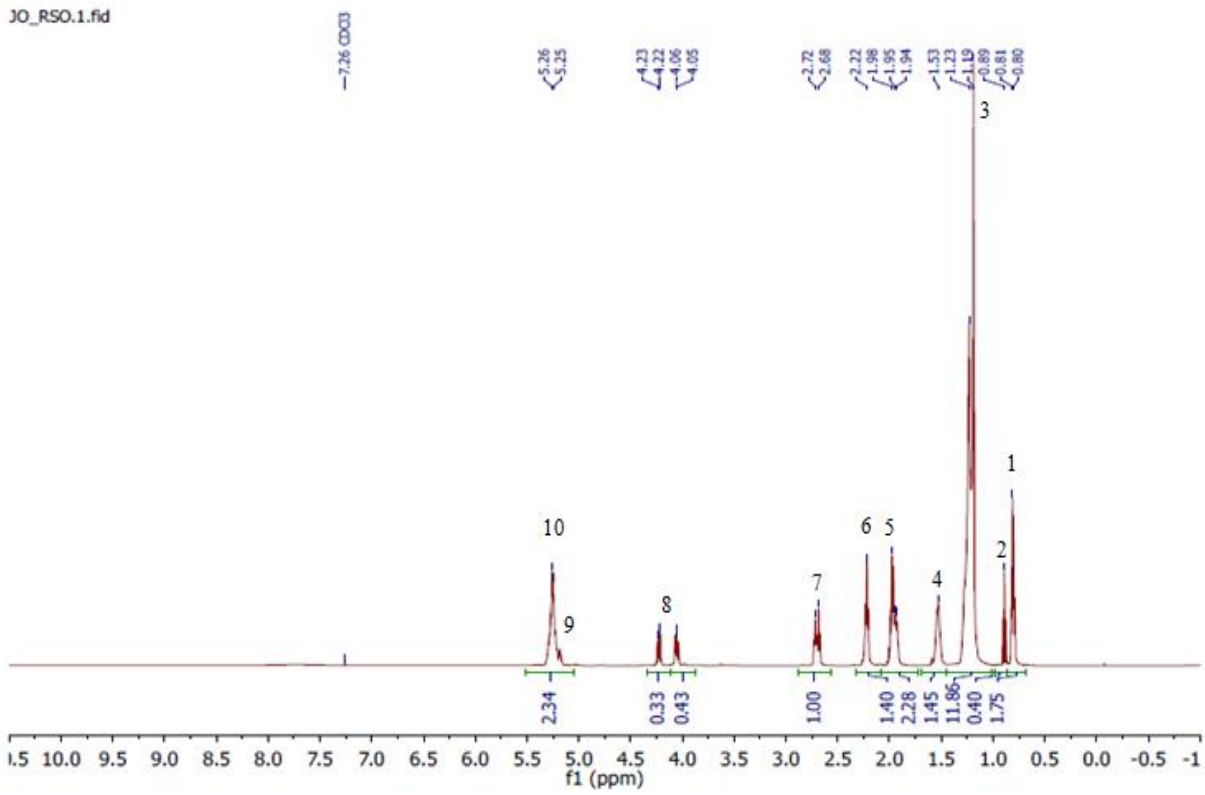


Figure 4.4: ^{1}H NMR spectrum of the rubber seed oil

4.3.10.3 ^{13}C NMR analysis of the seed oil

The ^{13}C NMR spectrum for the oil under study is depicted in Figure 4.5 and presented in Figures G.1 through G.5 of Appendix G. The spectrum could be grouped into four distinct spectra regions (A, B, C, and D) as presented in Table 4.6 (Onoji et al., 2016b). The results are similar to previous studies by other researchers on rubber seed oil (Okieimen et al., 2005b). When the ^{13}C NMR is compared with spectra in Figure G.6 of Appendix G (Sadowska et al., 2008), it shows the possible absence of linolenic and linoleic acids as confirmed by the data from GC-MS analysis (Table 4.3).

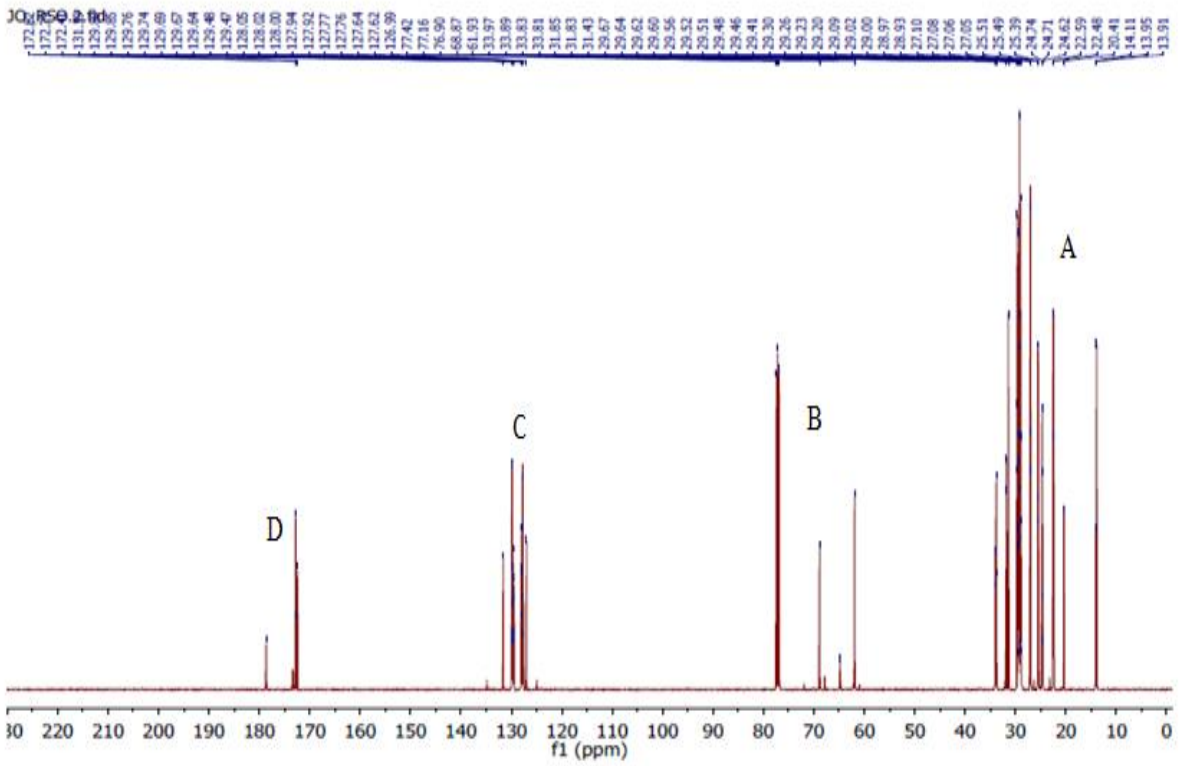


Figure 4.5: ^{13}C NMR spectrum of the rubber seed oil

Table 4.6: ^{13}C NMR analysis of carbon type present in the rubber seed oil

Group	Carbon environment	Chemical shift, δ (ppm)	Functional group
A	Aliphatic	13.91–33.97	CH_3
B	Glyceryl	61.93–77.16	CH_2–OCOR
C	unsaturated alkenes	126.99–131.99	CH=CH
D	carbonyl	172.41–172.82	C=O
	carboxylic acid	178.64	COOH

4.4 Kinetic study of thermo-oxidative degradation of the seed oil

When vegetable oils are heated under extreme conditions experienced in frying or in industrial applications, they undergo thermal oxidative reactions that are reflected in remarkable changes

in peroxide, iodine, and refractive index values, respectively (Oderinde et al., 2009). The average values of the peroxide, iodine, and refractive index of the *Hevea brasiliensis* seed oil used in this study with respect to temperature and time on heating obtained from Table E.1 of Appendix E are summarized in Table 4.7 (Onoji et al., 2016b).

Table 4.7: Effect of heating on peroxide, iodine, and refractive index values of rubber seed oil

Temp (°C)	Time (min)	Peroxide value (mequiv O_2/kg oil)	Iodine value (g I_2/100 g oil)	Refractive index @ 20 °C
100	30	4.02 ± 0.25	117.72 ± 1.10	1.4651 ± 0.013
	60	4.50 ± 0.12	117.43 ± 0.16	1.4322 ± 0.048
	120	4.81 ± 0.01	117.24 ± 0.05	1.4147 ± 0.018
	180	5.00 ± 0.22	117.02 ± 0.02	1.3514 ± 0.043
	240	5.40 ± 0.28	116.98 ± 0.66	1.3011 ± 0.001
	300	5.61 ± 0.15	116.84 ± 0.05	1.2430 ± 0.011
150	30	4.38 ± 0.04	117.56 ± 0.36	1.4630 ± 0.004
	60	4.66 ± 0.08	117.32 ± 0.16	1.4290 ± 0.001
		4.98 ± 0.12	117.12 ± 0.24	1.4130 ± 0.019
	180	5.24 ± 0.05	116.84 ± 0.32	1.3850 ± 0.005
	240	5.56 ± 0.35	116.60 ± 0.87	1.3651 ± 0.006
	300	5.82 ± 0.16	115.40 ± 0.84	1.3436 ± 0.002
200	30	4.62 ± 0.12	117.38 ± 0.09	1.3647 ± 0.002
	60	4.88 ± 0.08	117.02 ± 0.02	1.3230 ± 0.001
	120	5.00 ± 0.12	116.61 ± 0.38	1.2991 ± 0.002
	180	5.34 ± 0.05	116.32 ± 0.31	1.2911 ± 0.001
	240	5.76 ± 0.08	115.68 ± 0.98	1.2834 ± 0.002
	300	5.94 ± 0.04	115.24 ± 0.05	1.2433 ± 0.001
250	30	4.74 ± 0.02	117.21 ± 0.50	1.3020 ± 0.002
	60	4.90 ± 0.07	116.60 ± 0.28	1.2750 ± 0.001
	120	4.98 ± 0.11	116.20 ± 0.28	1.2331 ± 0.001
	180	5.20 ± 0.07	115.40 ± 0.28	1.2311 ±0.001
	240	5.50 ± 0.07	114.82 ± 1.32	1.2212 ± 0.005
	300	5.70 ± 0.14	114.48 ± 0.22	1.2011 ± 0.010

values are mean ± standard deviation of duplicate data

This shows that rubber seed oil undergoes thermal degradation that results to oxidative rancidity and formation of unstable hydroperoxides. Moisture present in rubber seed oil hastens its oxidation process (hydrolysis) that generates free fatty acids (FFAs) and their oxidized compounds as depicted in Figure 4.6.

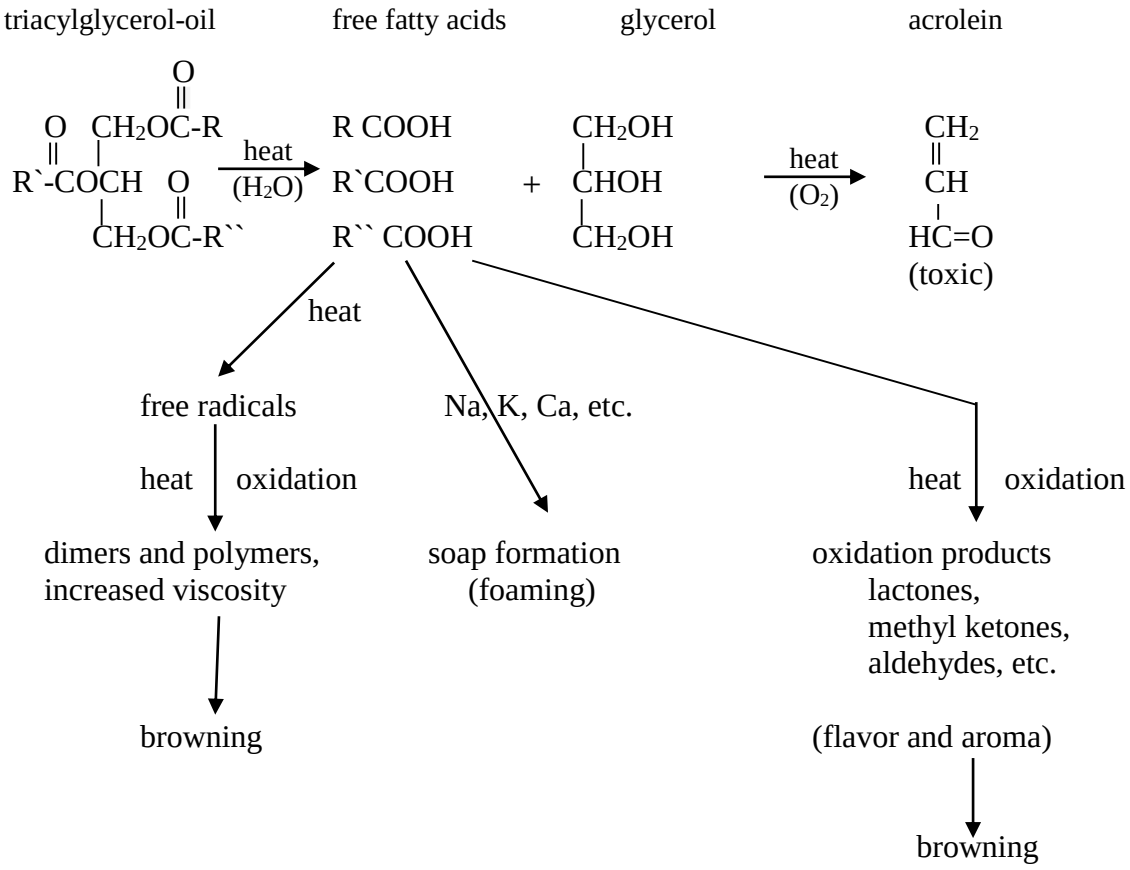


Figure 4.6: Overall process of oil degradation (Adapted from Onoji et al, 2016b)

During thermal hydrolysis, the oil decomposed to produce di- and mono-acylglycerol, glycerol, and FFAs that accelerate further the hydrolysis of the oil. The major thermal degraded byproducts of rubber seed oil are low molecular volatile compounds, such as aldehydes, ketones, carboxylic acids, and short chain alkanes and alkenes (Tables 4.4, 4.5, and 4.6) and non-volatile dimers and polymers. The rubber seed oil used in this study is rich in monounsaturated oleic acids (64.11 wt.%) and could form dehydroxydimer, ketohydrodimer, monohydrodimer, and dehydrodimer of oleic acid if defectively stored. Dimers and polymers are large molecules with molecular weight range of 692-1600 Da. These compounds are formed during thermal oxidation by a combination of ⁻C⁻C⁻, ⁻C⁻O⁻C⁻, and ⁻C⁻O⁻O⁻C⁻bonds and have hydroperoxy, epoxy, hydroxyl, carbonyl groups, and ⁻C⁻O⁻C⁻C⁻, and ⁻C⁻O⁻O⁻C⁻ linkages (Choe & Min, 2007). The aforementioned groups and linkages were present in the oil

used for this study as deduced from FT-IR and NMR results (Tables 4.4, 4.5, and 4.6). This establishes the possibility of generating dimers and polymers from rubber seed oil at elevated temperatures considered in the kinetic study. The mechanism for the formation of acyclic polymers generated from oleic acid component of the rubber seed oil during thermal degradation is shown in Figure 4.7. The degradation process also results in loss of unsaturation (iodine value) in the fatty acids as shown in Table 4.7.

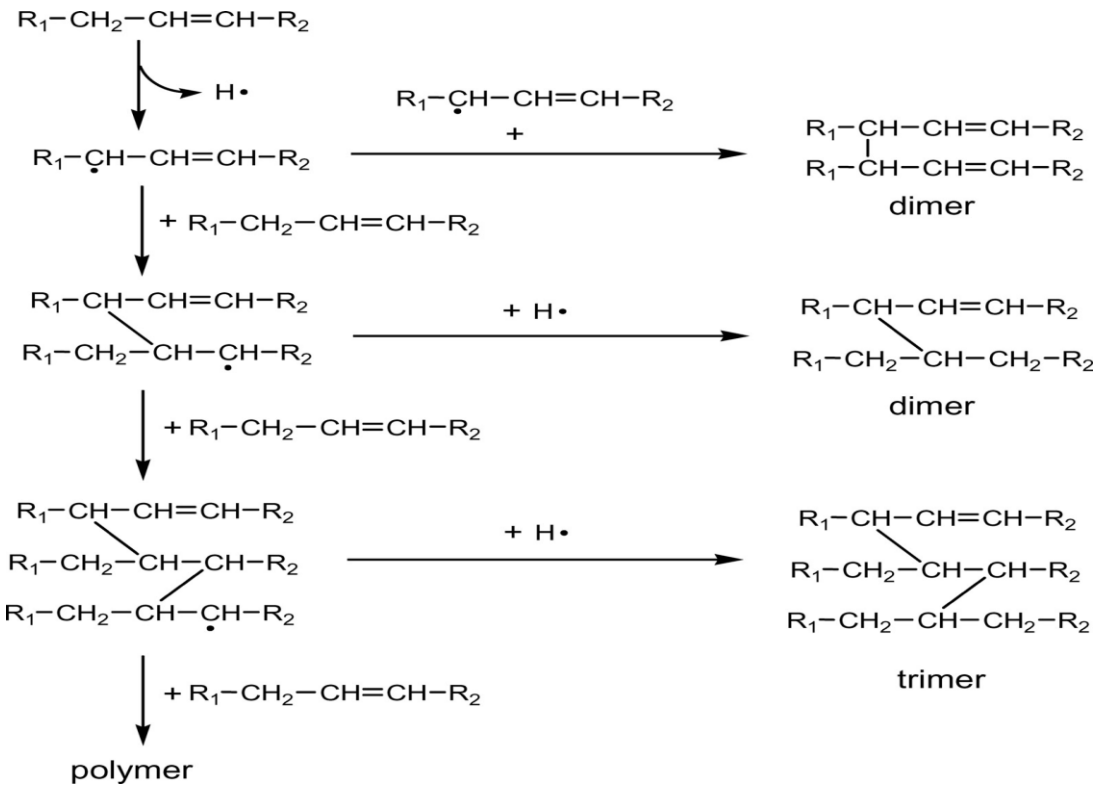


Figure 4.7: Acyclic polymer formations from oleic acid during thermal oxidation of oils (Adapted from Onoji et al., 2016b)

The iodine data in Table 4.7 were used to generate the kinetic data for the thermo-oxidative behaviour of the oil under heat treatment. The reaction follows a first order mechanism as depicted in Figure 4.8. The double bonds in vegetable oils increase the refractive index and the

progressive decrease in refractive index on heating as seen in Table 4.7 confirms loss of unsaturation.

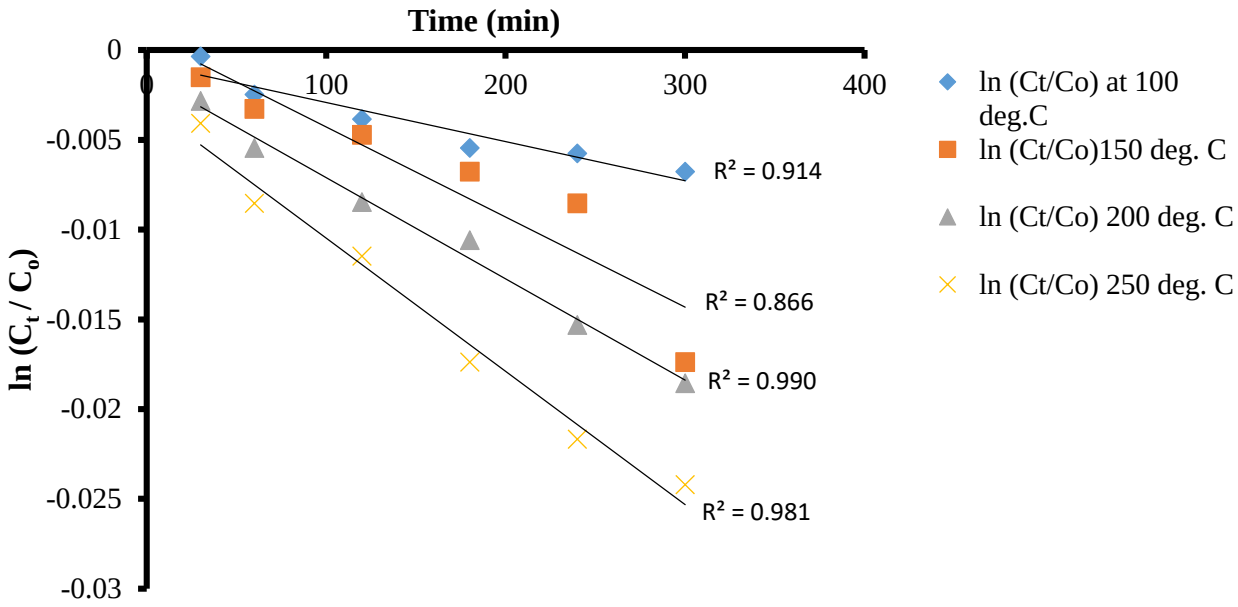


Figure 4.8: ln (C_t/C_o) vs. time for iodine values at 100, 150, 200 and 250 ºC (Adapted from Onoji et al., 2016b)

The kinetic parameters for degradation of rubber seed oil at 100, 150, 200, and 250 ºC are given in Table 4.8. The Arrhenius plot (lnk vs. 1/T) for the degradation kinetics in the temperature range 100-250 ºC is shown in Figure 4.9 with coefficient of determination R^2 equals 0.893. The activation energy (E_a) and the pre-exponential factor determined are 13.07 kJ/mol and $161x10^{-3}$ s^{-1}, respectively (Onoji et al., 2016b). The high activation energy suggests that the oil is less susceptible to thermal deterioration than other vegetable oils, such as *Hura crepitans* seed oil (E_a = 1.989 kJ/mol) (Oderinde et al., 2009). The proposed Arrhenius equation for the kinetics of degradation of rubber seed oil in the temperature range 100-250 ºC is given in Equation (4.9).

$$k\ (s^{-1}) = 161 \times 10^{-3}\ exp\ (-13.07/RT) \quad (4.9)$$

Table 4.8: Kinetic parameters for degradation of rubber seed oil

Parameters/Temperature	373 K	423 K	473 K	523 K
k (s^{-1})	2.0×10^{-3}	5.0×10^{-3}	6.0×10^{-3}	7.0×10^{-3}
E_a = 13.07 kJ/mol				
A_o = 161×10^{-3} s^{-1}				

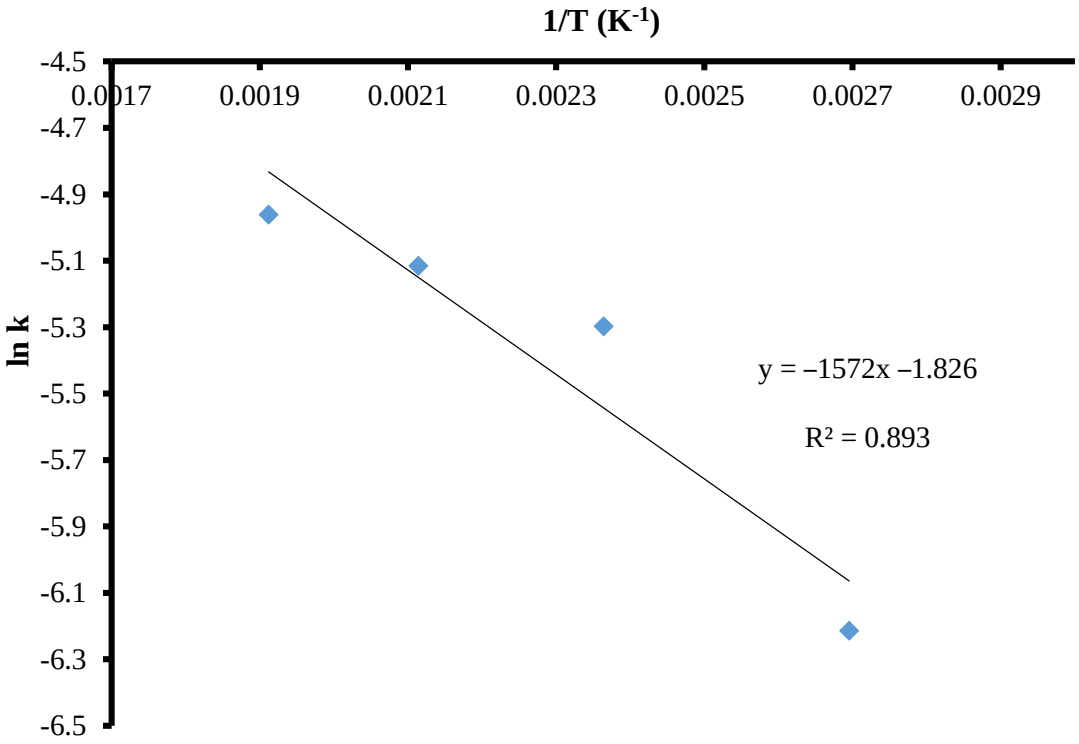


Figure 4.9: Arrhenius plot for kinetics of thermo-oxidative degradation of rubber seed oil

4.5 Parametric effects and optimization oil extraction using RSM

4.5.1 Full quadratic regression model

The RSM full quadratic regression model for the extraction of rubber seed oil using BBD based on Equation (3.7) is given in coded extraction process parameters as (Onoji et al., 2017a):

$$Y\ (\text{wt. \%}) = 36.66 + 1.71x_1 + 0.77x_2 + 3.69x_3 - 4.48x_1x_2 - 3.28x_1x_3 - 2.88x_2x_3 + 0.11x_1^2 - 1.24x_2^2 + 0.96x_3^2 \quad (4.10)$$

The mathematical model generated by Design-Expert software trial version 8.0.3.1 (*Stat-Ease Inc., Minneapolis, MN, USA*) was used for the analysis. The correlation between the predicted and experimental yields data is depicted in Figure 4.10, and data obtained from Table 4.9.

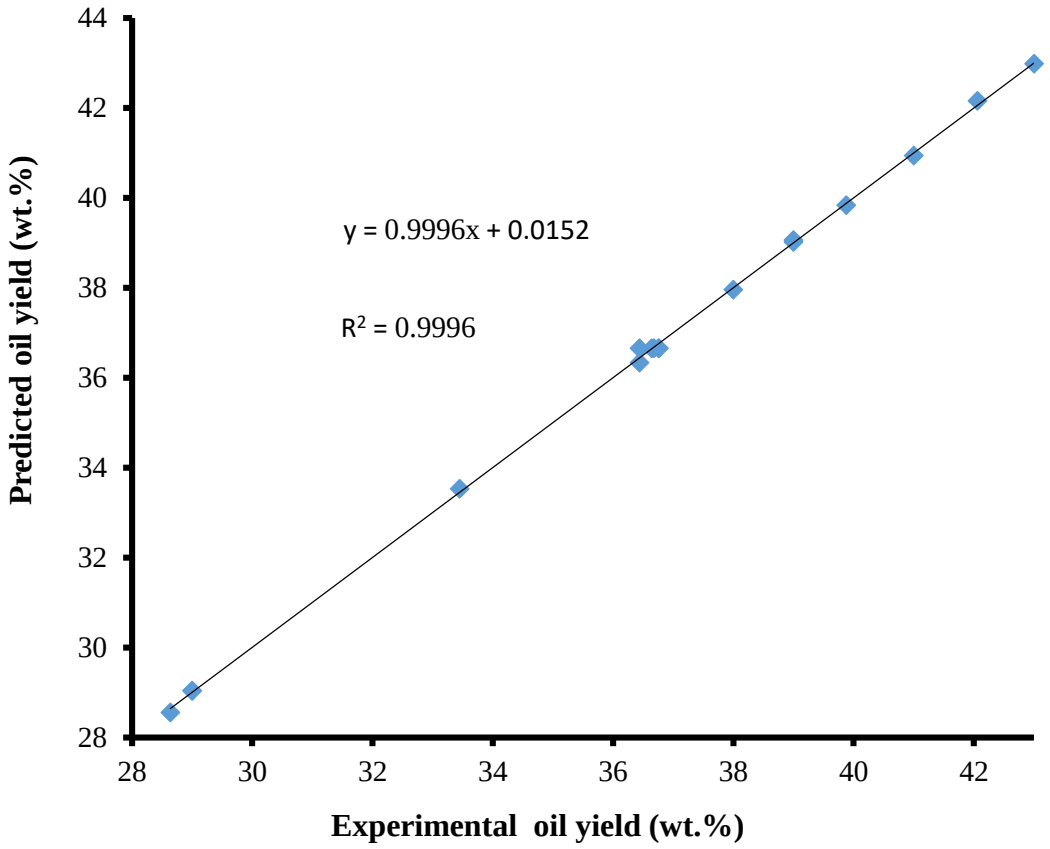


Figure 4.10: Correlation of predicted and experimental oil yields of rubber seed oil extraction

Table 4.9: Box–Behnken design for the rubber seed oil extraction process optimization by RSM and ANN (Onoji et al., 2017a)

Std. run	x_1	x_2	x_3	Oil yield (wt. %)	Predicted yield (wt. %)		Residual value	
					RSM	ANN	RSM	ANN
1	–1	–1	0	28.64	28.56	28.641	0.080	0.001195
2	1	–1	0	41.00	40.94	41.531	0.062	0.535070
3	0	0	0	36.44	36.66	36.656	–0.22	0.216070
4	0	0	0	36.64	36.66	36.656	–0.016	0.016071
5	–1	0	–1	29.00	29.04	29.000	–0.042	0.000305
6	1	0	–1	39.00	39.02	39.000	–0.024	0.000257
7	–1	0	1	43.00	42.98	43.000	0.024	0.000470
8	0	0	0	36.76	36.66	36.656	0.01	0.103930
9	0	–1	–1	29.00	29.04	29.000	–0.038	0.000497
10	0	1	–1	36.44	36.34	36.440	0.10	0.000012
11	0	–1	1	42.06	42.16	41.529	–0.10	0.530890
12	0	1	1	38.00	37.96	38.000	0.038	0.000005
13	–1	1	0	39.00	39.06	39.000	–0.062	0.000093
14	1	1	0	33.45	33.53	33.450	–0.080	0.000063
15	1	0	1	39.88	39.84	39.883	0.042	0.000197
16	0	0	0	36.68	36.66	36.656	0.024	0.023929
17	0	0	0	36.76	36.66	36.656	0.10	0.10393

X_1: rubber seed powder weight (g), X_2: solvent volume (mL), X_3: extraction time (min)

The analysis of the regression coefficients showed that the linear terms of x_1, x_2 and x_3 were positive, whereas the quadratic term of x_2 was negative. This means that the oil yield was enhanced by X_1, X_2 and X_3. However, at a certain level of solvent and with more seed powder weight, the oil yield decreases as the solvent becomes saturated. The curvature of the surface response was significantly determined by x_2^2. The coefficient of determination (R^2) of the model in predicting the yield was 0.9996. The residual values (Table 4.9) for the RSM in each case were found to be less than unity and confirm that the R^2 value for the model is close to 1.

4.5.2 Optimization of oil extraction process variables based on RSM

The BBD within the experimental range of data for the independent process parameters, predicted optimal rubber seed oil yield of 42.98 wt. % at the following conditions: rubber seed powder weight (RSPW) 60 g, solvent volume 250 mL, and extraction time 45 min. Using these predicted values, the experiment was validated in triplicate and the average optimum rubber seed oil yield was 42.64 wt. % (Section D.2 of Appendix D). This is close to the model predicted value (within ± 0.797 % relative error) at same optimum conditions based on Equation (4.11) (Zahedi & Azarpour, 2011). The absolute average deviation (AAD) obtained from Table 4.9 and based on Equation (4.12) (Betiku & Ajala, 2014) was ±0.385 %. Evaluation of R^2 and AAD values together was used to check the accuracy of the model (Baş & Boyaci, 2007b). The low value of AAD and R^2 = 0.9996 (close to unity) confirms the validity of the model in predicting the oil. Hence, the regression model gave a good estimate of the response of the process for low values obtained.

$$Percent\ relative\ error = \frac{experimental\ value - predicted\ value}{experimental\ value} \times 100 \quad (4.11)$$

$$AAD = \left\{\left[\sum_{i=1}^{n}\left(\frac{Y_{i,exp} - Y_{i,pred}}{Y_{i,exp}}\right)\right]\frac{1}{n}\right\} \times 100 \quad (4.12)$$

Where n is the number of experimental runs, while $Y_{i,\,exp}$ is the experimental oil yield and $Y_{i,\,pred}$ is the predicted oil yield.

4.5.3 Analysis of variance (ANOVA) study for seed oil extraction

The statistical significance of the quadratic regression model equation, the individual factors, their interactions and the goodness of the fit by analysis of variance (ANOVA) are shown in Table 4.10. The quality of the model fit was evaluated by the Fisher's test (F-value), the probability value (p-value), the 'lack of fit', the coefficient of determination (R^2) and adjusted coefficient of determination (R^2_{adj}). The *p-value* should be less than 0.05 for the variables to have a significant effect on the response value - in this case, RSO yield (Onoji et al., 2017a).

Table 4.10: Analysis of variance (ANOVA) for response surface quadratic model

Source of variance	Sum of squares	Degrees of freedom	Mean square	*F-value*	*p-value*
Model	303.18	9	33.69	1980.33	<0.0001
RSPW, x_1	23.44	1	23.44	1377.89	<0.0001
Solvent, x_2	4.79	1	4.79	281.56	<0.0001
Extraction time, x_3	108.81	1	108.81	6396.43	<0.0001
x_1x_2	80.19	1	80.19	4714.29	<0.0001
x_1x_3	43.01	1	43.01	2528.56	<0.0001
x_2x_3	33.06	1	33.06	1943.66	<0.0001
x_1^2	0.047	1	0.047	2.79	0.1388
x_2^2	6.47	1	6.47	380.39	<0.0001
x_3^2	3.87	1	3.87	227.49	<0.0001
Residual	0.12	7	0.017		
Lack of fit	0.05	3	0.017	0.96	0.4917
Pure error	0.069	4	0.017		
Corrected total	303.29	16			

RSM: R^2 = 0.9996, $R^2_{adj.}$ = 0.9991, Root mean square error (*RMSE*) = 0.088,
Mean = 36.57, Standard deviation = 0.13, Adequate precision = 144.2,
Absolute average deviation (*AAD*) = ± 0.385 %, % Coefficient of variation = 0.355,
F- Fisher; *p*- probability.

The quadratic regression model has an *F*-value of 1980.33 and a *p*-value <0.0001, which indicates that the derived model is statistically significant at the 95% confidence level. The higher the *F*-value for the specific independent process parameter, the higher will be the effect of that variable. *The* main effects, i.e. x_1, x_2 and x_3 are significant terms based on their calculated *p*-values (<0.0001). The quadratic effect terms of x_2^2 and x_3^2 are significant, but x_1^2 term is not significant (p>0.05), with a small *F*-value of 2.79. The cross-product terms of x_1x_2, x_1x_3 and x_2x_3, are all significant. In Table 4.11, 95% confidence levels (low and high) represent the range

that the true coefficients are found in 95% of the time. If one limit is positive and the other is negative, then the coefficient zero could be true, which indicates that the factor has no effect. In this study, x_1^2 has no significant effect on RSO yield having both negative and positive values as shown in Table 4.11. However, even though x_1^2 has a *p*-value >0.05 (Table 4.10), indicating that it has no significant effect on the RSO yield, the magnitude of the change caused is insignificant; hence, it was retained in the regression model Equation (4.10). In general, if there is large number of insignificant model terms, model reduction by reducing the ranges of parameters may improve the model (Dharma et al., 2016). If a model displays a 'lack of fit', it means that several important terms were excluded from the model, or the presence of unusually large residuals arising from fitting the model (Dharma et al., 2016). In that case, the model does not sufficiently describe the relationship between the independent process variables and the response variable. In this study, the 'lack of fit' of low *F*-value of 0.96 and high *p*-value of 0.4917 implied that the model was not significant relative to pure error (0.069). The *p*-value of the 'lack of fit' parameter is greater than 0.05, indicating that there is good fit between the quadratic regression model and the experimental oil yield obtained (Dharma et al., 2016). The R^2 reflects the variability of the dependent variable, which is explained by its relationship with the independent process variables. In this study, the R^2 value is 0.9996, which indicates that 99.96% of the variability in the rubber seed oil yield is attributed to the independent factors considered (rubber seed powder weight, solvent volume and extraction time), and only 0.04% was not explained by the model (Onoji et al., 2017a). The R^2_{adj} value is 0.9991 and the root mean squared error (RMSE) is 0.088. These indicate that the estimated model fits the experimental data satisfactorily, as suggested by Lee et al. (2010). The low values of standard error observed in the intercept and all the model terms (Table 4.11) confirm that the regression model equation fits the data well, with acceptable prediction. The variance inflation factor (VIF) values shown in Table 4.11 indicate that the center points are orthogonal to all other

factors in the model. The signal-to-noise ratio is measured by the statistical parameter called 'adequate precision'. In general, an adequate precision >4 is desirable for a good model (Dharma et al., 2016). In this study, the calculated adequate precision is 144.2 (Table 4.10), indicating that the signal is adequate and the quadratic model can be used to navigate the designed space. In addition, the 'coefficient of variation' is low (0.355%), which indicates that the experimental data are accurate and reliable.

Table 4.11: RSM regression analysis for rubber seed oil extraction

Factor	Regression coefficient	Degrees of freedom	Standard error	95% Cnf. level (low)	95% Cnf. level (high)	VIF
Intercept	36.66	1	0.058	36.52	36.79	1.00
x_1	1.71	1	0.046	1.60	1.82	1.00
x_2	0.77	1	0.046	0.66	0.88	1.00
x_3	3.69	1	0.046	3.58	3.80	1.00
x_1x_2	-4.48	1	0.065	-4.63	-4.32	1.00
x_1x_3	-3.28	1	0.065	-3.43	-3.12	1.00
x_2x_3	-2.88	1	0.065	-3.03	-2.72	1.00
x_1^2	0.11	1	0.046	-0.044	0.26	1.01
x_2^2	-1.24	1	0.046	-1.39	-1.09	1.01
x_3^2	0.96	1	0.046	0.81	1.11	1.01

Cnf: confidence; VIF: variance inflation factor

4.5.4 Parametric effects of interactive factors on the seed oil yield

Figure 4.11 (a) shows the response surface plot that indicates the influence of solvent volume and rubber seed powder weight on the extraction yield when extraction time was held constant at 45 min. It was observed that a higher seed powder weight significantly increases the oil yield at low solvent volume. However, a slight reduction in oil yield was observed when a higher solvent volume and low seed powder weight was used.

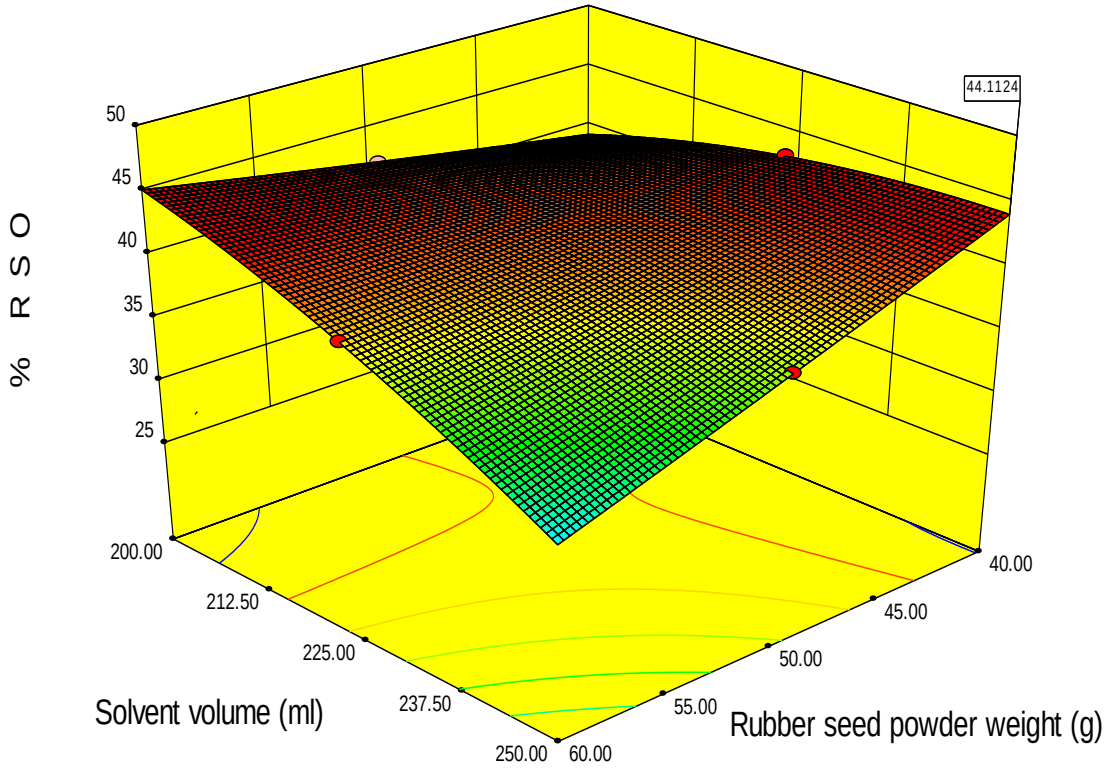


Figure 4.11 (a): Interactive effects between solvent volume and rubber seed powder weight on oil yield for RSM response surface (3D) plot

Figure 4.11 (b) depicts the response surface plot on the mutual interaction between extraction time and rubber seed powder weight at constant solvent volume (225 mL). It was observed that oil yield increased significantly with extraction time at low rubber seed powder weight. This may be the result of more interaction between rubber seed weight and solvent (Onoji et al., 2017a). This agrees with the findings of Reshad et al. (2015). Nevertheless, a reduction in oil yield was observed at higher rubber seed weight and low extraction time.

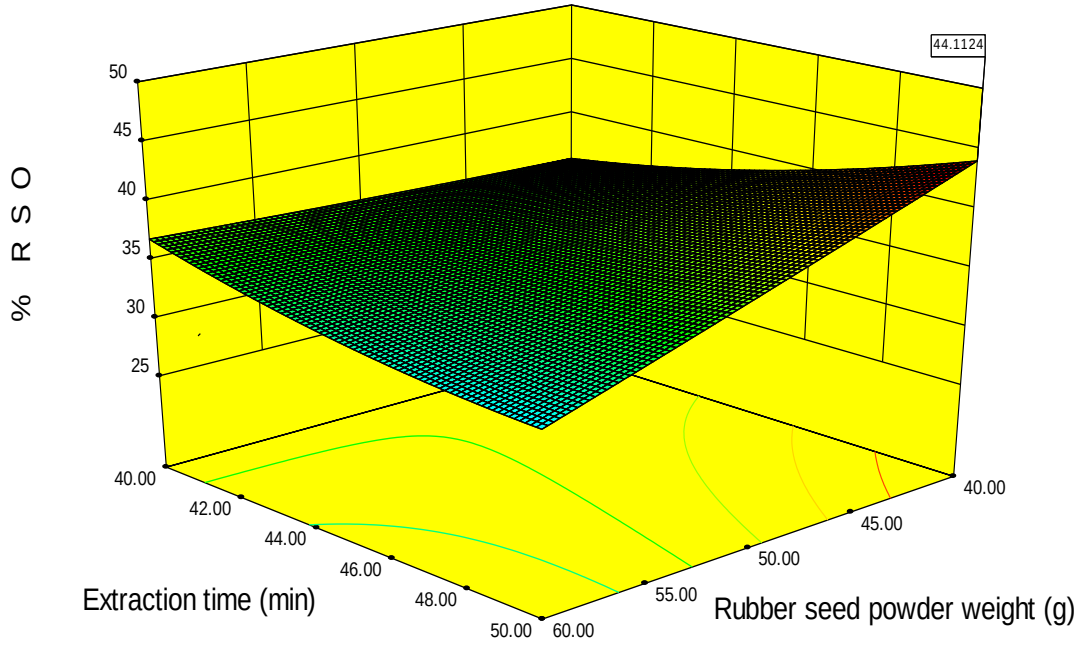


Figure 4.11 (b): Interactive effects between extraction time and rubber seed powder weight on oil yield for RSM response surface (3D) plot

Figure 4.11 (c) describes surface plot for the relationship between extraction time and solvent volume when the rubber seed powder weight was held constant at 50 g. A significant increase in oil yield was observed at low solvent volume and high extraction time. However, a marginal reduction (9.6%) in oil yield was observed when solvent volume and extraction time are both at high levels.

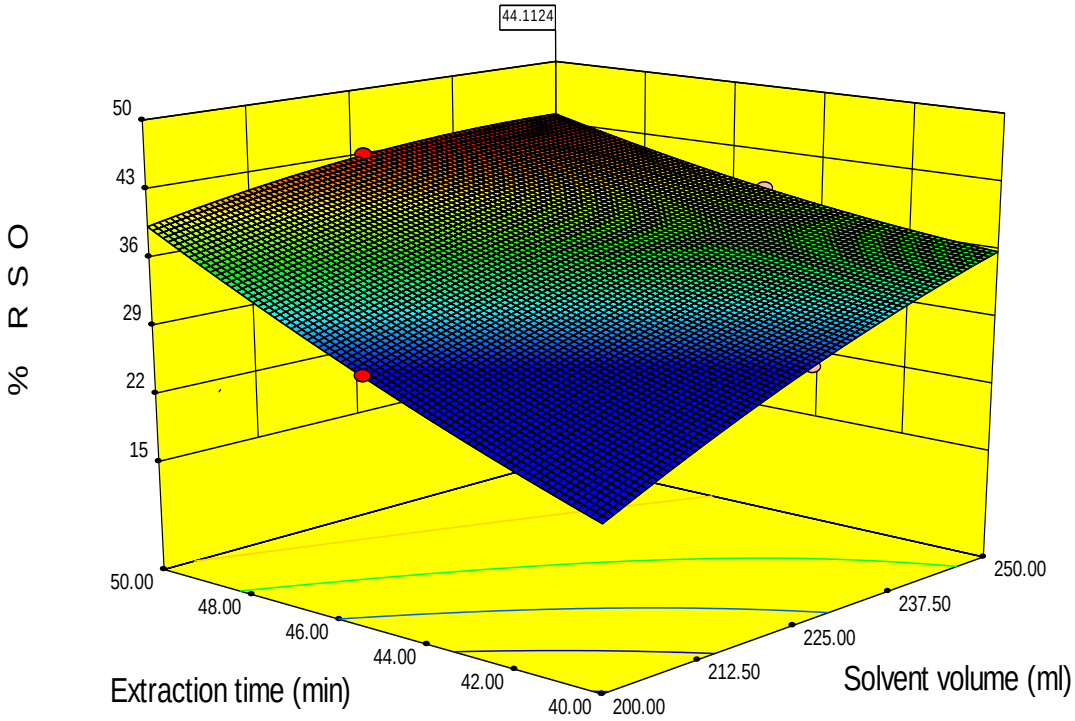


Figure 4.11 (c): Interactive effects between extraction time and solvent volume on oil yield for RSM response surface (3D) plot

4.6 Parametric effects and optimization of oil extraction using ANN model

The optimum number of neurons in the hidden layer that gave good prediction of the outputs of both training and cross validation sets in this study was iteratively obtained as three. The genetic algorithm (GA) of the model predicted rubber seed oil yield of 43 wt. % at the following conditions: rubber seed powder weight 40 g, solvent volume 202 mL, and extraction time 49.99 min. Using these values, the experiment was validated in triplicate, and average optimum rubber seed oil yield was 42.96 wt. % (Section D.3 of Appendix D). This is close to the model predicted value (within ±0.093 % relative error) at same extraction conditions. The model was found to have an R^2 value of 0.9982, R^2_{adj} value of 0.9964, RMSE of 0.2054, and AAD of ±0.064%. Figure 4.12 compares the predicted and experimental values of the rubber seed oil

yield, and the R^2 obtained (0.997) shows a good correlation between the data obtained. This confirms that the model proved suitable for adequate representation of the actual relationship among the selected factors.

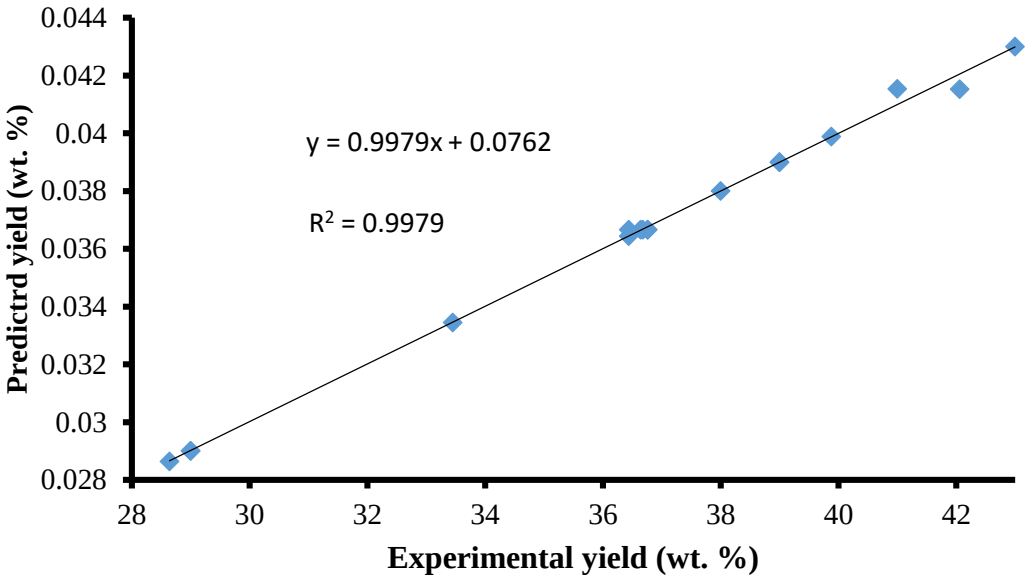
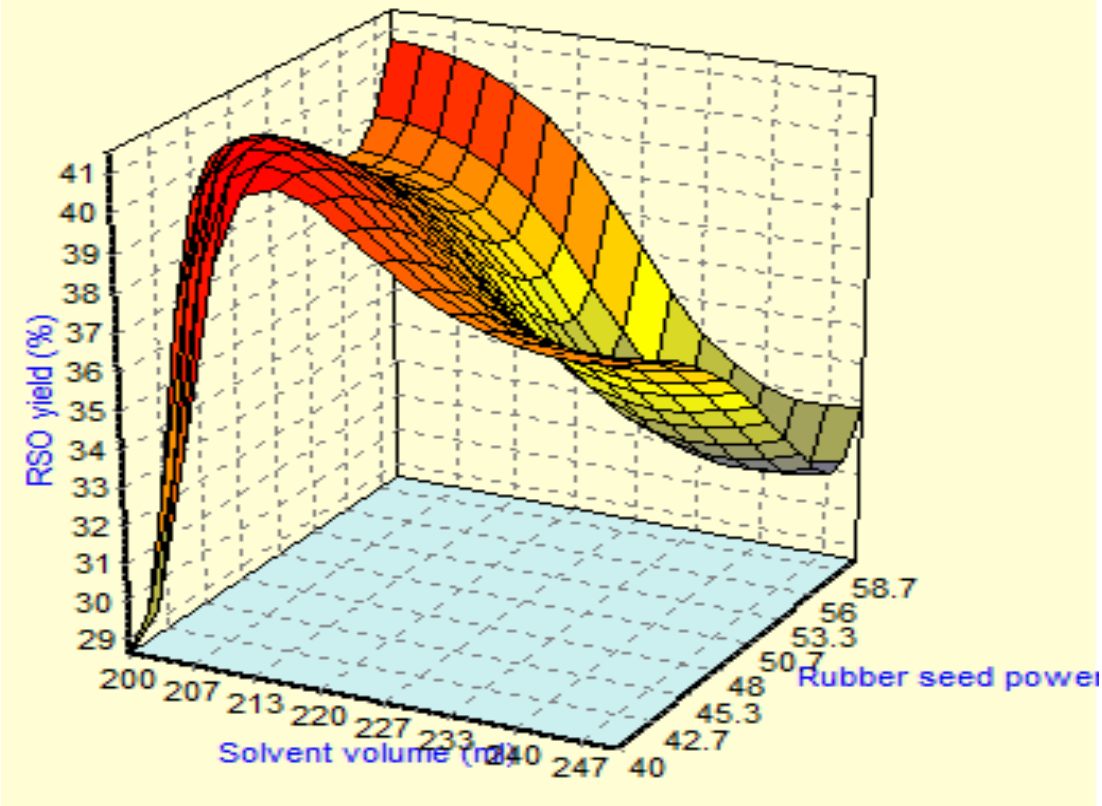


Figure 4.12: Correlation of predicted and experimental rubber seed oil yields by ANN model

Figures 4.13 (a–c) depicts the interactive effects on oil yield between two extraction independent variables while maintaining the third variable at constant level. The curvature nature of the 3D surfaces suggests significant interactions of solvent volume with rubber seed powder weight, extraction time with rubber seed powder weight, and solvent volume with extraction time. It was also observed that the contour plots obtained by the ANN model were very similar to those obtained by the RSM model.



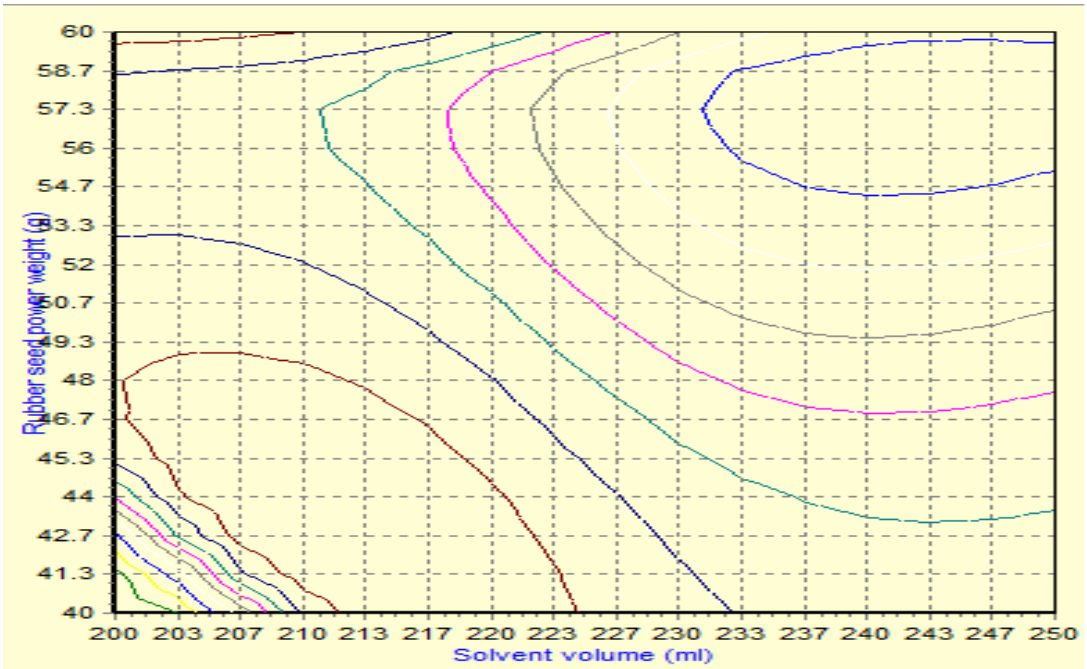


Figure 4.13 (a): Interactive effects of rubber seed powder weight and solvent volume on oil yield for ANN response surface (3D) and contour (2D) plots

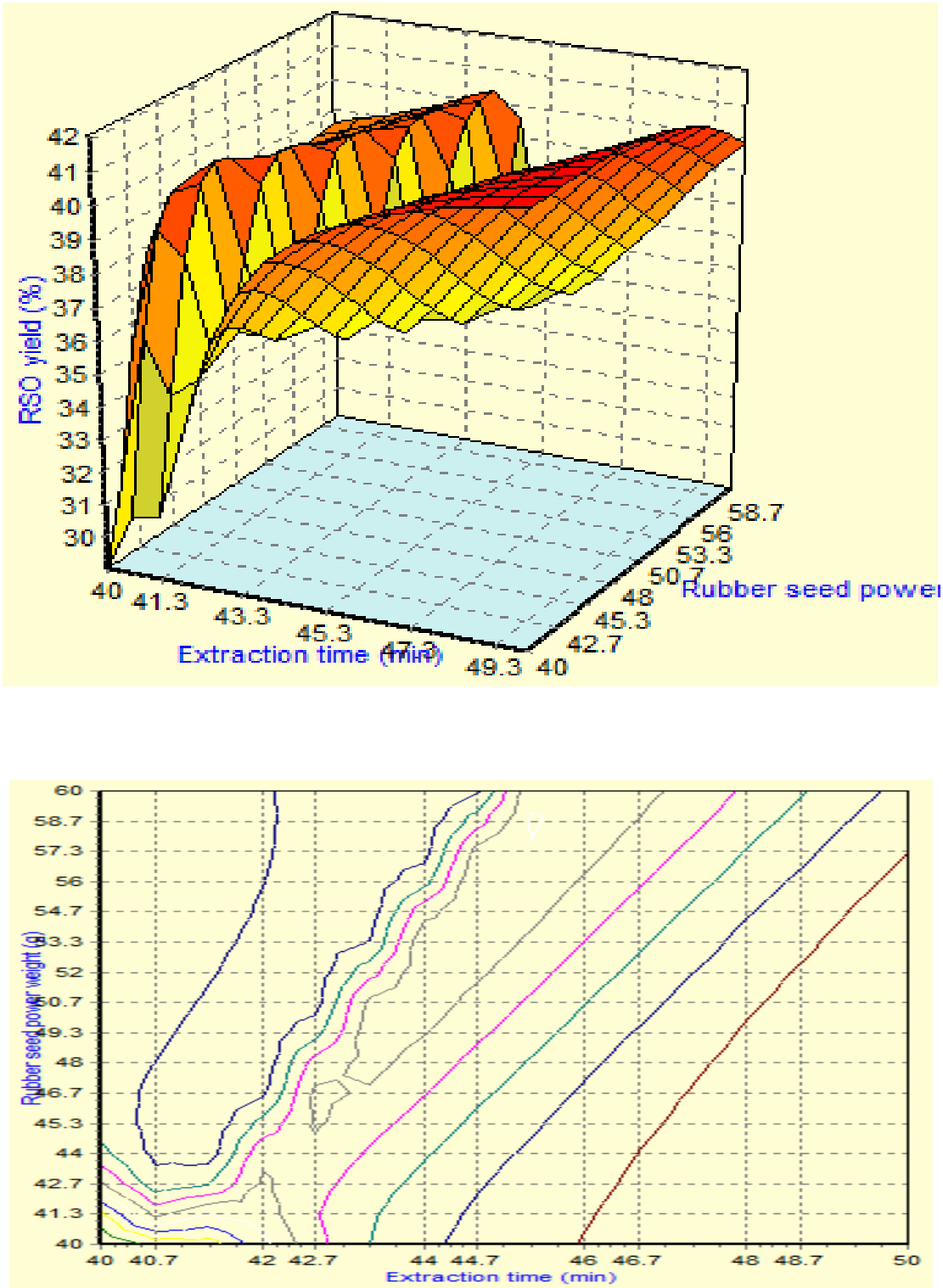
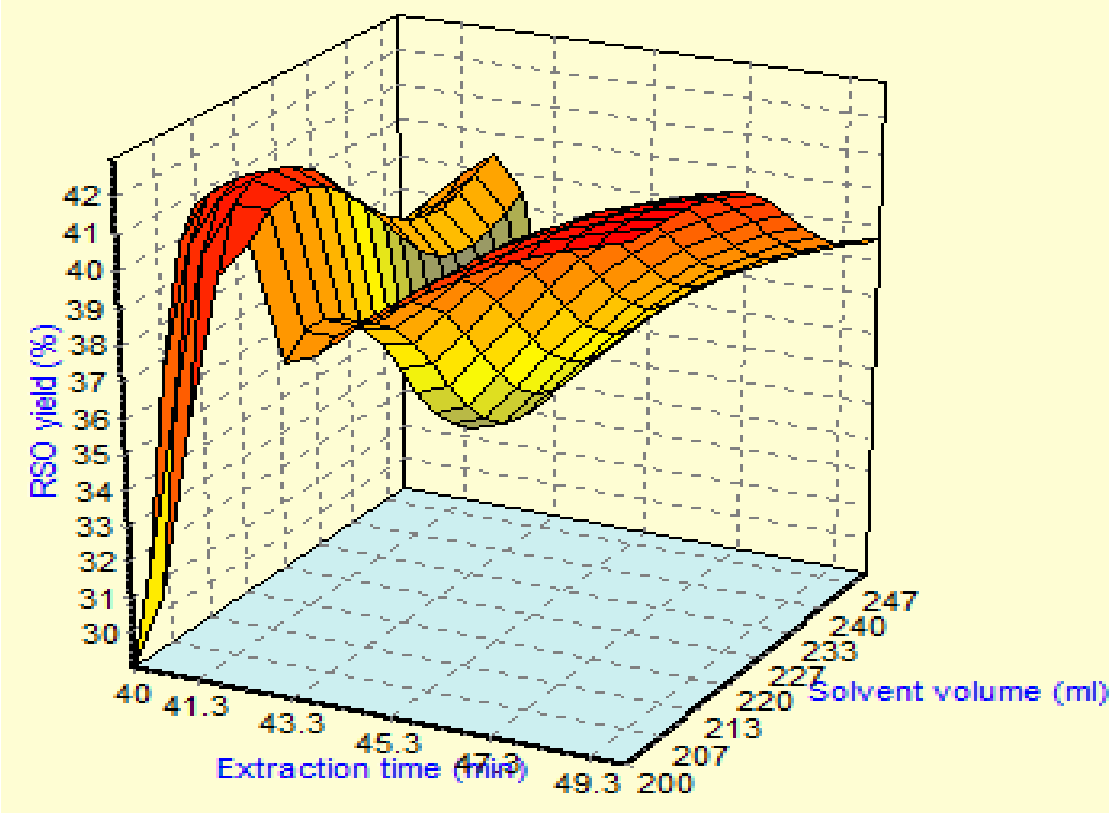


Figure 4.13 (b): Interactive effects of rubber seed powder weight and extraction time on oil yield for ANN response surface (3D) and contour (2D) plots.



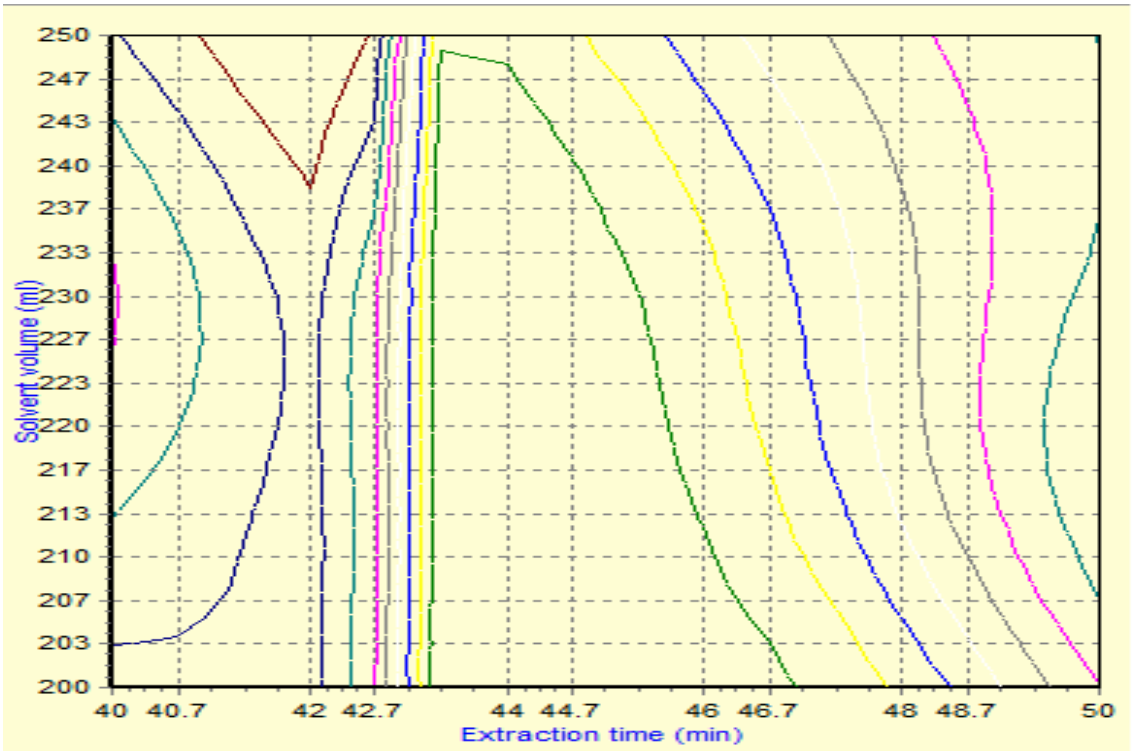


Figure 4.13 (c): Interactive effects of extraction time and solvent volume on oil yield for ANN response surface (3D) and contour (2D) plots

The level of importance of the process variables considered for the rubber seed oil extraction is shown in Figure 4.14, and it is apparent that solvent volume of 50.06% is the most significant variable on rubber seed oil yield, followed by rubber seed powder weight of 42.47% and lastly, extraction time of 7.471%.

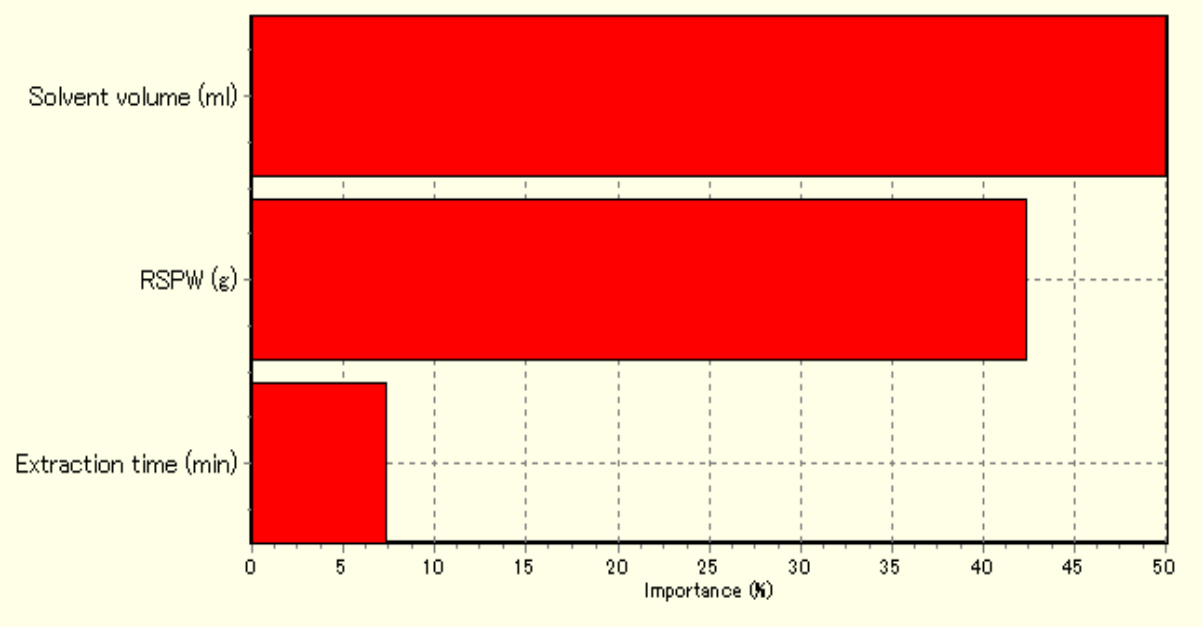


Figure 4.14: Percentage contribution of process variables to seed oil extraction via ANN model (solvent volume 50.06%; RSPW 42.47%; extraction time 7.471%)

4.7 Comparison of RSM and ANN models for the seed oil extraction

The accuracies of both RSM and ANN models were evaluated based on the values obtained for R^2, *AAD* and % relative error. The results show that both optimization techniques gave good predictions, due to the values of R^2 that are relatively close to unity (i.e. 0.9996 and 0.9982 for RSM and ANN, respectively). However, ANN proved to be a superior model, with lower values of % relative error (±0.093 %) and AAD (±0.064 %) compared to the RSM model with relative error ±0.797 % and AAD ±0.385 % (Onoji et al., 2017a).

4.8 Catalyst preparation and characterization

This section discusses the preparation of the catalyst derived from rubber seed shells, and the characterization of the catalyst for biodiesel production.

4.8.1 Thermo-gravimetric analysis of the rubber seed shell catalyst

To study the influence of calcination temperature on weight loss (%), the powdered RSS was subjected to thermal analysis (30–950 ^{o}C) in a nitrogen atmosphere at 10 ^{o}C/min heating rate. The thermogram of RSS in Figure 4.15 shows that less water was evaporated from the surface of the catalyst in the temperature range 30–348 ^{o}C. This indicates that less water moisture from air was adsorbed on the surface of the catalyst than for the common heterogeneous catalysts and it confirms its superior hydrophobicity (Onoji et al., 2017b)

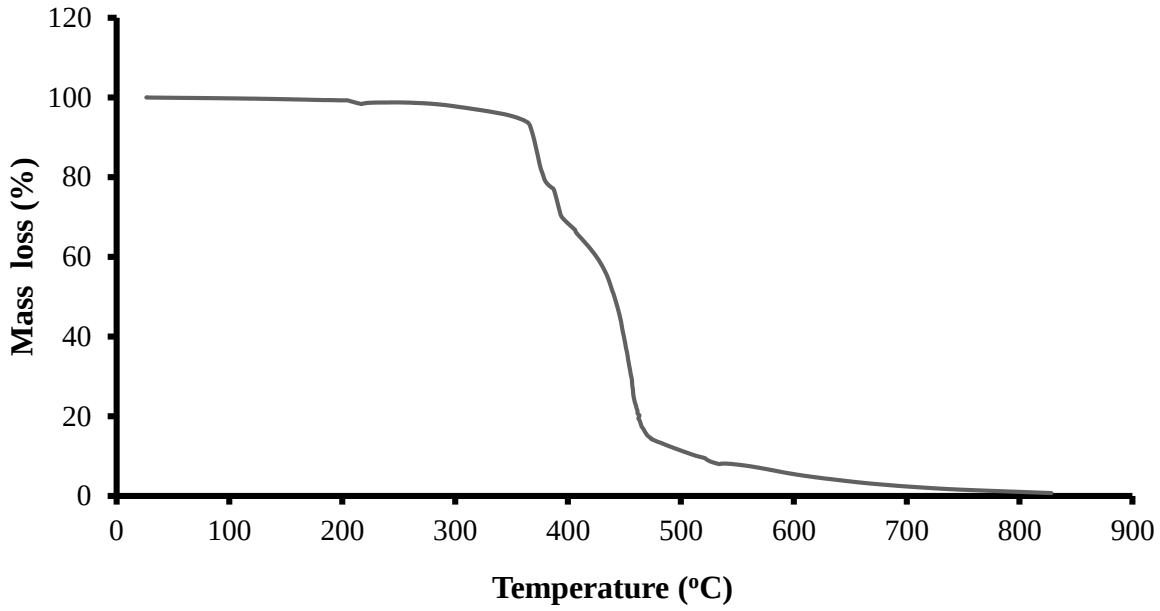


Figure 4.15 TGA profile for the rubber seed shell (RSS) catalyst

The result also shows that the decomposition temperature of RSS catalyst was about 348 ^{o}C. This confirms the stability of the catalyst for the transesterification reaction. The TGA result from this study is similar to the TGA curve for RSS by other researchers (Sun & Jiang, 2010).

Major mass loss (about 90%) was observed between 348 and 465 ^{o}C, which resulted from decomposition of macromolecules and removal of organic compounds such as cellulose and hemicelluloses (348–400 ^{o}C), and lignin (220–465 ^{o}C). At temperature range 465-800 ^{o}C, an additional small and steady mass loss was also observed. This may be attributed to the formation of gaseous components because of decomposition process. Figure 4.15 also shows that the RSS calcined at 800 ^{o}C or above did not indicate any further mass loss, which means that the composition of the calcined RSS was mainly CaO and SiO_2 as observed from XRD results. It also confirms the high thermal stability of the calcined RSS at 800 ^{o}C and above. Based on TGA results, 800 ^{o}C was chosen as the calcination temperature of RSS to produce the catalyst (Onoji et al., 2017b).

4.8.2 XRF elemental analysis and basic property of rubber seed shell catalyst

XRF spectra of raw and calcined RSS are depicted in Figure 4.16 (a & b). The elemental compositions are presented in Table H.1 of Appendix H. The pH for raw and calcined (800 ^{o}C) RSS was found to be 7 and 12.5, respectively. This confirms the basic nature of the derived catalyst. Background adjustment of peaks for trace metals such as niobium, molybdenum, tin, and antimony brought them within the range. The results show that the major elements present are calcium, silicon, potassium, aluminum, and iron. Trace metals such as zinc, tungsten, cobalt, manganese chromium, tin and antimony are present in minute quantities after calcination. The absence of heavy metals such as cadmium, arsenic, titanium, and lead confirms that the catalyst synthesized is non-toxic and environmentally friendly.

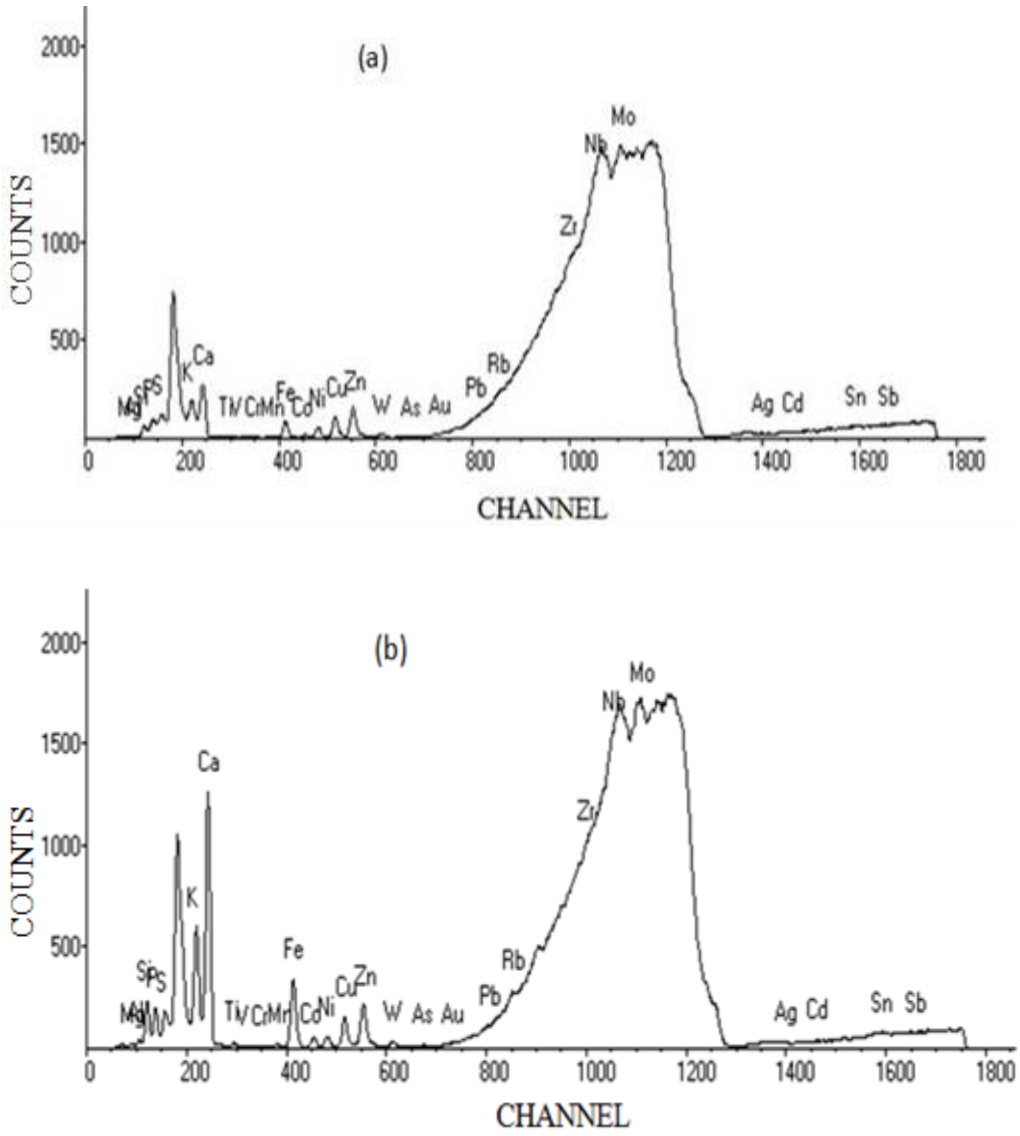
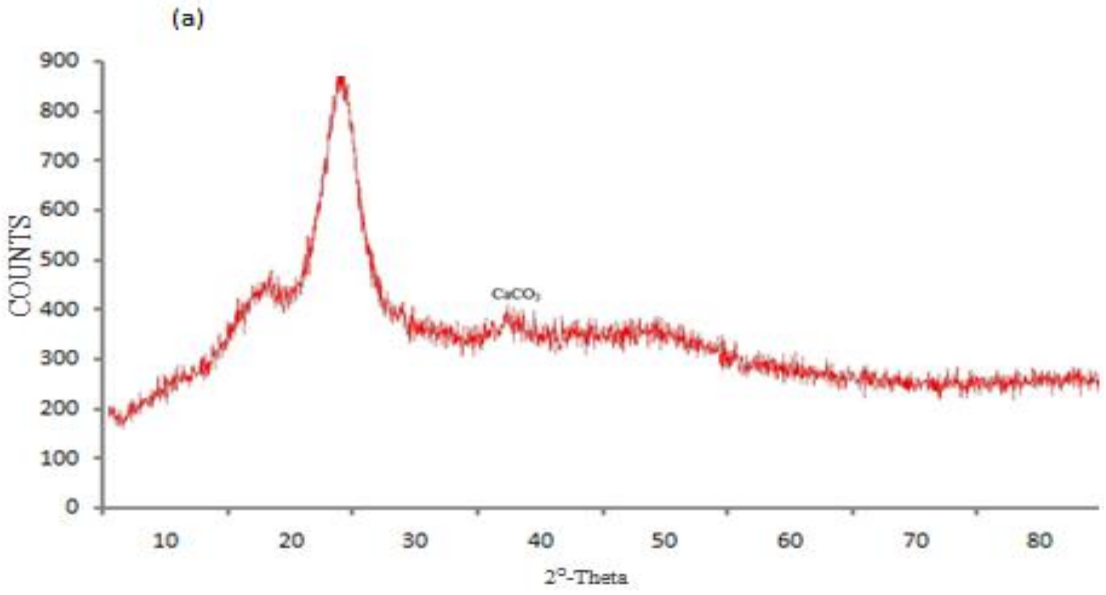


Figure 4.16: XRF analysis of RSS: (a) raw and (b) calcined at 800 ºC (Adapted from Onoji et al., 2017b)

4.8.3 XRD analysis of the rubber seed shell (RSS) catalyst

The XRD diffractograms of the raw and calcined (800 ºC) RSS are depicted in Figure 4.17 (a & b). As shown in Figure 4.17 (a), a wide diffraction peak centered at $2\theta = 23^{o}$ was observed in the XRD pattern of the raw RSS that suggests its amorphous structure (D'Cruz et al., 2007). The diffractograms of the calcined RSS show that the catalytic property was improved by the presence of lime (CaO) and quartz (SiO_2), which enhances its thermal stability. The analysis

of the crystal using XRD illustrates that the raw RSS is made of $CaCO_3$ and quartz. During calcination, $CaCO_3$ present in the raw RSS decomposes to CaO, and quartz to SiO_2. The diffractogram patterns of the calcined RSS are similar to the diffractograms CaO nano-particles reported in the literature (Tang et al., 2008). The CaO generated from RSS during calcination acts as a solid base catalyst for transesterification of rubber seed oil to biodiesel. CaO has been utilized as a base catalyst for soybean oil transesterification to biodiesel (Liu et al., 2008). The mechanisms of CaO as a base catalyst for oil transesterification are well described in the literature (Issariyakul & Dalai, 2014; Guo & Fang, 2011; Liu et al., 2008). In the presence of a little water, CaO generates methoxide anions that act as the real catalyst in transesterification reactions (Liu et al., 2008).



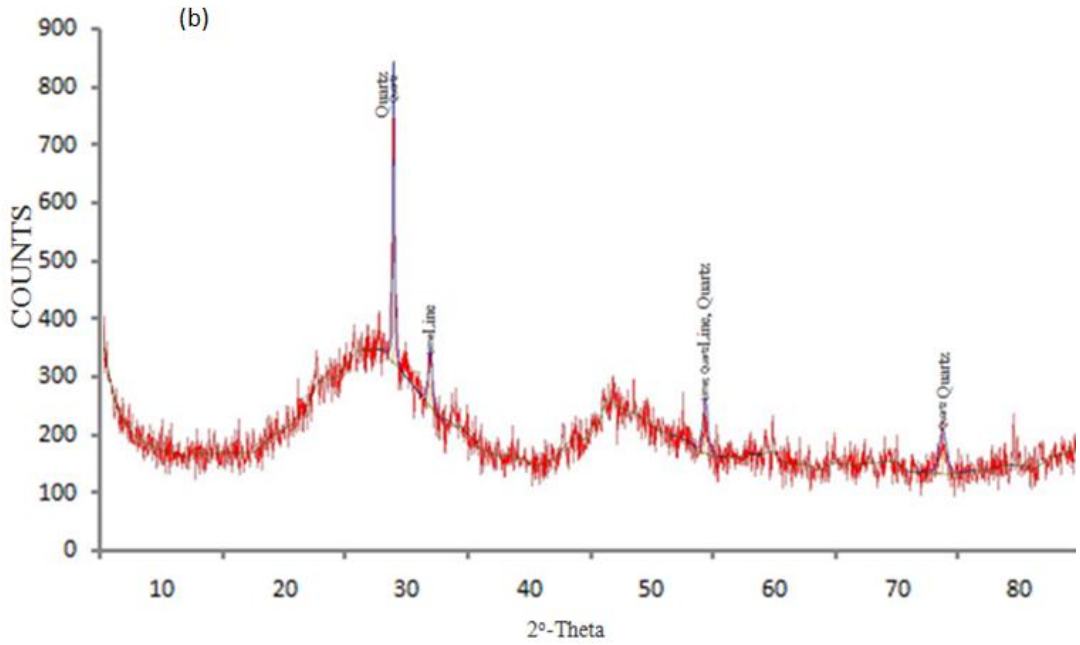


Figure 4.17: XRD diffractograms of RSS: (a) raw, and (b) calcined at 800 ºC (Adapted from Onoji et al., 2017b)

4.8.4 SEM analysis of the rubber seed shell catalyst

Scanning electron micrographs (SEM) of the raw and calcined rubber seed shell (RSS) are presented in Figure 4.18 (a & b). The morphology of the raw RSS looks like a mass aggregate that has less surface area as compared to the RSS calcined at 800 ºC, that shows major alteration in its morphology. There is an observed maximum particle size reduction in the calcined RSS, thereby exhibiting a higher surface area, an important characteristic of heterogeneous catalysts. The SEM image of calcined RSS clearly shows regular particle shapes with clusters of well-developed cubic crystals with obvious reduction in particle sizes, indicating higher surface area useful for transesterification reaction (Onoji et al., 2017b).

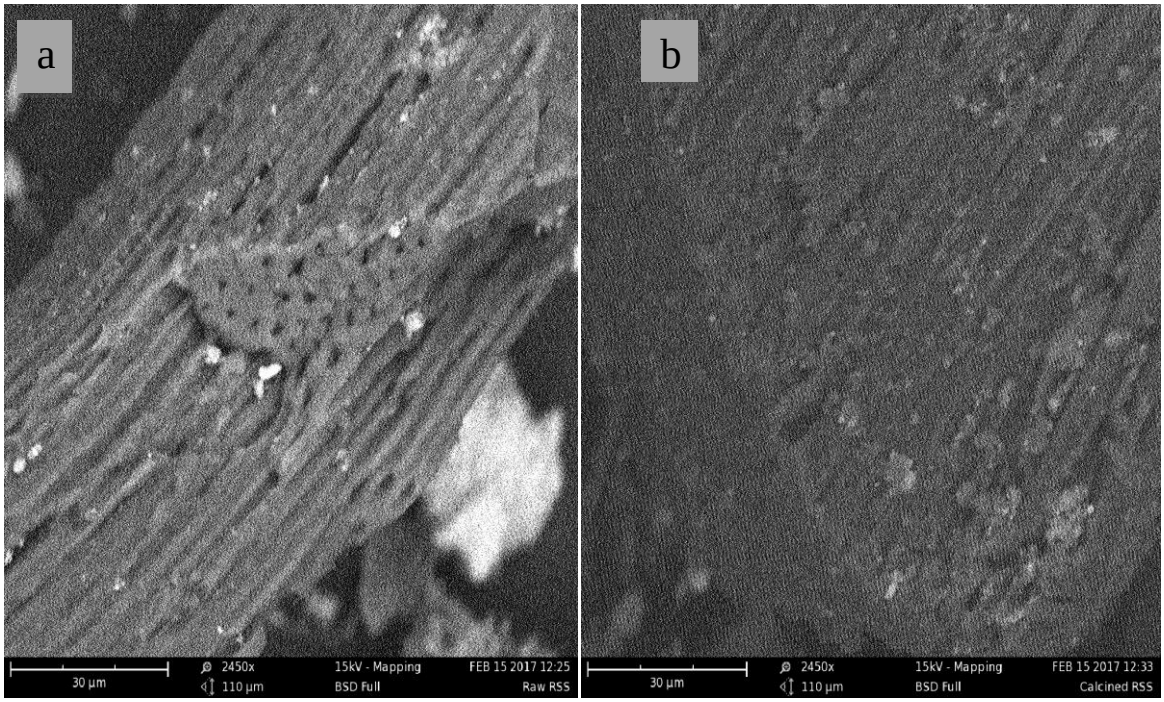


Figure 4.18: SEM images for (a) raw, and (b) calcined RSS catalyst at magnification 2450x

4.8.5 Surface properties of the rubber seed shell catalyst

The physical properties of the raw and calcined catalyst at 800 ^{o}C, such as specific surface area, pore volume, and pore-size distribution, were obtained by N_2 adsorption/desorption at 77.3 K using *Gold App surface area and porosity analyzer* (*Model: V-sorb 2800p*). All samples were outgassed prior to the measurement at 250 ^{o}C and 10^{-4} mbar for 11 h. The adsorption-desorption isotherms for the raw and calcined RSS are depicted in Figure 4.19 (Onoji et al., 2017b). The adsorption isotherm at low P/P_o for the calcined RSS is similar to type I isotherms that are characteristic of microporous adsorbent. At higher P/P_o, there was increase in the volume adsorbed caused by adsorption in mesopores as well as a hysteresis loop (0.5–0.9 P/P_o) developed that is typical of type IV isotherms caused by a weak capillary condensation below the expected condensation pressure of nitrogen (Storck et al., 1998).

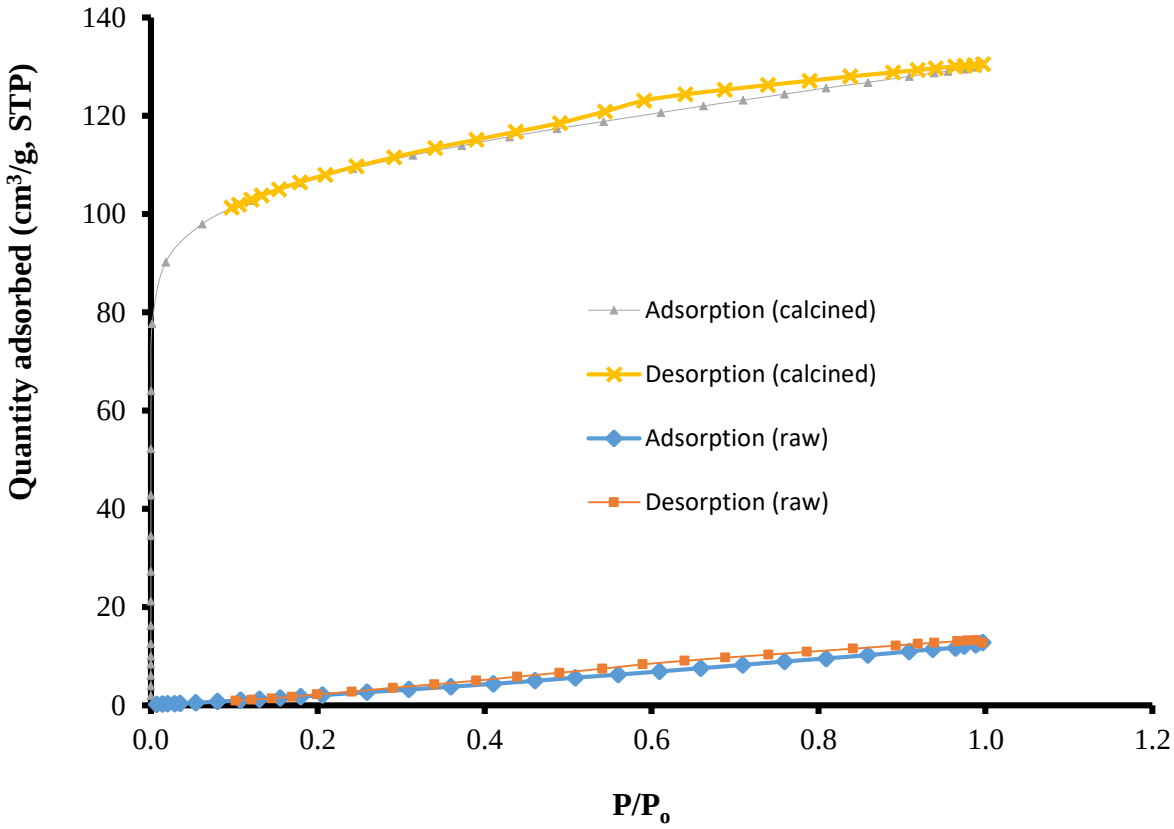


Figure 4.19: Nitrogen adsorption/desorption isotherms for raw and calcined RSS

The nitrogen adsorption/desorption isotherm log plot (Figure H.1 of Appendix H) presents an "*S*" shaped isotherm in the low P/P_o region, reaffirming the presence of micropores and mesopores in the calcined RSS. The nitrogen adsorption/desorption isotherm log plot for the raw RSS displayed a type III isotherm which is typical of multilayer adsorption in non-porous solids as shown in Figure H.2 of Appendix H. *Brunauer-Emmett-Teller* (BET) estimated the surface area of the raw and the calcined RSS as 21.83 and 352.51 m^2/g, respectively. The high surface area for the calcined RSS clearly shows its superiority over the raw RSS in catalyst formulation. The pore size for the raw and calcined RSS is 3.61 and 2.29 nm, respectively. The pore volume for the calcined RSS was estimated at 0.1208 cm^3/g, while the raw RSS was a non-porous material (Onoji et al., 2017b). The increase in BET surface area and pore volume correlate with the mass loss steps in the TGA curve and probably due to a modification of the

sample composition during calcination and crystal growth of calcium oxide (Syazwani et al., 2015). The derived catalyst has an estimated micropore and external surface areas of 250.71 and 101.8 m^2/g, respectively. The surface area of the calcined RSS catalyst, which depends on the calcination temperature, relates to its catalytic activity. The mesopore-size distribution analyzed by the *Barrett-Joyner-Halenda* (BJH) model is depicted in Figure H.3 of Appendix H. The summary of the nitrogen adsorption/desorption results for the raw and calcined RSS are shown in Tables 4.12 and 4.13, respectively (Onoji et al., 2017b). The single point surface area at $P/P_o = 0.3139$ was estimated at 334.23 m^2/g for the calcined catalyst, and 8.53 m^2/g for raw RSS at $P/P_o = 0.2589$. The results of the N_2 adsorption-desorption listed in Table 4.13 indicate that RSS catalyst provided a relatively large contact area with reactants that enhances the yield of the biodiesel produced.

Table 4.12: Summary report of N_2 adsorption/desorption analysis for raw RSS

S/N	Items	Description	Results
Surface area			
1	Single point surface area	$P/P_o = 0.258$	8.525 m^2/g
2	BET surface area	Point range: 0.053–0.206	21.838 m^2/g
3	Langmuir surface area	Monolayer adsorption model calculations	62.401 m^2/g
4	t-plot micropore area	A: Harkins-Jura adsorbed thickness (nm): 0.351–0.540	0.000 m^2/g
5	t-plot external surface area	S_{BET} - S_{micro}	21.837 m^2/g
6	BJH adsorption cumulative surface area	Pore width (nm): 2.092–587.658	18.965 m^2/g
7	BJH desorption cumulative surface area	Pore width (nm): 2.053–587.658	24.832 m^2/g
	Pore volume		
1	Single point adsorption total pore volume	$P/P_o = 0.996$, total pore volume of the critical pore width less than 587.658 nm	0.019 cm^3/g
2	t-plot micropore volume	-	0.000 cm^3/g
3	SF micropore volume	$P/P_o = 0.080$, total pore volume of the critical pore width less than 1.914 nm	0.001 cm^3/g
4	BJH adsorption cumulative volume	Pore width range (nm): 2.092–587.658	0.024 cm^3/g
5	BJH desorption cumulative volume	Pore width range (nm): 2.053–587.658	0.026 cm^3/g
Pore size			
1	Total adsorption average pore width	By 4V/A, A: adsorption BET specific surface area value	3.607 nm
2	BJH adsorption average pore width	By 4V/A, A: adsorption cumulative pore surface area	5.070 nm
3	BJH desorption average pore width	By 4V/A, A: desorption cumulative pore surface area	3.872 nm
4	BJH median pore width	Pore width range (nm): 2.226–587.658	2.500 nm
5	SF median pore width	Pore width range (nm): 1.119–1.914	1.510 nm

Table 4.13: Summary report of N_2 adsorption/desorption analysis for calcined (800 °C) rubber seed shell catalyst

S/N	Items	Description	Results
Surface area			
1	Single point surface area	$P/P_o = 0.313$	334.229 m^2/g
2	BET surface area	Point range: 0.061–0.242	352.518 m^2/g
3	Langmuir surface area	Monolayer adsorption model calculations	489.503 m^2/g
4	t-plot micropore area	A: Harkins-Jura adsorbed thickness (nm): 0.382–0.549	250.713 m^2/g
5	t-plot external surface area	$S_{BET} - S_{micro}$	101.804 m^2/g
6	BJH adsorption cumulative surface area	Pore width (nm): 1.959–675.818	62.630 m^2/g
7	BJH desorption cumulative surface area	Pore width (nm): 2.104–587.658	60.893 m^2/g
Pore volume			
1	Single point adsorption total pore volume	$P/P_o = 0.997$, total pore volume of the critical pore width less than 675.818 nm	0.201 cm^3/g
2	t-plot micropore volume	-	0.120 cm^3/g
3	SF micropore volume	$P/P_o = 0.096$, total pore volume of the critical pore width less than 3.053 nm	0.156 cm^3/g
4	BJH adsorption cumulative volume	Pore width range (nm): 1.959–675.818	0.060 cm^3/g
5	BJH desorption cumulative volume	Pore width range (nm): 2.104–675.818	0.058 cm^3/g
Pore size			
1	Total adsorption average pore width	By 4V/A, A: adsorption BET specific surface area value	2.290 nm
2	BJH adsorption average pore width	By 4V/A, A: adsorption cumulative pore surface area	3.855 nm
3	BJH desorption average pore width	By 4V/A, A: desorption cumulative pore surface area	3.965 nm
4	BJH median pore width	Pore width range (nm): 2.226–587.658	2.115 nm
5	SF median pore width	Pore width range (nm): 1.119–1.914	0.654 nm

4.9 Biodiesel production from the extracted seed oil and analysis

This section discusses the characterization of the produced biodiesel, optimization of the biodiesel process variables and testing of the biodiesel in an internal compression ignition engine.

4.9.1 Characterization of the rubber seed oil biodiesel

The biodiesel was characterized by following the procedures outlined by ASTM, AOAC (1990), and the results are presented in Table 4.14. The properties compared favourably with similar reports on biodiesel synthesized from *Hevea brasiliensis* oil (rubber seed) (Dhawane et al., 2015), and they were in agreement with the ASTM D 6751 and EN 14214 biodiesel standards. From the results, the methyl ester content of the biodiesel determined by GC-MS was 96.7%, while the calculated value using the correlation developed by Felizardo et al. (2006) was 96.9%. The results show that biodiesel produced from rubber seed oil using waste rubber seed shell as catalyst could be used in modern diesel engines without technical modifications.

Table 4.14: Fuel properties of biodiesel produced from rubber seed oil

Properties	Methods	ASTM D 6751 standards	EN 14214 standards	Literature values	This study
Density @ 15 °C (kg/m^3)	ASTM D 1298	870–900	860–900	885[a], 842[b], 880[c]	876
Water and sediment (vol %)	ASTM D 2709	< 0.05	< 0.05	0.042[a]	0.0062
Acid value (mg KOH/g)	ASTM D 664	< 0.8	< 0.5	0.42[a], 0.12[b], 0.06[c]	0.56
Iodine value (g I_2/100 g)	Wijs'		120 maximum		85.34
Saponification value (mg KOH/g)					182.53
Kinematic viscosity @ 40 °C (mm^2/s)	ASTM D 445	1.9–6.0	3.5–5.0	3.89[a], 5.642[b], 4.91[c]	4.32
Flash point (°C)	ASTM D 93	93 minimum	120 minimum	152[a], 183[b], 151[c]	158
Fire point (°C)				189[b]	172
Cloud point (°C)	ASTM D 2500	–3 to 12		3.2[a], 3[b], –7[c]	4.8
Pour point (°C)	ASTM D 97	–15 to 10	0	–2[a], –6[b], –10[c]	–8
Cold filter plugging point (°C)	ASTM D 6371			–2[a]	–0.62
Calorific value (MJ/kg)	ASTM D 240			39.70[a], 42.372[b]	40.67
Oxidation stability: @ 110 °C (h)	Rancimat[d]	≥ 3	≥ 6	8.54[a]	7.8
@ 140 °C (min)	PetroOXY[e]	≥ 17			21.55
Cetane number	ASTM D 613	47 minimum	51 minimum	54[a], 53[b]	57
Metals: Group II (Ca-ppm)	EN 14538		5		3.26
Ester content (%)	EN 14103		≥ 96.5	96.8[a]	96.7

[a]Ahmad et al. (2014b); [b] Dhawane et al. (2015); [c] Dhawane et al. (2016); [d] EN 14112; [e] ASTM D 7545-1

4.9.2 Reusability of the catalyst for biodiesel production

As shown in Figure 4.20 and Table H.2 of Appendix H, the biodiesel yield (%) at optimum catalyst loading of 2.2 g was higher than 80% when the catalyst was used in the fourth cycle and the value decreased to 77.3% in the fifth cycle of usage. The possible reason for the loss of catalytic activity was the blockage of active sites by the deposition of organic matter on the catalyst surface, and the leaching of the active metals from the catalyst into the reaction medium (Dhawane et al., 2016). This was facilitated by the breakage of bonds and the creation of CH_3O^- and Ca^{2+} ions. The AAS analysis of the biodiesel shows that the concentration of Ca^{2+} ion was 3.26 ppm (mg/kg). This value is within the limits of 5 mg/kg set by ASTM D 6751 and EN 14214 biodiesel standards. The effects of leaching of Ca^{2+} ions from the catalyst on the biodiesel are elucidated in Figure 4.21.

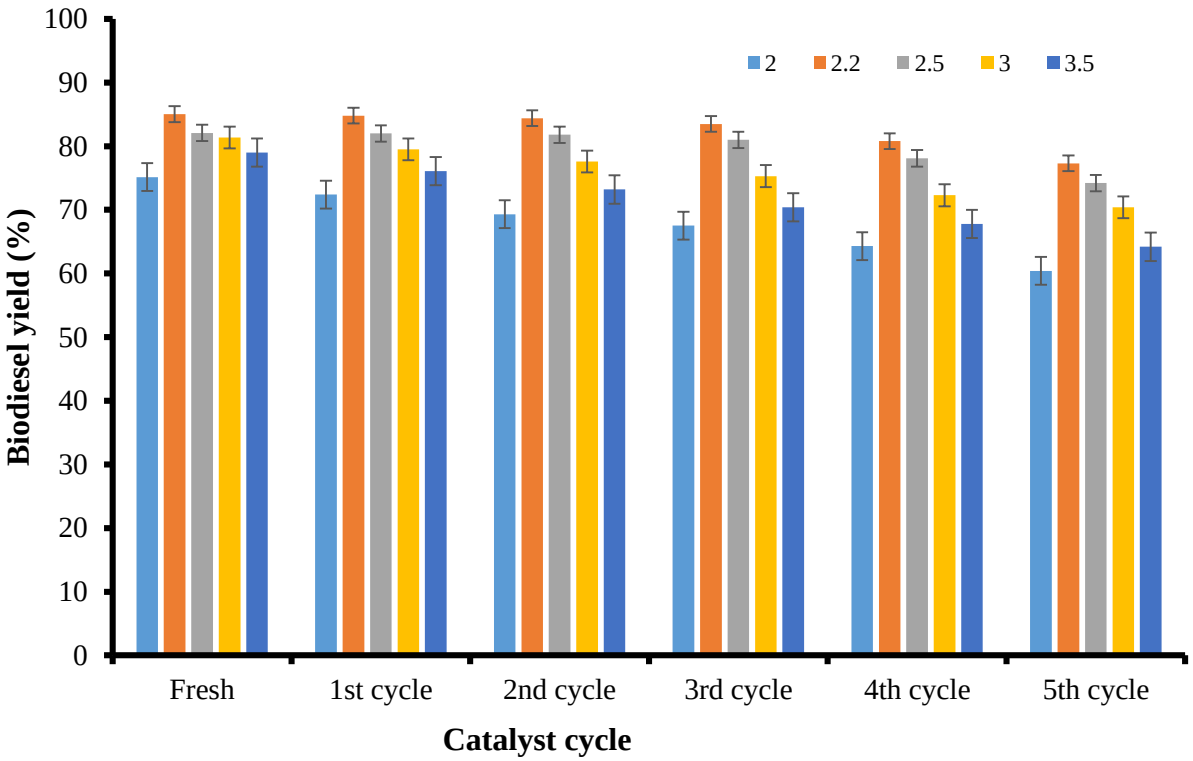


Figure 4.20: Effects of reuse of different catalyst loadings (2, 2.2, 2.5, 3, and 3.5 g) on biodiesel yield (%) at optimum conditions

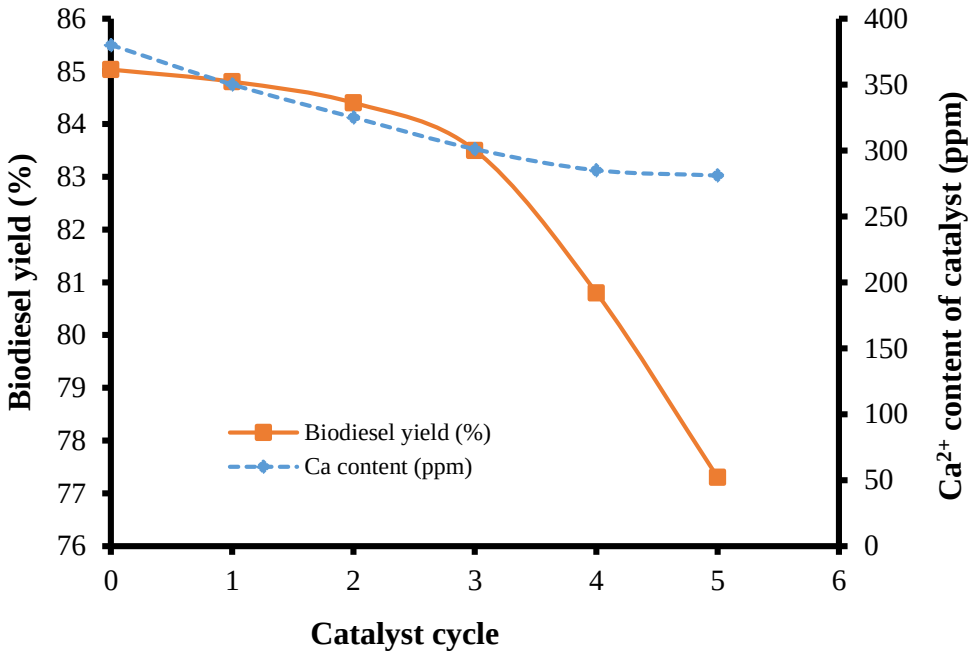


Figure 4.21: Effects of Ca^{2+} ion leaching from reused catalyst on biodiesel yield (%) at optimum conditions

4.10 Parametric effects and optimization of biodiesel production process variables

The optimization of the process variables for the biodiesel production, and the parametric effects of these variables on the yield of biodiesel as described by RSM and ANN models are discussed in this section.

4.10.1 Modeling and optimization of biodiesel production by RSM

The results of the transesterification step based on CCD as depicted in Table 4.15 were statistically analyzed by RSM. Design-Expert® dx8 software version 8.0.7.1(*Design Ease Inc., USA*) generated the quadratic mathematical model. The full quadratic regression model for rubber seed oil methyl ester (RSOME) production in coded process variables is given in Equation (4.13).

$$\textit{Biodiesel yield}\ (\%) = 83.46 + 0.008629x_1 + 0.21x_2 - 0.34x_3 + 0.26x_1x_2 + 0.21x_1x_3 + 0.16x_2x_3 - 0.11x_1^2 - 0.34x_2^2 - 0.30x_3^2 \quad (4.13)$$

A good correlation exists between the predicted yields and the experimental yields as shown in Figure 4.22. The coefficient of determination (R^2) given as 0.918 indicates a well-fitted and reliable model.

Table 4.15: Central composite design for optimization of biodiesel production process by RSM and ANN

Std. run	x_1	x_2	x_3	biodiesel yield (%)	Predicted biodiesel yield (%)		Residual	
					RSM	ANN	RSM	ANN
1	–1	–1	–1	83.50	83.50	83.50	0.033	0.00000046
2	1	1	–1	82.50	82.50	82.50	–0.044	0.00000005
3	–1	1	–1	83.00	83.04	83.00	–0.044	0.00000001
4	1	1	–1	83.20	83.16	83.20	0.039	0.00000012
5	–1	–1	1	82.00	82.04	82.00	–0.044	0.00000004
6	1	–1	1	82.00	81.96	82.00	0.039	0.00000001
7	–1	1	1	82.30	82.26	82.30	0.039	0.00000033
8	1	1	1	83.18	83.22	83.18	–0.039	0.00000055
9	–2	0	0	83.00	83.00	83.00	0.0023	0.00000021
10	–2	0	0	83.00	83.00	83.00	0.0023	0.00000021
11	0	–2	0	82.00	81.70	81.70	0.30	0.30000000
12	0	–2	0	81.40	81.70	81.70	–0.30	–0.30000000
13	0	0	–2	82.90	82.95	82.95	–0.047	–0.05000000
14	0	0	–2	83.00	82.95	82.95	0.053	0.05000000
15	0	0	0	83.19	83.46	83.458	–0.27	–0.26833000
16	0	0	0	83.56	83.46	83.458	0.10	0.10167000
17	0	0	0	83.70	83.46	83.458	0.24	0.24167000
18	0	0	0	83.20	83.46	83.458	–0.26	–0.25833000
19	0	0	0	83.20	83.46	83.458	–0.26	–0.25833000
20	0	0	0	83.90	83.46	83.458	0.44	0.44167000

Coded values x_1: reaction time (min), x_2: methanol/oil ratio (v/v), x_3: RSS catalyst (g)

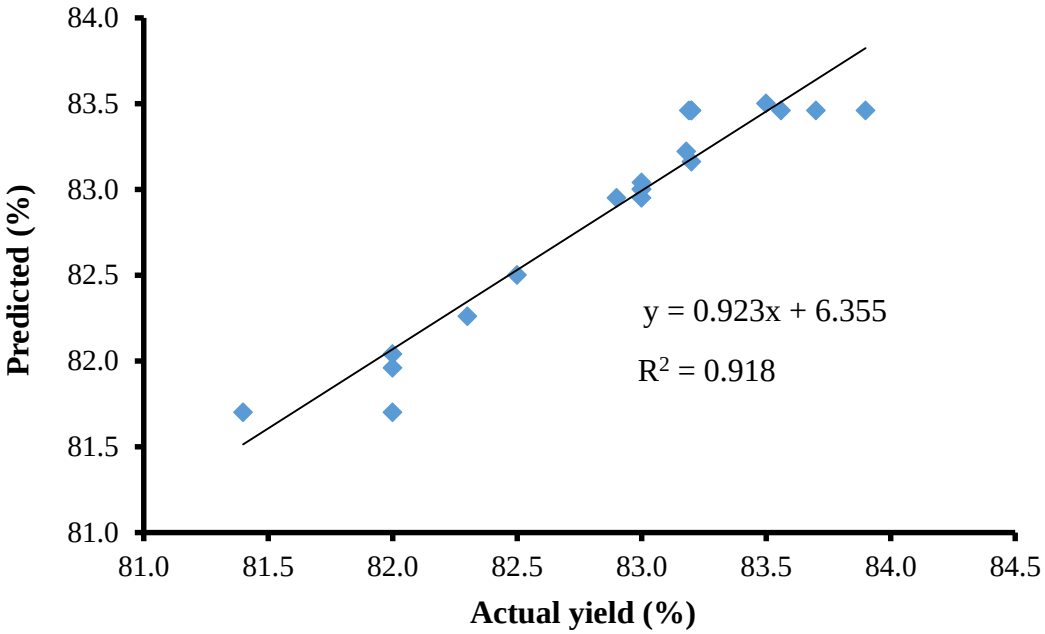


Figure 4.22: Correlation of predicted vs. actual biodiesel yields (%) for the RSM model

The residual values for RSM indicated in Table 4.15 were in each case, less than unity, and this confirms the closeness of R^2 to unity. The analysis of regression coefficients (Table 4.16) shows that the linear terms of x_1 and x_2 are positive, while x_3 is negative. The yield of RSOME (biodiesel) is enhanced by increase in X_1 and X_2 and reduction in X_3. The negativity of the coefficients of quadratic terms x_1^2, x_2^2, and x_3^2 suggests that the curvature effect of the surface response is determined by these terms.

The derived model predicted an optimal rubber seed oil methyl ester yield of 83.11% at optimum conditions of 60 min reaction time (X_1), 0.20 vol/vol methanol/oil ratio (X_2), and 2.50 g catalyst (X_3). The experiment was validated in triplicate using the optimum conditions to obtain an average RSOME yield of 83.06±0.013%. This value is close to the model predicted value, and within ±0.06% relative error based on Equation (3.27). The absolute average deviation (AAD) calculated from Table 4.15 and based on Equation (3.28) was ±0.022%. Hence, the developed model gave a good estimate of the response of the process to the process variables for low values obtained.

Table 4.16: RSM regression coefficients analysis for the biodiesel

Factor	Coefficient of Estimate	Degree of freedom	standard error	95%confidence level (low)	95%confidence level (high)	Variance inflation factor
*Intercep*t	83.46	1	0.10	83.23	83.69	–
x_1	0.008629	1	0.087	–0.18	0.20	1.72
x_2	0.21	1	0.087	0.015	0.40	1.72
x_3	–0.34	1	0.087	–0.53	–0.15	1.72
x_1x_2	0.26	1	0.091	0.057	0.46	1.00
x_1x_3	0.21	1	0.091	0.007	0.41	1.00
x_2x_3	0.16	1	0.091	–0.043	0.36	1.00
x_1^2	–0.11	1	0.066	–0.26	0.035	1.75
x_2^2	–0.34	1	0.066	–0.48	–0.19	1.75
x_3^2	–0.30	1	0.066	–0.44	–0.15	1.75

4.10.2 Analysis of variance (ANOVA) for biodiesel production

The statistical significance and the goodness of fit of the developed second-order quadratic model, as well as the effect of individual terms and their interactions were analyzed by ANOVA, and the results are summarized in Table 4.17. The quality of the model fit was evaluated by the Fisher's test (*F*-value), the probability value (*p*-value), the "lack of fit", the coefficient of determination (R^2), adjusted R^2 (R^2_{adj}), and predicted R^2 (R^2_{pred}). The *p*-value should be less than 0.05 for the variables to have significant effect on the response (RSOME yield). The polynomial model has an *F*-value of 12.38 and *p*-value <0.0003, which indicates that the developed model is statistically significant at the 95% confidence level. The higher the *F*-value for the specific independent process variable, the higher will be the effect of that variable. Two main effects, i.e. x_2 and x_3 are significant based on their estimated *p*-values (<0.05). This shows that biodiesel produced from rubber seed oil could be effectively catalyzed using indigenously prepared RSS catalyst. From the ANOVA analysis, the interactive effects of x_1x_2 and x_2x_3 on the biodiesel yield are significant ($p<0.05$) even though x_1 appears insignificant. The effects of individual process variable as shown in Table 4.16 indicate that the contribution of reaction time is low compared to other variables. However, there is a strong interaction between reaction time and other variables as presented in Tables 4.16 and 4.17.

In the present study, the "lack of fit" of low *F*-value of 0.079 and high *p*-value of 0.9246 implied that the model was not significant relative to pure error (0.65). The *p*-value of the "lack of fit" parameter is greater than 0.05, indicating that there is good fit between the second-order quadratic model and the experimental esters yield obtained (Dharma et al., 2016).

The coefficient of determination (R^2) reflects the variability of the dependent response variable, which is explained by its relationship with the independent process variables (Dharma et al., 2016).

In the present study, the R^2 value is 0.9187, which indicates that 91.87% of the variability in the biodiesel yield is attributed to the independent factors considered (reaction time, methanol/oil ratio, and catalyst amount), and only 8.13% was not explained by the model. The R^2 value is close to unity and signifies that the experimental data obtained linearly fits in the chosen model equation. The adjusted and predicted R^2 for the present study was obtained as 0.8436 and 0.7887, respectively. The difference between the adjusted R^2 and predicted R^2 values, which is 0.0549, is below the maximum allowable difference of 0.2 (Dhawane et al., 2016). This explains that the model is capable of predicting the response in a reasonable acceptable range. The adequate precision value measures the signal-to-noise ratio, and the present study gave adequate precision of 9.83, which was higher than the critical value of 4, thereby indicating that the model has strong signal to navigate the design space for the optimization purpose (Kostićet al., 2016; Betiku & Ajala, 2014; Cerino Córdovaet al., 2011). The coefficient of variance (C.V.) obtained for the present study was found to be low (0.313%), which indicates that the experimental data are accurate and reliable to suggest that the quadratic model is capable of optimizing the process.

Table 4.17 Analysis of variance (ANOVA) for the biodiesel production using RSM model

Source of variance	Sum of squares	degree of freedom	Mean square	*F*-value	*p*-value
Model	7.44	9	0.83	12.38	0.0003[a]
x_1	0.0006595	1	0.0006595	0.009884	0.9228
x_2	0.39	1	0.39	5.78	0.0371[a]
x_3	1.03	1	1.03	15.47	0.0028[a]
x_1x_2	0.54	1	0.54	8.11	0.0173[a]
x_1x_3	0.35	1	0.35	5.29	0.0443[a]
x_2x_3	0.20	1	0.20	3.07	0.1103
x_1^2	0.19	1	0.19	2.85	0.1224
x_2^2	1.75	1	1.75	26.18	0.0005[a]
x_3^2	1.38	1	1.38	20.66	0.0011[a]
Residual	0.67	10	0.067		
Lack of fit	0.013	2	0.006478	0.079	0.9246
Pure error	0.65	8	0.082		
Corrected total	8.10	19			
Statistical parameters:					
Standard deviation: 0.26			R^2: 0.9187		
Mean of response: 82.89			Adjusted R^2: 0.8436		
Coefficient of variance (%): 0.313			Predicted R^2: 0.7887		
Adequate precision: 9.83					

x_1: reaction time (min), x_2: methanol/oil ratio (vol/vol), x_3: catalyst amount (g)

[a] statistically significant at the confidence level of 95%

4.10.3 Parametric effects of interactive factors on biodiesel yield by RSM

In design of experiments (DOEs), the 3D model equation facilitates examination of the effects of process variables on the response variable. The surface plot depicted in Figure 4.23 (a) shows the interaction between reaction time (min) and methanol/oil ratio (vol/vol), with the catalyst amount constant at the center point. Rubber seed oil methyl ester yield, marginally (0.4%) increased with increase in reaction time from 60 to 70 min as shown in Figure 4.23 (a). At this condition, 0.6 vol/vol (coded) that translates to 0.28 vol/vol (actual) methanol/oil ratio was found to be the optimum for attaining 83.4% of yield when methanol/oil ratio varies from 0.20 to 0.30 vol/vol (actual). This shows that the interactive effect is not significant enough at these conditions of low range of reaction time (Onoji et al., 2017b).

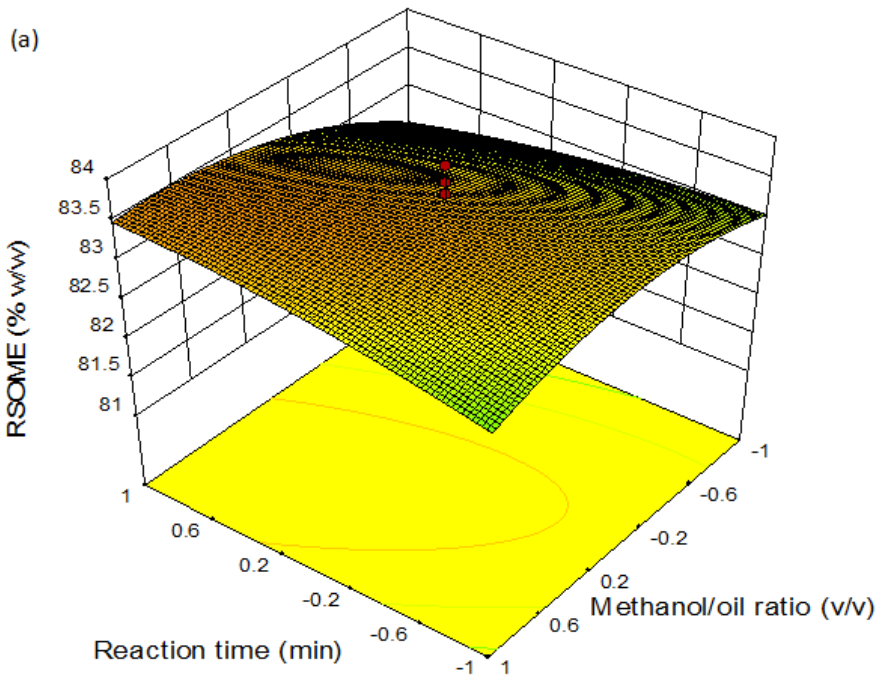


Figure 4.23 (a): RSM 3D plot for the interactive effect between reaction time and methanol/oil ratio on biodiesel (RSOME) yield

Figure 4.23 (b) depicts the interaction effect between reaction time and catalyst amount on rubber seed oil methyl ester yield, with methanol/oil ratio constant at the center point. It was evident that the reaction time's effect had the same trend as in Figure 4.23 (a). The effect of the reaction time alone on the yield as shown in Tables 4.16 and 4.17 is not significant, although it has significant interactions with methanol/oil ratio and catalyst amount as previously observed.

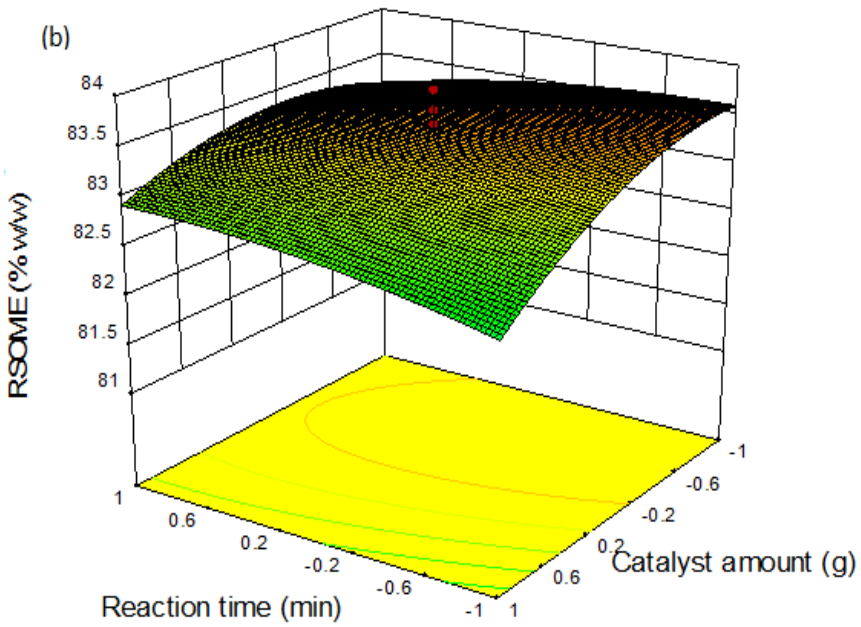


Figure 4.23 (b): RSM 3D plot for the interactive effect between reaction time and catalyst amount on biodiesel (RSOME) yield

Similar observations, but with slight reduction in yield (83%), were noticed for the plot of Figure 4.23 (c) that represents the interaction between methanol/oil ratio and catalyst amount, when the reaction time is constant at the center point. Marginal reduction in yield was observed when methanol/oil ratio varies from 0.20 to 0.30 vol/vol, with catalyst optimum value of 2.5 g. It is worthy to note that each of the interactions in the surface plots exhibited a curvature that indicates good interactive effects between the process factors involved.

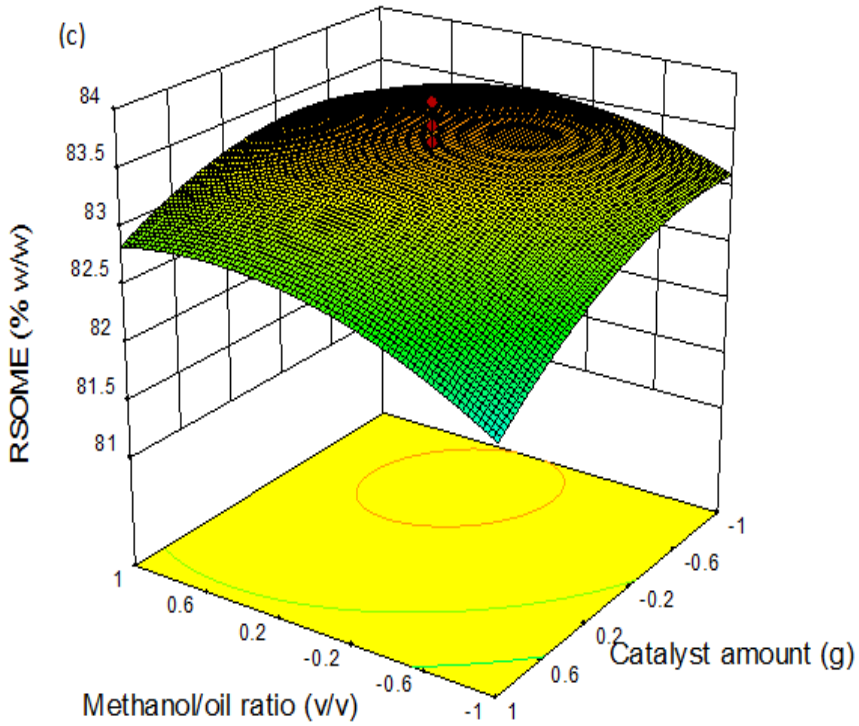


Figure 4.23 (c): RSM 3D plot for the interactive effect between methanol/oil ratio and catalyst amount on biodiesel (RSOME) yield

4.10.4 Optimization and interactive effects of process variables on biodiesel yield by ANN model

Iteratively, three neurons were obtained in the hidden layer that gave a good prediction of the outputs of training and validation sets in the present study. A network of 3-3-1 topology was developed, and the genetic algorithm of the model predicted optimal biodiesel (RSOME) yield of 85.07% at the following conditions: reaction time (X_1=56.70 min), methanol/oil ratio (X_2=0.21 vol/vol), and catalyst amount (X_3=2.20 g). The experiment was validated in triplicates using the optimum conditions, and the average optimal biodiesel yield was 85.03±0.0012%. This value is close to the model predicted value, and within ±0.051% relative error based on Equation (3.27). The % absolute average deviation (AAD) calculated from Table 4.15, and based on Equation (3.28) was ±0.000473%. Hence, the developed model gave a good estimate of the response of the process for the low values obtained. The model has a coefficient of

determination (R^2) value of 0.9198, R^2_{adj} value of 0.9182, and R^2_{pred} value of 0.9168. These values indicate a good and reliable model as was obtained for RSM.

Figure 4.24 compares the predicted and experimental values of the biodiesel yield, and the coefficient of determination (R^2 = 0.9198) shows a good correlation between the data obtained. This confirms that the model is suitable for adequate representation of the actual relationship among the selected factors.

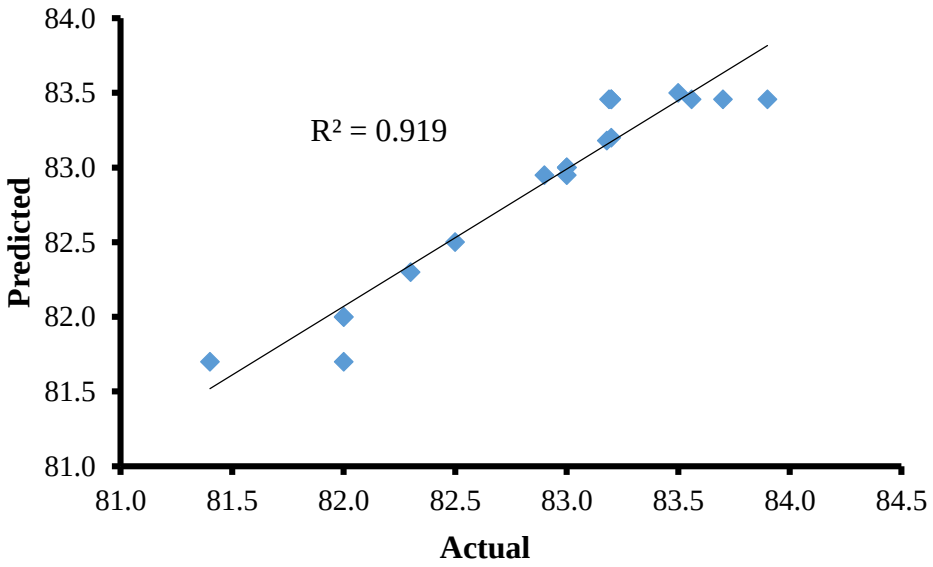


Figure 4.24: Correlation of predicted vs. actual biodiesel yields for ANN model

Figures 4.25, 4.26, and 4.27 depict the interactive effects on biodiesel (RSOME) yield between two process variables while maintaining the third variable constant at center point. The curvatures nature of the 3D surfaces suggested significant interactions of methanol/oil ratio with reaction time, catalyst amount with reaction time, and methanol/oil ratio with catalyst amount. Figure 4.26 shows steep decrease in the biodiesel yield as catalyst loading increases. This could be observed as excess catalyst negates the mixing of methanol, oil and catalyst, which led to phase separation and subsequent reduction in biodiesel yield. The observation is similar to the reports of other researcher that as catalyst loading increases, biodiesel yield

increases until optimum catalyst loading is attained (Syazwani et al., 2015). The level of importance of the process variables considered for the RSOME synthesis is depicted in Figure 4.28. It is apparent that catalyst amount (45.62%) is the most significant variable, followed by methanol/oil ratio (36.87%) and lastly, reaction time (17.51%).

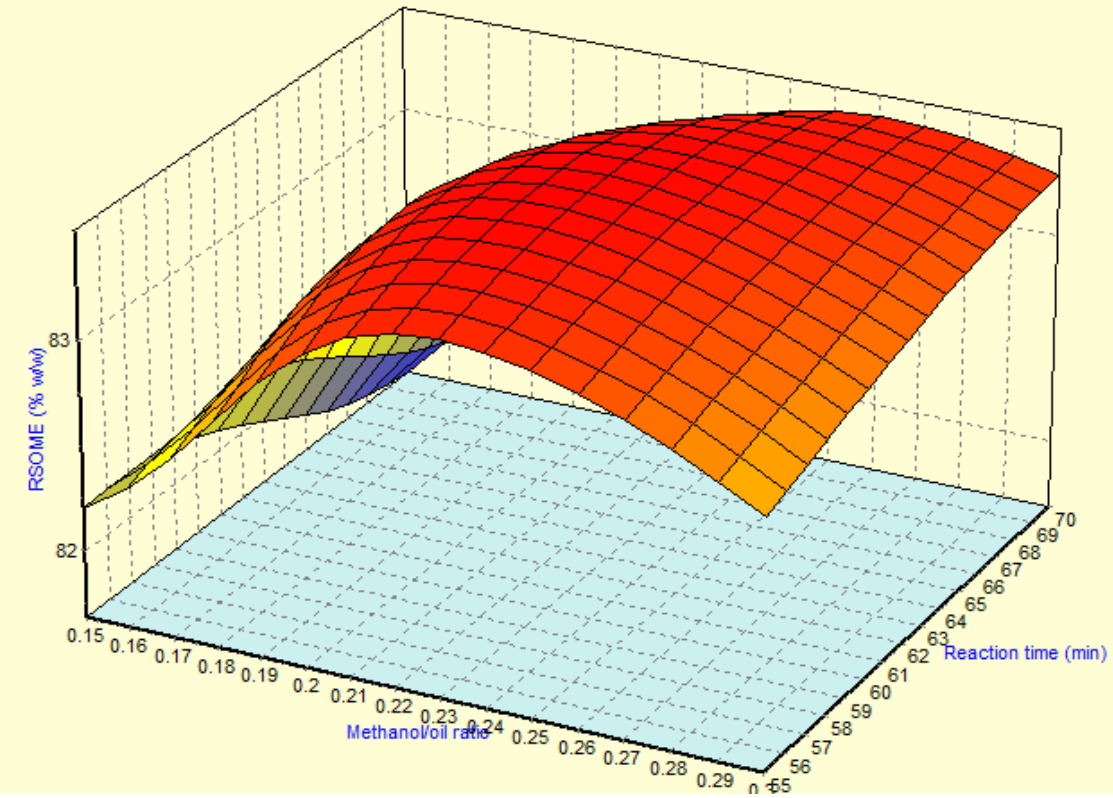


Figure 4.25: ANN Surface plot for the interactive effect of methanol/oil ratio with reaction time on (biodiesel) RSOME yield

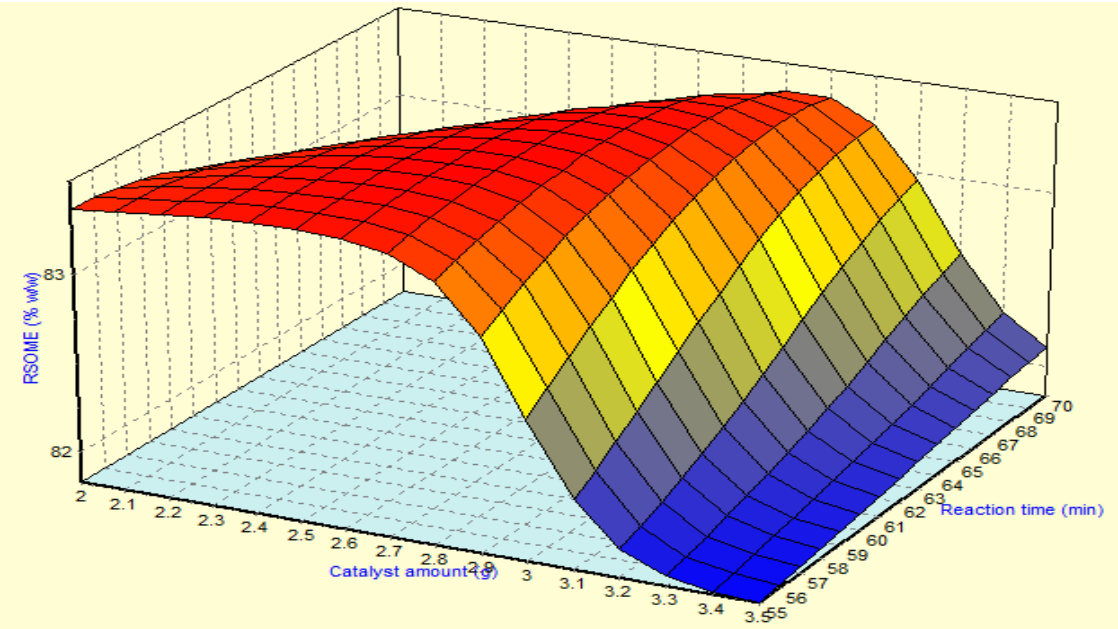


Figure 4.26: ANN Surface plot for the interactive effect of catalyst amount with reaction time on (biodiesel) RSOME yield

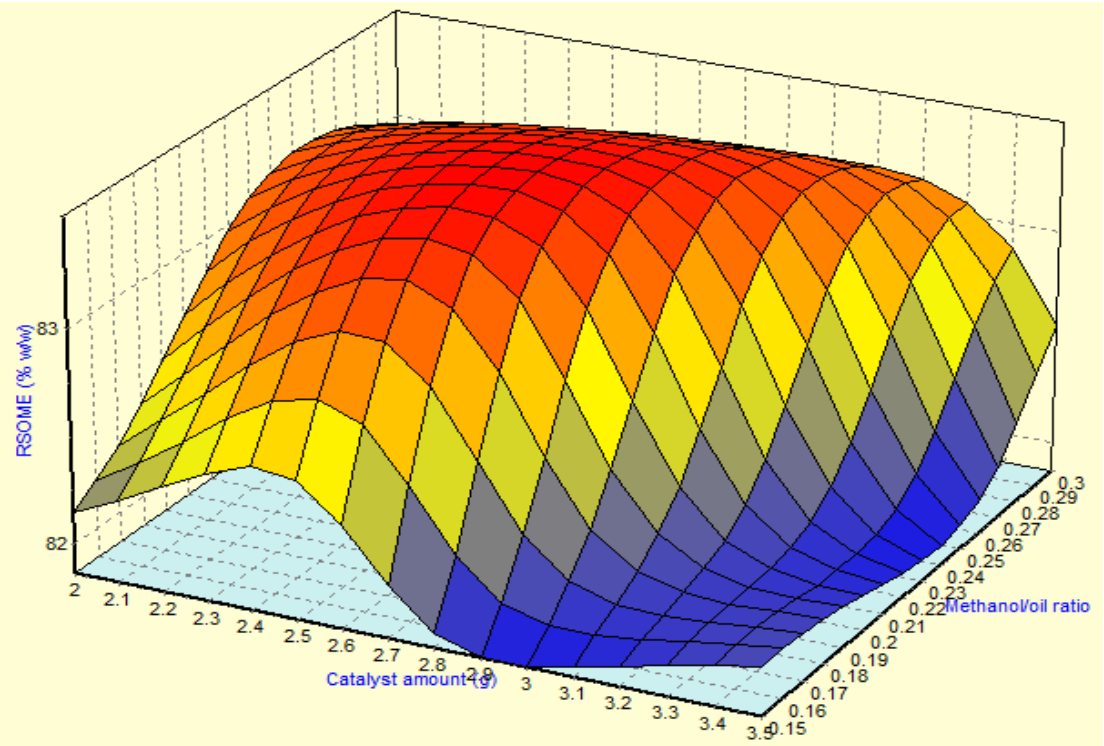


Figure 4.27: ANN Surface plot for the interactive effect of methanol/oil ratio with catalyst amount on biodiesel (RSOME) yield

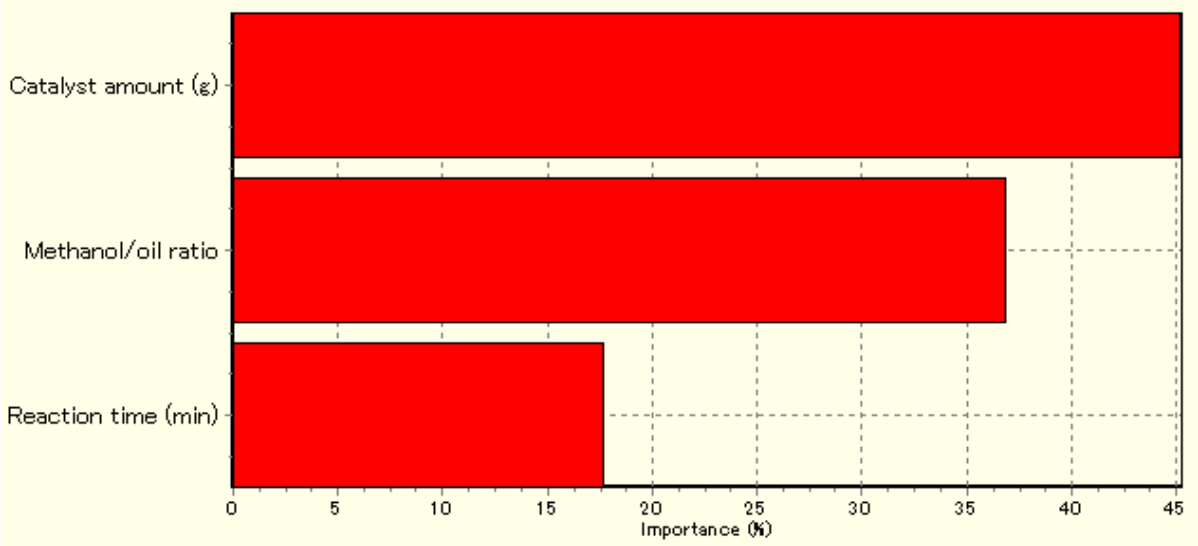


Figure 4.28: Percentage contribution of process variables to biodiesel production via ANN model (catalyst amount 45.62%, methanol/oil ratio 36.87%, and reaction time 17.51%)

4.10.5 Comparison of RSM and ANN models for the biodiesel production

The accuracies of both RSM and ANN models were evaluated based on the values obtained for R^2, *% AAD*, % relative error and the yields obtained at optimum conditions for the models. The RSM model equation at its optimum conditions (X_1 = 60 min, X_2 = 0.20 vol/vol and X_3 = 2.5 g) gave a yield of 83.11%. The ANN model at its optimum conditions (X_1 = 56.7 min, X_2 = 0.21 vol/vol and X_3 = 2.2 g) gave a higher biodiesel yield of 85.07%. The supremacy of the ANN model over RSM was further attested to by the lower values of relative error ($\pm$0.051%) and AAD ($\pm$0.000473%) compared to the values of RSM relative error ($\pm$0.06%) and AAD ($\pm$0.022%).

However, both optimization techniques gave good prediction due to the values of R^2 that are relatively close to unity (i.e. 0.9187 and 0.9198 for RSM and ANN, respectively). The non-linearity of the ANN may contribute to its superiority over RSM (Ma et al., 2016).

4.11 Performance and emissions analysis of test engine using biodiesel-diesel blends

The experimental analyses of the data for engine performance and emission characteristics obtained from the tested fuels (B00, B10, B20, B30, B50, and B100) used in this study are presented in this section. The properties of the tested fuels needed for the computation of combustion parameters are listed in Table 4.18.

Table 4.18: Properties of the test fuels

Fuel type	B00	B10	B20	B30	B50	B100
Density (kg/m^3)	850	853	855	858	863	876
LHV (kJ/kg)	42,900	42,400	41,900	41,500	40,500	38,200
Kinematic viscosity (mm^2/s)	3.21	3.32	3.43	3.54	3.76	4.32
Cetane number	52	52.5	53	53.5	54.5	57

4.11.1 Air/Fuel ratio (AFR)

The air-fuel mixture formation in the combustion chamber affects the combustion performance and emission characteristics of diesel engines (Li et al., 2016). The air-box differential pressure (ΔP) and the ambient air pressure (P_A) are important parameters for the computation of the flowrate of air. The flowrate of air and the air/fuel ratio were calculated using Equations (3.31) and (3.32), respectively. Figure 4.29 depicts the variation of air/fuel ratio with engine speed for the fuels tested (B00, B10, B20, B30, B50, and B100). The plots data were obtained from Tables I.1 through I.6 of Appendix I. The Figure depicts that B20 has the best air/fuel ratio, and biodiesel the least. A higher air/fuel ratio means lower amount of fuel was consumed for the given air flowrate. The lower value for biodiesel is attributed to its high density and

viscosity compared to other blends, and higher fuel consumption rate for biodiesel for same power output.

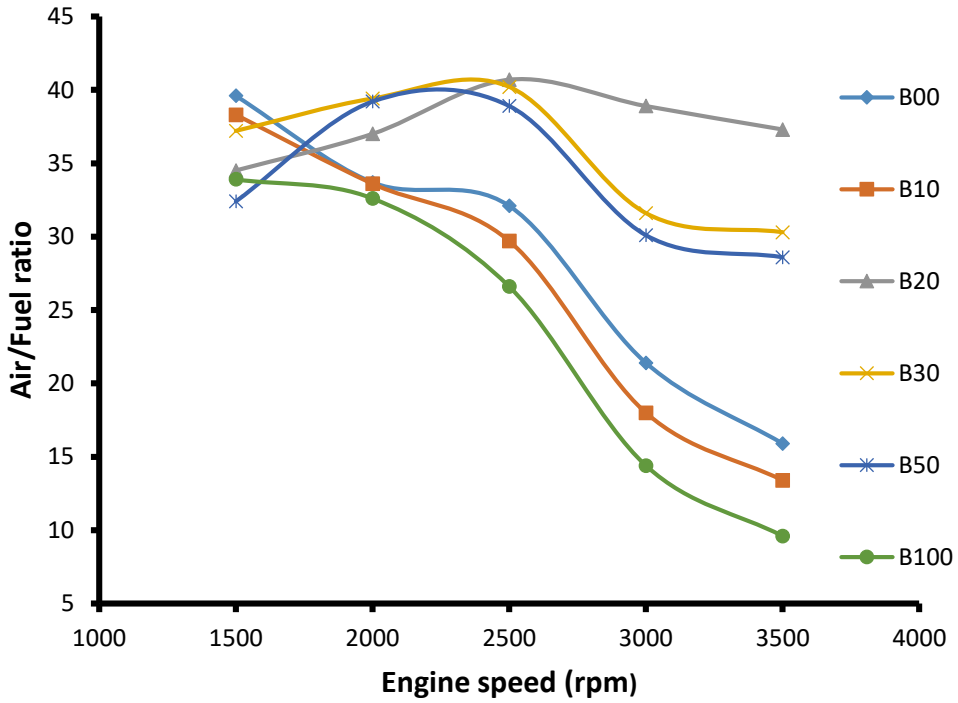


Figure 4.29: Variation of air/fuel ratio with speed for diesel and biodiesel blends

4.11.2 Brake mean effective pressure (BMEP)

The calculated BMEPs for the tested fuels are presented in Tables I.1 through I.6 of Appendix I, and were computed using Equation (3.33). The BMEP is a useful tool for comparing and evaluating similar types of engines. The maximum BMEP developed by the engine for all fuels tested was 4.75 bar for pure diesel (B00) at 2500 rpm and it was within the range of values reported for this engine using diesel fuel (TecQuipment Ltd, 2011). It was also observed that for all fuels tested, their maximum BMEP was obtained at 2500 rpm, which appears to be the ideal speed to operate the test engine for maximum efficiency.

4.11.3 Brake thermal efficiency (BTE%)

Brake thermal efficiency is the ratio between the effective power developed and the rate of energy introduced by fuel injection (Aldhaidhawi et al., 2017). The variation of BTE% of the engine with speeds for the biodiesel blends used in this study in relation to diesel fuel is depicted in Figure 4.30 with plot data obtained from Table I.7 of Appendix I. It was observed that BTE% decreases as the percentage of biodiesel in the blends increases at all speeds due to poor atomization of the blends coupled with high viscosity. Among the blends, B50 was found to have the maximum thermal efficiency of 42.8% at a brake power of 1.88 kW, while for diesel oil, it was 56% and biodiesel 28.2% at 2500 rpm. It can be shown that beyond the speed limit of 2500 rpm, the brake thermal efficiency trend is reverted and started decreasing. The lower BTE% obtained for B100 could be due to the low calorific value of biodiesel and increase in fuel consumption as compared to B50. Ramadhas et al. (2005a) reported this trend for a diesel engine fueled with rubber seed oil methyl esters (biodiesel).

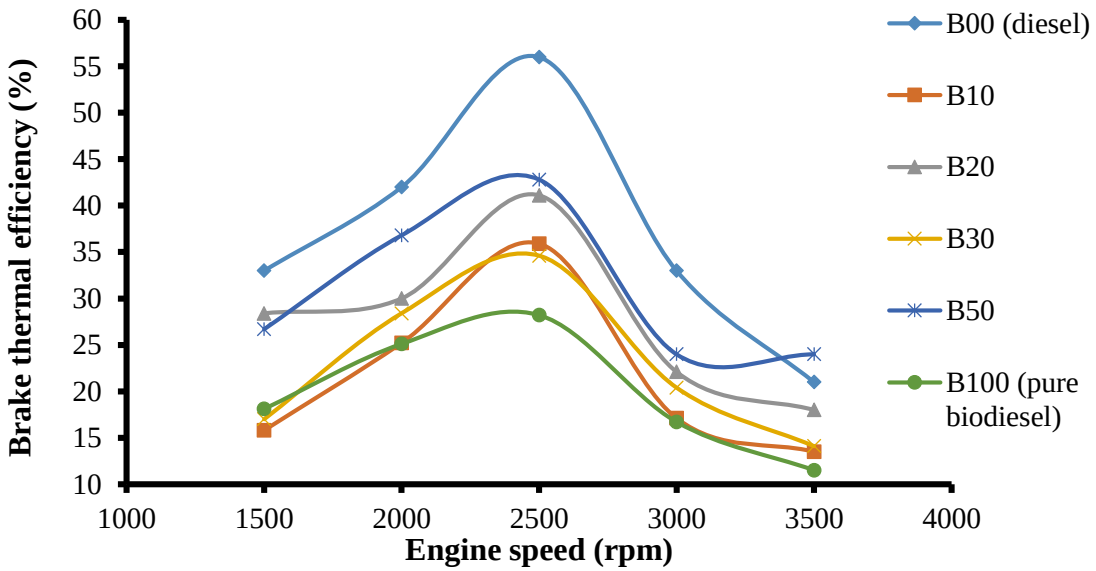


Figure 4.30: Variation of brake thermal efficiency with speed for diesel and biodiesel blends

4.11.4 Brake specific fuel consumption (BSFC)

The term brake specific fuel consumption (BSFC) refers to fuel consumption quantities which have been normalized by the engine power representing actual fuel consumed to produce 1 kW of power output (Aldhaidhawi et al., 2017). Figure 4.31 depicted below, and obtained from data presented in Table I.8 of Appendix I shows the variation of BSFC of diesel and biodiesel blends at full load conditions with engine speeds. It was found that the BSFC for the blend B20 was close to that of diesel. For higher blends, the BSFC was found to be much higher than diesel at all speeds. This is the result of the combined effects of lower heating value and the high fuel flow rate due to high viscosity of the blends as reported by other researchers (Celikten et al., 2012). The finding of this study is consistent with findings of past studies (Labeckas & Slavinskas, 2006; Raheman & Ghadge, 2008).

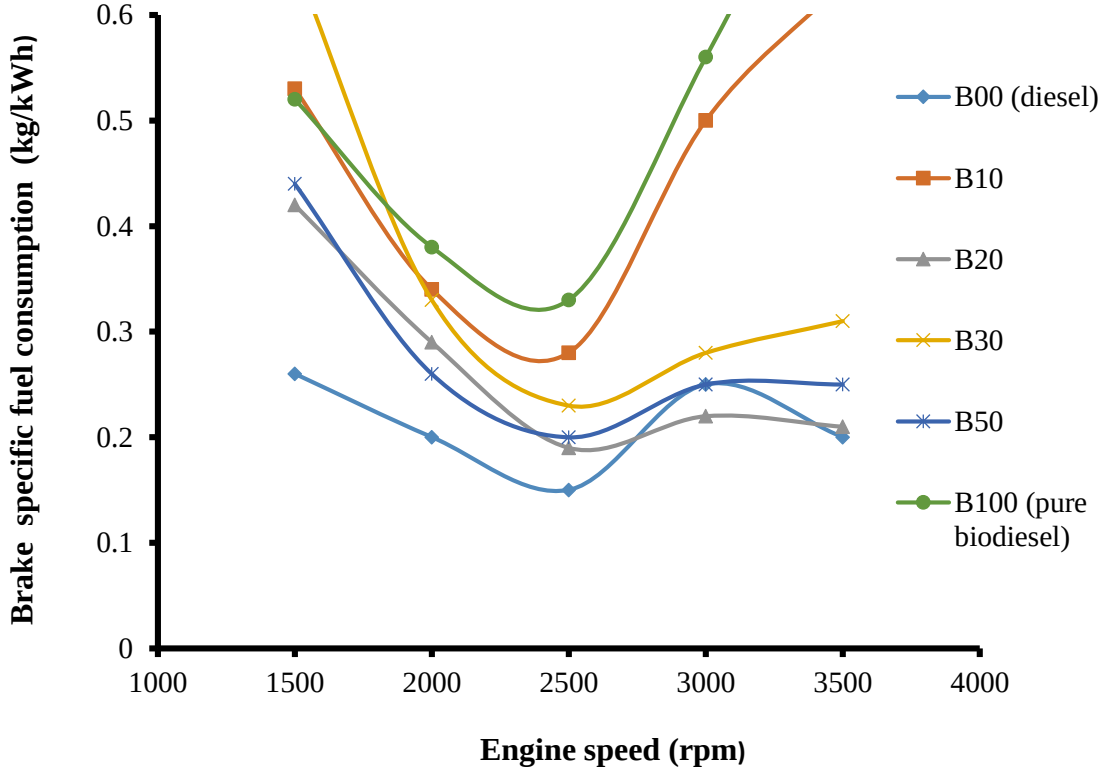


Figure 4.31: Variation of brake specific fuel consumption with speed for diesel and biodiesel blends

4.11.5 Engine brake power

Figure 4.32 obtained from data presented at Table I.9 of Appendix I shows that the brake power (BP) increases progressively for all types of fuels tested (B00, B10, B20, B30, B50 and B100) all speeds at full load conditions. The value of BP recorded followed similar trends for all fuels blends. The BP value increment was related to the increase in engine speed, since at high speeds the combustion inside the cylinder was close to completion, which produced increasing brake power. The lower value of engine power for biodiesel and its blends is related to its lower calorific value compared to fossil diesel, and it is a natural phenomenon (Mohsin, et al., 2014). However, since the difference for biodiesel in each fuel blend was 10–20%, the data showed similar results, but B20 and B50 showed characteristics that are similar to pure diesel with respect to brake power. It may be argued that the higher brake specific fuel consumption of rubber seed biodiesel and its blends will compensate this power loss and maintain the fuel quantity, finally yielding the same engine output. Mohsin et al. (2014) reported a similar trend at full load conditions using biodiesel blends in a test engine.

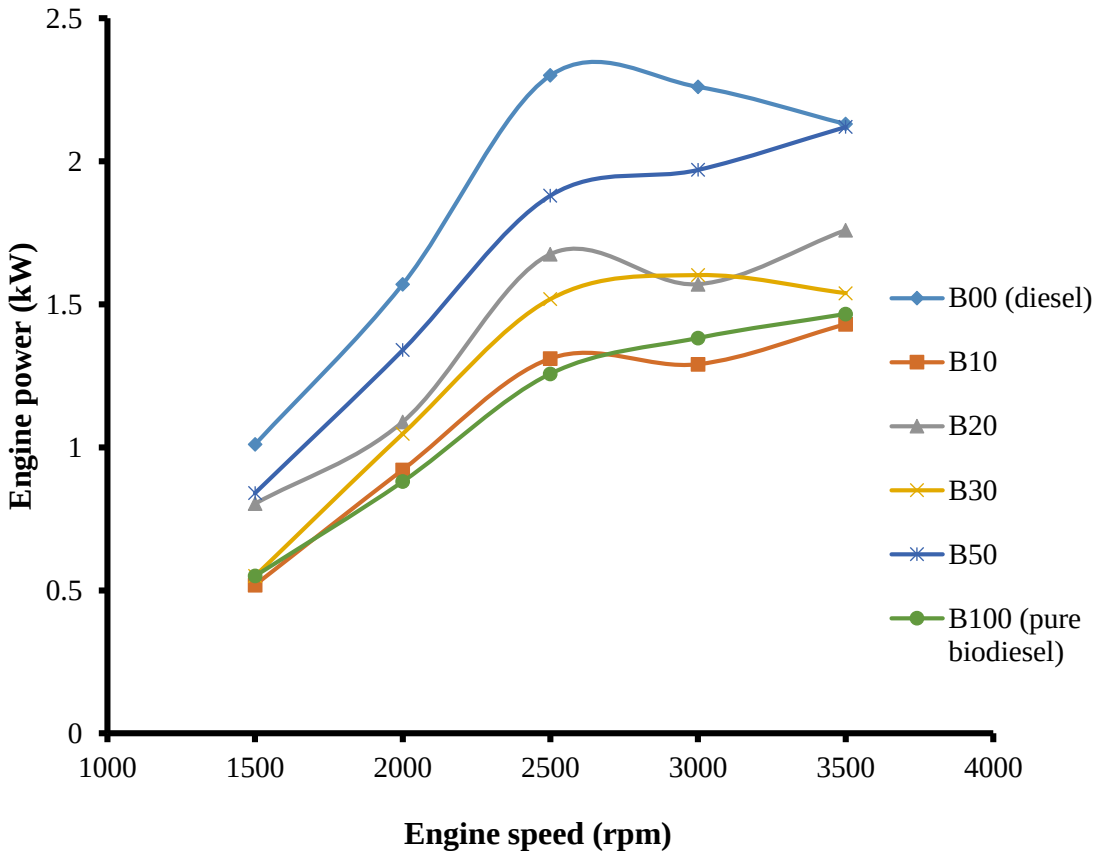


Figure 4.32: Variation of engine power with speed for diesel and biodiesel blends

4.11.6 Engine torque

As shown in Figure 4.33 below, there was reduction in the engine torque for each type of fuels blends used in the present study beyond 2500 rpm. The data for the plots are recorded in Table I.10 of Appendix I. The value of torque decreased as the engine speed increased beyond 2500 rpm, because of less force needed to push the engine piston at high speed. This decreasing value of torque for high speed is considered normal for every type of engine (Mohsin et al., 2014). Lower torque value at a higher engine speed is one of the criteria that ensure positive reaction of the fuel inside the cylinder.

For all fuels tested, maximum torque was achieved at 2500 rpm, but biodiesel fuel gave the lowest torque value at all speeds. A similar trend was reported by Mohsin et al. (2014), which

showed maximum torque for all blends at 2400 rpm but tended to decrease with further increase in speed.

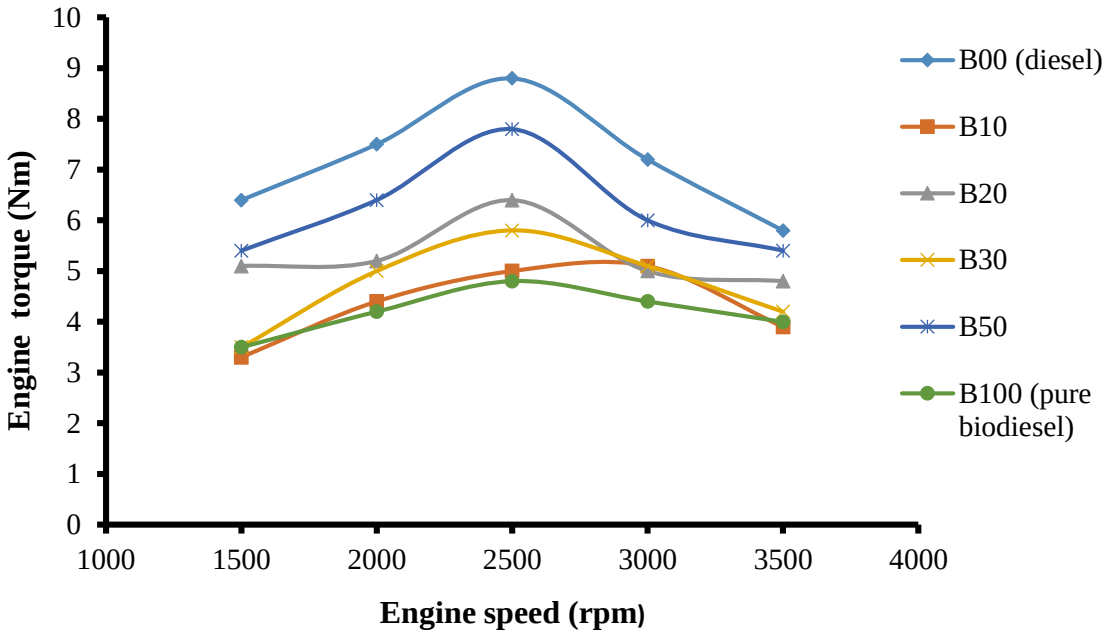


Figure 4.33: Variation of engine torque with speed for diesel and biodiesel blends

4.11.7 Exhaust gas temperature (EGT)

Figure 4.34 shows the plots of exhaust gas temperature (EGT) with engine speeds for biodiesel blends and diesel obtained from Table I.11 of Appendix I. The results show that the EGT increases with increase in engine speed for all fuels tested. At all speeds, fossil diesel was found to have the lowest temperature and the temperature for various blends show an upward trend with increasing volume of biodiesel in the blends. The ester molecule in the biodiesel contains oxygen atoms that enhance the combustion process, which results to higher EGTs. In addition, air-coded engines run hotter resulting to higher EGTs. The high EGT for biodiesel resulted to higher concentration of NO_x in the exhaust gas emission. These findings are consistent with those reported by other researchers (Ramadhas et al., 2005a; Elango & Senthilkumar, 2011).

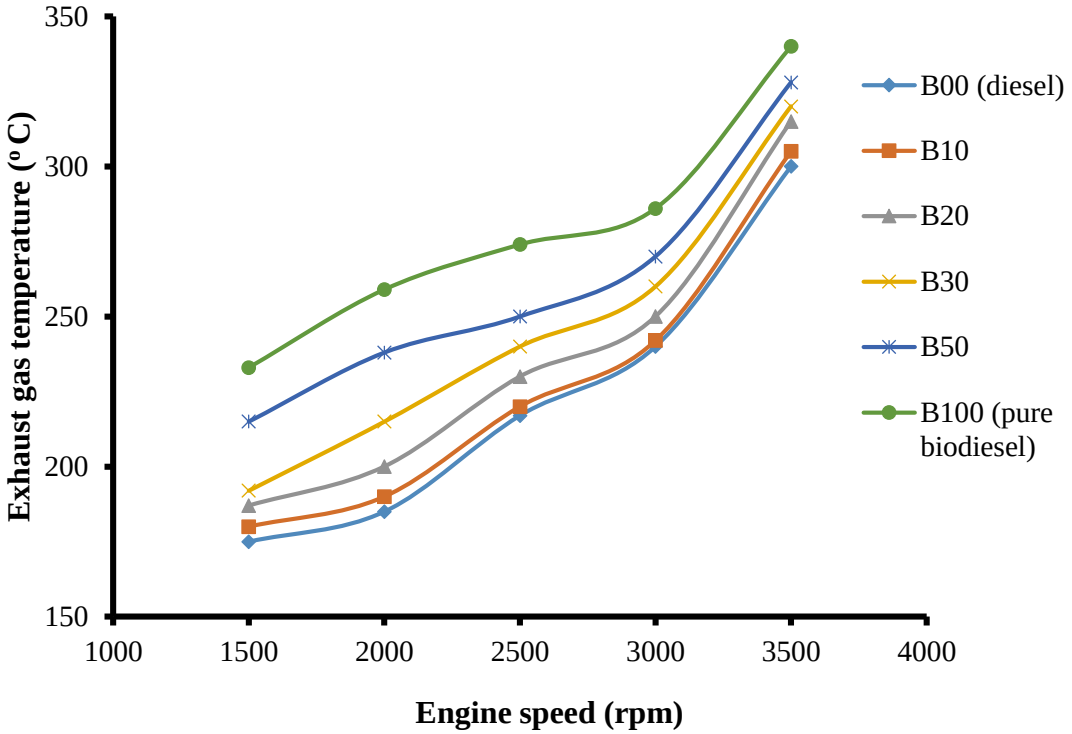


Figure 4.34: Variation of exhaust gas temperature with speed for diesel and biodiesel blends

4.11.8 CO emissions

Carbon monoxide (CO) is the result of incomplete combustion of fuel such as fossil diesel that lacks oxygen molecule in its molecular structure. Several factors such as air-fuel ratio, engine speed, injection timing, injection pressure, and type of fuels affect CO emissions. The different CO emission values of diesel and biodiesel blends with their trend lines at various engine speeds are depicted in Figure 4.35 with data obtainable from Table I.12 of Appendix I. In all causes considered, CO emission at 2500 rpm recorded the lowest values and it could be considered as the ideal speed for the engine operation. It is interesting to note that the engine emits more CO using diesel as compared to that of biodiesel and blends at all speeds. This result can be attributed to the higher oxygen content and cetane number of the biodiesel fuel than diesel fuel. As the percentage of biodiesel increased in the blend, the higher oxygen

content to biodiesel allows more carbon molecules to burn and facilitates the completion of combustion process (Mofijur et al., 2014).

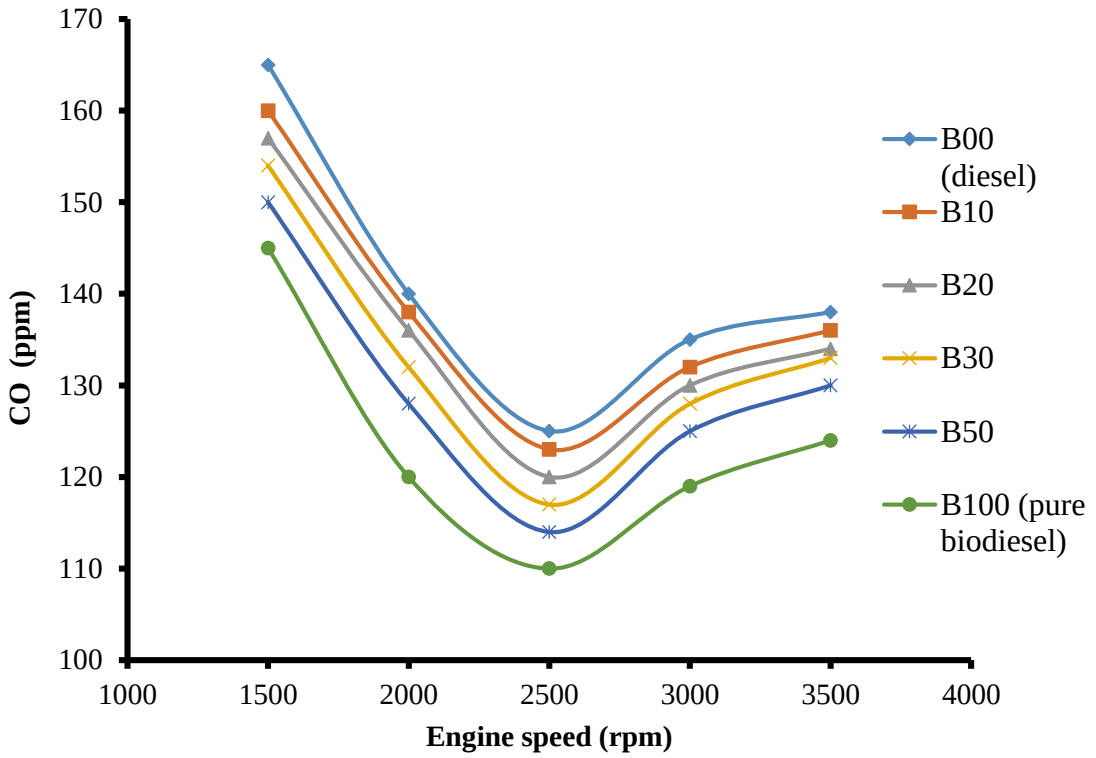


Figure 4.35: Variation of carbon monoxide emissions with speed for diesel and biodiesel blends

4.11.9 CO_2 emissions

Figure 4.36 compares the CO_2 emissions of various fuel blends tested in the diesel engine at different speeds. Naturally, emission of CO_2 from the engine is due to complete combustion of the fuel in the combustion chamber. The release of more CO_2 indicates the closeness to complete combustion of fuel. In the present study as shown in Figure 4.36, and data obtained from Table I.13 of Appendix I, and the blend of B20, gave the highest amount of CO_2 emission starting from 1500 through 3500 rpm. This supports the higher values of exhaust gas temperature. In all the cases considered, diesel (B00) produces the lowest amount of CO_2 due to incomplete combustion. Although, CO_2 is considered a greenhouse gas that causes increased

global warming, from the engine performance point of view, it achieved complete combustion and that the CO_2 emitted are readily absorbed by plants for food production process (photosynthesis) that keeps the level of CO_2 in the atmosphere balance (Mohsin et al., 2014).

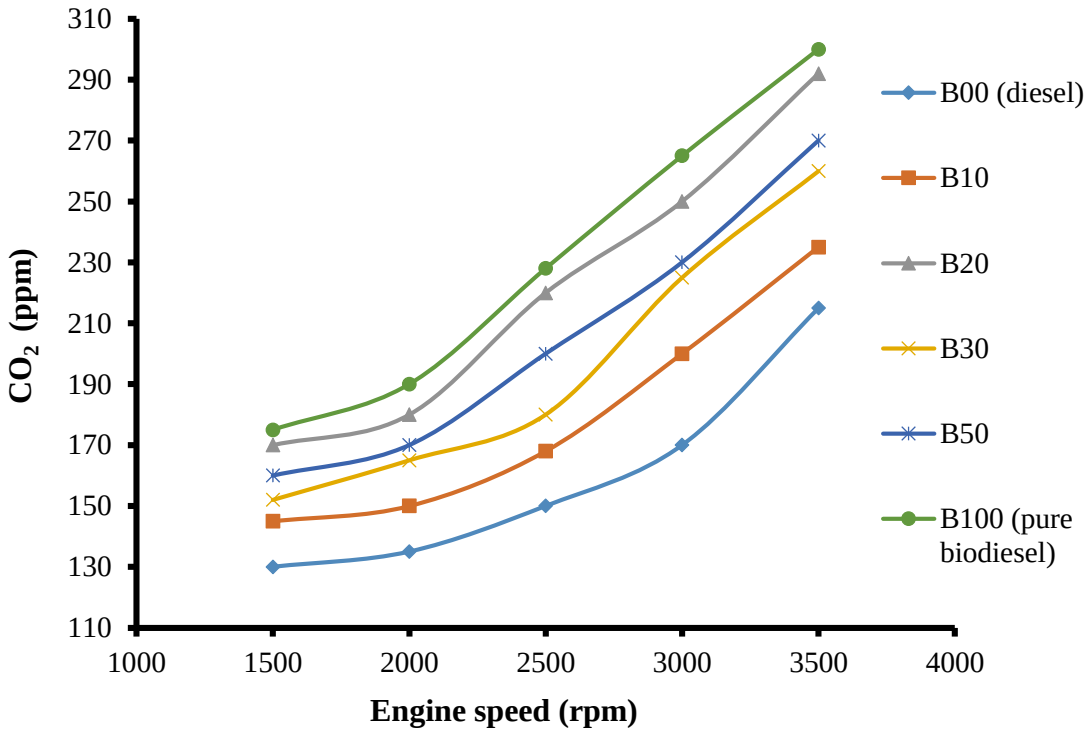


Figure 4.36: Variation of carbon dioxide emissions with speed for diesel and biodiesel blends

4.11.10 NO_x emissions

The variation of NO_x emissions of biodiesel-diesel blends with speeds obtained from Table I.14 of Appendix I is depicted in Figure 4.37. The NO_x emission for biodiesel and the blends followed are increasing trend with respect to engine speed. In all the fuels tested, NO_x emission was higher than the neat diesel (B00) with biodiesel and B50 exhibiting higher values than other blends. NO_x emission is directly related to the engine combustion chamber temperatures which in turn indicated by the prevailing exhaust gas temperature. With increase in the value of exhaust gas temperature, NO_x emission also increases (Ramadhas et al., 2005a). The results

of the present study are in agreement with the reports of researchers cited in the literature (Özener et al., 2014). Most researchers proposed that oxygen content of biodiesel, unexpected advance in the fuel injection timing, extended combustion timing, and higher combustion temperature trigger higher formation of NO_x (Ozsezen & Canakci, 2011; Murillo et al., 2007).

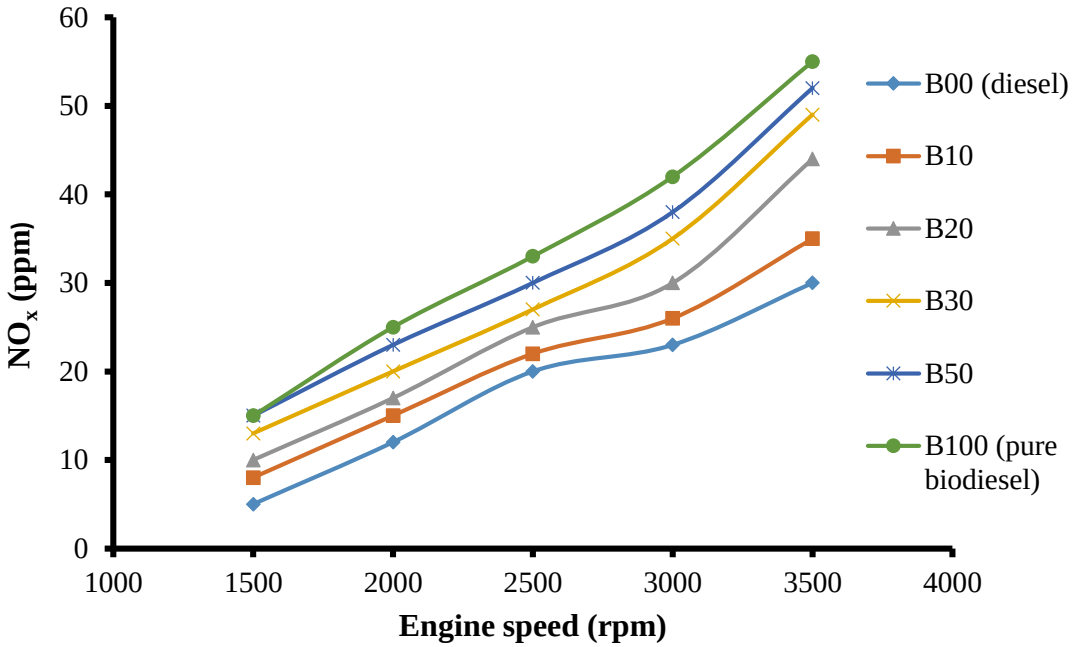


Figure 4.37: Variation of nitrogen oxides emissions with speed for diesel and biodiesel blends

4.11.11 Total hydrocarbons (THCs)

Figure 4.38 with plot data obtained from Table I.15 of Appendix I shows that the amount of THCs decreased with the increasing amount of biodiesel in the blends. This indicates that most of the total hydrocarbons emissions present in the combustion chamber were generated from the pure diesel used since the amount of fuel injected was constant for each type of blend tested. In all cases considered, engine speed at 3000 rpm produces the lowest amount of THCs, after which there was sudden increase in the content of THCs emitted at higher speeds.

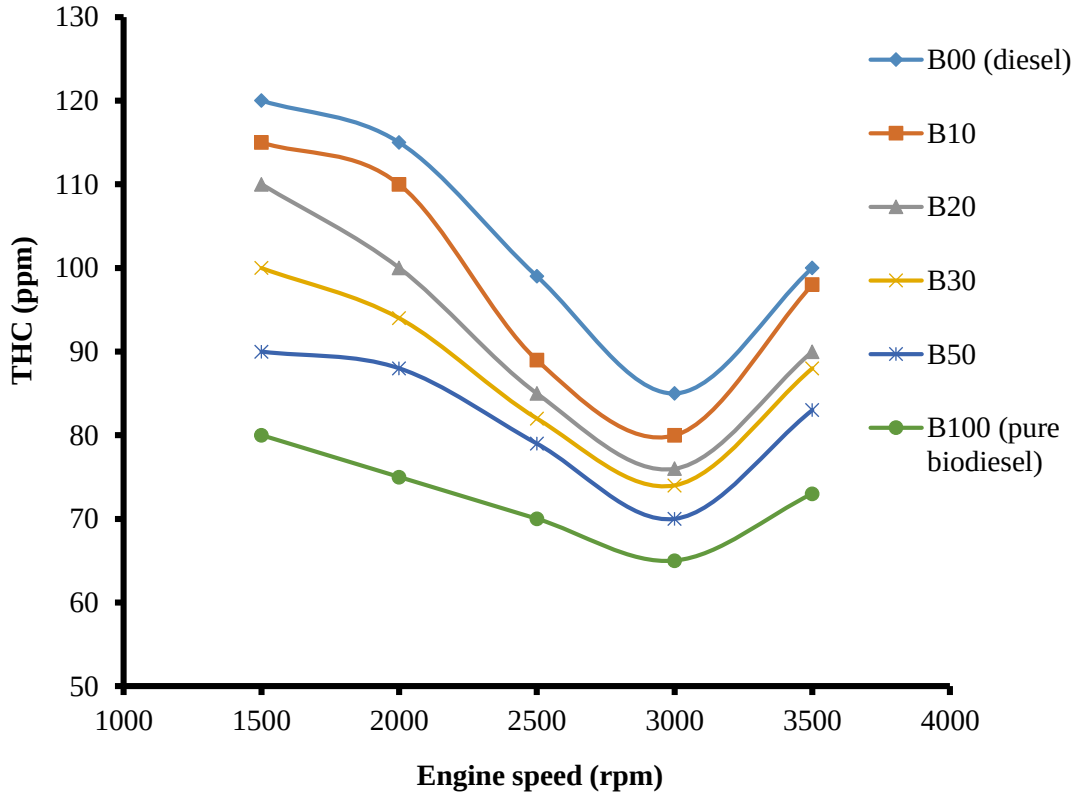


Figure 4.38: Variation of total hydrocarbons emissions with speed for diesel and biodiesel blends

4.11.12 Smoke opacity

The variation of smoke density with respect to different fuels considered is depicted in Figure 4.39, with plot data presented in Table I.16 of Appendix I. The smoke density for biodiesel and blends is generally lowered than that of diesel. B20 blend gave the lowest smoke intensity compared to other blends. Higher cetane number and lower compressibility of the biodiesel resulted in a lower ignition delay compared to that of diesel. A lower ignition delay reduces the accumulation of fuel in the combustion chamber and reduces smoke emissions (Geo et al., 2009). The formation of smoke primarily results from the unburnt molecules of fuels because of partial reaction of carbon in the liquid fuel (Özener et al., 2014). As shown in Figure 4.39, the smoke opacity decreases as the content of biodiesel in the blends increases. The reduction

in the smoke opacity with increase in biodiesel content can also be attributed to the decrease in the carbon content, and increase in the concentration of oxygen in biodiesel fuel.

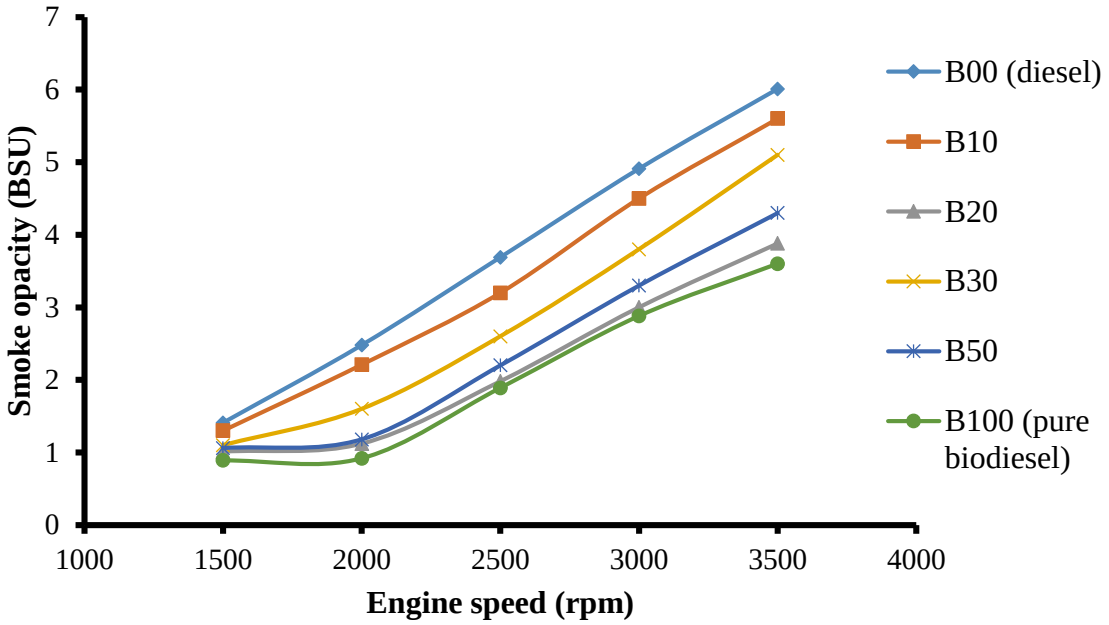


Figure 4.39: Variation of smoke opacity with speed for diesel and biodiesel blends

CHAPTER 5: CONCLUSION AND RECOMMENDATIONS

5.1 Conclusion

Energy security has been the major hindrance to the development of African countries. Biomass in the form of charcoal and fuelwood continues to be the main fuel source in these countries. Biodiesel, a sustainable energy whose properties are similar to petro-diesel could reduce the dependency on fossil diesel. Over 90% of biodiesel produced is sourced from edible oils that compete with food uses. Food is a necessity of man after shelter; and the use of edible vegetable oils as biodiesel source materials is counterproductive. Non-edible low-cost rubber seed oil obtained from abundant waste rubber seeds in Nigeria was exploited for biodiesel production in this study. The oil was chemically extracted from the Nigerian NIG800 clonal seeds using n-hexane solvent in a soxhlet extractor, and the physicochemical properties determined were in the range previously reported by researchers for rubber seed oil.

The oil extraction process variables were optimized using the response surface methodology and artificial neural network techniques via Box-Behnken experimental design. The developed models were effective in describing the parametric effect of the considered operating variables on the extraction of oil from rubber seeds. The high oleic acid content and the presence of *cis*-erucic acid indicate the potential use of the oil as a source material for oleo chemical and steel industries in the future. The kinetics of thermo-oxidative degradation of the oil follows first-order kinetics with activation energy of 13.07 kJ/mol and thermally stable up to 250 ^{o}C.

The applicability of the waste rubber seed shell obtained during oil extraction was investigated as a base catalyst for the oil transesterification to biodiesel.

The lower energy content of the produced rubber seed oil biodiesel affects the brake specific fuel consumption, but it was compensated by the improved combustion efficiency and lower environmental pollution as observed for total hydrocarbon, carbon monoxide, and smoke opacity emissions compared to fossil diesel. Optimal performance of the fuel was observed

with the B20 blend followed by B50 and the engine operated at 2500 rpm. To ensure timely dissemination of the findings in this study, results have been communicated to colleagues and researchers in the field via four published journal articles and one communication in an international conference.

5.2 Recommendations

It is recommended that further studies should be undertaken on such as:

1. The developed basic heterogeneous rubber seed shell catalyst doped with sulphuric acid via wet impregnation method be investigated for biodiesel production. This will ensure that both esterification and transesterification reactions are carried out in a single stage expected to generate a higher yield of biodiesel at a lower processing time;
2. The mechanisms of the developed catalyst used in this thesis should be investigated further to offer insight into its anticipated behaviour during biodiesel production;
3. A zero-dimensional simulation model should be employed to predict performance characteristics of the engine using biodiesel produced from rubber seed oil catalyzed by rubber seed shell catalyst;
4. Development of a differential thermodynamic equation system to obtain the pressure inside the cylinder as a function of the crank angle (θ) for differential engine conditions is recommended as future work;
5 Effects of the biodiesel on the engine components such as plunger, injectors, cylinder head, valves, piston and rings should be investigated in an endurance test to determine the level of components wear.

5.3 Contributions to knowledge

1. The outcomes of this research will serve as a pool of information for the relevant Government Ministries, Parastatals, Departments, Research Institutes, Industries, and Agencies that will serve as advocates for the implementation of the National Biofuels Policy across Nigeria's business strata with respect to biodiesel production from rubber seed oil and other African nations where rubber trees are cultivated;

2. This research provides valuable information to the global community that the genetic engineered rubber seed obtained from Nigerian NIG800 series contains high content of oleic acid and *cis*-erucic acid as a source material for oleo chemicals currently sourced from non-renewable fossil materials;

3. The performance and emission analyses of diesel engine show that the biodiesel produced from rubber seed oil via calcined waste rubber seed shell as catalyst could be used in the modern diesel engines without technical modifications.

REFERENCES

Abassi, A., Khalilarya, Sh., & Jafarmadar, S. (2010). The influence of the inlet charge temperature on the second law balance under the various operating engine speed in DI diesel engine. *Fuel*, *89*, 2425–2432.

Abdulkadir, B.A., Danbature, W., Yirankinyuki, F.Y., Magaji, B., & Muzakkir, M. M. (2014). Insitu transesterification of rubber seeds (Hevea brasiliensis). *Greener Journal of Physical Sciences*, *4* (3), 038–044.

Abila, N. (2012). Biofuels development and adoption in Nigeria: Synthesis of drivers, incentives and enablers. *Energy Policy*, *43*, 387–395.

Ahmad, J., Yusup, S., Bokhari, A., & Kamil, R. N. M. (2014a). Biodiesel production from the high free fatty acid "Hevea brasiliensis" and fuel properties characterization. *Applied Mechanics and Materials*, *625*, 897–900.

Ahmad, J., Yusup, S., Bokhari, A., & Kamil, R. N. M. (2014b). Study of fuel properties of rubber seed oil based biodiesel. *Energy Conversion and Management*, *78*, 266–275.

Ahmad, J., Bokhari, A., & Yusup, S. (2014c). Optimization and parametric study of free fatty acid (FFA) reduction from rubber seed oil (RSO) by using response surface methodology (RSM). *Australian Journal of Basic and Applied Sciences*, *8*(5), 299–303.

Ahmad, M., Teong, L.K., Zafar, M., Sultana, S., Sadia, H., & Khan, M. A. (2013). *Prospects and potential of green fuel from some non-traditional seed oils used as biodiesel. In: Z. Fang (Ed.),*. (Zheng fang, Ed.). https://doi.org/10.5772/52031

Aigbodion, A.I., & Pillai, C. K. S. (2000). Preparation, analysis and applications of rubber seed oil and its derivatives in surface coatings. *Progress in Organic Coatings*, *38*, 187–192.

Ajiwe, V.I.E., Okeke, C.A., & Agbo, H. U. (1995). Extraction and utilization of *Afzelia africana* seed oil. *Bioresource Technology*, *53*, 89–90.

Aldhaidhawi, M., Chirac, R., & Badescu, V. (2017). Ignition delay, combustion and emission

characteristics of diesel engine fueled with rapeseed biodiesel-A literature review. *Renewable and Sustainable Energy Reviews*, *73*, 178–186.

Ali, M., & Watson, I. A. (2014). Comparison of oil extraction methods, energy analysis and biodiesel production from flax seeds. *International Journal of Energy Research*, *38*, 614–625.

Alkida, A. C. (1988). The application of availability and energy balances to a diesel engine. *Journal of Engineering for Gas Turbines and Power*, *110* (3), 462–469.

Amigun, B., Musango, J.K., & Stafford, W. (2011). Biofuels and sustainability in Africa. *Renewable and Sustainable Energy Reviews*, *15*, 1360–1372.

Amigun, B., Sigamoney, R., & Blottnitz, H. von. (2008). Commercialization of biofuel industry in Africa: a review. *Renewable and Sustainable Energy Reviews*, *12*, 690–711.

Anastopoulos, G., Zannikou, Y., Stournas, S., & Kalligeros, S. (2009). Transesterification of vegetable oils with ethanol and characterization of the key fuel properties of ethyl esters. *Energies*, *2*, 362–376.

Aniamaka, E.E., & Uriah, O. B. C. (1990). Collection of preparation of rubber (Hevea brasiliensis) seeds for seedling production In: Proceedings of a National Workshop on Fruit/tree production. (p. 75–79.). NAERLS Zaria, Nigeria.

Antczak, M.S., Kabiak, A., Antczak, T., & Bielecki, S. (2009). Enzymatic biodiesel synthesis-Key factors affecting efficiency of the process. *Renewable Energy*, *34* (5), 1185–1194.

Aransiola, E.F., Ojumu, T.V., Oyekola, O.O., Madzimbamuto, T.F. & Ikhu-Omoregbe, D. I. O. (2014). A review of current technology for biodiesel production: State of the art. *Biomass and Bioenergy*, *61*, 276–297.

Aravind, A., Joy, M.L., & Nair, K. P. (2015). Lubricant properties of biodegradable rubber tree seed (Hevea brasiliensis Muell. Arg) oil. *Industrial Crops and Products*, *74*, 14–19.

Ashraful, A.M., Masjuki, H.H., Kalam, M.A., Rizwanul Fattah, I.M., Imtenan, S., Shahir, S.

A., & & Mobarak, H. M. (2014). Production and comparison of fuel properties, engine performance and emission characteristics of biodiesel from various non-edible vegetable oils: a review. *Energy Conversion and Management*, *80*, 202–228.

Association of Official Analytical Chemists. (1990). *AOAC. Official methods of analysis, 15th ed.*, (15th ed.). Washington D.C.

Asuquo, J.E., Anusiem, A.C.I., & Etim, E. E. (2012). Extraction and characterization of rubber seed oil. *International Journal of Modern Chemistry*, *1* (3), 109–115.

Atabani, A.E., Silitonga, A.S., Ong, H.C., Mahlia, T.M.I., Masjuki, H.H., Badruddin, I.A., & Fayaz, H. (2013). Non-edible vegetable oils: A critical evaluation of oil extraction, fatty acid compositions, biodiesel production, characteristics, engine performance and emissions production. *Renewable and Sustainable Energy Reviews*, *18*, 211–245.

Awolu, O.O., & Layokun, S. K. (2013). Optimization of two-step transesterification production of biodiesel from neem (Azadirachta indica) oil. *International Journal of Energy and Environment Engineering*, *4* (39), 1–9.

Aylmore, L. A. G. (1974). Hysteresis in gas sorption isotherms. *Journal of Colloid and Interface Science*, *46* (3), 410–416.

Azoumah, Y., Blin, J., & Daho, T. (2009). Exergy efficiency applied for the performance optimization of a direct injection compression ignition (CI) engine using biofuels. *Renewable Energy*, *34*, 1494–1500.

Bakare, I.O., Pavithran, C., Okieimen, F.E., & Pillai, C. K. . (2006). Polyesters from renewable resources: preparation and characterization. *Journal of Applied Polymer Science*, *100*, 3748–3755.

Banković-Ilić, I.B., Stamenković, O.S., & Veljković, V. B. (2012). Biodiesel production from non-edible plant oils. *Renewable and Sustainable Energy Reviews*, *16*, 3621–3647.

Baş, D., & Boyaci, I. H. (2007a). Modeling and optimization II: comparison of estimation

capabilities of response surface methodology with artificial neural networks in a biochemical reaction. *Journal of Food Engineering*, *78* (3), 846–854.

Baş, D., & Boyaci, I. H. (2007b). Modeling and optimization I: usability of response surface methodology. *Journal of Food Engineering*, *78* (3), 836–845.

Bayindir, H., Işik, M.Z., Argunhan, Z., Yücel, H.L., & Aydin, H. (2017). Combustion, performance and emissions of a diesel power generator fueled with biodiesel-kerosene and biodiesel-kerosene-diesel blends. *Energy*, *123*, 241–251.

Bayraktar, H. (2005). Experimental and theoretical investigation of using gasoline-ethanol blends in spark-ignition engines. *Renewable Energy*, *30*, 1733–1747.

Betiku, E., & Ajala, S. O. (2014). Modeling and optimization of Thevetia peruviana (yellow oleander) oil biodiesel synthesis via Musa paradisiacal (plantain) peels as heterogeneous base catalyst: A case of artificial neural network vs. response surface methodology. *Industrial Crops and Products*, *53*, 314–322.

Bhuiya, M.M.K., Rasul, M.G., Khan, M.M.K., Ashwath, N., Azad, A.K., & Mofijur, M. (2015). Optimization of oil extraction process from Australian native beauty leaf seed (Calophyllum inophyllum). *Energy Procedia*, *75*, 56–61.

Bohre, A. (2013). *Immobolization of radioactive waste in ceramic-based hosts: Radioactive waste immobolization*. Hamburg: Anchor Academic Publishers.

Bokhari, A., Yusup, S., & Ahmad, M. M. (2012). Optimization of the parameters that affects the solvent extraction of crude rubber seed oil using response surface methodology (RSM). In C. C. L. Dmitriev A. (Ed.), *Recent Advance in Engineering* (pp. 28–30). Paris: WSEAS.

Bokhari, A., Yusup, S., Kamil, R.N.M., & Ahmad, J. (2014). Blending study of palm oil methyl esters with rubber seed oil to improve biodiesel blending properties. *Chemical Engineering Transactions*, *37*, 571–576.

Bora, M.M., Gogoi, P., Deka, D.C., & Kakati, D. K. (2014). Synthesis and characterization of yellow oleander (Thevetia peruviana) seed oil-based alkyd resin. *Industrial Crops and Products*, *52*, 721–728.

Boro, J., Deka, D., & Thakur, A. J. (2012). A review on solid oxide derived from waste shells as catalyst for biodiesel production. *Renewable and Sustainable Energy Reviews*, *16*, 904– 910.

Borugadda, V.B., & Goud, V. V. (2013). Comparative studies of thermal, oxidative and low temperature properties of waste cooking oil and castor oil. *Journal of Renewable and Sustainable Energy*, *5* (63104), 1–15.

Botella, L., Bimbela, F., Martin, L., Arauzo, J., & Sánchez, J. L. (2014). Oxidation stability of biodiesel fuels and blends using the Rancimat and PetroOXY methods. Effect of 4-allyl-2, 6-dimethoxyphenol and catechol as biodiesel additives on oxidation stability. *Frontiers in Chemistry*, *2* (43), 1–9.

Caton, J. A. (2000). On the destruction of availability (exergy) due to combustion processes-with specific application to internal combustion engines. *Energy*, *25*, 1097–1117.

Celikten, I., Mutlu, E., & Solmaz, H. (2012). Variation of performance and emission characteristics of a diesel engine fueled with diesel, rapeseed oil and hazelnut oil methyl ester blends. *Renewable Energy*, *48*, 122–126.

Çengel, Y.A., & Boles, M. A. (1994). *Thermodynamics: an engineering approach* (2nd ed.). New York: McGraw-Hill, Inc.

Cerino Córdova, F.J., Garcia León, A.M., Garcia Reyes, R.B., Garza González, M.T., Soto Regalado, E., Sánchez González, M.N., & Quezada López, I. (2011). Response surface methodology for lead biosorption on Aspergillus terreus. *International Journal Environmental Science Technology*, *8* (4), 695–704.

Ceylan, S., & Goldfarb, J. L. (2015). Green tide to green fuels: TG-FTIR analysis and kinetic

study of Ulva prolifera pyrolysis. *Energy Conversion and Management*, *101*, 263–270.

Charles, S. (2002). Noble obsession, Charles Goodyear, Thomas Hancock, and the race to unlock the greatest industrial secret of the 19th century. *Hyperion*.

Choe, E., & Min, D. B. (2007). Chemistry of deep-fat frying oils. *Journal of Food Science*, *72* (5), 77–86.

Christmann, K. (2012). Thermodynamics and Kinetics of Adsorption. Institut für Chemie und Biochemie. *IMPRS-Lecture Series*, 1–58.

Chuahy, F.D.F., & Kokjohn, S. L. (2017). High efficiency dual-fuel combustion through thermochemical recovery and diesel reforming. *Applied Energy*, *195*, 503–522.

Claude, V., Courson, C., Köhler, M., & Lambert, S. D. (2016). Overview and essentials of biomass gasification technologies and their catalytic cleaning methods. *Energy & Fuels*, *30* (11), 8791–8814.

Coats, A.W., & Redfen, J. P. (1963). Thermogravimetric analysis: A review. *Analyst*, *88* (1053), 906–924.

Cullity, B. D. (1978). *Elements of X-ray Diffraction* (2nd ed.). Reading, Massachusetts: Addison-Wesley Publishing Company Inc.

D'Cruz, A., Kulkarni, M.G., Meher, L.C., & Dalai, A. K. (2007). Synthesis of biodiesel from canola oil using heterogeneous base catalyst. *Journal of American Chemists' Society*, *84* (10), 937–943.

De Boer, J.H., Lippens, B.C., Lisen, B.G., Broekhoff, J.C.P., van den Heuvel, A., & Osinga, T. J. (1966). The t-curve of multimolecular N_2-adosorption. *Journal of Colloid and Interface Science*, *21*, 405–414.

Demirbaş, A. (2009). Political, economic and environmental impacts of biofuels: A review. *Applied Energy*, *86*, S108–S117.

Demirbaş, A. (1998). Fuel properties and calculation of higher heating values of vegetable oils.

Fuel, *77* (9/10), 1117–1120.

Demirbaş, M.F., Balat, M., & Balat, H. (2009). Potential contribution of biomass to the sustainable energy development. *Energy Conversion and Management, 50, 1746*–1760.

Desjardins R. (1997). *Water treatment.* Editions of University of Montreal, Canada: Presses inter Polytechnique.

Dharma, S., Masjuki, H.H., Ong, H.C., Sebayang, A.H., Silitonga, A.S., & Kusumo, F. (2016). Optimization of biodiesel production process for mixed Jatropha *curcas*–Ceiba pentandra biodiesel using response surface methodology. *Energy Conversion and Management*, 178–190.

Dhawane, S.H., Kumar, T., & Halder, G. (2015). Central composite design approach towards optimization of flamboyant pods derived steam activated carbon for its use as heterogeneous catalyst in transesterification of Hevea brasiliensis oil. *Energy Conversion and Management*, *100*, 277–287.

Dhawane, S.H., Kumar, T., & Halder, G. (2016). Parametric effects and optimization on synthesis of Iron (II) doped carbonaceous catalyst for the production of biodiesel. *Energy Conversion and Management*, *122*, 310–320.

Di Serio, M., Tesser, R., Pengmei, L., & Santacesaria, E. (2008). Heterogeneous catalysts for biodiesel production. *Energy & Fuels*, *22* (1), 207–217.

Dizge, N. & Keskinler, B. (2008). Enzymatic production of biodiesel from canola oil using immobilized lipase. *Biomass and Bioenergy*, *32* (12), 1274–1278.

Dwivedi, G., Jain, S., & Sharma, M. P. (2013). Diesel engine performance and emission analysis using biodiesel from various oil sources-reviews. *Journal of Materials and Environmental Science*, *4* (4), 434–447.

Dwivedi, G., & Sharma, M. P. (2015). Application of Box-Behnken design in optimization of biodiesel yield from Pongamia oil and its stability analysis. *Fuel*, *145*, 256–262.

Ebewele, R.O., Iyayi, A.F., & Hymore, F. K. (2010a). Considerations of the extraction process and potential technical applications of Nigerian rubber seed oil. *International Journal of Physical Sciences, 5* (6), 826–831.

Ebewele, R.O., Iyayi, A.F., & Hymore, F.K. (2010b). Deacidification of high acidic rubber seed oil by re-esterification with glycerol. *International Journal of Physical Sciences, 5* (6), 841–846.

Eka, H.D., Tajul Aris, Y., & Wan Nadiah, W. A. (2010). Potential use of Malaysia rubber (Hevea brasiliensis) seed as food, feed and biofuel. *International Food Research Journal*, *17*, 527–534.

El-Seesy, A.I., Abdel-Rahman, A.K., Bady, M., & Ookawara, S. (2017). Performance, combustion, and emission characteristics of a diesel engine fueled by biodiesel-diesel mixtures with multi-walled carbon nanotubes additives. *Energy Conversion and Management*, *135*, 373–393.

Elango, T., & Senthilkumar, T. (2011). Performance and emission characteristics of CI engine fuelled with non-edible vegetable oil and diesel blends. *Journal of Engineering Science and Technology*, *6* (2), 240–250.

Elkhaleefa, A., & Shigidi, I. (2015). Optimization of sesame oil extraction process conditions. *Advances in Chemical Engineering Science*, *5*, 305–310.

Encinar, J.M., Susan, F., Gonzalez, J.F., & Rodriguez-Reinares, A. (2007). Ethanolysis of used frying oils: Biodiesel preparation and characterization. *Fuel Processing Technology*, *88* (5), 513–522.

Felizardo, P., Correia, M.J.N., Raposo, I., Mendes, J.F., Berkemeier, R., & Bordado, J. M. (2006). Production of biodiesel from waste frying oil. *Waste Management*, *26*, 487–494.

Fillières, R., Benjelloun-Mlayal, B., & Delmas, M. (1995). Ethanolysis of rapeseed oil:

Quantitation of ethyl esters, mono-, di-, and triglycerides and glycerol by high-performance size-exclusion chromatography. *Journal of American Oil Chemists' Society*, *72*(4), 427–432.

Fogler, H. S. (2008). *Elements of Chemical Reaction Engineering* (4th ed.). singapore: John Wiley & Sons (Asia).

Food and Agriculture Organization of the United Nations (2014). Natural rubber plantation areas harvested (hectares) for all countries. http://www.factfish.com/catalog/crop%3E [accessed 18.05.15].

Freedman, B., Butterfield, R.O., & Pryde, E. H. (1986). Transesterification kinetics of soybean oil. *Journal of American Oil Chemists' Society*, *63*, 1375–1380.

Gan, M., Pan, D., Ma, L., Yue, E., & Hong, J. (2009). The kinetics of the esterification of free fatty acids in waste cooking oil using Fe2 (SO4)3/C catalyst. *Chinese Journal of Chemical Engineering*, *17* (1), 83–87.

Geo, V.E., Nagarajan, G., & Nagalingam, B. (2010). Studies on improving the performance of rubber seed oil fuel for diesel engine with DEE port injection. *Fuel*, *89*, 3559–3567.

Geo, V.E., Nagarajan, G., Kamalakannan, J., & Nagalingam, B. (2009). Experimental investigations to study the characteristics of rubber-seed-oil-fueled diesel engine supplemented with diethyl ether. *Energy & Fuels*, *23*, 533–538.

Gimbun, J., Ali, S., Kanwal, C.C.S.C., Shah, L.A., Gazali, N.H.M., Cheng, C.K., & Nurdin, S. (2012). Biodiesel production from rubber seed oil using a limestone based catalyst. *Advances in Materials Physics and Chemistry*, *2* (4), 138–141.

Gog, A., Roman, M., Toşa, M., Paizs, C., & Irimie, F. . (2012). Biodiesel production using enzymatic transesterification-Current state and perspectives. *Renewable Energy*, *39* (1), 10–16.

Gouveia de Souza, A., Oliveira Santos, J.C., Conceiçáo, M.M., Dantas Silva, M.C., & Prasad,

S. (2004). A thermoanalytic and kinetic study of sunflower oil. *Brazilian Journal of Chemical Engineering*, *21* (2), 265–273.

Guardiola, C., Martín, J., Pla. B., & Bares, P. (2017). Cycle by cycle NOx model for diesel engine control. *Applied Thermal Engineering*, *110*, 1011–1020.

Gueguim Kana, E.B., Oloke, J.K., Lateef, A., & Adesiyan, M. O. (2012). Modeling and optimization of biogas production on saw dust and other co-substrates using Artificial Neural network and Genetic Algorithm. *Renewable Energy*, *46*, 276–281.

Guillèn, M.D., & Cabo, N. (2002). Fourier transform infrared spectra data versus peroxide and anisidine values to determine oxidative stability of edible oils. *Food Chemistry*, *77*, 503–510.

Guillèn, M.D., & Ruiz, A. (2003). ^{1}H nuclear magnetic resonance as a fast tool for determing the composition of acyl chains in acylglycerol mixtures. *European Journal of Lipid Science and Technology*, *105*, 502–507.

Guo, F., & Fang, Z. (2011). Biodiesel production with solid catalyst, Biodiesel-feedstocks and processing technologies, In: M. Stoytcheva (Ed.), ISBN: 978-953-307-713-0, InTech. www.intechopen.com/books/biodiesel-feedstocks-and-processing-technologies/biodiesel-production-with-solid. In M. Stoytcheva (Ed.).

Guo, F., Peng, Z.-G., Dai, J.-Y., & Xiu, Z.-L. (2010). Calcined sodium silicate as solid base catalyst for biodiesel production. *Fuel Processing Technology*, *9*, 322–328.

Hago, W., & Morin, A. (2010). An internal combustion engine with CO2 capture. *Efficient Hydrogen Motors*, 7–9.

Harris, L. B. (1969). Adsorption of a patchwise heterogeneous surface II. Heats of adsorption from the condensation approximation. *Surface Science*, *13*, 377–392.

Hassan, S.N.A.M., Ishak, M.A.M., Ismail, K., Ali, S.N., & Yusop, M. F. (2014). Comparison study of rubber seed shell and kernel (*Hevea brasiliensis*) as raw material for bio-oil

production. *Energy Procedia*, *52*, 610–617.

Heywood, J. B. (1988). *Internal Combustion Engine Fundamentals* (Int. ed.). New York: McGraw-Hill Book Company.

Hincapie, G.M., Valange, S., Barrault, J., Moreno, J.A., & Lopez, D. P. (2014). Effect of microwave assisted system on transesterification of castor oil with ethanol. *Universitas Scientiarum*, *19* (3), 193–200.

Hosamani, K.M., & Katagi, K. S. (2008). Characterization and structure elucidation of 12-hydroxyoctadec-cis-9-enoic acid in Jatropha gossypifolia and Hevea brasiliensis seed oils: a rich source of hydroxy fatty acid. *Chemistry and Physics of Lipids*, *152*, 9–12.

Hosmani, S. S. (2014). *Introduction to Surface Alloying of Metals*. new york: Springer Science & Business.

Hrušovský, I., Martinka, J., & Chrebet, T. (2013). Evaluation of thermal oxidation of vegetable oils by means of safety calorimeter SEDEX. *European Journal of Environmental and Safety Sciences*, *1* (1), 13–17.

Ibrahim, A.M., & Pillai, B. C. (2011). Optimization of process parameters for biodiesel extraction from rubber seed oil using central composite design. *International Journal of Production and Management Research*, *2* (1), 23–31.

Ibrahim, A. (2016). Investigating the effect of using diethyl ether as a fuel additive on diesel engine performance and combustion. *Applied Thermal Engineering*, *107*, 853–862.

Igeleke, C.L., & Omorusi, V. I. (2007). Review of post-harvest deterioration of rubber Seeds. *Journal of Agriculture and Social Research*, *7* (2), 11–19.

Ishola, M.M., Brandberg, T., Sanni, S.A., & Taherzadeh, M. J. (2013). Biofuels in Nigeria: A critical and strategic evaluation. *Renewable Energy*, *55*, 554–560.

Islam, M.A., Auta, M., Kabir, G. & Hameed, B. . (2016). A thermogravimetric analysis of the combustion kinetics of karanja (Pongamia pinnata) fruit hulls char. *Bioresource*

Technology, *200*, 335–341.

Ismail, A., Van de Voort, F., Emo, G., & Sedman, J. (1993). Rapid quantitative determination of free fatty acids in fats and oils by Fourier transform infrared spectroscopy. *Journal of American Oil Chemists' Society*, *70* (4), 335−341.

Issariyakul, T., & Dalai, A. K. (2014). Biodiesel from vegetable oils. *Renewable and Sustainable Energy Reviews*, *31*, 446−471.

Iyayi, A.F., Akpaka, P.O., & Ukpeoyibo, U. (2008). Rubber seed processing for value-added latex production in Nigeria. *African Journal of Agricultural Research*, *3* (7), 505–509.

Iyer, K.P.D., & Kunji, A. S. (1992). Extension of Harkins-Jura adsorption isotherm to solute adsorption. *Colloids and Surfaces*, *63*, 235–240.

Jaya, N., & Ethirajulu, K. (2011). Kinetic studies of heterogeneously catalyzed transesterification of cottonseed oil to biodiesel. *Journal of Environmental Research and Development*, *5* (3A), 689–695.

Karger, B.L., Synder, L.R., & Horvath, C. (1973). *An Introduction to Separation Science* (1st ed.). new york: John Wiley and Sons, New York.

Kawashima, A., Matsubara, K., & Honda, K. (2008). Development of heterogeneous base catalysts for biodiesel production. *Bioresource Technology*, *99*, 3439–3443.

Khan, F. A. (2014). *Biotechnology in Medical: Sciences*. Boca Raton: CRC Press.

Kim, S.J., Kim, M.Y., Jeong, S.T., Jang, M.S., & Chung, I. M. (2012). Analysis of the biomass content of various Miscanthus genotypes for biofuel production in Korea. *Industrial Crops and Products*, *38*, 46–49.

Kings, A.J., Raj, R.E., Miriam, L.M.M., & Visvanathan, M. A. (2017). Cultivation, extraction and optimization of biodiesel production from potential microalgae Euglena sanguinea using eco-friendly natural catalyst. *Energy Conversion and Management*, *141*, 224–235.

Kittigowittana, K., Wongsakul, S., Krisdaphong, P., Jimtaisong, A., & Saewan, N. (2013). Fatty acid composition and biological activities of seed oil from rubber cultivar RRIM 600 (*Hevea brasiliensis*). *International Journal of Applied Research in Natural Products*, *6* (2), 1–7.

Knothe, G. (1999). Rapid monitoring of transesterification and assessing biodiesel fuel quality by near-infrared spectroscopy using a fiber-optic probe. *Journal of American Oil Chemists' Society*, *76* (7), 795–800.

Koh, M.Y., & Mohd. Ghazi, T. I. (2011). A review of biodiesel production from Jatropha curcas L. oil. *Renewable and Sustainable Energy Reviews*, *15* (5), 2240–2251.

Kostić, M.D., Joković, N.M., Stamenković, O.S., Rajković, K.M., Milić, P.S., & Veljković, V. B. (2013). Optimization of hampseed oil extraction by n-hexane. *Industrial Crops and Products*, *48*, 133–143.

Kostić, M.D., Veličković, A.V., Joković, N.M., Stamenković, O.S., & Veljković, V. B. (2016). Optimization and kinetic modeling of esterification of the oil obtained from waste plum stones as a pretreatment step in biodiesel production. *Waste Management*, *48*, 619–629.

Krishnakumar, U., Sivasubramanian, V., & Selvaraju, N. (2013). Physico-chemical properties of the biodiesel extracted from rubber seed oil using solid metal oxide catalysts. *International Journal of Engineering Research and Applications*, *3* (4), 2206–2209.

Kumar, A., & Sharma, S. (2011). Potential non-edible oil resources as biodiesel feedstock: An Indian perspective. *Renewable and Sustainable Energy Reviews*, *15*, 1791–1800.

Kumar, A., Jones, D.D., & Hanna, M. . (2009). Thermochemical biomass gasification: A review of the current status of the technology. *Energies*, *2* (3), 556–581.

Kumar, S.S., & Purushothaman, K. (2010). High FFA rubber seed oil as an alternative fuel for diesel engine-an overview. *International Journal of Engineering and Science*, *10* (1), 16–24.

Labeckas, G., & Slavinskas, S. (2006). Performance of direct-injection off-road diesel engine on rapeseed oil. *Renewable Energy*, *31*, 849–863.

Lee, A., Chaibakhsh, N., Rahman, M.B.A., Basri, M., & Tejo, B. A. (2010). Optimized enzymatic synthesis of levulinate ester in solvent-free system. *Industrial Crops and Products*, *32*, 246–251.

Levenspiel, O. (2005). *Chemical Reaction Engineering (4th ed.)*. New Delhi: Prentice-Hall of India, New Delhi.

Li, .H, Pordesimo, L.O., Weiss, J., & Wilhelm, L. R. (2004). Microwave and ultrasound assisted extraction of soybean oil. *Transactions of the ASAE, 47* (4), 1187–1194.

Li, J., Zu, Y.-G., Luo, M., Gu, C.-B., Zhao, C.-J., Efferth, T., & Fu, Y.-J. (2013). Aqueous enzymatic process assisted by microwave extraction of oil from yellow horn (*Xanthoceras sorbifolia* Bunge) seed kernels and its quality evaluation. *Food Chemistry*, *138*, 2152–2158.

Li, X.R., Zhou, H., Su, L., Chen, Y., Qiao, Z., & Liu, F. (2016). Combustion and emission characteristics of a lateral swirl combustion system for DI diesel engines under low excess air ratio conditions. *Fuel, 84*, 672–680.

Lior, N., & Ruddy, G. J. (1988). Second law analysis of an ideal Otto cycle. *Energy Conversion and Management, 28* (4), 327–334.

Liu, X.J., He, H., Wang, Y.J., Zhu, S.L., & Piao, X. (2008). Transesterification of soybean oil to biodiesel using CaO as a solid base catalyst. *Fuel*, *87*, 216–221.

Lowell, S., Shields, E., Thomas, M., & Thommes, M. (2004). *Characterization of Porous Materials and Powders: Surface Area, Pore size and Density* (1st ed.). Norwell: Kluwer Academic Publishers.

Ma, F., & Hanna, M. A. (1999). Biodiesel production: a review. *Bioresource Technology*, *70*, 1–15.

Ma, L., Lv, E., Du, L., Lu, J., & Ding, J. (2016). Statistical modeling/optimization and process intensification of microwave-assisted acidified oil esterification. *Energy Conversion and Management*, *122*, 411–418.

Madani, M. (2004). *Contribution to the study of the adsorption of imazethapyr and catalyzed photodegradation of imazethapyr and diuron*. *PhD* Thesis, University Mohammed V. Faculty of Sciences, Rabat (Morocco).

Malik, U.S., Ahmed, M., Sombilla, M.A., & Cueno, S. L. (2009). Biofuels production for smallholder producers in the greater Mekong sub-region. *Applied Energy*, *86*, S58–68.

Man, Y. C., & Setiowaty, G. (1999). Determinations of anisidine value in thermally oxidized palm olein by Fourier transform infrared spectroscopy. *Journal of American Oil Chemists' Society*, *76* (2), 243−247.

Marchetti, J.M., & Errazu, A. F. (2008). Esterification of free fatty acids using sulfuric acid as catalyst in the presence of triglycerides. *Biomass and Bioenergy*, *32* (9), 892−895.

Mazumdar, P., Borugadda, V.B., Goud, V.V., & Sahoo, L. (2012). Physico-chemical characteristics of Jatropha *curcas* L. of North East India for exploration of biodiesel. *Biomass Bioenergy*, *46*, 546−554.

Mechrafi, E. (2002). *Adsorption, desorption and mobility of herbicides in contact with organic and inorganic adsorbents. PhD Thesis*. University Mohammed V, Faculty of Sciences, Rabat (Morocco).

Meisami, F., Ajam, H., & Tabasizadeh, M. (2017). Thermo-economic analysis of diesel engine fueled with blended levels of waste cooking oil biodiesel in diesel engine. *Biofuels*, 1–10. doi:10.1080/17597269.2017.1284475.

Menkiti, M.C., Agu, C.M., & Udeigwe, T. K. (2015). Extraction of oil from Terminalia catappa L.: Process parameter impacts, kinetics, and thermodynamics. *Industrial Crops and Products*, *77*, 713–723.

Misra, D. N. (1969). Adsorption on heterogeneous surfaces: A Dubinin-Radushkevich equation. *Surface Science*, *18* (2), 367–372.

Mitropoulos, A. C. (2008). The Kelvin equation. *Journal of Colloid and Interface Science*, *317*, 643–648.

Modi, M.K., Reddy, J.R.C., Rao, B.V.S.K., & Prasad, R. B. N. (2007). Lipase-mediated conversion of vegetable oils into biodiesel using ethyl acetate as acyl acceptor. *Bioresource Technology*, *98* (6), 1260–1264.

Mofijur, M., Masjuki, H.H., Kalam, M.A., Atabani, A.E., Arbab, M.I., Cheng, S.F., & G., & S.W. (2014). Properties and use of moringa oleifera biodiesel and diesel fuel blends in a multi cylinder diesel engine. *Energy Conversion and Management*, *82*, 169–176.

Mohsin, R., Majid, Z.A., Shihnan, A.H., Nasri, N.S., & Sharer, Z. (2014). Effect of biodiesel blends on engine performance and exhaust emission for diesel dual fuel engine. *Energy Conversion and Management*, *88.*, 821–828.

Molintas, H., & Gupta, A. K. (2011). Kinetic study for the reduction of residual char particles using oxygen and air. *Applied Energy*, *88* (1), 306–315.

Morshed, M., Ferdous, K., Khan, M.R., Mazumder, M.S.I., Islam, M.A., & Uddin, M. T. (2011). Rubber seed oil as a potential source for biodiesel production in Bangladesh. *Fuel*, *90*, 2981–2986.

Murga, R., Ruiz, R., Beltrán, S., & Cabezas, J. L. (2000). Extraction of natural complex phenols and tannins from grape seeds by using supercritical mixtures of carbondioxide and alcohol. *Journal of Agriculture and Food Chemistry*, *48*, 3408–3412.

Murillo, S., Miguez, J.L., Porteiro, J., Granada, E., & Morán, J. C. (2007). Performance and exhaust emissions in the use of biodiesel in outboard diesel engines. *Fuel*, *86*, 1765–1771.

Ng, W.P.Q., Lam, H.L., & Yusup, S. (2013). Supply network synthesis on rubber seed oil

utilisation as potential biofuel feedstock. *Energy*, *55*, 82–88.

Nguyen, C., & Do, D. D. (2001). The Dubinin-Radushkevich equation and the underlying microscopic adsorption description. *Carbon*, *39*, 1327–1336.

NIS (1992). *Nigerian Industrial Standards. Standards for edible vegetable oils.*

Nisar, J., Razaq, R., Farooq, M., Iqbal, M., Khan, R.A., Sayed, M., Shah, A., & Rahman, I. (2017). Enhanced biodiesel production from Jatropha oil using calcined waste animal bones as catalyst. *Renewable Energy*, *101*, 111–119.

Norazahar, N., Yusup, S., Ahmad, M.M., Abubakar, S., & Ahmad, J. (2012). Parametric optimization of kapok (*Ceiba pentandra*) oil methyl ester production using Taguchi approach. *International Journal of Energy and Environment Engineering*, *6* (6), 541–548.

Noureddini, H., Gao, X., & Philkana, R. S. (2005). Immobilized *pseudomonas cepecia* lipase for biodiesel fuel production from soybean oil. *Bioresource Technology*, *96* (7), 769–777.

Oderinde, R.A., Ajayi, I.A., & Adewuyi, A. (2009). Characterization of seed and seed oil of Hura crepitans and the kinetics of degradation of the oil during heating. *Electronic Journal of Environmental, Agricultural and Food Chemistry*, *8* (3), 201–208.

Ogbu, I.M., & Ajiwe, V. I. E. (2016). FTIR studies of thermal stability of the oils and methyl esters from Afzelia africana and Hura crepitans seeds. *Renewable Energy*, *96*, 203–208.

Ohimain, E. I. (2013). A review of the Nigeria biofuel policy and incentives (2007). *Renewable Energy and Sustainable Energy Review*, *22*, 246–256.

Okieimen, F.E., Okieimen, C.O., & Ojokoh, F. I. (2005a). Rubber seed shell carbon as sequestrant of heavy metals and organic compounds from acqueous solution. *Indian Journal of Chemical Technology*, *12*, 181–186.

Okieimen, F.E., Pavithran, C., & Bakare, I. O. (2005b). Epoxidation and hydroxiation of rubber

seed oil: one-pot multi-step reactions. *European Journal of Lipid Science and Technology, 107*, 330–336.

Olajide, J.O., Igbeka, J.C., Afolabi, T.J., & Emiola, O. A. (2007). Prediction of oil yield from groundnut kernels in an hydraulic press using artificial neural network (ANN). *Journal of Food Engineering, 81* (4), 643–646.

Om Tapanes, N.C., Gomes Aranda, D.A., de Mesquita Varneiro, J.W., & Ceva Antunes, O. A. (2008). Transesterification of jatropha curcas oil glycerides: Theoretical and experimental studies of biodiesel reaction. *Fuel*, *87* (10/11), 2286–2295.

Omo-Ikerodah, E.E., Omokhafe, K.O., Akpobome, F.A., & Mokwunye, M. U. (2009). An overview of the potentials of natural rubber (*Hevea brasiliensis*) engineering for the production of valuable proteins. *African Journal of Biotechnology*, *8* (25), 7303–7307.

Omorogbe, S.O., Ikhuoria, E.U., Aigbodion, A.I., Obazee, E.O., & Momodu, V. M. (2013). Production of rubber seed oil based biodiesel using different catalysis. *Current Research in Chemistry*, *5* (1), 11–18.

Onoji, S.E., Iyuke, S.E., Igbafe, A.I., & Nkazi, D. B. (2016a). Rubber seed oil: A potential renewable source of biodiesel for sustainable development in sub-Saharan Africa. *Energy Conversion and Management*, *110*, 125–134.

Onoji, S.E., Iyuke, S.E., & Igbafe, A. I. (2016b). *Hevea brasiliensis* (Rubber seed) oil: Extraction, characterization, and kinetics of thermo-oxidative degradation using classical chemical methods. *Energy & Fuels*, *30* (12), 10555–10567.

Onoji, S.E., Iyuke, S.E., Igbafe, A.I., & Daramola, M. O. (2017a). *Hevea brasiliensis* (Rubber seed) oil: Modeling and optimization of extraction process parameters using response surface methodology and artificial neural network techniques. *Biofuels*, 1–11. doi:10.1080/17597269.2017.1338122.

Onoji, S.E., Iyuke, S.E., Igbafe, A.I., & Daramola, M. O. (2017b). Transesterification of rubber

seed oil to biodiesel over a calcined waste rubber seed shell catalyst: Modeling and optimization of process variables. *Energy & Fuels*, *31* (6), 6109–6119.

Oyedeji, F., & Oderinde, R. (2006). Characterization of isopropanol extracted vegetable oils. *Journal of Applied Science*, *6*, 2510–2513.

Özener, O., Yüksek, L., Ergenç, A.T., & Özkan, M. (2014). Effects of soybean biodiesel on a DI diesel engine performance, emission and combustion characteristics. *Fuel*, *115*, 875–883.

Özkan, M. (2015). A comparative study on energy and exergy analyses of a CI engine performed with different multiple injection strategies at port load: Effect of injection pressure. *Entropy*, *17* (1), 244–263.

Ozsezen, A.N., & Canakci, M. (2011). Determination of performance and combustion characteristics of a diesel engine fueled with canola and waste palm oil methyl esters. *Energy Conversion and Management*, *52*, 108–116.

Peduzzi, E., Boissonnet, G., & Maréchal, F. (2016). Biomass modelling: Estimating thermodynamic properties from the elemental composition. *Fuel*, *181*, 201–217.

Piker, A., Tabah, B., Perkas, N., & Gedanken, A. (2016). A green and low-cost room temperature biodiesel production method from waste oil using egg shells as catalyst. *Fuel*, *182*, 34–41.

Polany, M., Smisek, M., & Cerney, S. (1970). Active carbon manufacture, properties and application. *Analytical Chemistry*, *42* (14), 81A–81A.

Portet-Koltalo, F., & Machour, N. (2013). Analytical methodologies for the control of particle phase polycyclic aromatic compounds from diesel engine exhaust. In S. Bari (Ed.), *Diesel engine-combustion, emission and condition monitoring* (p. 91–117.). InTech e-Publishing company. https://doi.org/10.5772/53725

Prabhahar, M., Manohar, R.M., & Sendilvelan, S. (2012). Performance and emission studies

of a diesel engine with pongamia methyl ester at different load conditions. *International Journal of Engineering Research and Applications*, *2* (3), 2707–2713.

Raheman, H., & Ghadge, S. (2008). Performance of diesel engine with biodiesel at varying compression ratio and ignition timing. *Fuel 87, 2659–2666.*

Rahman, S.M.A., Masjuki, H.H., Kalam, M.A., Abedin, M.J., Sanjid, A., & Rahman, M. M. (2014). Assessing idling effects on a compression ignition engine fueled with Jatropha and Palm biodiesel blends. *Renewable Energy*, *68*, 644–650.

Rakopoulos, C.D., & Giakoumis, E. G. (1997). Development of cumulative and availability rate balances in a multi-cylinder turbocharged indirect injection diesel engine. *Energy Conversion and Management*, *38* (4), 347–369.

Rakopoulos, C.D., & Giakoumis, E. G. (2006). Second-law analyses applied to internal combustion engines operation. *Progress in Energy and Combustion Science*, *32* (1), 2–47.

Ramadhas, A.S., Jayaraj, S., & Muraleedharan, C. (2005). Biodiesel production from high FFA rubber seed oil. *Fuel*, *84* (4), 335–340.

Ramadhas, A.S., Muraleedharan, C., & Jayaraj, S. (2005a). Performance and emission evaluation of a diesel engine fueled with methyl esters of rubber seed oil. *Renewable Energy*, *30* (12), 1789–1800.

Ramadhas, A.S., Jayaraj, S., & Muraleedharan, C. (2005b). Characterization and effect of using rubber seed oil as fuel in the compression ignition engines. *Renewable Energy*, *30*, 795–803.

Ramaswamy, H.S., Van De Voort, F.R., & Ghazala, S. (1989). An analysis of TDT and Arrhenius methods for handling process and kinetic data. *Journal of Food Science*, *54* (5), 1322–1326.

Raventós, M., Duarte, S., & Alarcón, R. (2002). Application and possibilities of supercritical

CO_2 extraction in food processing industry: an overview. *Food Science Technology International*, *8*, 269–284.

Reshad, A.S., Tiwari, P., & Goud, V. V. (2015). Extraction of oil from rubber seeds for biodiesel application: Optimization of parameters. *Fuel*, *150*, 636–644.

Rodríguez-Solana, R., Salgado, J.M., Domínguez, J.M., & Cortés-Diéguez, S. (2014). Estragole quantity optimization from fennel seeds by supercritical fluid extraction (carbon dioxide– methanol) using a Box–Behnken design. Characterization of fennel extract. *Industrial Crops and Products Crops and Products*, *60*, 186–192.

Roschat, W., Kacha, M., Yoosuk, B., Sudyoadsuk, T., & Promarak, V. (2012). Biodiesel production based on heterogeneous process catalyzed by solid waste coral fragment. *Fuel*, *98*, 194–202.

Sabarish, C.S., Sebastian, J., & Muraleedharan, C. (2016). Extraction of oil from rubber seed through hydraulic press and kinetic study of acid esterification of rubber seed oil. *Procedia Technology*, *25*, 1006–1013.

Sadowska, J., Johansson, B., Johannessen, E., Friman, R., Broniarz-Press, L., & Rosenholm, J. B. (2008). Characterization of ozonated vegetable oils by spectroscopic and chromatographic methods. *Chemistry and Physics of Lipids*, *151*, 85–91.

Sajjadi, B., Raman, A.A.A., & Arandiyan, H. (2016). A comprehensive review on properties of edible and non-edible vegetable oil-based biodiesel: Composition, specifications and prediction models. *Renewable and Sustainable Energy Reviews*, *63*, 62–92.

Sanjel, N., Gu, J.H., & Oh, S. C. (2014). Transesterification kinetics of waste vegetable oil in supercritical alcohols. *Energies*, *7*, 2095–2106.

Santos, J.C.O., Dos Santos, I.M.G., De Souza, A.G., Prasad, S., & Dos Santos, A. V. (2002). Thermal stability and kinetic study on thermal decomposition of commercial edible oils by thermogravimetry. *Journal of Food Science*, 67 (4), 1393–1398.

Sasmal, S., Goud, V.V, & Mohanty, K. (2012). Characterization of biomass available in the region of North-East India for production of biofuels. *Biomass and Bioenergy*, *45*, 212–220.

Sayyar, S., Abidin, Z.Z., Yunus, R., & Muhammad, A. (2009). Extraction of oil from jatropha seeds-optimization and kinetics. *American Journal of Applied Science*, *6*, 1390–1395.

Schwab, A.W., Bagby, M.O. & Freedman, B. (1987). Preparation and properties of diesel fuels from vegetable oils. *Fuel*, *66*, 1372–1378.

Senthilkumar, S., & Purushothaman, K. (2012). High FFA rubber seed oil as an alternative fuel for diesel engine-An overview. *International Journal of Engineering and Science*, *1* (10), 16–24.

Shanavas, S., Kunji, A.S., Varghese, H.T., & Panicker, C. Y. (2011). Comparison of Langmuir and Harkins-Jura adsorption isotherms for the determination of surface area of solids. *Oriental Journal of Chemistry*, *27* (1), 245–252.

Shokri, A., Hatami, T., & Khamforoush, M. (2011). Near critical carbon dioxide extraction of Anise (*Pimpinella Anisum* L.) seed: Mathematical and artificial neural network modeling. *Journal of Supercritical Fluids*, *58*, 49–57.

Siboni, S., & Volpe, C. D. (2008). Some mathematical aspects of the Kelvin equation. *Computers and Mathematics with Applications*, *55* (1), 51–65.

Singh, J., & Bargale, P. C. (2000). Development of a small capacity double stage compression screw press for oil expression. *Journal of Food Engineering*, *43* (2), 75–82.

Skoog, D.A., Holler, F.J., & Crouch, S. R. (2007). *Principle of Instrumental Analysis* (6th Ed.). Thomson Publishing, USA.

Slopiecka, K., Bartocci, P., & Fantozzi, F. (2012). Thermogravimetric analysis and kinetic study of poplar wood pyrolysis. *Applied Energy*, *97*, 491–497.

Smith, B. C. (2011). *Fundamentals of Fourier Transform Infrared Spectroscopy* (2nd ed.).

Boca Raton: CRC Press.

SON (2000). Standard Organization of Nigeria. Standards for edible refined palm oil and its processed form.

Stepanov, V.S. (1995). Chemical energies and exergies of fuels. *Energy 20* (3), 235–242.

Storck, S., Bretinger, H., & Maier, W. F. (1998). Characterization of micro- and mesoporous solids by physisorption methods and pore-size analysis. *Applied Catalysis A: General*, *174*, 137–146.

Subramaniam, D., Murugesan, A., Avinash, A., & Kumaravel, A. (2013). Bio-diesel production and its engine characteristics: An expatiate view. *Renewable and Sustainable Energy Reviews*, *22*, 361–370.

Subroto, E., Manurung, R., Heeres, H.J., & Broekhuis, A. A. (2015). Optimization of mechanical oil extraction from Jatropha curcas L. kernel using response surface method. *Industrial Crops and Products*, *63*, 294–302.

Sun, K., & Jiang, J. c. (2010). Preparation and characterization of activated carbon from rubber seed shell by physical activation with steam. *Biomass and Bioenergy*, *34*, 539–544.

Syazwani, O.N., Rashid, U., & Yap, Y. H. T. (2015). Low-cost solid catalyst derived from waste Cyrtopleura costata (Angel Wing Shell) for biodiesel production using microalgae oil. *Energy Conversion and Management*, *101*, 749–756.

Takase, M., Zhao, T., Zhang, M., Chen, Y., Liu, H., Yang, L., & Wu, X. (2015). An expatiate review of neem, jatropha, rubber and karanja as multipurpose non-edible biodiesel resources and comparison of their fuel, engine and emission properties. *Renewable and Sustainable Energy Reviews*, *43*, 495–520.

Tang, Z.-X., Clavean, D., Corcuff, R., Belkacemi, K., & Arul, J. (2008). Preparation of nano-CaO using thermal-decomposition method. *Materials Letters*, *62*, 2096–2098.

TecQuipment Ltd. (2011). *TD200 Small Engine Test Set User Guide Manual for TecQuipment*

Test Engines. Nottingham, UK.

Thanh, L.T., Okitsu, K., Boi, L.V., & Maeda, Y. (2012). Catalytic technologies for biodiesel fuel production and utilization of glycerol: a review. *Catalysts*, *2*, 191–222.

Toscano, G., Riva, G., Pedretti, E.F., & Duca, D. (2012). Vegetable oil and fat viscosity forecast models based on iodine number and saponification number. *Biomass Bioenergy*, *46*, 511–516.

UNFCCC (2015). United Nations Framework Convention on Climate Change. Adoption of the Paris Agreement. http://unfccc.int/resource/dos/2015/COP21/eng/109r01.pdf

Ude, C.N., Onukwuli, O.D., Nwobi-Okoye, C., Anisiji, O.E., Atuanya, C.U., & Menkiti, M.C. (2017). Performance evaluation of cottonseed oil methyl esters produced using CaO and prediction with an artificial neural network. *Biofuel*, *1*–8, doi: 10.1080/17597269.2017.1345355.

Uprety, B.K., Chaiwong, W., Ewelike, C., & Rakshit, S. K. (2016). Biodiesel production using heterogeneous catalysts including wood ash and the importance of enhancing byproduct glycerol purity. *Energy Conversion and Management*, *115*, 191–199.

Valente, V.S.B., Vieira, A. dos S., & Teixeira, R. M. (2016). Physicochemical characterization of commercial biodiesel/diesel blends and evaluation of unconventional spectroscopic vibrational techniques in the monitoring of their oxidation and hydrolysis during storage. *Energy & Fuels*, *30*, 8399–8409.

Van Boekel, M. A. J. S. (1996). Statistical aspects of kinetic modeling for food science problems. *Journal of Food Science*, *6* (3), 477–489.

Van Dongen, R.H. & Broekhoff, J. C. P. (1969). The isosteric heat of adsorption on homogeneous and patchwise heterogeneous surfaces. *Surface Science*, *18*, 462–469.

Vasudevan, M., Sakaria, P.L., Bhatt, A.S., Mody, H.M., & Bajaj, H. C. (2011). Effect of concentration of aminopropyl groups on the surface of MCM-41 on adsorption of Cu^{2+}.

Industrial & Engineering Chemistry Research, *50* (19), 11432–11439.

Venkatachalam, P., Geetha, N., Sangeetha, P., & Thulaseedharan, A. (2013). Natural rubber producing plants: An overview. *African Journal of Biotechnology*, *12* (12), 1297–1310.

Verma, P., Sharma, M.P., & Dwivedi, G. (2016). Impact of alcohol on biodiesel production and properties. *Renewable and Sustainable Energy Reviews*, *56*, 319–333.

Vipin, V.C., Sebastian, J., Muraleedharan, C., & Santhiagu, A. (2016). Enzymatic transesterification of rubber seed oil using *rhizopus oryzae* lipase. *Procedia Technology*, *25*, 1014–1021.

Widayat, W., & Kiono, B. F. T. (2012). Ultrasound assisted esterification of rubber seed oil for biodiesel production. *International Journal of Renewable Energy Development*, *1*, 1–5.

Widayat, W., Wibowo, A.D.K., & Hadiyanto (2013). Study on production process of biodiesel from rubber seed (*Hevea brasiliensis*) by in situ (trans) esterification method with acid catalyst. *Energy Procedia*, *32*, 64–73.

Widyarani; Ratnaningsih, E., Sanders, J.P.M., & Bruins, M. E. (2014). Biorefinery methods for separation of protein and oil fractions from rubber seed kernel. *Industrial Crops and Products*, *42*, 323–332.

Willard, H.W., Merritt, Jr., Dean, J.A., & Seattle, J. (1981). *Instrumental Methods of Analysis* ((6th Ed.)). Belmont, CA, USA, Wadsworth Publishing Company.

Willems, P., Kuipers, N.J.M., & De Haan, A. B. (2008). Hydraulic pressing of oilseeds: Experimental determination and modeling of yield and pressing rates. *Journal of Food Engineering*, *89* (1), 8–16.

Wohlgemutgh, N. (1999). Cost benefits indicators associated with the integration of alternative energy sources: a system approach for Carinthia, Austria. *Renewable Energy*, *16*, 1147–1150.

Wu, J. (2004). *Modeling adsorption of organic compounds on activated carbon: A multivariate approach. PhD Thesis*. University of Neuchâtel, Schweiz.

Yang, L., Takase, M., Zhang, M., Zhao, T., & Wu, X. (2014). Potential non-edible oil feedstock for biodiesel production in Africa: A survey. *Renewable and Sustainable Energy Reviews*, *38*, 461–477.

Yuan, X., Liu, J., Zeng, G., Shi, J., Tong, J., & Huang, G. (2008). Optimization of conversion of waste rapeseed oil with high FFA to biodiesel using response surface methodology. *Renewable Energy*, *33* (7), 1678–1684.

Zabeti, M., Daud, W.M.A.W., & Aroua, M. K. (2009). Activity of solid catalysts for biodiesel production: A review. *Fuel Processing Technology*, *90*, 770–777.

Zahedi, G., & Azarpour, A. (2011). Optimization of supercritical carbon dioxide extraction of Passiflora seed oil. *Journal of Supercritical Fluids*, *58*, 40–48.

Zhang, L., Xu, C., & Champagne, P. (2010). Overview of recent advances in thermo-chemical conversion of biomass. *Energy Conversion and Management*, *51*, 969–982.

Zhang, S., Zu, Y.G, Fu, Y.J., Luo, M., Zhang, D.Y., & Efferth, T. (2011). Rapid microwave-assisted transesterification of yellow horn oil to biodiesel using a heteropolyacid solid catalyst. *Bioresource Technology 101* (3), 931–936.

Zheng, Y.L., Wiesenborn, D.P., Tostenson, K., & Kangas, N. (2003). Screw pressing of mode and de-hulled flax seed for organic oil. *Journal of the American Oil Chemists' Society*, *80* (10), 1039–1045.

Zhu, Y., Xu, J., Li, Q., & Mortimer, P. E. (2014). Investigation of rubber seed yield in Xishuangbanna and estimation of rubber seed oil based biodiesel potential in Southeast Asia. *Energy*, *69*, 837–842.

APPENDIX

Appendix A

Energy Conversion and Management 110 (2016) 125–134

Contents lists available at ScienceDirect

Energy Conversion and Management

journal homepage: www.elsevier.com/locate/enconman

Review

Rubber seed oil: A potential renewable source of biodiesel for sustainable development in sub-Saharan Africa

Samuel E. Onoji [a,b,*], Sunny E. Iyuke [a], Anselm I. Igbafe [c], Diakanua B. Nkazi [a]

[a] School of Chemical & Metallurgical Engineering, University of the Witwatersrand, 1 Jan Smuts Avenue, Braamfontein 2050, Private Bag 3, Johannesburg, South Africa
[b] Petroleum and Natural Gas Processing Department, Petroleum Training Institute, PMB 20, Effurun, Nigeria
[c] School of Chemical & Petroleum Engineering, Afe Babalola University, PMB 5454, Ado-Ekiti, Nigeria

ARTICLE INFO

Article history:
Received 11 September 2015
Accepted 2 December 2015

Keywords:
Rubber seed oil
Transesterification
Biodiesel
Sustainable energy
SSA countries

ABSTRACT

The global energy demand is currently met by the use of non-renewable fossil fuels. The challenges of non-availability of these fuels in the future, instability in prices of crude oil and its negative environmental impacts, stimulated researchers in the global community in search of renewable energies for replacement of fossil fuels in future. Biodiesel has been identified as a good complement and plausible replacement of fossil diesel because of the overwhelming characteristic properties similar to fossil diesel in addition to its good lubricity, biodegradability, non-toxicity and eco-friendliness when used in diesel engines. The production of biodiesel from edible vegetable oils competes with food consumption and consequently high cost of food and biodiesel. Studies have shown that rubber seed contains 35–45 wt.% oil which portrays a better competitor to other non-edible oil bearing plants in biodiesel production. Biodiesel produced from non-edible rubber seed oil (RSO) is an attractive option for the sustainable development of sub-Saharan Africa (SSA) countries that depend heavily on fossil diesel. The application of abundant plantain (*Musa paradisiacal*) peels considered as waste in SSA countries as heterogeneous base catalyst in RSO biodiesel production will further reduce the cost of biodiesel. Rubber trees (*Hevea brasiliensis*) are grown domestically in large plantations solely for latex production in most tropical SSA countries and the seeds fall out as waste to the ground either to germinate or are collected and discarded annually. However, SSA countries have an estimated combined capacity of 717,750 ha of rubber trees equivalent to 251 million trees that can generate on annual basis, about 107,662.5 ton of rubber seed, 17,947.339 ton of rubber seed oil and an equivalent 16,691.025 ton of biodiesel. The cultivation of natural rubber trees will sustain the production of rubber products from latex and seed oils for biodiesel which would create additional financial benefits to the plantation farmers and reinvigorates the economies of the local communities in SSA countries.

© 2015 Elsevier Ltd. All rights reserved.

Contents

1. Introduction . . . 126
2. Benefits of biodiesel policies in sub-Saharan Africa . . . 126
3. Rubber seed capacity in SSA . . . 127
   3.1. Industrial applications of rubber seed . . . 127
   3.2. Rubber seed oil extraction methods . . . 128
      3.2.1. Conventional method (mechanical and chemical) . . . 128
      3.2.2. Gas-assisted mechanical expression method . . . 128
      3.2.3. Microwave-assisted method . . . 128
      3.2.4. Ultrasonic-assisted method . . . 128
      3.2.5. Aqueous enzymatic method . . . 128
   3.3. Rubber seed oil production . . . 129

* Corresponding author at: School of Chemical & Metallurgical Engineering, University of the Witwatersrand, 1 Jan Smuts Avenue, Braamfontein 2050, Private Bag 3, Johannesburg, South Africa.
E-mail address: samonoji@yahoo.co.uk (S.E. Onoji).

http://dx.doi.org/10.1016/j.enconman.2015.12.002
0196-8904/© 2015 Elsevier Ltd. All rights reserved.

energy&fuels

Article

pubs.acs.org/EF

Hevea brasiliensis (Rubber Seed) Oil: Extraction, Characterization, and Kinetics of Thermo-oxidative Degradation Using Classical Chemical Methods

Samuel E. Onoji,*[,†,‡] Sunny E. Iyuke,[†,‡] and Anselm I. Igbafe[§]

[†]School of Chemical & Metallurgical Engineering, University of the Witwatersrand, 1 Jan Smuts Avenue, Braamfontein 2050, Private Bag 3, Johannesburg, South Africa

[‡]Petroleum and Natural Gas Processing Department, Petroleum Training Institute, PMB 20, Effurun, Nigeria

[§]School of Chemical & Petroleum Engineering, Afe Babalola University, PMB 5454, Ado-Ekiti, Nigeria

Supporting Information

ABSTRACT: In the present study, nonedible seed oils from underutilized Nigerian NIG800 clonal rubber seeds were extracted using a solvent method to obtain a yield of 43 wt % after extraction for 1 h using a 0.5 mm kernel particle size. The oil was characterized by GC-MS, FT-IR, and NMR analyses, and found to possess several potential industrial applications. The physicochemical properties determined agreed with reported values in the literature. The low ash content (0.001 wt %) indicates the absence of trace metals that catalyze oxidation reactions. The low moisture (1.73 wt %) and carbon residue (0.4 wt %) contents, high volatile matter (97.869 wt %), and low freezing point (−18 °C) properties of the oil indicate a better source material for biodiesel synthesis for use in cold regions compared to other vegetable oils. The higher heating value of 39.37 kJ/kg for the oil is within the range of values reported by researchers for other nonedible vegetable oils. The high content of saturated fatty acids (30.67 wt %) and moderately low monounsaturated fatty acids (69.33 wt %) confer a good shelf life compared to other oils. A closer examination of results of the NMR and GC-MS show a satisfactory agreement that these genetically modified rubber seeds have an insignificant proportion of polyunsaturated fatty acids (linoleic, linolenic, etc.). This insignificant presence of polyunsaturated fatty acids supports higher thermal stability, and slower rate of oxidation of the oil compared to other vegetable oils. The kinetics of thermal oxidative degradation follows a first-order reaction. The activation energy of 13.07 kJ/mol was obtained within the temperature range 100−250 °C.

1. INTRODUCTION

The depletion of fossil materials and the concern for the degraded environment motivated researchers in the global community to search for alternative source routes for energy. Vegetable oils are seen as plausible source materials for renewable energy production.[1] To avert a food-fuel crisis, nonedible vegetable oils, considered as low-grade oils that are not suitable for food uses, could be an attractive preference to edible oils for industrial applications.[2] These nonedible oil plants can be grown in rural, unproductive, and degraded lands, as they are well adapted to a semiarid and low moisture/fertility environment.[3]

Vegetable seed plants are abundant in every region of the world, and over 350 of them have been identified with domestic and industrial uses. One of the few versatile bioenergy crops with nonedible oil that has attracted the attention of researchers in recent times is the rubber tree (*Hevea brasiliensis*). The tree belongs to the plant family *Euphorbiaceae* and the subfamily genus *Hevea*, and is native to the Amazon region of Brazil in South America, but is mainly grown in Southeast Asia countries (90.5%), sub-Saharan Africa (7%), South America (1.5%), and others (1%).[1]

Hevea brasiliensis is economically cultivated for the production of latex as a source of natural rubber for the production of various rubber products in use globally, while the seeds are underutilized.[1,4,5] However, the oil from the underutilized seeds is the second most valuable product after the latex.[6] The combined production capacity of rubber seed oil in the sub-Saharan Africa countries is projected at about 18 kiloton annually.[1] This value is expected to increase substantially with the expansion of rubber plantations to generate nonedible oils that will make up the greatest proportion of renewable raw materials for the chemical industries in the future. Rubber seed oil has several industrial applications, such as biodiesel synthesis,[1,7,8] biolubricant and hydraulics oil formulations,[9,10] linseed oil substitute,[10] oleochemicals production,[11] and cosmetic and pharmaceutical products.[5] Other uses include paint and coating formulations, as semidrying oil,[3] alkyd resin, and polyurethane biocomposites production.[12,13] The reported rubber seed oil (RSO) yield of 35−50 wt % in the literature is high to encourage its extraction and commercialization for industrial uses.[1]

Industrially, several methods are employed for oil extraction, such as mechanical pressing, solvent extraction, enzymatic, aqueous, and their combinations.[1,14,15] Mechanical pressing (batch or continuous) is widely used and well adapted to rural areas with moderate initial and operating costs, but oil yield is low.[16−18] Recent studies revealed solvent extraction using *n*-

Received: September 7, 2016
Revised: November 8, 2016
Published: November 9, 2016

ACS Publications © 2016 American Chemical Society

DOI: 10.1021/acs.energyfuels.6b02267
Energy Fuels 2016, 30, 10555−10567

BIOFUELS, 2017
https://doi.org/10.1080/17597269.2017.1338122

Taylor & Francis
Taylor & Francis Group

Check for updates

Hevea brasiliensis (rubber seed) oil: modeling and optimization of extraction process parameters using response surface methodology and artificial neural network techniques

Samuel Erhigare Onoji [a,b], Sunny E. Iyuke[a,b], Anselm I. Igbafe[c] and Michael O. Daramola[a]

[a]School of Chemical & Metallurgical Engineering, University of the Witwatersrand, 1 Jan Smuts Avenue, Braamfontein 2050, Private Bag 3, Johannesburg, South Africa; [b]Petroleum and Natural Gas Processing Department, Petroleum Training Institute, PMB 20, Effurun, Nigeria; [c]School of Chemical & Petroleum Engineering, Afe Babalola University, PMB 5454, Ado-Ekiti, Nigeria

ABSTRACT

In the present study, results of parametric effects and optimization of extraction of rubber seed oil from under-utilized rubber seeds using response surface methodology (RSM) and artificial neural network (ANN) based on a statistically designed experimentation via the Box–Behnken design (BBD) are reported. A three-level, three-factor BBD was employed using rubber seed powder weight (X_1), solvent volume (X_2) and extraction time (X_3) as process variables. A quadratic polynomial model was obtained to predict oil yield. The RSM model predicted an optimal oil yield of 42.98 wt.% at conditions of X_1 (60 g), X_2 (250 mL) and X_3 (45 min) and validated experimentally as 42.64 wt.%. The ANN model predicted optimal oil yield of 43 wt.% at conditions of X_1 (40 g), X_2 (202 mL) and X_3 (49.99 min) and validated as 42.96 wt.%. Both models are effective in describing the parametric effect of the considered operating variables on the extraction of oil from the rubber seeds. However, the ANN describes the effect more accurately than the RSM model, with a lower percentage relative error and absolute average deviation (AAD). The extracted oil possesses physicochemical properties that support biodiesel production and other industrial applications.

ARTICLE HISTORY
Received 26 September 2016
Accepted 21 April 2017

KEYWORDS
Rubber seed oil extraction; Box–Behnken design; modeling and optimization; response surface methodology; artificial neural network

Introduction

The rubber tree (*Hevea brasiliensis*) which belongs to the plant family Euphorbiaceae and the genus *Hevea* is indigenous to the Amazon basin of Brazil in South America [1]. It is economically cultivated for the production of latex as a source of natural rubber for the production of various rubber products [2,3]. The global harvested area of rubber plantations (according to data available in 2013) is 10,315,732 ha [4]. The sub-Saharan African countries account for about 7%, and the rest is mainly from Southeast Asian countries [1]. *Hevea* exhibits morphological variability, with nine species recognized ranging from large forest trees to little more than shrubs with latex in their parts. The plant possesses the highest potential yield of natural rubber with viable genetic variability [5,6].

The rubber tree is a versatile bioenergy crop with several potential and industrial uses. The oil from the wasted seeds is the second-most valuable product after the latex [7]. The rubber seed weighs 2–6 g, and is about 2–5 cm long and mottled brown in color, with a glossy surface [1,8]. The seeds are enclosed in a pod of three ellipsoidal capsules and contain 40–63 wt.% kernel [1,2,7,9–11], 35–51 wt.% shell [1,2,10,11], and are a source of proteins, fat, carbohydrates and amino acids [1,12,13]. The shell is a potential source of powdered activated carbon and bio-oil [3,14]. When latex and seed production is no longer sustainable due to aging, the trees are felled and used for the production of rubber hardwood as a source of pulp for the paper industry and furniture making, and its sawdust can be pyrolyzed into useful products [3,15].

Recently, researchers classified rubber seed oil (RSO) as a second-generation non-edible vegetable oil. The potentials of the oil as a plausible substitute for edible oils in industrial applications such as production of biodiesel [1,8,11,16,17], semi-drying oil [1,18], paints, coating, printing ink, cosmetic and pharmaceutical products [1,3,18] have been investigated. It could also be used to produce soap and shampoo [18], bio-lubricants [18–20], alkyd resin [20,21], oleo-chemicals and nylon-11 [22], cracked liquid biofuels [23], kaolin intercalates [14], hydraulic oils [18,19] and linseed oil substitute [3,18]. The oil content of rubber seed varies from 30 to 60 wt.% [2,3,7,8,21]. The de-oiled cake from the kernel after preliminary treatment to remove toxic substances is a source of proteins for animal and poultry feeds [3,10,19].

Mechanical, enzymatic, and chemical methods are commonly utilized for oil seed extraction [1,24]. The mechanical type (hydraulic and screw press) is relatively inexpensive after initial capital costs, but the oil yield is low compared to other extractive methods [1]. Ali and Watson [25] also reported that this method is relatively

CONTACT Samuel Erhigare Onoji samonoji@yahoo.co.uk

© 2017 Informa UK Limited, trading as Taylor & Francis Group

energy&fuels

Article

pubs.acs.org/EF

Transesterification of Rubber Seed Oil to Biodiesel over a Calcined Waste Rubber Seed Shell Catalyst: Modeling and Optimization of Process Variables

Samuel Erhigare Onoji,*[,†,‡] Sunny E. Iyuke,[†,‡] Anselm I. Igbafe,[§] and Michael O. Daramola[†]

[†]School of Chemical & Metallurgical Engineering, University of the Witwatersrand, 1 Jan Smuts Avenue, Braamfontein 2050, Private Bag 3, Johannesburg, South Africa

[‡]Petroleum and Natural Gas Processing Department, Petroleum Training Institute, PMB 20, Effurun, Nigeria

[§]School of Chemical & Petroleum Engineering, Afe Babalola University, PMB 5454, Ado-Ekiti, Nigeria

Supporting Information

ABSTRACT: In the present study, waste rubber seed shell (RSS) obtained from our previous study was investigated as a plausible solid base catalyst for the transesterification of esterified rubber seed oil (RSO) to biodiesel. TGA, XRF, XRD, SEM, and N_2 adsorption/desorption analysis (BET) were used to characterize the catalyst. Central composite design (CCD) was employed to design the experiments conducted to study the influence of the process variables (reaction time, methanol/oil ratio, and catalyst loading) on biodiesel yield. Response surface methodology (RSM) technique, was used to optimize the process, and the quadratic model developed was statistically significant with *F*-value of 12.38 and *p*-value (<0.05). The optimum conditions obtained from RSM are as follows: reaction time (60 min), methanol/oil ratio (0.20 vol/vol), and catalyst loading (2.2 g) with a maximum biodiesel yield of 83.11% which was validated experimentally as 83.06 ± 0.013%. Reusability test of the catalyst at optimum conditions shows that the biodiesel yield was over 80% after fourth cycle of usage and the leached Ca^{2+} ion content of biodiesel was 3.26 mg/kg (ppm). The ester content determined by a precalibrated gas chromatography and the oxidation stability of the biodiesel are 96.7% and 7.8 h, respectively. The characterized biodiesel complied with ASTM D 6751 and EN 14214 biodiesel standards.

1. INTRODUCTION

One of the main issues confronting humanity from creation to date and taken much of man's attention is that of energy security. From time immemorial, man has always looked for a way to satisfy this energy demand. Over 3000 years ago, the discovery of fossil materials such as oil, natural gas, and coal seems to have solved the crisis. The discovery brought about the industrial revolution, urbanization, and modernization of facilities, leading to an improved standard of living.[1] As the world population grew, the demand for energy also increased. With the concepts of sustainable development, the environment became a major concern. Fossil materials account for over 80% of the world energy source, with attendant environmental problems, such as increased greenhouse gases (causing climate change), degradation of the ecosystems (land, water, and air), and the depletion of the ozone layer, associated with their usage.[2,3] Besides the environmental issues, fossil materials are nonrenewable, nonbiodegradable, nonavailability in most regions, associated with price instability, and unaffordable to a larger population of the world. Biodiesel, a more environmentally friendly fuel, is a long chain fatty acid monoalkyl ester popularly accepted as a complement to fossil diesel.[4,5] Biodiesel is associated with renewability, biodegradability, lower emission profile, and excellent lubricity among others.[2,6] Biodiesel is produced by the transesterification of vegetable oils, animal fats, and other sources of oils/fats with primary alcohols in the presence of suitable catalysts (homogeneous, heterogeneous, and enzymes).[1,5,6] Over 90% biodiesel produced is sourced from edible vegetable oils that compete with food use.[1,2] Food is a necessity of man after shelter; and the use of edible vegetable oils as biodiesel source materials is counterproductive.

Feedstock accounts for about 60−75% of the total cost of biodiesel,[2] and the production of biodiesel from low-cost materials will reduce its price and makes it more competitive with fossil-diesel. Nonedible rubber seed oil could be exploited as low-cost industrial oil for biodiesel production. This will reduce biodiesel cost and avoid a food-fuel crisis in the future. Homogeneous base catalysts such as NaOH, KOH, and methoxides of sodium and potassium are most suitable for industrial transesterification of edible vegetable oils that are generally low in free fatty acids (FFAs). However, associated problems, such as difficulty in catalyst−products separation, initial catalyst cost, soap formation, low-grade byproduct glycerol, reactor corrosion, and large volume washing water requirements, induced further research for environmentally benign heterogeneous catalysts for biodiesel synthesis from nonedible oils.[5,7] Heterogeneous (solid) catalysts are separated from reaction mixtures by a simple filtration process. They are reused and recycled multiple times to produce a high-grade glycerol.[8] In the recent past, successful ventures were reported on the utilization of calcined waste materials such as eggshell[9] and animal bones[10] to generate low-cost CaO solid base catalysts for

Received: February 2, 2017
Revised: May 17, 2017
Published: May 19, 2017

ACS Publications © 2017 American Chemical Society

DOI: 10.1021/acs.energyfuels.7b00331
Energy Fuels 2017, 31, 6109−6119

Appendix B

Section B.1

Rubber seed analysis:

1st Experiment:

Amount of rubber seed used = 500 g

Amount of shell present = 249.65 g

∴ Amount of kernel (solid + moisture) = 250.35 g

2nd Experiment:

Amount of rubber seed used = 500 g

Amount of shell present = 248.65 g

Amount of kernel (solid + moisture) = 251.35 g

Mass % shell (1st reading) = $\frac{249.65}{500} \times 100 = 49.93\%$

Mass % shell (2nd reading) = $\frac{248.65}{500} \times 100 = 49.73\%$

Average mass % shell = $\frac{1}{2}(49.93 + 49.73) = 49.83\%$

Standard deviation, $\sigma = \sqrt{\frac{\Sigma(X - \overline{X})^2}{n-1}}$ (B.1)

Where $\overline{X}$ = mean of the data (49.93, 49.73)

n = number of data

∴ Standard deviation for shell = ± 0.14

Mass % of kernel and moisture calculations:

Average mass of kernel and moisture = $\frac{1}{2}(250.35 + 251.35) = 250.85g$

Mass % (kernel + moisture) = $\frac{250.85}{500} \times 100 = 50.17\%$

Determination of moisture content of the kernel:

1st Experiment:

Amount of kernel used = 100 g

Amount of kernel after drying to constant mass at 105 ^{o}C for 5 h = 90.35 g

Mass of moisture = (100 – 90.35) g = 9.65 g

$\therefore$ Mass % moisture = $\frac{9.65}{100} \times 100 = 9.65\%$

2nd Experiment:

Amount of kernel used = 100 g

Amount of kernel after drying to constant mass at 105 ^{o}C for 5 h = 90.25 g

Mass of moisture = (100 – 90.25) g = 9.75 g

$\therefore$ Mass % moisture = $\frac{9.75}{100} \times 100 = 9.75\%$

$\therefore$ Average mass % moisture = $\frac{1}{2}(9.65+9.75) = 9.7 \pm 0.07\%$

Therefore, average mass % kernel in the seed = 50.17 – 9.7 = 40.47$\pm$ 0.07%

Appendix C

Section C.1

This section shows the experimental setup for rubber seed oil extraction using the n-hexane–soxhlet extractor.



Weighing of milled kernel Milled kernel in muslin cloth

Figure C.1: Preparation of milled kernel for oil extraction



Figure C.2: Oil soxhlet extractor used for the study



Figure C.3: Rotary evaporator used in the study

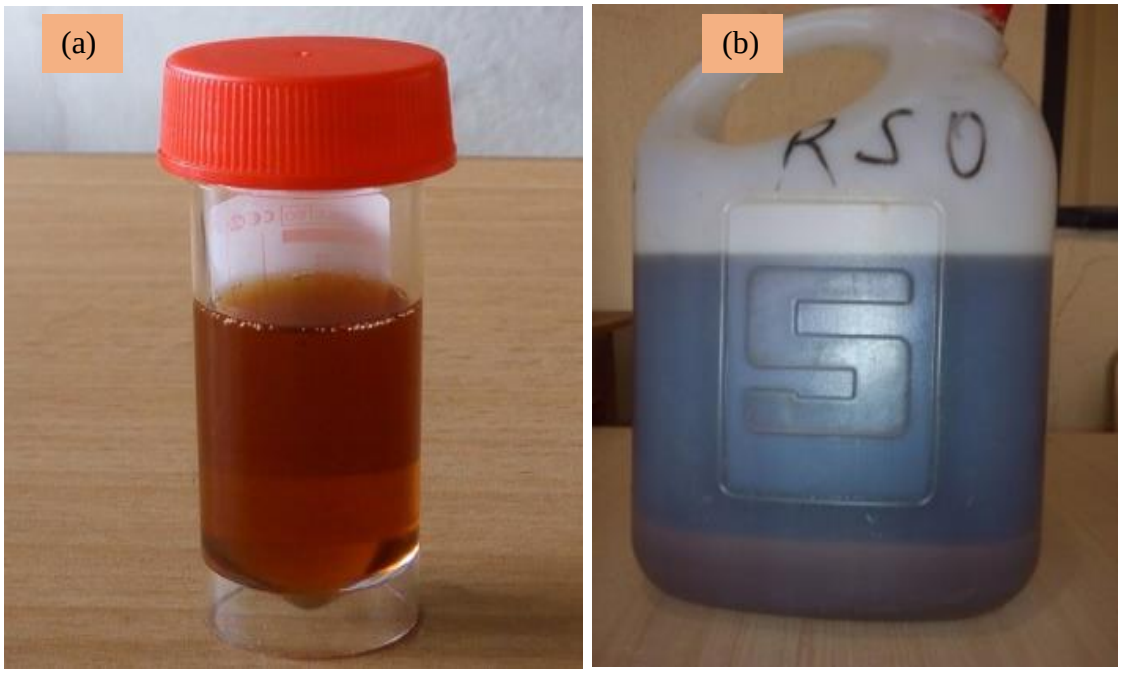


Figure C.4: Extracted rubber seed oil: (a) filtered, (b) crude

Appendix D

Section D.1

This section deals with the determination of the oil yield (%) using the experimental setup in Appendix C. The oil yield was calculated based on Equation (3.1) for each particle size (0.5, 1, 1.5, 2 and 2.5 mm) considered. The experimental procedures are described in Section 3.2.2.

Calculation of oil yield for 0.5 mm particle size:

1st Experiment:

Mass of kernel charged into extractor = 50 g

Volume of n-Hexane used = 225 mL

Mass of extracted oil = 20.12 g

Oil yield = $\frac{20.12}{50} \times 100 = 40.24\%$

2nd Experiment:

Mass of kernel charged into extractor = 50 g

Volume of n-Hexane used = 225 mL

Mass of extracted oil = 20.18 g

Oil yield = $\frac{20.18}{50} \times 100 = 40.36\%$

$\therefore$ Average oil yield for 0.5 mm kernel size = $\frac{1}{2}(40.24 + 40.36) = 40.3 \pm 0.085\%$

Similar experiments were conducted in duplicates, and the oil yields obtained for 1, 1.5, 2, and 2.5 mm particle size are 39.95, 40.25; 37.8, 37.4; 32.7, 32.3; and 29.5, 29.1%, respectively. The average results are tabulated in Table D.1, and plotted in Figure 4.1.

Table D.1: Variation of oil yield with kernel particle size

Particle size (mm)	0.5	1	1.5	2	2.5
Oil yield (%)	40.3±0.085	40.1±0.212	37.6±0.283	32.5±0.283	29.3±0.283

Section D.2: Validation of optimal oil yield for RSM model

The RSM model predicted an optimum oil yield of 42.98% at the following conditions:

Rubber seed milled kernel = 60 g

Solvent volume = 250 mL

Extraction time = 45 min

60 g of milled kernel of 0.5 mm particle size was charged into the n-hexane extractor with 250 mL hexane. The experiment was conducted for a period of 45 min and repeated in triplicates. The procedures in Section D.1 were followed and the average oil yield calculated is shown below.

1st Experiment:

Mass of milled kernel used = 60 g

Mass of extracted oil = 25.572 g

Oil yield = $\frac{25.572}{60} \times 100 = 42.62\%$

2nd Experiment:

Mass of milled kernel used = 60 g

Mass of extracted oil = 25.59 g

Oil yield = $\frac{25.59}{60} \times 100 = 42.65\%$

3rd Experiment:

Mass of milled kernel used = 60 g

Mass of extracted oil = 25.59 g

Oil yield = $\frac{25.59}{60} \times 100 = 42.65\%$

Average oil yield = $\frac{1}{2}(42.62 + 42.65 + 42.65) = 42.64 \pm 0.017\%$

The experimental validated oil yield value of 42.64% is close to the model predicted optimum value of 42.98% within an error of 0.8%.

Section D.3: validation of optimal oil yield for ANN model

The ANN model predicted on optimum oil yield of 43% at the following conditions:

Rubber seed milled kernel = 40 g

Solvent volume = 202 mL

Extraction time = 49.99 min

Using these optimum conditions, the experiment was conducted in triplicates as described in Section D.1.

1st Experiment:

Mass of milled kernel used = 40 g

Mass of extracted oil = 17.148 g

Oil yield = $\frac{17.148}{40} \times 100 = 42.87\%$

2nd Experiment:

Mass of milled kernel used = 40 g

Mass of extracted oil = 17.16 g

Oil yield = $\frac{17.16}{40} \times 100 = 42.9\%$

3rd Experiment:

Mass of milled kernel used = 40 g

Mass of extracted oil = 17.244 g

Oil yield = $\frac{17.244}{40} \times 100 = 43.11\%$

Average oil yield = $\frac{1}{2}(42.87 + 42.9 + 43.11) = 42.96 \pm 0.131\%$

The experimental validated oil yield value of 42.96% is close to the model predicted optimum value of 43% within an error of 0.09%.

Appendix E

Section E.1

This section deals with the procedures and calculations of the physicochemical properties of the extracted rubber seed oil based on the procedures described in ASTM and AOAC methods.

Section E.1.1 Determination of the density (ρ) and specific gravity (SG) of the oil

This was determined using 25 mL capacity density bottles at 15 ^{o}C. The SG was calculated as the ratio of the density of the oil to that of water at 15 ^{o}C.

$$\rho = \frac{mass}{volume} \tag{E.1}$$

$$SG = \frac{\rho_o}{\rho_w} \tag{E.2}$$

Section E.1.2 Determination of the ^{o}API gravity

Equation (E.3) determined the ^{o}API of the oil as shown below.

$$^{o}API = \frac{141.5}{SG@15^{o}C} - 131.5 \tag{E.3}$$

Section E.1.3 Conradson carbon residue of the seed oil

The conradson carbon residue was determined following the procedures described in ASTM D189-IP 13. The determination of carbon residue left after evaporation and pyrolysis of oil is intended to provide some indication of its relative coke-forming propensity when used as source material for fuel. In this study, 3 ± 0.1 g of oil was weighed and placed in a porcelain crucible containing 0.3149 g of glass bead to maintain uniform heating (Onoji et al., 2016b). The crucible was placed in the center of the skidmore iron crucible (Stanhope-Seta apparatus) with a lid. Heat was applied and pre-ignition period observed was 30 ± 5 min when smoke appeared above the chimney. The experiment lasted for 60 ± 5 min in an air-free environment. At the end of the specified heating period, the test crucible containing the carbonaceous residue was cooled in a desiccator and weighed again. The residue remaining was calculated as a percentage of the original sample, and reported as non-combustible carbon residue. The experiment was carried out in duplicate and average value computed as shown below.

1st Experiment:

Amount of oil and glass bead placed in a porcelain crucible = 3.3149 g

Mass of oil = 3.0 g

Mass of carbon residue and bead after evaporation and pyrolysis of the oil = 0.3263 g

∴ Mass of carbon residue = (0.3263 – 0.3149) g = 0.0114 g

% mass carbon residue = $\frac{0.0114}{3} \times 100 = 0.38\%$

2nd Experiment:

Amount of oil and glass bead placed in a porcelain crucible = 3.3149 g

Mass of oil = 3.0 g

Mass of carbon residue and bead after evaporation and pyrolysis of the oil = 0.3275 g

∴ Mass of carbon residue = (0.3275 – 0.3149) g = 0.0126 g

% mass carbon residue = $\frac{0.0126}{3} \times 100 = 0.42\%$

$\therefore$ Average mass % carbon residue = $\frac{1}{2}(0.38+0.42) = 0.4\%$

Section E.1.4 Moisture content analysis of the seed oil

The moisture content was determined using a standard laboratory U CLEAR oven (*Model: DHG-9053A*) operated at 105 ^{o}C. About 20 g of the sample was placed in a clean porcelain crucible, and weighed. The process of heating and cooling was repeated every 10 min after weighing until constant weight was obtained. All analyses were done in duplicates, and moisture content was determined by calculating the weight difference of the sample before and after oven drying as documented below.

1st Experiment:

Amount of oil used = 20 g

Amount of oil after drying to constant mass at 105 ^{o}C = 19.658 g

Amount of moisture removed = (20 – 19.658) g = 0.342 g

% moisture content = $\frac{0.342}{20} \times 100 = 1.71\%$

2nd Experiment:

Amount of oil used = 20 g

Amount of oil after drying to constant mass at 105 ^{o}C = 19.65 g

Amount of moisture removed = (20 – 19.65) g = 0.35 g

% moisture content = $\frac{0.35}{20} \times 100 = 1.75\%$

$\therefore$ Average mass % moisture = $\frac{1}{2}(1.71+1.75) = 1.73\%$

Section E.1.5 Ash content analysis of the seed oil

The ash content was determined by burning 20 g of oven-dried sample in a porcelain crucible placed in an electric muffle furnace (Carbolite, Parson Lane, Hope Valley S33 6RB, England, *Model: RWF 12/5*) maintained at 550 ± 25 ^{o}C for an initial 20 min, cooled in a desiccator and weighed again. The heating and cooling process was repeated every 10-min interval until the carbonaceous residue was reduced to an ash. The results were expressed on a dry weight basis according to procedures prescribed in ASTM D 482-IP 4, and documented as shown below.

1st Experiment:

Amount of oven-dried oil placed in a porcelain crucible = 20 g

Amount of cooled ash content after combustion at 550 ± 25 ^{o}C = 0.00018 g

% Ash content of oil = $\frac{0.00018}{20} \times 100 = 0.0009\%$

2nd Experiment:

Amount of oven-dried oil placed in a porcelain crucible = 20 g

Amount of cooled ash content after combustion at 550 ± 25 ^{o}C = 0.00022 g

% Ash content of oil = $\frac{0.00022}{20} \times 100 = 0.0011\%$

$\therefore$ Average mass % ash = $\frac{1}{2}(0.0009 + 0.0011) = 0.001\%$

Section E.1.6 Determination of the seed oil volatile matter

The percentage of volatile matter in the oil was obtained by using Equation (E.4).

$$Volatile\ matter\ (\%) = 100 - (carbon\ residue + moisture + ash) \quad \text{(E.4)}$$

Therefore, % volatile matter = 100 – (0.4 + 1.73 + 0.001) = 97.869%

Section E.1.7 Determination of the peroxide value (PV) of the oil

About 2 g of oil sample was weighed into a 250-mL pyrex flask and 40 mL of solvent mixture (2:1 glacial acetic acid/chloroform) was added. The content was swirled until it was dissolved completely and 2 g of KI powder was then added. The mixture was boiled briskly in a water bath maintained at 70 ^{o}C for 1 min. The boiled mixture was added to a flask containing 40 mL of 5% KI and the resultant mixture was then washed with 50 mL of distilled water. The content of the flask was titrated with 0.004M $Na_2S_2O_3$ solution using 1 mL of 0.5% starch solution as indicator. The experiment was repeated and peroxide value (mequiv O_2/kg oil) was calculated as indicated in Equation (E.5).

$$\text{Peroxide value} = \frac{\text{V} \times \text{M}}{\text{w}} \tag{E.5}$$

where:

V = volume of $Na_2S_2O_3$ used for titration

M = molarity of $Na_2S_2O_3$

w = weight of oil sample

Section E.1.8 Determination of the iodine value (IV) of the oil (Wijs' method)

About 0.26 g of oil was dissolved in 10 mL of carbon tetrachloride and agitated in a stopper flask. 20 mL of Wijs solution was added and allowed to stand for 30 min in the dark at room temperature. 20 mL of 10% potassium iodide solution and 100 mL distilled water was added to the mixture in the flask and titrated with 0.1M $Na_2S_2O_3$ (sodium thiosulphate) standard solution using 1 mL of 0.5% starch solution as indicator. The iodine value was calculated using Equation (E.6).

$$IV = \frac{12.69 \times M \times (B - S)}{w} \tag{E.6}$$

where:

B = volume of $Na_2S_2O_3$ titrated in blank

S = volume of $Na_2S_2O_3$ titrated in test

M = molarity of standard $Na_2S_2O_3$

w = mass of oil used

Section E.1.9 Determination of the refractive index (RI) of the oil

A digital Abbe Refractometer (Model: 60/ED) was used to determine the refractive index of the oil that was maintained at 20 ^oC in a water bath to keep the temperature of the glass slide uniform. Then, few drop of oil sample was dropped into the glass slide of the refractometer by means of syringe and needle. This was repeated twice and the values were converted using a calibrated chart, and average value was recorded.

Section E.1.10 Determination of the saponification value (SV) of the oil

About 4 g of oil was weighed into a 250-mL pyrex flask and 50 mL of 0.5M ethanolic KOH was added. The setup was connected to a reflux condenser and heated gently for 30 min. The mixture formed (soap solution) was cooled and titrated with 0.5M HCl solution using 2 drops of phenolphthalein indicator. The endpoint is reached when the pink colour of the indicator disappeared. The experiment was conducted for the blank titration and repeated. The saponification value was calculated according to Equation (E.7).

$$SV = \frac{56.1 \times M \times (B - S)}{w} \quad \text{(E.7)}$$

where:

B = volume of HCl used during blank titration

S = volume of HCl used for test

M = molarity of standard HCl

w = mass of oil used in gram; Molecular mass of KOH = 56.1

Section E.1.11 Determination of acid value (AV) of the oil

The acid value was determined by dissolving 5 g of oil sample in a hot mixture of 25 mL (95% vol/vol) diethyl ether and 25 mL ethanol in a 250-mL flask. The hot solution was titrated with 0.1M KOH solution using 3 drops of phenolphthalein indicator. The acid value was calculated using Equation (E.8). It is important to note that %FFA is half the acid value.

$$AV = \frac{56.1 \times M \times V}{w} \tag{E.8}$$

where:

M = molarity of standard KOH

V = volume of titrant (KOH) in cm^3

w = mass of oil sample

56.1 = molecular mass of KOH

Section E.1.12 Determination of the pH value of the oil

About 2 g of the oil sample was poured into a clean dry 100 mL beaker and 12.5 mL of hot distilled water was added to the sample in the beaker and stirred gradually. The resulting solution was cooled in a water bath at temperature of 28 ^{o}C. A standardized pH meter with buffer solution and the electrode immersed into the sample was used to read up the pH value of the oil sample. The experiment was repeated and the average value recorded.

Section E.2

This section deals with the effects of temperature and time parameters on the peroxide, iodine, and refractive index values of the oil during heat treatment. At each temperature and time indicated, the values are determined as described in Section E.1, and they are recorded in Table E.1. The average values and their standard deviations are presented in Table 4.7.

Table E.1: Variation of peroxide, iodine, and refractive index values of rubber seed oil with temperature and time

Temp (°C)	Time (min)	Peroxide (mequiv O_2/kg oil)		Iodine (I_2/100 g oil)		Refractive index @ 20 °C	
		1st Reading	2nd Reading	1st Reading	2nd Reading	1st Reading	2nd Reading
100	30	3.84	4.20	118.50	116.94	1.4555	1.4747
	60	4.41	4.59	117.31	117.55	1.3982	1.4662
	120	4.80	4.82	117.20	117.28	1.4018	1.4276
	180	4.84	5.16	117.00	117.04	1.3820	1.3208
	240	5.20	5.60	116.51	117.45	1.3001	1.3021
	300	5.50	5.72	116.80	116.88	1.2580	1.2352
150	30	4.35	4.41	117.30	117.82	1.4601	1.4659
	60	4.60	4.72	117.20	117.44	1.4281	1.4299
	120	4.89	5.07	116.95	117.29	1.3991	1.4269
	180	5.20	5.28	116.61	117.07	1.3811	1.3889
	240	5.31	5.81	115.98	117.22	1.3700	1.3602
	300	5.70	5.94	114.80	116.00	1.3420	1.3452
200	30	4.53	4.71	117.31	117.45	1.3628	1.3666
	60	4.82	4.94	117.00	117.04	1.3225	1.3235
	120	4.91	5.09	116.34	116.88	1.2970	1.3012
	180	5.30	5.38	116.10	116.54	1.2900	1.2922
	240	5.70	5.82	114.98	116.38	1.2815	1.2853
	300	5.91	5.97	115.20	115.28	1.2431	1.2435
250	30	4.72	4.76	116.85	117.57	1.3001	1.3039
	60	4.85	4.95	116.40	116.80	1.2745	1.2755
	120	4.90	5.06	116.00	116.40	1.2326	1.2343
	180	5.15	5.25	115.20	115.60	1.2319	1.2303
	240	5.45	5.55	113.88	115.76	1.2254	1.2170
	300	5.60	5.80	114.32	114.64	1.2085	1.1937

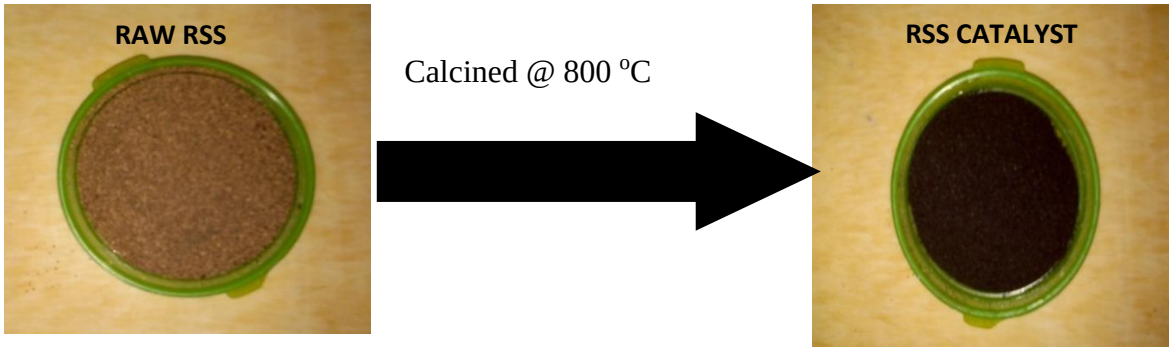


Figure E.1: Calcination of rubber seed shell (RSS) catalyst for biodiesel production

Appendix F

Section F.1

Esterification of rubber seed oil:

Prior to transesterification reaction, the acid value of the oil is reduced to ≤ 1% FFA to avoid the consumption of the base catalyst during biodiesel production through saponification reaction (soap formation). The initial value of the rubber seed oil was 18.02 mg KOH/g oil. For each concentration of H_2SO_4 catalyst (1.5, 3, 4.5, and 6 % vol/vol) used, the experiment was carried out in duplicates as described in Section 3.8.1. The acid value in each case was determined as discussed in Section E.1.11 of Appendix E, and the values recorded in Table F.1.

Table F.1: Esterification parameters of the rubber seed oil (Onoji et al., 2017b)

Std run	H_2SO_4 (% vol/vol)	Acid value (mg KOH/g oil)	FFA (%)
0	0	18.20±0.141	9.10±0.07
1	1.5	12.50±0.125	6.25±0.0625
2	3	4.82±0.021	2.41±0.01
3	4.5	3.98±0.01	1.96±0.005
4	6	1.78±0.005	0.86±0.0025



Figure F.1: Esterified oil separation into two layers



Figure F.2: Gravity settling of biodiesel, catalyst and glycerol phases



Figure F.3: Processed rubber seed oil methyl ester (biodiesel) for analysis

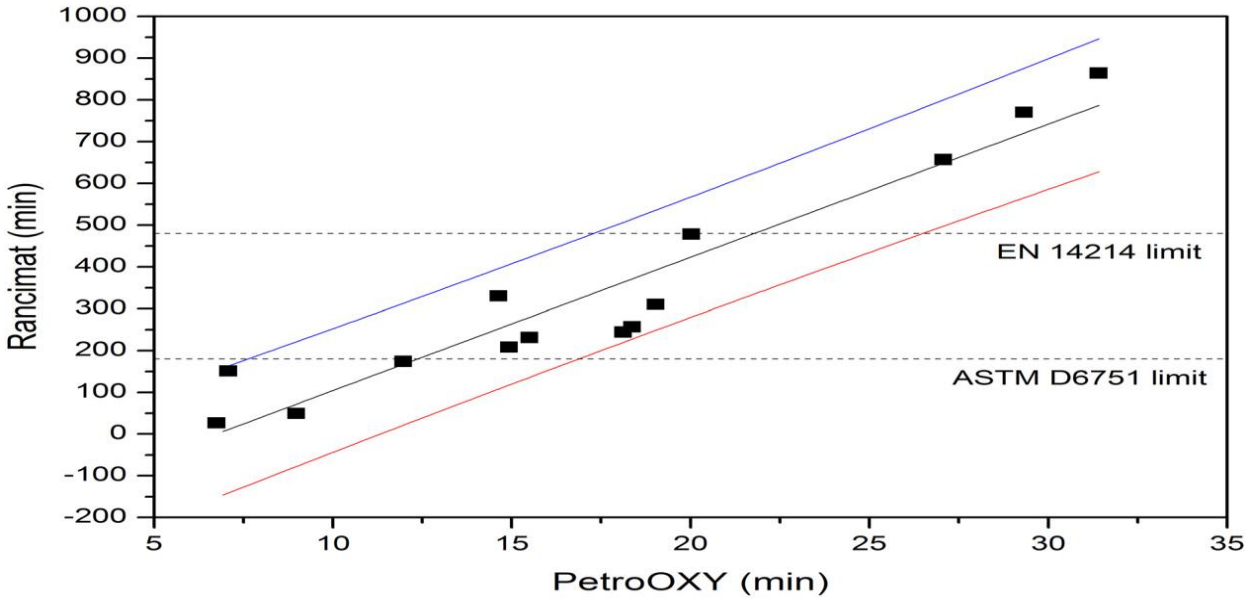


Figure F.4: Regression line (−), upper (−), and lower (−) prediction intervals and experimental data (■) of oxidation stability determination for biodiesel without additive (Adapted from Botella et al., 2014)

Appendix G

Table G.1: Infrared group absorption frequencies (Onoji et al., 2016b)

Type of bond	Functional group	Type of vibration	Wavenumber (cm^{-1})	Wavelength (μ)	Intensity (I)
C–H	Alkanes	stretch	3000-2850	3.33-3.51	s
	$–CH_3$	bend	1450 and 1375	6.90-7.27	m
	$–CH_2–$	bend	1465	6.83	m
	Alkenes	stretch	3100-3000	3.23-3.33	m
		bend	1700-1000	5.88-10.0	s
	Aromatics	stretch	3150-3050	3.17-3.28	s
		out-of-plane bend	1000-700	10.0-14.3	s
	Alkynes	stretch	ca. 3300	ca. 3.03	s
	Aldehydes		2900-2800	3.45-3.57	w
			2800-2700	3.57-3.70	w
C–C	Alkanes	not usually useful			
C=C	Alkenes		1680-1600	5.95-6.25	m-w

	Aromatics		1600-1400	6.25-7.14	m-w
C≡C	Alkyne		2250-2100	4.44-4.76	m-w
C=O	Aldehyde Ketone Carboxylic acids Esters Amide Anhydride Acyl chloride		1740-1720 1725-1705 1725-1700 1750-1730 1700-1640 ca. 1810 ca. 1760 1800	5.75-5.81 5.80-5.87 5.80-5.88 5.71-5.78 5.88-6.10 ca. 5.52 ca. 5.68 5.55	s s s s s s s s
C–O	Alcohols, Ethers, Esters, Carboxylic acids		1300-1000	7.69-10.0	S
O–H	Alcohols, Phenols: Free H-bonded Carboxylic acids (2)		 3650-3600 3400-3200 3300-2500	 2.74-2.78 2.94-3.12 3.03-4.00	 m m m

N–H	Primary and secondary amines		ca. 3500	ca. 2.86	M
C≡N	Nitriles		2260-2240	4.42-4.46	M
N=O	Nitro (R–NO_2)		1600-1500 1400-1300	6.25-6.67 7.14-7.69	s s
C-X	Fluoride Chloride Bromide, Iodide		1400-1000 800-600 <600	7.14-10.0 12.5-16.7 >16.7	s s s

(I): s = strong, m = medium and w = weak

Table G.2: Assignment of signals of ^{1}H NMR spectra for vegetable oils (hazel nut and walnut) (Guillèn & Ruiz, 2003)

Signal	Chemical shift (ppm)	Functional group
1	0.83–0.93	$–CH_3$(saturated, oleic and linoleic acyl chains)
2	0.93–1.03	$–CH_3$ (linolenic acyl chains)
3	1.22–1.42	$– (CH_2)_n$ -(acyl chains)
4	1.52–1.70	$–OCO–CH_2–CH_2–$ (acyl chains)
5	1.94–2.14	$–CH_2–CH=CH$ (acyl chains)
6	2.23–2.36	$–OCO–CH_2–$ (acyl chains)
7	2.70–2.84	$=HC–CH_2–CH=$ (acyl chains)
8	4.10–4.32	$–CH_2OCOR$ (glyceryl group)
9	5.20–5.26	>CHOCOR (glyceryl group)
10	5.26–5.40	–CH=CH– (acyl chains)

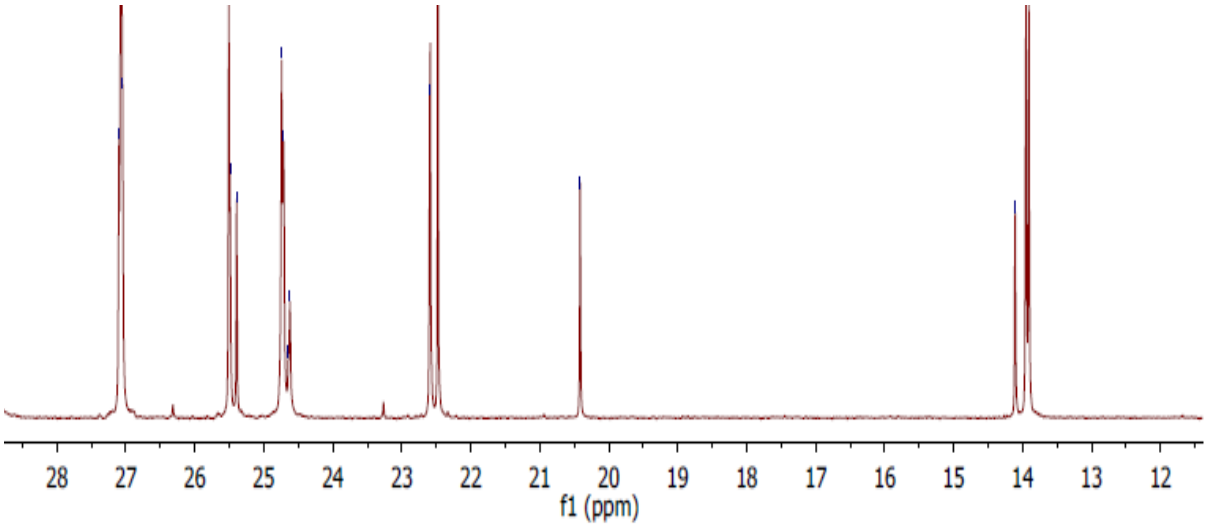


Figure G.1: ^{13}C NMR spectra of rubber seed oil (12–28 ppm)

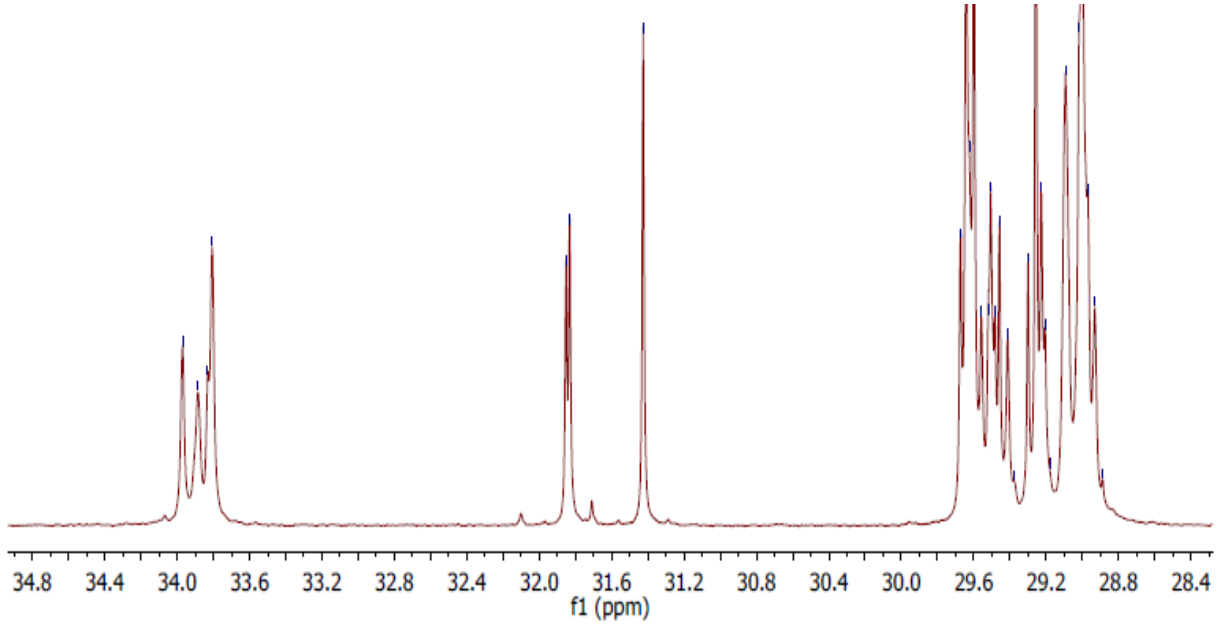


Figure G.2: ^{13}C NMR spectra of rubber seed oil (28.4–34.8 ppm)

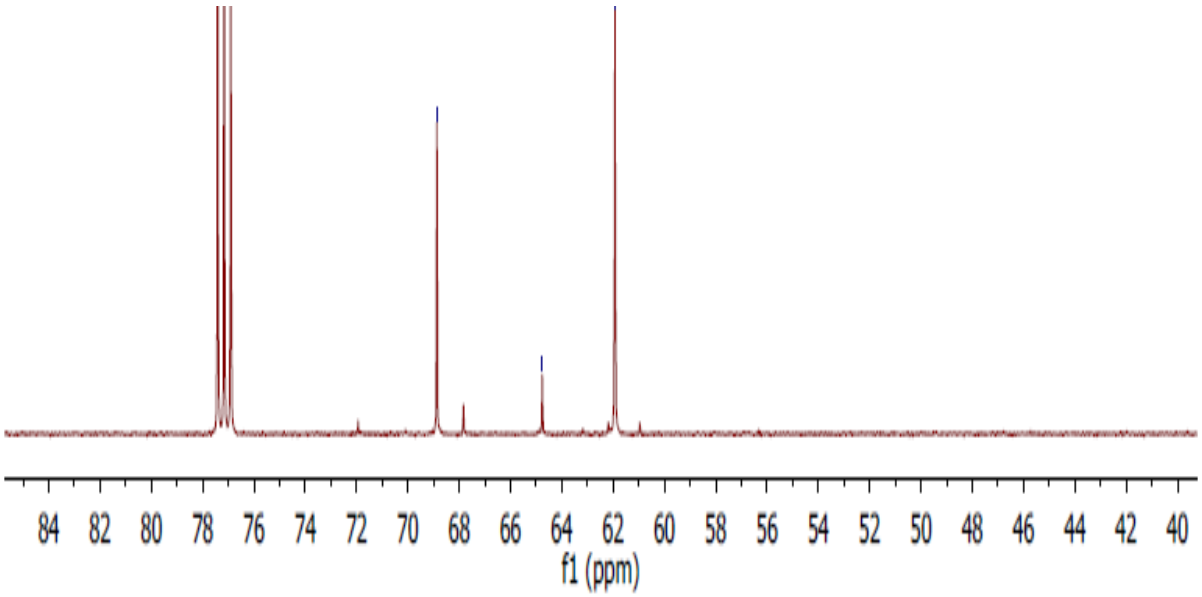


Figure G.3: ^{13}C NMR spectra of rubber seed oil (40–84 ppm)

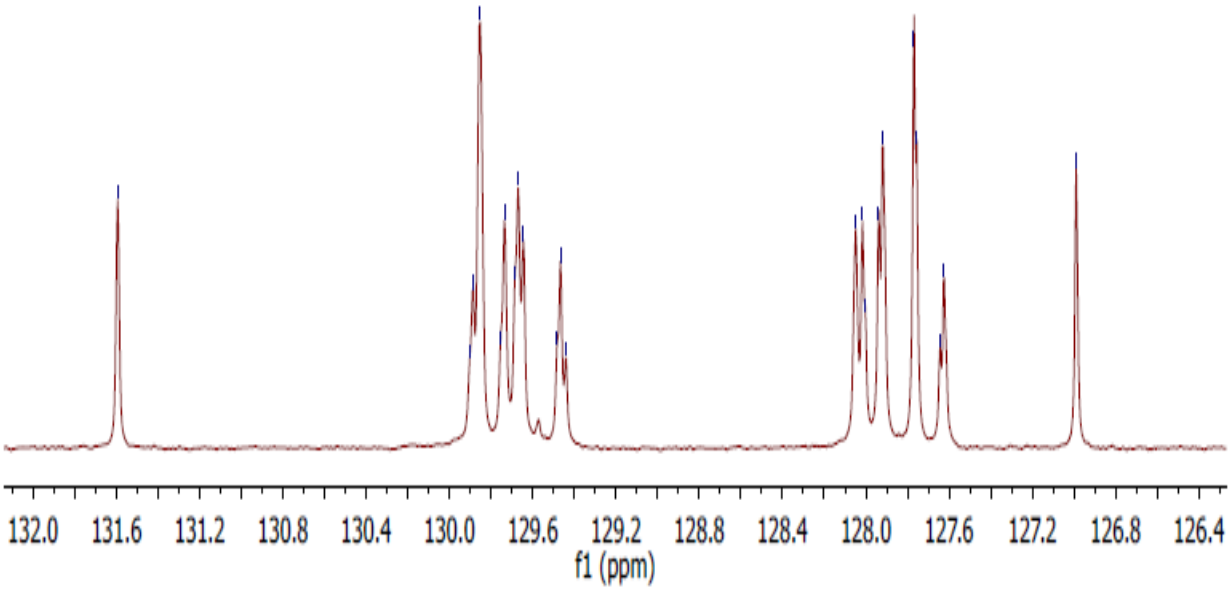


Figure G.4: ^{13}C NMR spectra of rubber seed oil (126.4–132.0 ppm)

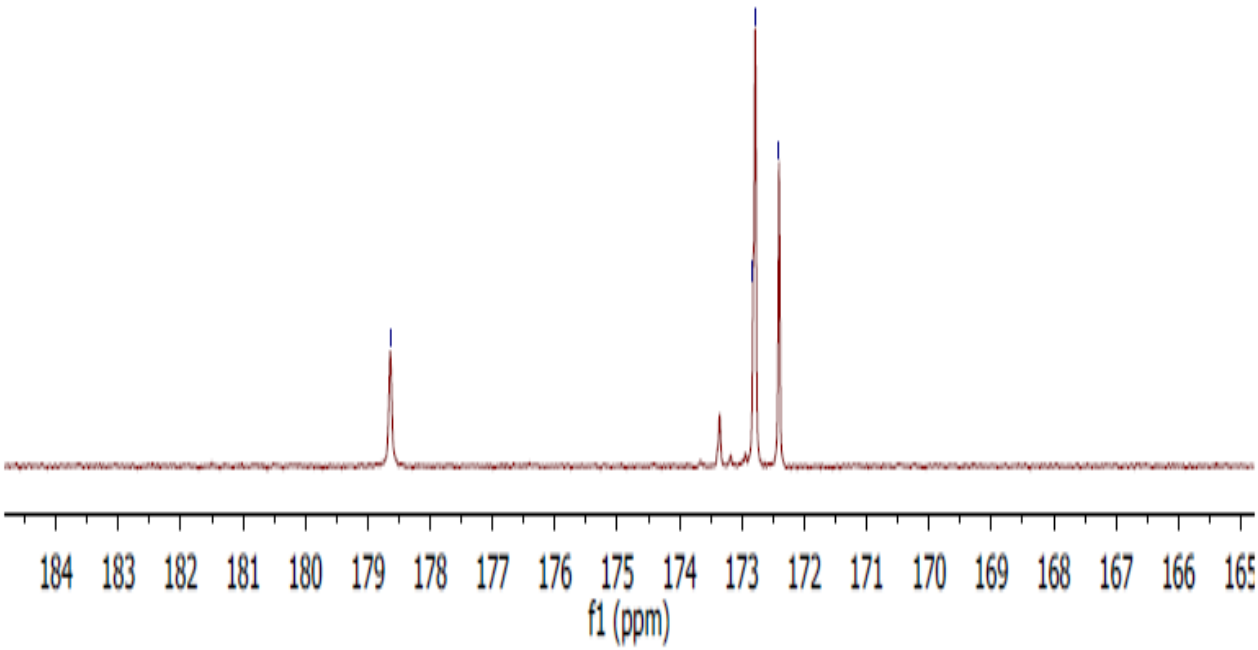


Figure G.5: ^{13}C NMR spectra of rubber seed oil (165–184 ppm)

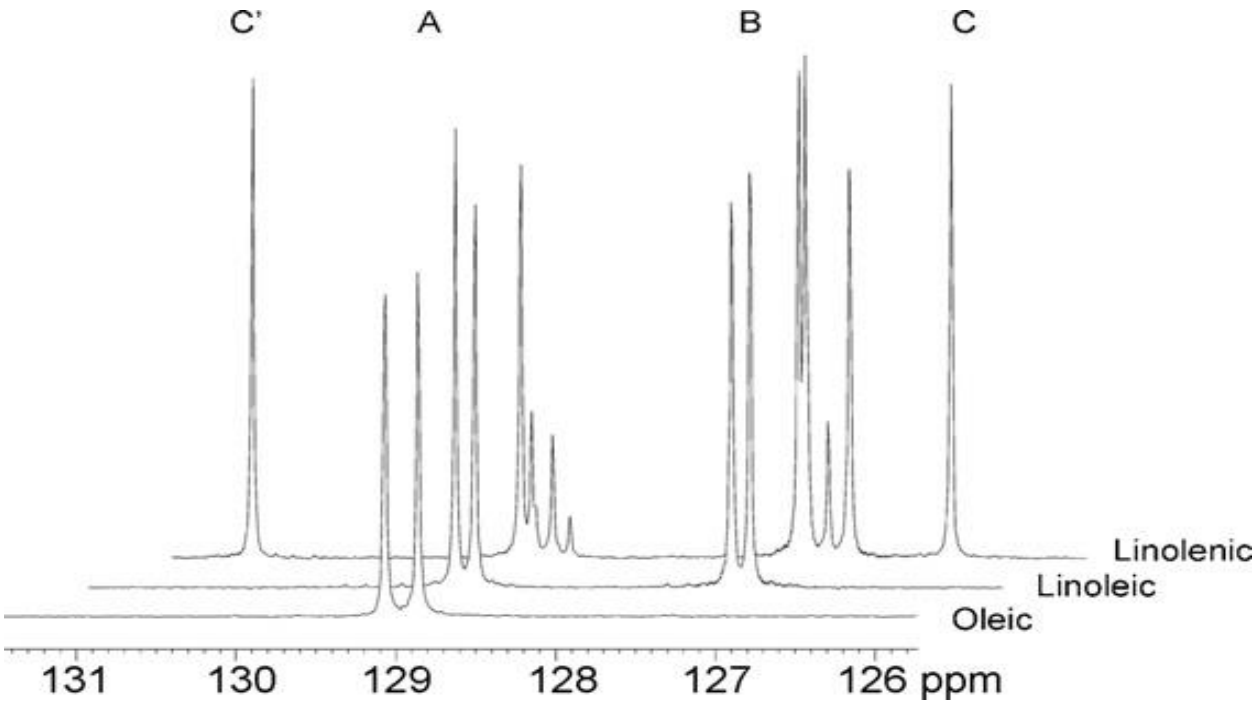


Figure G.6: Double bond peaks in the ^{13}C NMR spectrum for pure oleic acid, linoleic acid, and linolenic acid. Peaks for each characteristic double bond carbon are assigned the letters A for the peak found in all acids, B for the peak found in both linoleic and linolenic acid, and C and C' for the peaks found only in linolenic acid (Adapted from Sadowska et al., 2008)

Appendix H

Table H.1: XRF spectroscopic elemental analysis of rubber seed shells catalyst (Onoji et al., 2017b)

Elements	Raw (uncalcined) RSS pH=7.0			Calcined RSS at 800 ^{o}C for 3 h pH=12.5		
	Intensity	Concentration (mg/mL)	wt.%	Intensity	Concentration (mg/mL)	wt.%
Magnesium, Mg	0.0000	0.0267	0.5801	0.0001	0.1349	1.9423
Aluminum, Al	0.0003	0.0817	1.7749	0.0007	0.2048	2.9487
Silicon, Si	0.0015	0.0533	1.1579	0.0043	0.3392	4.8838
Phosphorus, P	0.0026	0.1202	2.6113	0.0037	0.1746	2.5132
Sulfur, S	0.0055	0.3847	8.3576	0.0059	0.4225	6.0832
Potassium, K	0.0020	0.1566	3.4021	0.0081	0.6516	9.3817
Calcium, Ca	0.0071	0.1195	2.5961	0.0243	0.7247	10.434
Vanadium, V	0.0002	0.0082	0.1781	0.0002	0.0093	0.1339
Chromium, Cr	0.0003	0.0111	0.2411	0.0002	0.0066	0.0950
Manganese, Mn	0.0003	0.0160	0.3476	0.0005	0.0284	0.4089
Cobalt, Co	0.0002	0.0017	0.0369	0.0001	0.0013	0.0187
Iron, Fe	0.0021	0.2766	6.0091	0.0076	0.8000	11.518
Nickel, Ni	0.0018	0.1079	2.3441	0.0015	0.0931	1.3405
Copper, Cu	0.0034	0.0630	1.3687	0.0037	0.1334	1.9207
Zinc, Zn	0.0050	0.1707	3.7085	0.0056	0.1947	2.8033
Tungsten, W	0.0006	0.1971	4.2820	0.0007	0.2528	3.6398
Rubidium, Rb	0.0000	0.0000	0.0000	0.0005	0.0018	0.0259
Niobium, Nb	0.0058	0.0675	1.4664	0.0054	0.0633	0.9114
Molybdenum	0.0035	0.1890	4.1060	0.0045	0.1592	2.2922
Tin, Sn	0.0074	1.3830	30.0456	0.0077	1.4414	20.753
Antimony, Sb	0.0093	1.1685	25.3856	0.0089	1.1078	15.950

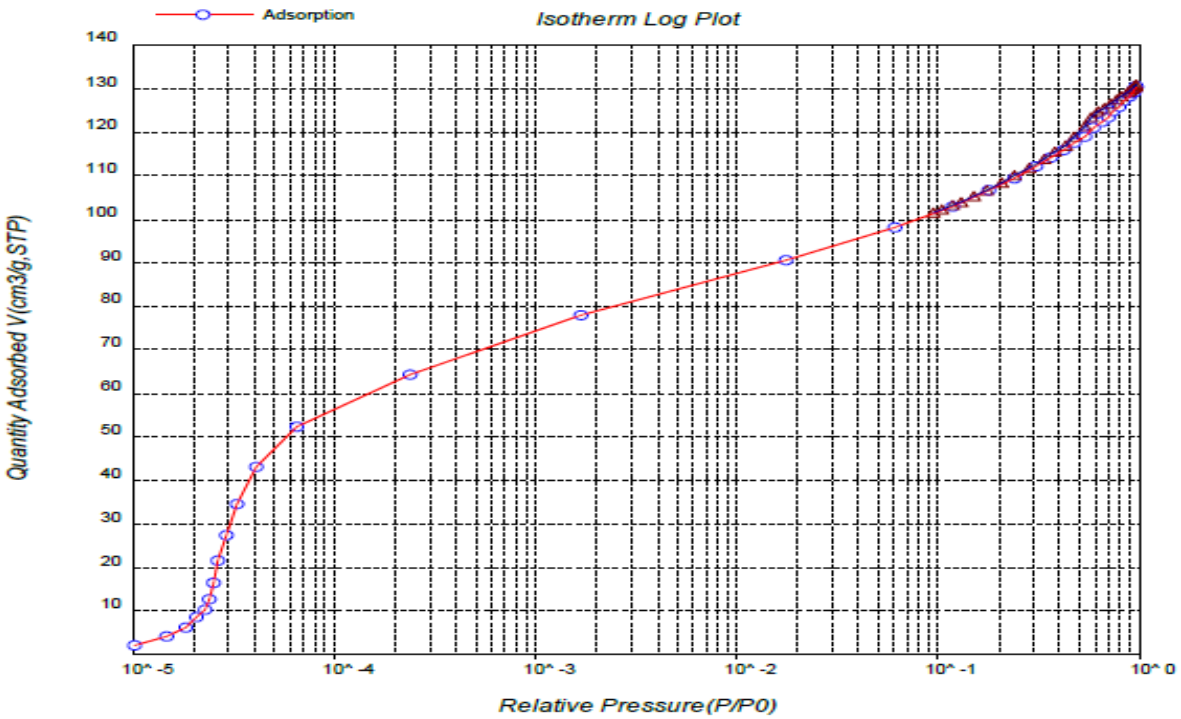


Figure H.1: Nitrogen adsorption/desorption log plot for calcined RSS (Adapted from Onoji et al., 2017b)

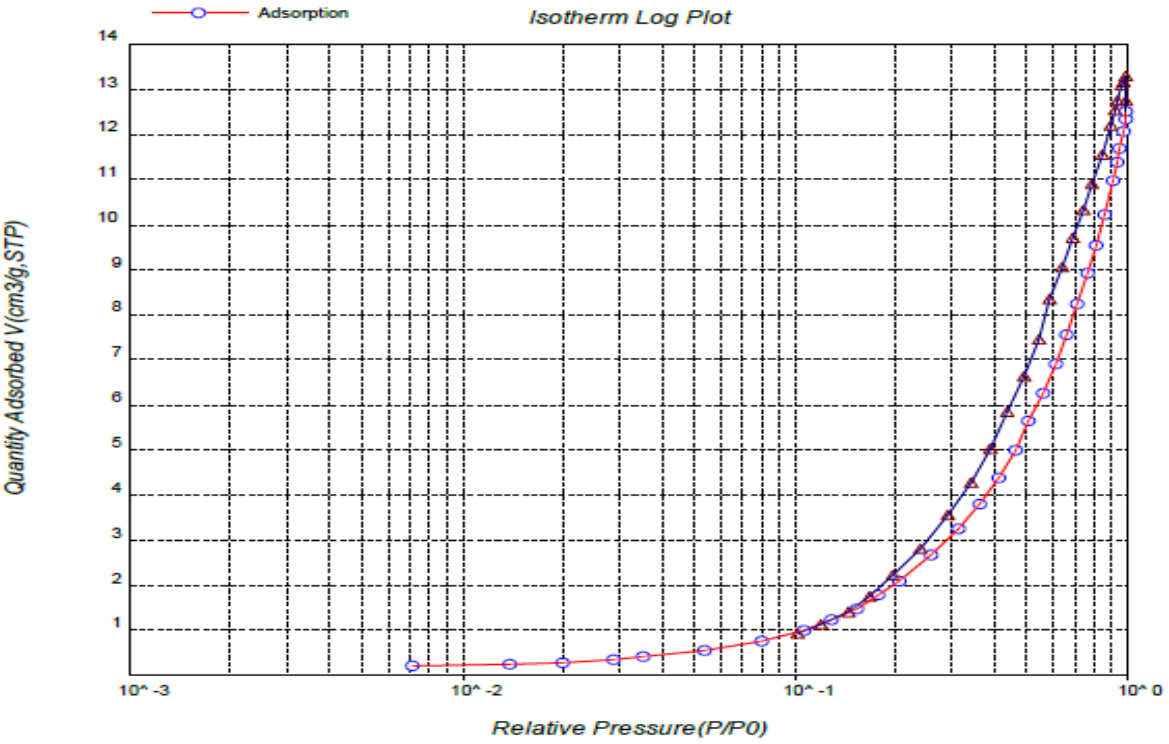


Figure H.2: Nitrogen adsorption/desorption log plot for raw RSS (Adapted from Onoji et al., 2017b)

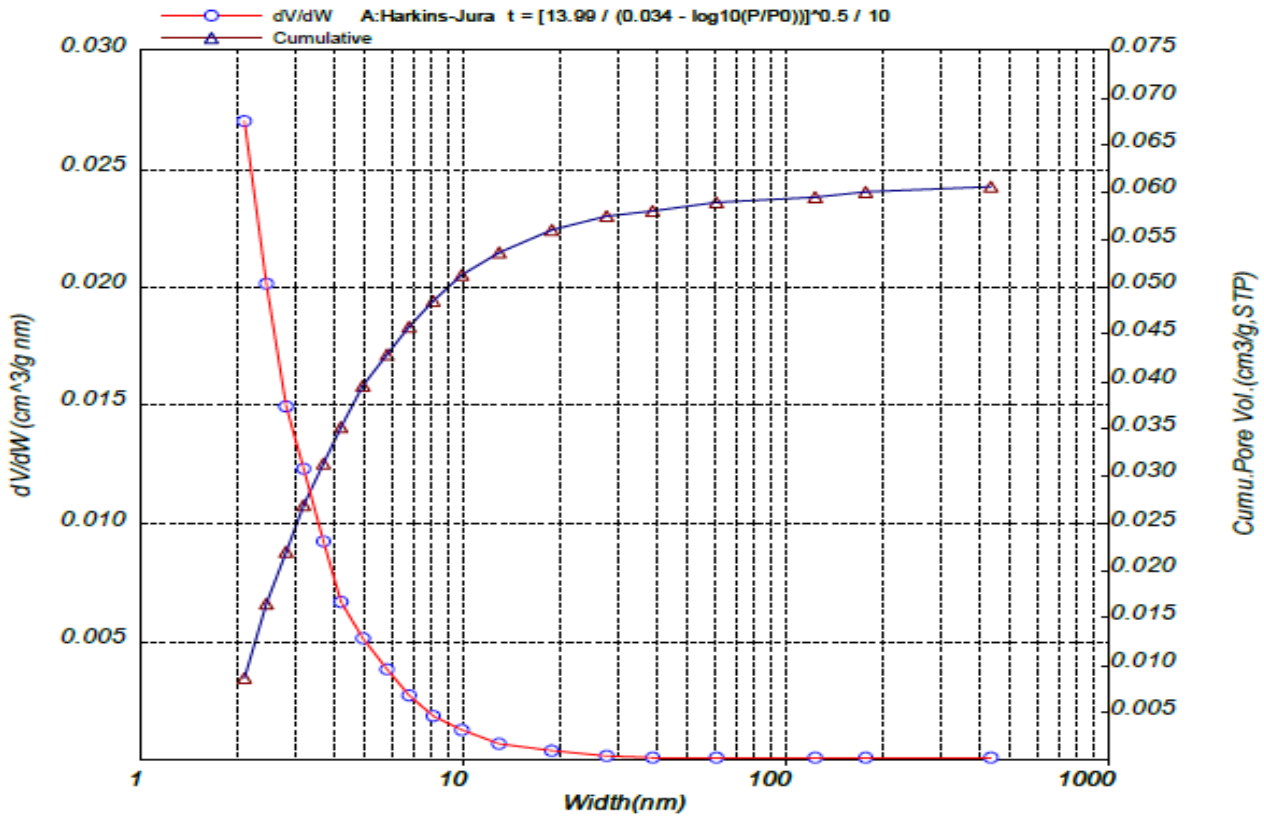


Figure H.3: BJH adsorption pore-size distribution log plot for calcined RSS (Adapted from Onoji et al., 2017b)

Table H.2: Biodiesel yields for fresh and reused catalyst loadings at optimum conditions

Catalyst loading (g)	Yield with fresh catalyst (%)	Yield with reused catalyst (%)				
		1st cycle	2nd cycle	3rd cycle	4th cycle	5th cycle
2.0	75.15 ± 1.25	72.4 ± 1.31	69.31 ± 1.12	67.52 ± 1.3	64.3 ± 1.18	60.4 ± 1.11
2.2	85.03 ± 1.13	84.8 ± 1.09	84.4 ± 1.11	83.5 ± 1.16	80.8 ± 0.04	77.3 ± 0.12
2.5	82.08 ± 1.27	82.01 ± 1.17	81.8 ± 1.32	81.0 ± 1.4	78.1 ± 1.39	74.2 ± 0.94
3.0	81.36 ± 1.18	79.5 ± 1.09	77.6 ± 1.31	75.3 ± 2.04	72.3 ± 1.99	70.4 ± 1.16
3.5	79.01 ± 2.01	76.1 ± 1.23	73.2 ± 1.35	70.4 ± 1.88	67.8 ± 2.04	64.2 ± 1.67

value ± standard deviation of duplicate data**.**

Appendix I

Section I.1

The combustion efficiency of diesel engines has resulted to increase in its usage in the transportation sector in the last few decades. Thus, the environmental concerns are growing and the fuels used in road transportation are subject to increasing stringent regulations (Aldhaidhawi et al., 2017). Biodiesel sourced from non-edible rubber seed oil is considered as a solution to the existing emission problems arising from the use of fossil diesel.

The experimental data for the analyses of the engine performance and emissions arising from the use of the rubber seed oil biodiesel-diesel blends used in the study are presented in this section. This includes air/fuel ratio, brake mean effective pressure, brake thermal efficiency, brake specific fuel consumption, engine brake power, engine torque, exhaust gas temperature, and emissions of CO, CO_2, NO_x, total hydrocarbons, and smoke opacity.

Table I.1: Variation of engine speed with fuel and air parameters for B00 (diesel)

Engine speed (rpm)	Fuel volume (cm^3)	Fuel drain time (s)	Fuel density (ρ), (gcm^{-3})	Fuel flowrate, $\dot{m}_f$ (kgh^{-1})	Ambient air temp., T_A (^oC)	Air differential pressure, ΔP (Pa)	Ambient air pressure, P_A (Pa)	Air velocity (ms^{-1})	Air flowrate, $\dot{m}_a$ (kgh^{-1})	Air/Fuel ratio, $\frac{\dot{m}_a}{\dot{m}_f}$	BMEP (bar)
1500	8	94	0.85	0.26	28.6	-136	100,900	14.6	10.32	39.6	3.48
2000	8	79	0.85	0.31	29.0	-140	100,900	14.8	10.46	33.7	4.06
2500	8	72	0.85	0.34	29.3	-153	100,800	15.5	10.93	32.1	4.75
3000	8	44	0.85	0.56	30.1	-184	100,800	17	11.97	21.4	3.89
3500	8	29	0.85	0.83	31.1	-225	100,800	18.75	13.21	15.9	3.14

Table I.2: Variation of engine speed with fuel and air parameters for B10

Engine speed (rpm)	Fuel volume (cm^3)	Fuel drain time (s)	Fuel density (ρ), (gcm^{-3})	Fuel flowrate, $\dot{m}_f$ (kgh^{-1})	Ambient air temp., T_A (^oC)	Air differential pressure, ΔP (Pa)	Ambient air pressure, P_A (Pa)	Air velocity (ms^{-1})	Air flowrate, $\dot{m}_a$ (kgh^{-1})	Air/Fuel ratio, $\frac{\dot{m}_a}{\dot{m}_f}$	BMEP (bar)
1500	8	91	0.853	0.27	30.1	-138	100,500	14.7	10.35	38.3	1.79
2000	8	79	0.853	0.31	30.2	-140	100,500	14.8	10.42	33.6	2.39
2500	8	66	0.853	0.37	30.5	-156	100,500	15.6	10.99	29.7	2.71
3000	8	38	0.853	0.64	30.7	-171	100,400	16.3	11.5	18	2.22
3500	8	27	0.853	0.90	30.8	-188	100,400	17.1	12.06	13.4	2.11

Table I.3: Variation of engine speed with fuel and air parameters for B20

Engine speed (rpm)	Fuel volume (cm^3)	Fuel drain time (s)	Fuel density (ρ), (gcm^{-3})	Fuel flowrate, $\dot{m}_f$ (kgh^{-1})	Ambient air temp., T_A (^oC)	Air differential pressure, ΔP (Pa)	Ambient air pressure, P_A (Pa)	Air velocity (ms^{-1})	Air flowrate, $\dot{m}_a$ (kgh^{-1})	Air/Fuel ratio, $\frac{\dot{m}_a}{\dot{m}_f}$	BMEP (bar)
1500	8	72	0.855	0.34	31.7	-178	100,400	16.7	11.72	34.5	2.76
2000	8	77	0.855	0.32	31.6	-182	100,400	16.9	11.85	37	2.81
2500	8	77	0.855	0.32	31.7	-220	100,400	18.5	13.03	40.7	3.46
3000	8	70	0.855	0.35	31.6	-240	100,500	19.4	13.6	38.9	2.71
3500	8	66	0.855	0.37	31.6	-247	100,500	19.6	13.8	37.3	2.6

Table I.4: Variation of engine speed with fuel and air parameters for B30

Engine speed (rpm)	Fuel volume (cm^3)	Fuel drain time (s)	Fuel density (ρ), (gcm^{-3})	Fuel flowrate, $\dot{m}_f$ (kgh^{-1})	Ambient air temp., T_A (^oC)	Air differential pressure, ΔP (Pa)	Ambient air pressure, P_A (Pa)	Air velocity (ms^{-1})	Air flowrate, $\dot{m}_a$ (kgh^{-1})	Air/Fuel ratio, $\frac{\dot{m}_a}{\dot{m}_f}$	BMEP (bar)
1500	8	67	0.858	0.36	30.5	-230	101,000	19	13.39	37.2	1.89
2000	8	71	0.858	0.35	31.0	-244	101,000	19.5	13.78	39.4	2.71
2500	8	71	0.858	0.35	29.5	-253	100,900	19.9	14.06	40.2	3.14
3000	8	55	0.858	0.45	29.5	-259	100,900	20.1	14.22	31.6	2.76
3500	8	51	0.858	0.48	30.9	-272	100,900	20.6	14.54	30.3	2.27

Table I.5: Variation of engine speed with fuel and air parameters for B50

Engine speed (rpm)	Fuel volume (cm^3)	Fuel drain time (s)	Fuel density (ρ), (gcm^{-3})	Fuel flowrate, $\dot{m}_f$ (kgh^{-1})	Ambient air temp., T_A (^oC)	Air differential pressure, ΔP (Pa)	Ambient air pressure, P_A (Pa)	Air velocity (ms^{-1})	Air flowrate, $\dot{m}_a$ (kgh^{-1})	Air/Fuel ratio, $\frac{\dot{m}_a}{\dot{m}_f}$	BMEP (bar)
1500	8	67	0.863	0.37	31.6	-186	100,700	17	12	32.4	2.89
2000	8	71	0.863	0.35	31.6	-243	100,700	19.5	13.71	39.2	3.47
2500	8	65	0.863	0.38	31.5	-282	100,700	21	14.78	38.9	3.88
3000	8	51	0.863	0.49	32.2	-282	100,700	21	14.76	30.1	3.39
3500	8	47	0.863	0.53	32.4	-298	100,600	21.6	15.16	28.6	3.13

Table I.6: Variation of engine speed with fuel and air parameters for B100 (biodiesel)

Engine speed (rpm)	Fuel volume (cm^3)	Fuel drain time (s)	Fuel density (ρ), (gcm^{-3})	Fuel flowrate, $\dot{m}_f$ (kgh^{-1})	Ambient air temp., T_A (^oC)	Air differential pressure, ΔP (Pa)	Ambient air pressure, P_A (Pa)	Air velocity (ms^{-1})	Air flowrate, $\dot{m}_a$ (kgh^{-1})	Air/Fuel ratio, $\frac{\dot{m}_a}{\dot{m}_f}$	BMEP (bar)
1500	8	87	0.876	0.29	31.1	-125	100,400	14	9.83	33.9	1.89
2000	8	76	0.876	0.33	31.1	-150	100,400	15.3	10.76	32.6	2.26
2500	8	62	0.876	0.41	31.5	-154	100,400	15.5	10.90	26.6	2.60
3000	8	33	0.876	0.77	31.6	-160	100,400	15.8	11.11	14.4	2.38
3500	8	21	0.876	1.19	31.8	-171	100,400	16.3	11.48	9.6	2.17

Table I.7: Variation of brake thermal efficiency (BTE %) with engine speed

Engine speed (rpm)	BTE (%)					
	B00	B10	B20	B30	B50	B100
1500	33	15.8	28.4	17	26.7	18.1
2000	42	25.2	30	28.4	36.8	25.1
2500	56	35.9	41.1	34.6	42.8	28.2
3000	33	17.1	22.1	20.4	24	16.7
3500	21	13.5	18	14.1	24	11.5

Table I.8: Variation of brake specific fuel consumption (BSFC) with engine speed

Engine speed (rpm)	BSFC ((kg/kWh)					
	B00	B10	B20	B30	B50	B100
1500	0.26	0.53	0.42	0.65	0.44	0.52
2000	0.20	0.34	0.29	0.33	0.26	0.38
2500	0.15	0.28	0.19	0.23	0.20	0.33
3000	0.25	0.50	0.22	0.28	0.25	0.56
3500	0.39	0.63	0.21	0.31	0.25	0.81

Table I.9: Variation of engine brake power (BP) with engine speed

Engine speed (rpm)	BP (kW)					
	B00	B10	B20	B30	B50	B100
1500	1.01	0.518	0.803	0.55	0.84	0.55
2000	1.57	0.921	1.089	1.047	1.34	0.88
2500	2.30	1.31	1.675	1.518	1.88	1.257
3000	2.26	1.29	1.57	1.602	1.97	1.382
3500	2.13	1.43	1.759	1.539	2.12	1.466

Table I.10: Variation of engine torque with engine speed

Engine speed (rpm)	Torque (Nm)					
	B00	B10	B20	B30	B50	B100
1500	6.4	3.3	5.1	3.5	5.4	3.5
2000	7.5	4.4	5.2	5.0	6.4	4.2
2500	8.8	5.0	6.4	5.8	7.8	4.8
3000	7.2	4.1	5.0	5.1	6.0	4.4
3500	5.8	3.9	4.8	4.2	5.4	4.0

Table I.11: Variation of exhaust gas temperature (EGT) with engine speed

Engine speed (rpm)	EGT (^oC)					
	B00	B10	B20	B30	B50	B100
1500	175	180	187	192	215	233
2000	185	190	200	215	238	259
2500	217	220	230	240	250	274
3000	240	242	250	260	270	286
3500	300	305	315	320	328	340

Table I.12: Variation of carbon monoxide emissions with engine speed

Engine speed (rpm)	CO (ppm)					
	B00	B10	B20	B30	B50	B100
1500	165	160	157	154	150	145
2000	140	138	136	132	128	120
2500	125	123	120	117	114	110
3000	135	132	130	128	125	119
3500	138	136	134	133	130	124

Table I.13: Variation of carbon dioxide emissions with engine speed

Engine speed (rpm)	CO_2 (ppm)					
	B00	B10	B20	B30	B50	B100
1500	130	145	170	152	160	175
2000	135	150	180	165	170	190
2500	150	168	220	180	200	228
3000	170	200	250	225	230	265
3500	215	235	292	260	270	300

Table I.14: Variation of oxides of nitrogen emissions with engine speed

Engine speed (rpm)	NO_x (ppm)					
	B00	B10	B20	B30	B50	B100
1500	5	8	10	13	15	15
2000	12	15	17	20	23	25
2500	20	22	25	27	30	33
3000	23	26	30	35	38	42
3500	30	35	44	49	52	55

Table I.15: Variation of total hydrocarbons emissions with engine speed

Engine speed (rpm)	THCs (ppm)					
	B00	B10	B20	B30	B50	B100
1500	120	115	110	100	90	80
2000	115	110	100	94	88	75
2500	99	89	85	82	79	70
3000	85	80	76	74	70	65
3500	100	98	90	88	83	73

Table I.16: Variation of smoke opacity emissions with engine speed

Engine speed (rpm)	Smoke (BSU)					
	B00	B10	B20	B30	B50	B100
1500	1.41	1.3	1.01	1.1	1.06	0.89
2000	2.48	2.21	1.12	1.6	1.18	0.92
2500	3.69	3.2	1.98	2.6	2.2	1.89
3000	4.91	4.5	3	3.8	3.3	2.88
3500	6.01	5.6	3.88	5.1	4.3	3.6

BSU: Bosch smoke unit